Sustainable Regional Aircraft

Final Report

DSE Group 20

Delft University of Technology

TU Delft

This page is intentionally left blank

Delft University of Technology

Delft, The Netherlands

Design Synthesis Exercise Spring 2020

AE3200

Sustainable Regional Aircraft

Final Report

Authors:	
Jorn van Beek	4544439
Sasho Ivanov	4681657
Jari Malfliet	4668626
Manuel Martin	4137361
Matteo Rebosolan	4664973
Rick van Rooijen	4646878
Paul Simon Schön	4531515
George Tzanetos	4667638
Tobias Veselka	4451848
Martijn Vroom	4666372

Submission Date:	June 30, 2020
Group:	20
Supervisors:	Ir. Jos Sinke
	Dimosthenis Giannopoulos
	Sumit Tambe

TU Delft Delft University of Technology

Preface

This report is the culmination of the Design Synthesis Exercise of Group 20 at the Technical University of Delft. This endeavor has taken the 10 bachelor aerospace students of Group 20, 9 weeks to complete, in which their engineering and organizational skills have been tested like never before.

This project is all about trying to solve the current paradox society finds itself in, where the demand for air travel is only increasing, and is increasing at the same rate as people's desire to not harm the environment. The objective of the project is to design a more sustainable option for a regional aircraft. Readers that are interested in future sustainable solutions for the air transport industry will most likely find this report engaging.

The team, group 20, would like to extend our sincere gratitude to all those that have helped this project become reality. A special thanks to Professor Jos Sinke, Dimosthenis Giannopoulos, Sumit Tambe, and Robert Coenen for their indispensable guidance throughout the entire Design Synthesis Exercise process. Many thanks to Dr. Arvind Gangoli Rao, Davide Nardi, and Dr. Rene Alderliesten, for taking time out of their busy schedule to lend the team a supporting hand. The input of the organizational committee of the DSE was highly appreciated. And a final thanks to all family members and loved ones that have supported everyone through the span of this project.

Executive Overview

Project Objectives The aviation industry is following suit with the growing world demand of becoming more environmentally conscious/friendly. However, the demand for commercial aviation has only been increasing with time, resulting in an ever growing source of pollution. The challenge is to manage this paradox, meet the demand increase with an overall reduction in pollution. The project objective is best described in the mission need statement which is to "provide a design for a regional aircraft with an environmental footprint which is at least 25% lower than for the reference aircraft, the Bombardier CRJ700 series, and which can fly 75 passengers over a distance of 2000km." Reducing the design's environmental footprint is mainly achieved by lowering the climate effects of the product, including its production, fuel and end-of-life handling. The project focuses on developing new strategies and design solutions to reduce the environmental footprint of all three stages of the life-cycle: production, operation, and end of life. Currently operational emissions, greenhouse gasses, are the main contributor to climate change in the aviation industry. Therefore, minimizing the operational emissions will put a large dent in the overall carbon footprint. The social aspects, impact of the design on human well-being, and economical aspects of being sustainable also have to be considered. A balance must be struck between improving sustainability and cost to ensure competitiveness and affordability with the current market.

Name of the Aircraft The to-be-designed regional aircraft is named "RELIGHT". RELIGHT is short for REgionaL Innovative Green Hydrogen Transport. As the name suggests, hydrogen will be the main source of propulsion, which is considered innovative w.r.t. the current market. The acronym RELIGHT is chosen as it contains the word "LIGHT", which refers to the lightweight application of hydrogen combustion due to its high mass-specific energy density.

Mission Characteristics The achievable range will vary from $2000km$ at maximum payload weight to a range of $4595km$ with no payload on board. RELIGHT's flight profile goes as follows: RELIGHT takes off and starts climbing to a cruise altitude of $10km$. RELIGHT will cruise for approximately $2000km$ at an average cruise speed of $807.6km/h$. RELIGHT will touch-down, taxi to the gate and shut down the engines. However, in case a diversion is needed, RELIGHT will be able to cruise for another $200km$ at a speed of approximately $646km/h$. Then the loitering phase starts, the aircraft will have enough reserve fuel to loiter for 45 minutes at a speed of approximately $485km/h$.
RELIGHT will require a massive shift in operations and logistics from the current norm. It demands a structural change at airports to be able to provide green hydrogen. The idea is to remove the greenhouse effect directly and indirectly. For this to become a reality the production of hydrogen must be green. The teams vision is that green energy sources provided by the countries' economy are used for producing hydrogen at airports. On top of this a few hurdles need to be dealt with before being able to use cryogenic hydrogen as a fuel source. During the life-cycle of the aircraft, the swing in temperatures due to the cryogenic hydrogen fuel will introduce massive strain and cyclic loads to the fuel tanks and pipes. Therefore, frequent and careful inspections will be required. Managing and transporting fuel to the aircraft without an overall increase in temperature is another logistical challenge that result in drastic changes in conventional ground operations.

Market Analysis The market RELIGHT aims to get a foothold in is predominantly developing economies such like those in South East Asia, Africa and South America due to their rapid growth rates. In order for RELIGHT to be successful it is necessary to establish a hydrogen fuel infrastructure at regional airports. The emphasis on serving major destinations in developing economies has a significant impact on the design. This set the range requirement to $2000km$ as well as the purchasing price which was set to be less than 44.4 million USD. After analyzing the cost of manufacture for RELIGHTS subsystems, it was found that a price of 37 million USD was realizable. The cost break down structure also revealed that the total development cost of RELIGHT would be less than 1 billion US$.
It was found that using the high bypass ratio turbofan at a low combustion temperature, the operational costs would decrease by 1%. In conjunction with the unit cost this could lead to a return on investment of less than 7 years, under constant utilization. Therefore it can be concluded that this aircraft would achieve a market foothold in two decades, when the hydrogen infrastructure has been provided to several regional airports.

Sustainable Development Strategy To guarantee sustainable development of RELIGHT, the three pillars of sustainability are assessed. These are the environment, the economy and society. Environmental sustainability

entails the impact to the natural environment, in which emission of pollutants plays a large role. Economical sustainability focuses on profit, such that the program has purpose and can function a long time. To be sustainable with respect to society, RELIGHT offers quality to all stakeholders involved: project employers and employees, certification organizations, airliners, airports, passengers and people living near airports.

For the carbon footprint, the operational emissions are analysed. These are compared with the emissions of the Bombardier CRJ700. The large difference is due to the fuels used; hydrogen for RELIGHT and kerosene for the CRJ700, since hydrogen emits no carbon. The water feedstock needed for RELIGHT is somewhat larger, since hydrogen electrolysis from green energy and H_2O requires slightly more fresh water than kerosene production. Even though the development, fuel and unit costs are estimated to be lower than the CRJ700, the profit achieved is lower and hence the return on investment is longer. This is due to the smaller range and cruise speed compared to the CRJ700. However, as it is likely that kerosene will increase in cost and hydrogen decrease in the coming decade(s), RELIGHT will end up being more profitable. Noise results being slightly larger, however the analysis is based on older aircraft technology and therefore not entirely accurate. The pollutants that cause damage to human health are decreased drastically, since RELIGHT emits no Particulate Matter. A visualization for the sustainability comparison of RELIGHT and the CRJ700 is presented in Figure 1.

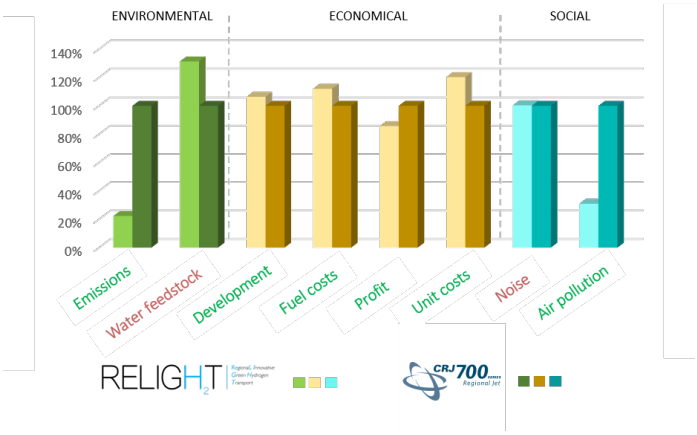

Figure 1: Sustainability comparison between RELIGHT and Bombardier CRJ700

Preliminary Concept Description During the preliminary phases of the project several design concepts were investigated. The three concepts that showed the most potential were the blended wing body concept, the strutted wing concept and the hybrid hydrogen concept. These three concepts were put through a trade-off and their performance was evaluated with respect to different categories. From this analysis the hybrid hydrogen concept achieved the highest score, meaning it is the concept on which detailed design is performed. The hybrid hydrogen concept is defined as using a combination between hydrogen and kerosene. The ratio between the two needs to be determined based on several factors like weight, cost, emissions and overall viability.

A Class I weight estimation is performed to provide values for the MTOM, OEM and fuel weight. Different calculations are made where the hydrogen fraction is varied to investigate the effect on hybrid fuel. To start the Class I weight estimation several parameters were found. This includes the payload weight which is $7975kg$, which include both passengers, their luggage, and additional cargo. The OEM is determined using a regression line based on existing aircraft. A mass of 1.5 tonnes is added to the OEM to account for the hydrogen fuel tank. The fuel weight is calculated based on the fuel fractions method during different flight phases, where the changing fuel flow rate is accounted for when considering different hybrid mixtures. This is done by assuming that the energy of the mixture remain the same.

Based on the results of this analysis a full hydrogen aircraft has been chosen. From emission perspective this configuration performs really well. Also the complexity associated with the hybrid system is omitted when choosing a full hydrogen system.

The parameters from the Class I estimations are refined using a Class II weight estimation, where the different system masses are calculated. These two methods are then connected into an iterative loop until the results

converge within 1%. The method used for the Class II weight estimation was of Torenbeek [1]. The results can be viewed in Table 1. The results from the weight estimation were used in the subsystem design. Along with the Class II, a flight envelope is built, which constrains the speeds and loads the aircraft is allowed to operate in. The maximum load factor n_{max} resulting from the envelope is 2.537, with the limit load n_{limit} factor being 2.656.

Table 1: Class II weight estimation overview

MTOM [kg]	OEM [kg]	Payload mass [kg]	Fuel mass [kg]	Fuselage [kg]	Propulsion [kg]	Wing [kg]	Equipment [kg]
28083	18276	7975	1848	3948	2743	2350	6427

Subsystem Design

Propulsion System The propulsion system development methodology aims to deliver the required thrust while minimizing the weight, emissions and cost. The design is based on a list of requirements that the propulsion systems needs to comply with for the aircraft to function as intended. These requirements were set to ensure that the realization of the engine remains realistic and achievable.
A high bypass ratio hydrogen turbofan engine was developed, having similar components as a regular turbofan. An analytical model of the engine was constructed using thermodynamic relations to model the temperature and pressure at various stations inside the engine. The model allows for iteration which is used when altering input parameters to get the desired performance. The analysis is performed for two stages during the mission profile, that being the take-off at $1500m$ and cruise. A bypass ratio of 10, together with an inlet diameter of 2.285m, resulted in a core flow of $27.3kg/s$ and a fuel mass flow of $0.1kg/s$ The results obtained at those conditions are $60.75kN$ and $44.6kN$ of thrust and a specific fuel consumption of $1.7g/kN/s$ and $3.6g/kN/s$, respectively.

After the engines have been sized, the hydrogen tank design can start. The aircraft will have three tanks, one tail tank and two auxiliary tanks placed on the wings. The cryogenic liquid in the tank is kept from boiling off by insulation that is placed around the tank. The amount of insulation limits the boil-off rate to 1% per 10 hours. Boil-off effects are taken into account as boil-off gases pose a big hazard. The insulation thickness is calculated by taking into account the heat flux coming from the hotter outside environment which can be quantified using thermodynamic principles. This results in an insulation thickness of $2.8cm$ for the tail tank, and $3.5cm$ for the external wing tank when closed cell polymethacrylimide is used.

The external wing-mounted tanks are placed at a distance of $7.44m$ from the centerline of the aircraft. This is the middle of the gap between the flap and aileron as the external wing tanks are placed on the back of the wing, with a portion of the tank showing behind the trailing edge. This is to allow for gradual transition of the aircraft's cross sectional area, which reduces the transonic and sonic drag. This position is the only possibility for the tank pylon where it does not interfere with the flaps or aileron operations.

Next, to connect the tanks and engines a fuel distribution system is needed. The system takes the liquid hydrogen from the tanks using a jet pump, then fed into the pipes using a low pressure pump. This is fed into the feed tanks located on the wing, from where the liquid hydrogen is pumped into a heat exchanger just before the engine, which heats the hydrogen to between 150-250K before it is injected into the combustion chamber. The reliability of the system is increased by doubling the pumps for redundancy. Multiple safety valves are placed at key locations to address safety issues in the event of an emergency. Furthermore, a purge system is added to clean the fuel system of leftover hydrogen or air at startup or shutdown as mixing the two could lead to unwanted combustion.

Fuselage and Tank Layout The fuselage not only provides seating space for 75 passengers, but also includes a cockpit, a front and aft galley, the necessary emergency aisle dimensions and doors, lavatories and cargo space. In case of the RELIGHT, hydrogen had to be stored inside the fuselage because of the large required tank volume of $28.28m^3$.
It was decided to place 5 seats (2 on the left, 3 on the right) per row. For 75 passengers, this results in 15 rows. A seat pitch of 32 inch is taken. Room is provided for an aisle, armrests, cabin luggage and wall clearance. Between the seventh and eight row, a type III emergency exit with emergency aisle is located. Floor and wall

thicknesses were also incorporated, both being 100mm. Under the floor, cargo storage is provided for a total of $1000kg$. 1/3 goes in the front hold ($6m$ from nose), 2/3 in the back hold ($19m$ from nose).

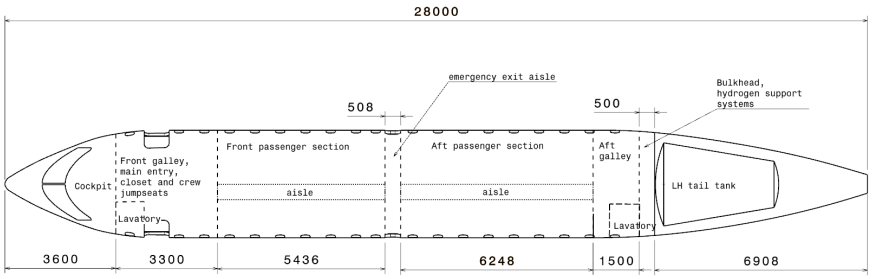

Figure 2: Top view of fuselage

The required tank volume was found to be $28.28m^3$, which is considerably bigger than a similar kerosene tank. Therefore, alternative storage methods needed to be explored. It was found that the tail could store half of the required volume. The other half either needed to be stored in a top tank (a longitudinal tank above the cabin) or external wing tanks below the wing. A drag trade-off was done between the two. The external wing tanks came out as winner, as it causes $600N$ less drag. Next, the tail tank and external wing tanks were sized. The diameter of the external wing tank is $1.39m$, for an assumed length of $5m$. The tail tank is shaped as an oblique truncated cone, with big diameter $2.7m$, small diameter $1.5m$ and length of $3.58m$. Both types of tanks include end caps. Alternative cabin lay-outs were also explored. If the customer wants to increase the passenger number, cargo hold weight needs to be sacrificed. If the customer wishes to have 5 passengers seats less, the tank volume of external tanks can be increased with 50% and then RELIGHT can fly to $3000km$. Control and stability needs to be adequately redesigned for this extended range version. Cabin lighting and cargo placement could also be further researched.

Wing Planform Consecutively, a thorough calculation procedure follows and is explained to the reader, concerning the sizing of the primary dimensions and aerodynamic values, those being portrayed right below. Next, the airfoil selection can take place. Therefore, in order to narrow it down correctly, the value for $C_{L_{des}}$ is obtained using solely the wing loading, and then corrected for compressibility and for the airfoil. In accordance to the result, the 7 parameters that dictate the selection are decided upon, and the Reynolds number of the flight mission calculated. As a result, for the above $C_{L_{des}}$, the best airfoils are picked, and a trade-off is performed. The resulting airfoil is the NACA-SC(2)0614, a supercritical airfoil that serves RELIGHT's mission perfectly.

Table 2: Wing planform characteristics, and outputs of aerodynamic analysis

Parameter	**Value**	**Unit**	**Parameter**	**Value**	**Unit**
Wing area - S	62.248	m^2	Tip chord - c_t	1.320	m
Aspect Ratio - AR	8	$-$	Mean aerodynamic chord - MAC	3.048	m
Span - b	22.316	m	Thickness-to-chord ratio - t/c	0.14	$-$
Taper ratio - λ	0.310	$-$	Dihedral - Γ	-1	deg
Root chord - c_r	4.259	m	Design lift coefficient - $C_{L_{des}}$	0.4567	

Next, the high lift devices are sized, with the driving parameter being $\Delta C_{L_{max}}$. Slats were deemed not necessary. The resulting lift curves for cruise, take-off and landing are displayed above in Figure 3a. The drag is split between the zero-lift drag and the lift-induced drag. The oswald efficiency factor is calculated, and the resulting drag polar can be found in Figure 3b.
The parameters are wing span (b), drag divergence Mach number (M_{dd}), and the zero-lift drag contribution of the landing gear ($C_{D_{0_{gear}}}$). Their values respectively are, calculated to be 22.32, 0.803, and 12.94. The requirements compliance part then brings the section back to the requirements listed in the beginning and links each one to the appropriate section part. Lastly, the weight of the system is discussed in accordance to the Class II weight estimation section, and several recommendations are put together, for valid assumptions made through the process or further accuracy in future development.

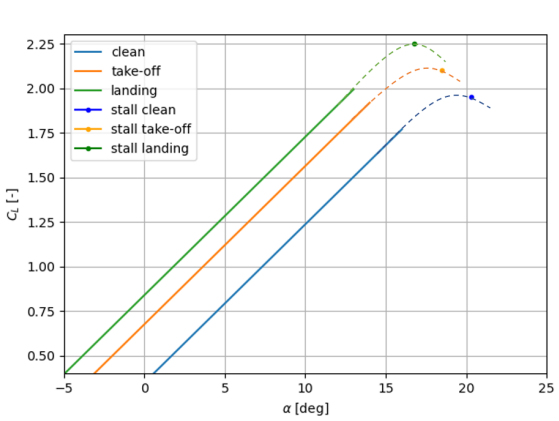

(a) Wing lift curves for clean, take-off and landing configuration

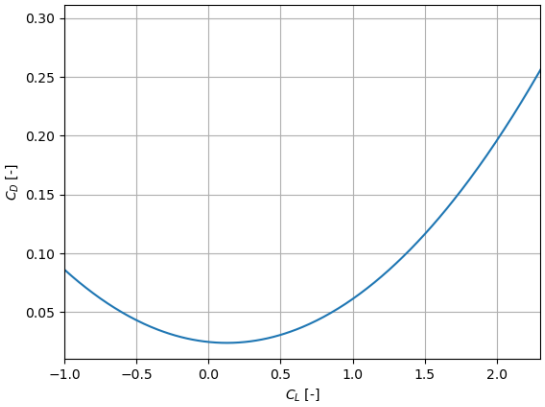

(b) Drag polar of RELIGHT

Figure 3: Aerodynamic properties

Stability and Control

Center of Gravity Before being able to size Stability and control subsystems, the center of gravity (C.G.) range must be determined. This is based on the operational empty weight (OEW), the payload weight and the fuel weight, together with the respective C.G. locations of each component.

The C.G. during loading will be kept between 31% and 53%, while the requirement for the in flight shift is more strict: between 31% and 44% of the mean aerodynamic chord (MAC). A large amount of the shift will be caused by the emptying of the hydrogen tank in the tail of the aircraft emptying during flight. The loading diagram that was made to visualize the calculation can be seen in Figure 4

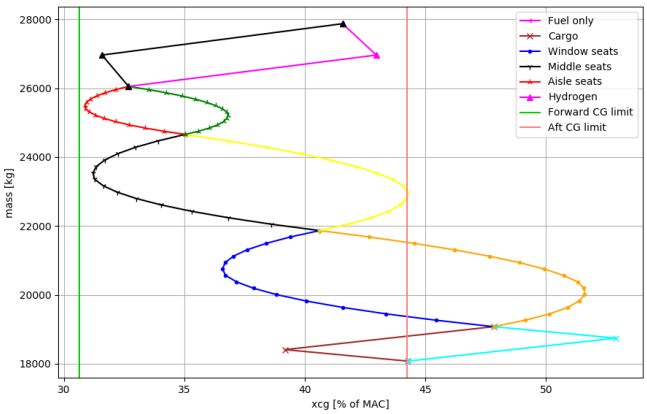

Figure 4: Loading Diagram of RELIGHT

Vertical Tail The vertical tail area is sized based on the One Engine Inoperative (OEI) requirement. If, during take-off, one of the engines shuts down, the aircraft still should be able to fly straight by deflecting the rudder accordingly, to counteract the yawing moment created by the asymmetric engine thrust. Based on statistics, the preliminary vertical tail volume and vertical tail area are estimated. Then, the vertical tail is sized with a simple rudder; this results in a very large vertical tail area, with a very high vertical tail volume. This is more resource intensive, as it is requires more material and a stronger structure, thus creating more drag. Therefore, as literature [2] suggests, a rudder with a double hinge line is used, which allows for further deflection of the rudder, with a maximum deflection of $40°$ instead of $25°$ for a simple rudder. Though this is certainly possible, a more detailed aerodynamic analysis on the effects of a larger deflection is recommended. In Table 3 all relevant values of the design of the vertical tail are tabulated.

Table 3: Vertical tail dimensions

Vertical tail area S_v/S [-]	Vertical tail span b_v/b [-]	Vertical tail AR A_v [-]	Vertical tail taper ratio λ_v [-]	Rudder area S_r/S_v [-]	Vertical tail volume $\bar{V}_v$ [-]	Maximum deflection rudder $[deg]$
0.224	0.207	1.7	0.6	0.303	0.117	40

The effect of several parameters on the required vertical tail area is worth mentioning: An increase in the MTOW is found to decrease the required tail area, due to the higher minimum control speed V_{mc}; a decrease in engine thrust will provide the same results. It is assumed that the ratio of rudder to chord area, equal to 0.303, is identical to the rudder chord to vertical tail chord ratio c_f/c. Both an increase and decrease of this ratio has adverse effects on the vertical tail area.

Landing Gear The weight of the aircraft is the deciding factor for determining the amount of landing gear struts and wheels; the aircraft has one nose gear and two main gear struts, with two wheels per strut. The position of the landing gear is determined based on several requirements: the tipover angle ϕ should be below $55°$; the tipback angle θ should be larger than $15°$ and the nose gear should be sufficiently loaded to allow for steering, whilst not being loaded too excessively to make the aircraft difficult to steer. The load on the nose landing gear should be between 8 and 15% of the take-off weight. Below, in Table 4, all relevant dimensions are provided.

Table 4: Landing gear location

Landing gear	Longitudinal position w.r.t. A/C nose [m]	Vertical position from ground w.r.t. Z_{cg} [m]	Lateral position Y_{LG} w.r.t. A/C symmetry plane [m]	Loading relative to W_{TO} [-]
Main	15.4311	3.203	2.295	0.9118
Nose	3.84	3.203	-	0.0882

Both the main and nose gear tires are selected in a trade-off based on the maximum tire speed, tire pressure and wheel loading. The dimensions for the Goodyear tires, operating at 906.22 kPa, are: 34x9.25-16 (Outer diameter x width - inner diameter in inches[1]) and 17.5x5.75-8 for the main and nose gear, respectively. Moreover, a detailed analysis on the shock absorbing design is performed. The require shock absorber stroke length of $0.341m$ is found to be similar to comparable aircraft. Lastly, the performed sensitivity analysis shows the impact of varying several parameters when sizing the landing gear. Especially the nose landing gear is very sensitive to a shift in C.G. location, if the entire C.G. range were to be moved by $\pm$ $1m$, the nose gear shifts almost twice that distance.

Horizontal Tail The horizontal tail must provide both stability and control to the aircraft in terms of pitch. Furthermore, the tail must be able to provide pitch control of the aircraft at take-off, while also keeping the trim drag at an acceptable level. Due to the in-flight gravity shift, sizing the tail to an acceptable size is a challenge. Figure 5 shows the scissor plot of RELIGHT. On the y-axis, the horizontal tail size ratio with respect to the wing is given, while the x-axis shows the C.G. The red line shows the actual tail size and C.G. range during flight. The blue line shows the aft limit of the C.G. limit for stability, while the yellow line shows the forward limit for controlability. Note that controlability is assessed during landing because of the large moment coefficient induced by the flaps, while the stability is assessed during cruise, as the neutral point moves forward at increasing Mach number. In green, the limit is shown due to the rotation requirement which is sizing in the case of RELIGHT. Furthermore, an overview of the designed horizontal stabilizer is given in Table 5.

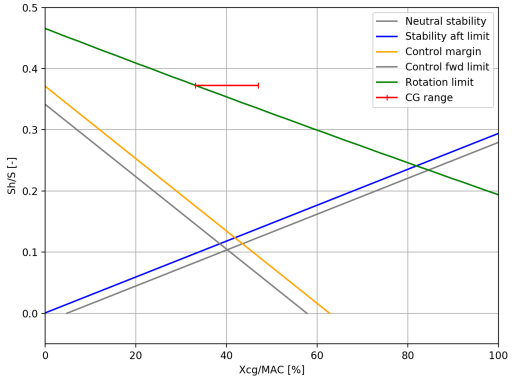

Figure 5: Scissor Plot of RELIGHT

Table 5: Horizontal tail data

Horizontal tail area S_h [m^2]	Tail area ratio $\frac{S_h}{S}$ [-]	Horizontal tail span b_h [m]	Horizontal tail AR A_v [-]
23.58	0.3788	9.7	4
Horizontal tail sweep $\Lambda_{0.5c}$ [deg]	**Horizontal tail type**	**Wing root chord location $x_{rootchord}$ [m]**	**Horizontal tail taper ratio λ_h**
25	Adjustable	10.7	0.5

[1]Tire data in tire catalogues and literature is listed in United States customary units; for reproducibility and consistency these units are used

Structural and Material Design The structures and materials of the aircraft have been chosen to minimize the overall carbon footprint of the aircraft. For the material a trade-off was made between a fully metal aircraft and composite aircraft. The fully metal aircraft results in an improvement of the production and end of life performance, and the composite aircraft results in a reduction in operational emissions. RELIGHT runs on hydrogen and therefore the operational emissions are very low, and further weight reduction does not lead to significant reduction in carbon footprint. Therefore the choice was made to go with a majority metal aircraft, specifically Al 2024-T351. This will not only reduce the footprint of production and increase the sustainability at end of life it also has the effect of making the aircraft less costly to manufacture.

The cryogenic tank material is made up of a CFRP (Hexcel 8552) pressure shell. The insulation will consist of Rohacell foam to ensure the cryogenic hydrogen can remain at cryogenic temperatures. The total weight is $300kg$.

The wing and fuselage structure is made such that it can cope with loads experienced without failing. This is done by identifying the limiting loads and sizing the structures for these loads. Structural idealization was used for both the fuselage and wing structure in order to find an optimal structure across the structural cross sections. Currently the wing skin has an average thickness of $6.5mm$, a total of 34 stringers with an area of $0.0015m^2$ each. For the fuselage, the structure has a thickness of $1.5mm$ for x<8m and x<16m and a thickness of $3mm$ for 8m<x<16m, a total of 55 stringers with an area of $0.00001m^2$ throughout the fuselage. The mode of failure that is currently considered is yield failure due to bending stress and the tresca criterion. The modes of failure that still need to be optimized for are those of buckling, fatigue, creep, deflection, and fracture.

Final Design Characteristics

Budget Breakdown

A mass budget breakdown and a contingency plan have been created to account for the resource spending occurring at the later design stages resulting from reducing uncertainty. That way the design is constrained, meaning suitable design choices need to be made to fit within the requirements. The contingency plan specifies the maximum values that different parameters should be designed for during the different phases. These values are lower than the final desired value, to allow for growth later in the design. This is done with the use of a performance index, which measures the relative difference between the current stage and the design value goal.

Aircraft Systems RELIGHT will make use of an extensive electrical system. Instead of a pneumatic system using bleed air from the engines and/or APU to start up the engines, provide anti-ice and provide air conditioning, electric starter motors, heating and compressors will be used. Additionally, the hydraulic system for the flight controls and landing gear will be powered by electrical pumps instead of mechanical pumps attached to the engine. The goal of this is to reduce complexity and weight. The electrical system will feature two redundant power controllers, with both controllers able to provide power to flight-critical systems. There will be four hydraulic systems on board of RELIGHT, of which one will be the backup system to control primary flight controls during contingencies. Each hydraulic system will feature two electric pumps, each connected to either the forward or aft power controller. The environmental control system will provide fresh air to passengers, which is similar to most airliners except for the electric air compressor. The APU will be very similar to the APU installed in the CRJ700, with the exception of the bleed air system. The bleed air system will not be featured on RELIGHT, while the electric generators will become more powerful.

RAMS The RAMS characteristics of RELIGHT need to be explored, those include the reliability, availability, maintainability and safety of the aircraft. Starting with reliability, the main difference with existing aircraft is the hydrogen propulsion system. The system uses multiple tanks and pumps to allow for redundancy thus also increasing the reliability. The availability of the aircraft comes down to the hydrogen availability at regional airports. It is assumed that in the coming years an increasing amount of regional airports will allow for hydrogen refueling. Maintenance is eased by the high wing configuration which allows for inspection and unscheduled maintenance of the external wing tanks and engines. The main safety concerns are connected with the hydrogen storage and transfer. Multiple safety systems are incorporated into the design to increase the safety such as pressure release valves and heat exchangers.

Aircraft Performance

Maneuvering With the subsystems being designed, a closer look can be taken at RELIGHT's maneuverability. This is expressed in terms of airfield performance, climb performance, cruise performance and turning performance. To comply with the user requirement of have a take-off distance of less than $1500m$, the take-off needs to be broken down into take-off ground run distance ($x_{gr_{to}}$), transition distance (x_{tr}) and total take-off distance (x_{to}). The team decided to achieve take-off within $1500m$ at both sea level and $1500m$, to be able to operate from elevated regional airports. The same applies to the landing distance, as the team imposed a requirement of being capable of taking-off from and landing at the same runway. Table 6 summarizes the resulting take-off and landing performance. It becomes clear that the landing requirements can be met at both altitudes. However, the take-off at $1500m$ of altitude exceeds the take-off requirement. It must be said that in these calculations, the effect of runway slope, wind and ground effect have not been included. Therefore, it is recommended to investigate the effect on the required take-off distance as this will improve the overall take-off performance. Moreover, the requirement itself might be reconsidered, as it turned out to be a critical constraint when sizing the engines. It was found that the required sea-level thrust to weight ratio had to be increased from 0.31 to 0.44. Hence, the design turned out to be very sensitive to the take-off requirement at $1500m$ which decreases overall efficiency. Since the team imposed this requirement above the one provided by the user, the requirement might be revisited in deliberation with the user.

Table 6: Airfield performance at sea level and 1500m altitude for a reverse thrust of 50% at sea level and 100% at 1500m; all instances of x reported in [m] and V in [m/s]

	Take-off				Landing					
	$x_{gr_{to}}$	V_{lof}	x_{tr}	x_{to}	x_{ap}	x_{fl}	V_{ap}	x_{rot}	x_{br}	x_{la}
sea level	737.4	59.5	293.2	1030.6	289.5	146.1	73.7	147.3	901.4	1484.4
1500 m	1160.1	66.7	368.8	1528.9	364.2	108.8	82.6	165.2	842.1	1480.3

Climb performance is quantified by means of the maximum achievable steady rate of climb. Since this condition changes with altitude, a plot is made which also shows the corresponding airspeed and maximum achievable climb angle as function of altitude. These plots are derived from the performance diagrams, which itself show the behavior of available power versus required power as function of airspeed and load factor. The resulting maximum rate of climb range from $61.5m/s$ at sea level to $27m/s$ at cruise altitude. This complies with the requirement of having a sea level rate of climb of at least $10m/s$.

Finally, the turning performance is expressed in terms of minimum turn radius, minimum time to turn and steepest turn in case of a steady level turn. Since these turn characteristics are dictated by the maximum attainable load factor, $n_{max} - V$ diagrams are constructed at different altitudes at which turn performance is computed. This results in allowable ranges of airspeed at different load factors, which enables quantification of the aforementioned turn characteristics. Furthermore, rate one turn characteristics are computed to check the compliance with the requirement: "The aircraft shall be able to perform a rate one turn at sea level, with a bank angle lower than 25 degrees." The turning performance is depicted in Figure 6 for the allowable airspeed ranges found from $n_{max} - V$ diagrams. The minimum turn radius (R_{min}), minimum time to turn (T_{min}) and corresponding airspeed at which this optimal performance is attained ($V_{R_{min}}$ and $V_{T_{min}}$), is summarized in Table 7. The steepest turn is achieved at a maximum load factor of 2.54, as derived from the flight envelope. This implies a corresponding maximum bank angle of 66.8 degrees. Lastly, the range and endurance characteristics of RELIGHT are provided in Table 8.

Table 7: Optimal turning characteristics

	n_{max} $[-]$	R_{min} $[m]$	$V_{R_{min}}$ $[m/s]$	T_{min} $[s]$	$V_{T_{min}}$ $[m/s]$
Sea level	2.54	356	90	25	90
Cruise	2.54	924	145	40	145

Table 8: Maximum range, ferry range and endurance

Range $[km]$	Ferry range $[km]$	Endurance $[hh:mm:ss]$
2159.3	4318.73	03 : 26 : 30

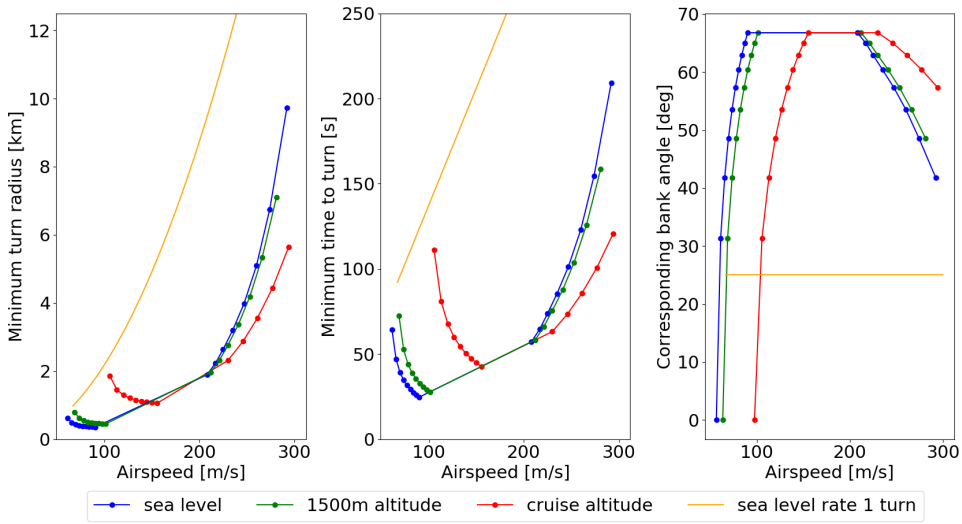

Figure 6: Minimum turn radius, minimum time to turn and corresponding bank angle

Noise As the noise pollution affects the social aspect of RELIGHT's environmental footprint, it is key to analyze noise levels. To show the compliance with the noise limits set by ICAO regulations, RELIGHT is put through an extensive noise calculation model. This model heavily relies on empirical data, derived from noise levels perceived from existing aircraft. A distinction is made between engine noise and airframe noise, as these are known to be the most dominant noise contributors. Engine noise is further split up into fan noise, combustion noise, turbine noise and jet noise. Jet shock cell noise is not considered as the engines are designed such that the exhaust flow mach number does not exceed one. Airframe noise is split up into the main airframe noise sources: clean wing, horizontal and vertical tail, flaps and main and nose landing gear. For each of the aforementioned noise sources, a 1/3 Octave Band sound spectrum is computed for central frequencies ranging from approximately 30 to 30000Hz. The total noise polluted is then found by combining the noise levels of each individual noise source, after which maximum noise levels are derived from the total noise spectra. The maximum noise levels during approach, flyover and landing, as stipulated by ICAO regulations, are summarized in Table 9. In here, also the maximum noise of the CRJ700 is stated to facilitate comparison.

Table 9: Maximum noise levels w.r.t. a reference acoustic pressure of 2E-5 Pa

	Approach noise	Flyover noise	Lateral noise	Cumulative noise
Limit	95	86	91	264 [dB]
RELIGHT	101	74	89	264 [dB]
CRJ700	93	83	89	265 [dB]

Looking at the noise limits, the flyover and lateral noise requirements are being met. However, the approach noise exceeds the noise limit stipulated by the ICAO, which implies that the aircraft cannot be certified. However, the empirical data used to build the noise model, which do not represent current technologies in the area of noise reduction. Therefore, the noise levels obtained can be reduced by 10dB, just by the application of noise reduction concepts like acoustic lining, flow mixers and silencing nozzles. Hence, the future project development will focus on the application of such concepts, to comply with the requirements in the first place and further lowering the environmental footprint in the second place.

Operational Emissions Since emissions during flight are a key indicator of RELIGHT's environmental footprint and hence sustainability, they are important to analyze. Arguably, operational emissions from combustion take up the largest part of an aircraft's life span. The top-level requirement was to at least reduce operational emission by 25% with respect to the reference aircraft, the Bombardier CRJ700. To obtain a measure for emissions, a few steps are taken. First, the Emission Index for the most harmful pollutants, CO_2, H_2O and NO_x, are determined for both kerosene and hydrogen combustion. These pollutants are selected as they have

a large Global Warming Potential (GWP) and take up the majority of the emission. Logically, the second step is to determine the GWP for each pollutant, which varies with altitude. Lastly, the operational emissions are expressed as the Carbon Footprint (CF), which equates each pollutants to the mass of CO_2 with equivalent climate impact on a 100 year scale. The CF is divided by passenger kilometers, such that RELIGHT and the CRJ700 can be compared. This yields a CF reduction of 77.69% and thereby the stakeholders requirement is complied with. This result also satisfies the top-level requirement of minimizing the environmental footprint.

Sustainability With three aspects of sustainability covered in noise, operational emissions and cost, it is paramount to analyze other aspects as well. As such a stronger baseline for sustainability is created. First and foremost, two footprints that are deemed important are the Water Footprint (WF) and the Air Pollution Footprint (APF). The WF entails analysis of the H_2O feedstock used for fuel production. RELIGHT needs 31.3% more water for hydrogen production from H_2O and green energy than the kerosene refinery needed for the CRJ700. The APF takes into account emissions that are harmful to human health: NO_x and Particulate Matter ($PM_{2.5}$). Due to hydrogen combustion producing no carbon containing pollutants, RELIGHT's APF is about 69.% lower than the CRJ700's.

Other aspects of sustainability that are touched upon, but do not incorporate detailed analysis, concern production and end-of-life. The main aspect that will decrease sustainability are the hydrogen tanks and systems, as they are harder to recycle and complex to produce. Overall however more use can be made of recycled parts and refurbished subsystems. Also, most of the aircraft in constructed from metals which can be recycled.
To conclude sustainability, the aspects that are analyzed in detail all show promising results, except for water use, profit per year and noise. However, water usage shows only a minor increase. Profit is highly dependent on hydrogen costs and will likely increase in the future. Lastly, noise levels should reduce by as much as $10dB$ if more contemporary analyses are conducted.

Future Aircraft Development The schedule for the RELIGHT program from the end of the DSE until the delivery of the first commercial unit has been developed. The three main phases of the post-DSE development are the continuation of the design, the testing program and series production.

In the first three years of design continuation the main aircraft aerodynamic, structural, control and system interaction characteristics will be designed and analyzed until all requirements are met. The following seven years of design will see that all details of the aircraft will be optimized to the highest possible degree. Also, all structural elements, such as ribs, rivets, metal/composite sheets will be sized accurately while systems such as hydraulic actuators, electronics, landing gears and actuators will be designed in detail. Once the design of the aircraft is complete, the testing program can take place. Both on-ground and flight-based tests will be performed. The former will ensure that RELIGHT is structurally sound, both in terms of maximum loads and resistance to fatigue. The flight tests will put the prototype aircraft through the most extreme weather conditions that it might run into during its operational lifetime. Then, once the testing program is complete and RELIGHT has been granted all the proper safety certifications, series production can start. The production process will follow lean production principles, such as Just-In-Time (JIT) delivery and closeness of workshops and assembly line. Finishing the design work will take approximately 10 years, testing and certifying will take 5 more and the production process for a single aircraft will take six months. The first RELIGHT aircraft is expected to enter service in late 2036.

Conclusion and Recommendations The design choices implemented in RELIGHT allowed to meet all the critical design requirements. Compared to the Bombardier CRJ700 series, the aircraft performs infinitely better from the emissions standpoint, featuring no CO_2 emissions during operation and extremely reduced NO_x emissions. Surprisingly, the 25% constraint on cost w.r.t to the CRJ700 has been met and, in case of cost per unit, exceeded, RELIGHT's unit cost is estimated at $ 37 million versus $41 million for the CRJ700.

The upcoming detailed design phase will present many challenges and opportunities, most of them related to the implementation of hydrogen fuel in the aircraft. For instance, the effect of the wing-mounted tanks on the aerodynamics must be analyzed in more detail, as well as the design of a fuel distribution system that has to work with hydrogen. Plenty of opportunities not related to hydrogen implementation are also present, especially in the aerodynamics and structural field.

Contents

Nomenclature

Abbreviations

A/C	Aircraft	-
APF	Air Pollution Footprint	-
APU	Auxiliary Power Unit	-
AR	Aspect Ratio	-
ATC	Air Trafic Control	-
BPR	Bypass Ratio	-
C.G.	Center of gravity	-
CAGR	Compound Annual Growth Rate	-
CF	Carbon Footprint	-
CFRP	Carbon Fibre Reinforced Polymer	-
dB	Decibels	-
DOC	Direct Operating Cost	-
DSE	Design Synthesis Exercise	-
EASA	European Aviation Safety Agency	-
EF	Environmental Footprint	-
EI	Emissions Index	-
EPS	Electrical Power System	-
ESWL	Equivalent Single Wheel Load	-
FAA	Federal Aviation Agency	-
FBS	Functional Breakdown Structure	-
FF	Form Factor	-
FFD	Functional Flow Diagram	-
Fwd	Forward	-
GHG	Greenhouse Gas	-
GWP	Global Warming Potential	-
HLD	High Lift Device	-
IATA	International Air Transport Association	-
ICAO	International Civil Aviation Organization	-
IF	Interference Factor	-
JIT	Just-In-Time	-
LCN	Load Classification Number	-
LEMAC	Leading Edge of Mean Aerodynamic Chord	-
LG	Landing Gear	-
LNG	Liquefied Natural Gas	-
MAC	Mean Aerodynamic Chord	-
MAI	Manufacturing, Assembly, & Integration	-
MLW	Maximum Landing Weight	-
MPH	Mile Per Hour	-
MTBM	Mean Time Between Maintenance	-
MTOW	Maximum Take-off Weight	-
MTTM	Mean Time To Maintain	-
MTTR	Mean Time To Repair	-
NF	Nitrogen Footprint	-
NPF	Noise Pollution Footprint	-
OEI	One Engine Inoperative	-
OEM	Operational Empty Mass	-
OEW	Operational Empty Weight	-
PSI	Pound-force per Square-Inch	-
RAMS	Reliability, Maintainability, Availability and Safety	-
RAT	Ram Air Turbine	-
RELIGHT	REgionaL Innovative Green Hydrogen Transport	-
RFL	Required Field Length	-
ROC	Rate of Climb	-
SFC	Specific Fuel Consumption	-
SPL	Sound Pressure Level	-
TET	Turbine Entry Temperature	-
TRL	Technology Readiness Level	-
UHCs	Unburnt-Hydrocarbons	-
WF	Water Footprint	-

Symbols

α	Angle of attack	deg
$\alpha_\delta)_{C_L}$ / $(\alpha_\delta)_{c_l}$	Effect of the aspect ratio and flap-chord ratio on 3D flap effectiveness	–

$\bar{q}_{mc}$	Dynamic pressure at minimum control speed V_{mc}	Pa
$\bar{V}_v$	Vertical tail volume	$-$
$\bar{x}_{ac}$	Distance from nose to aerodynamic center	m
$\bar{x}_{np}$	Distance from nose to nuetral point	m
β	Compressibility correction coefficient	$-$
Δn_{la}	Additional load factor during landing due to flare initiation	$-$
δ_a	Average of maximum upward and downward aileron deflection	m
δ_f	Flap deflection	deg
δ_r	Required rudder deflection	$1/rad$
η	1/3 Octave Band central frequency parameter	$-$
η_s	Energy absorption efficiency of shock absorber	$-$
η_{tire}	Energy absorption efficiency of the tire	$-$
η_t	Total efficiency	$-$
$\frac{\delta\epsilon}{\delta\alpha}$	Downwash angle	rad
$\frac{V_h}{V}$	Tail-wing speed ratio	$-$
$\frac{W}{S}$	Weight over wing area	kg/m^2
Γ	Dihedral	deg
γ	Heat capacity ratio	$-$
γ_{ap}	Approach angle	rad
γ_{cl}	Climb angle	rad
$\hat{C_L}$	Cruise lift coefficient	$-$
λ	Instantaneous failure rate	$/hour$
λ	Taper	$-$
$\Lambda_{c/2_v}$	Semi-chord sweep angle of the vertical tail	rad
$\Lambda_{c/2}$	Semi-chord sweep angle	rad
$\Lambda_{c/4}$	Quarter chord sweep	rad
$\langle p^2 \rangle^*$	Mean square accoustic pressure	rad
μ	Dynamic viscosity	$kg/(m\ s)$
μ	Rolling friction coefficient	$-$
μ_{br}	Landing braking coefficient	$-$
$\overline{D}$	Average drag force	N
$\overline{L}$	Average lift force	N
$\overline{T}$	Average thrust force	N
$\overline{T}_{rev}$	Average reverse thrust force during landing	N
$\overline{V}_{la}$	Average landing velocity	m/s
$\overline{V}_{to}$	Average take-off velocity	m/s
ϕ	Azimuthal directivity angle	rad
ρ	Density	kg/m^3
ρ_∞	Upstream flow density	kg/m^3
ρ_{to}	Density at take-off	kg/m^3
σ	Normal Stress	N/mm^2
τ	Aileron effectiveness	$-$
τ	Shear Stress	N/mm^2
θ	Clearance angle	deg
θ	Polar directivity angle	rad
A'	Correlation constant with Jet-A1 combustors	$-$
A^*	Normalized acoustic Power	$-$
A_a	Achieved Availability	$-$
A_i	Inherent Availability	$-$
A_o	Operational Availability	$-$
$A_{v(f)}/A_v$	Ratio of vertical tail AR in presence of fuselage to isolated vertical tail	$-$
$A_{v(hf)}/A_{v(f)}$	Ratio of vertical tail AR in presence of horizontal tail and fuselage to the vertical tail in presence of fuselage	$-$
$A_{v_{eff}}$	Effective aspect ratio of the vertical tail	$-$
A_v	Aspect ratio of the vertical tail	$-$
a_x/g	Braking coefficient for dry concrete with simple or anti-skid brakes	$-$
ac_v	Distance vertical tail aerodynamic center w.r.t. aircraft nose	m
b	Wingspan	m
$b1$	Aileron inside y-position measured from the center line of the aircraft	m

$b2$	Aileron outside y-position measured from the center line of the aircraft	m
b_v	Vertical tail span	m
$c(y)$	Wing chord length along the span	m
C_f	Skin friction coefficient	$-$
C_{Lmax}	Maximum wing lift coefficient	$-$
c_∞	Upstream flow speed of sound	m/s
$C_{d_{0_{al}}}$	Airfoil zero drag coefficient at aileron location	$-$
$C_{D_{opt}}$	Optimum drag coefficient at cruise	$-$
C_D	Drag Coefficient	$-$
c_f/c	flap-chord over chord ratio	$-$
c_{jk}	Specific fuel consumption when going fully kerosene	$g/s/kN$
$C_{L,Dmin}$	Wing lift coefficient at minimum drag	$-$
$C_{L\alpha A-h}$	Tail-less aircraft lift gradient	$1/\deg$
$C_{L\alpha h}$	Tail lift gradient	$1/\deg$
$C_{l_{\alpha_{al}}}$	Airfoil sectional lift gradient at aileron location	$1/rad$
$C_{L_{\alpha_v}}$	Vertical tail lift curve slope	$1/rad$
$C_{L_{\alpha v}}$	Vertical tail lift curve slope	$1/rad$
$c_{l_{\alpha_v}}$	Vertical tail airfoil lift curve slope	$1/rad$
$c_{l_\alpha})_{M_{to}}$	Airfoil lift curve slope with compressibility correction	$1/rad$
$C_{l_{\delta_a}}$	Aileron control derivative	$1/rad$
$c_{l_{\delta_{theory}}}$	Lift effectiveness of a plain flap	$1/rad$
C_{l_δ} / $c_{l_{\delta_{theory}}}$	Correction factor for plain flap lift	$-$
$C_{L_{des,M=0}}$	Design wing lift coefficient at 0 Mach	$-$
$C_{L_{des}}$	Design wing lift coefficient	$-$
$C_{l_{des}}$	Design airfoil lift coefficient	$-$
$C_{L_{max}}$	Maximum lift coefficient	$-$
$C_{L_{opt}}$	Optimum lift coefficient at cruise	$-$
C_{l_p}	Roll damping coefficient	$-$
C_L	Lift Coefficient	$-$
$C_{m_{ac}}$	Moment coefficient around the aerodynamic center	$-$
c_{MAC}	Mean aerodynamic chord length	m
C_m	Moment coefficient	$-$
$C_{n_{\delta_r}}$	Yaw moment due to rudder deflection control derivative	$-$
$C_{N_{max}}$	Maximum normal coefficient	-
$C_{p,0_{M_{cruise}}}$	Minimum cruise pressure coefficient	$-$
$C_{p,0}$	Minimum pressure coefficient	$-$
C_r	Wing root chord	m
C_t	Wing tip chord	m
c_T	Specific fuel consumption	N/Ns
$C_{y_{\delta_r}}$	Side force due to rudder derivative	$-$
D	Drag	N
D	Noise directivity	$-$
D/q	Drag area	m^2
D_o	Outer diameter of the main wheel tire	in
d_s	Diameter of the main gear shock absorber	in
$Diam_{pod}$	Pod diameter	m
E	Energy	J
e	Oswald Efficiency Factor	$-$
e_h	Specific energy of hydrogen	$-$
e_k	Specific energy of kerosene	$-$
E_{max}	Maximum glide ratio	J
E_t	Total kinetic energy at touchdown	$ft * lbs$
F	Force	N
F	Fuel flow	kg/s
F	Noise spectrum function	m/s
f	1/3 Octave Band central frequency	Hz
f/a	Fuel-to-air ratio	$-$
f_b	Blade passing frequency	Hz
G	Noise normalized geometry function	$-$
g	Gravitational acceleration	m/s^2
GW	Gross Weight	-
H	Heating value	J/kg

h_{pylon}	Pylon height	m
h_{sc}	Screen height	m/s^2
I	Impulse	Ns
k	Correction coefficient for effective aspect ratio of the vertical tail	–
K_b	Correction factor due to flap efficiency	–
k_E	Friction factor	–
K_{g_r}	Coefficient dependent on vertical wing position, used for landing gear mass estimation	–
K_{v_v}	Multiplication factor based on the vertical tail configuration	–
K_{vh}	Factor that accounts for the relative size of the horizontal and vertical tail	–
L	Lift	N
L	Noise normalized characteristic length	–
l_t	Tail length	m
l_{pod}	Pod length	m
l_{pylon}	Pylon length	m
l_v	Distance from aerodynamic center of the vertical tail to the center of gravity	m
l_v	Distance vertical tail aerodynamic center w.r.t. C.G.	m
LHV_{hydr}	Lower heating value of hydrogen	– -
$M^\dagger$	Airfoil technology factor	–
M_∞	Upstream flow mach number	–
M_{cruise}	Cruise mach number	–
M_{cr}	Critical Mach number	–
M_{dd}	Mach drag divergence number	–
m_h	Hydrogen mass contribution	kg
m_k	Kerosene mass contribution	kg
M_{to}	Mach number at take-off	–
n	Tone numbers within 1/3 Octave Band central frequency	–
n_s	Number of main gear struts	–
N_D	Fraction of drag induced yawing moment due to the inoperative engine w.r.t. $N_{t_{crit}}$	–
N_g	Landing gear load factor	–
$n_{lim_{pos}}$	Positive Limit Load Factor	-
N_{mw}	Number of main landing gear wheels	–
$N_{t_{crit}}$	Critical engine-out yawing moment	Nm
n_{to}	Take-off load factor	–
P	Achievable roll rate by maximum aileron deflection	rad/s
P	Power	W
P_3	Fuel injector inlet pressure	Pa
P_a	Power available	W
P_{drop}	Fuel injector air flow pressure drop	$\%$
P_m	Maximum static load on main landing gear per strut	lbs
P_{ref}	Reference acoustic pressure	N/m^2
P_{req}	Oswald Efficiency Factor	W
q	Dynamic pressure	Pa
R	Flare trajectory radius	m
r	Radius	mm
$R(t)$	Reliability	–
R^2	Regression rate	kg
R_{jet}	Range of jet aircraft in the unified range equation	m
$R_{max_{alt}}$	Maximum range at constant altitude	m
R_{max_v}	Maximum range at constant velocity	m
r_s*	Normalized distance between noise source and observer	–
Re	Reynolds number	–
$ROC_{s_{max}}$	Maximum steady rate of climb	m/s
S	Wing area	m^2
S_{ref}	Wing reference surface area	m^2
S_r	Rudder area	m^2
$s_{s_{nose}}$	Maximum allowable tire deflection of the nose landing gear	in
s_s	Shock absorber stroke	in

s_{snose}	Shock absorber stroke length of the nose landing gear	m
s_t	Maximum allowable tire deflection	in
S_v	Vertical tail area	m^2
S_{wf}	Reference flap area	m^2
T	Thrust	N
t	Thickness	mm
t/c	Thickness-to-chord ratio	$-$
T_3	Fuel injector inlet temperature	K
T_{TO_e}	Total engine thrust at take-off	N
T_{to}	Maximum take-off thrust	N
V	Airspeed	m/s
V/F	Specific range	m
V_D	Dive speed	m/s
V_{lof}	Lift-off velocity	m/s
V_{mc}	Minimum control speed	m/s
V_{min}	Minimum airspeed	m/s
V_{opt}	Optimal velocity at a specific moment in time	m/s
V_S	Stall Speed	-
$V_{TAS_{cruise}}$	True airpseed at cruise conditions	m/s
W	Aircraft weight at particular flight condition	N
w_t	Touchdown rate	ft/s
W_L	Weight at landing	lbs
W_{TO}	Take-off weight	kg
W_v	Weight of the vertical tail	kg
$x_{air_{la}}$	Landing horizontal airborne distance	m
$x_{air_{to}}$	Take-off horizontal airborne distance	m
x_{ap}	Landing horizontal approach distance	m
x_{br}	Landing braking distance	m
X_{CG}	Longitudinal distance of the aircraft C.G. from the nose	m
x_{cl}	Take-off horizontal climb distance until screen height	m
x_{fl}	Landing horizontal distance covered during flare	m
$x_{gr_{la}}$	Landing ground run distance	m
$x_{gr_{to}}$	Take-off ground run distance	m
x_{la}	Total horizontal distance covered during landing from screen height until complete stop	m
$X_{LG_{nose}}$	X-location of the nose landing gear measured from the nose	m
x_{rot}	Horizontal distance covered during rotation after touchdown of main landing gear	m
x_{to}	Total horizontal distance covered during take-off until screen height	m
x_{tr}	Take-off horizontal transition distance	m
y	Span-wise position with respect to the center line of the aircraft	m
Y_{LG}	Lateral distance from the aircraft symmetry plane to the contact point of the main landing gear with the ground	-
y_t	Moment arm of the engine thrust from the point of application to C.G.	m
z_h	Height of the horizontal stabilizer measured from the bottom of the vertical tail	m
k'	Correction factor for nonlinear lift behavior of plain flaps	$-$

1 Introduction

Modern aviation has occupied a large fraction of technology innovation, as it is a relatively new field compared to most that are being advanced. In the 21st century this has occurred due to room for novelty and safety demand as tragic accidents - although having low frequency - were considered too usual. Regarding speed, the market had been constantly on the rise before encountering the tragic incident of the Concorde crash in July 25, 2000, killing 100 passengers and all crew members. This event happened to the most successful and famous supersonic airliner, being used by British Airways and Air France, and so it marked the downfall of commercial supersonic aviation in several years, until recently, with multiple aircraft manufacturers unveiling new concepts in the late 2010s. Similar speed of advancement has been seen with the transition from as many mechanical components as possible towards electrical and hydraulics combinations, aspects which are discussed later in this report as well.

In general innovation terms, the industry has not remained at a standstill since its creation. Over the last decade though, regardless of industry, the whole global population has shifted the view towards the environment. From personal to public use and action, a vast amount of creations or ideas are judged principally on climate effects. Hence, over the same range of time, the idea of being innovative in many ways, has become synonymous to being environmentally friendly. For this reason, the group showed excitement when allocated to a design with large emphasis on sustainability since it was given maximum potential for novelty. Furthermore, the design concerns the regional aviation market. The industry has lately also put significant weight and investment on the regional market as it has been proven desirable by the traveling population. Consumer feedback has displayed an exponential demand on short regional flights countering train travel or even driving, a fact that is undoubtedly linked to the aforementioned demand for safety that is being consistently complied with. As a result, a design of a Sustainable Regional Aircraft design is a project that directly targets both the fast growing aviation market but also entails the modern primary characteristic of innovation, with environmental sustainability as its guiding objective.

This report shows the end result of a 10-week project completed by DSE group 20, targeting the above concept. Throughout this extensive journey, the idea has become a conceptual design process, and finally the preliminary design of the RELIGHT aircraft. Specifically, having initially spent a week in focus on a project plan, the team members were assigned roles, both organizational and technical, and all appropriate Project Management and Systems Engineering procedures were performed. Further down the timeline, the team went through the baseline phase, during which all significant background information was gathered, including a thorough literature study for innovative concepts of the various aircraft departments. Furthermore, basing the aircraft design on those novelty sub-concepts, strawman concepts were created for the entire aircraft which were then discussed in detail, and were narrowed down to three that were presented to the supervising coaches and tutor [3]. During the midterm phase that followed, the group performed a trade-off between the resulting concepts, including an analysis of the trade-criteria, and trading off all aspects separately, which resulted in a single final concept that was displayed together with its primary characteristics [4]. Having completed all of the above, group 20 reached the final phase, that also marks the preliminary design phase, which this report concerns. The general objective for this project is initially showed in Section 2.1, as well as the mission characteristics showed in Section 3, to give the reader a clear image of the end-goal to be achieved. Consecutively, the thorough sustainable development strategy that has carefully been created along the entire project is explained in Section 4, together with Section 5.1, where the aspects of the preliminary concept that set a base for the detail to be added. Moreover, and most importantly, the entire view of the subsystems in development is explored with clear processes of calculation and sizing in Section 6. This generates a final design, that obtains some design characteristics like resource allocation, safety, and more, that are portrayed right after, in Section 7, along with the analysis of the vehicle's performance inSection 8. Lastly, since the group has come to the end of the preliminary design, the process must still have a clear path to follow, which is presented in Section 9, and in Section 10, the conclusions and recommendations for the steps to be followed.

2 Project Objectives

The purpose of this section is to outline the project objectives, that have been derived from top-level user requirements. Section 2.1 describes such objectives. Furthermore, the name of the aircraft is introduced in Section 2.2. Finally, a closer look is taken at the market in Section 2.3.

2.1 General Objectives

The aviation industry is becoming more and more environmental friendly, mostly lead by policies set by organizations like the International Civil Aviation Organization (ICAO) and the International Air Transport Association (IATA). Since the environmental impact of air transport is hardly decreasing due to rapidly growing aviation sector, this project is centered around a single challenging goal: to create a design with the lowest possible environmental footprint. More specifically, the design shall be a regional aircraft that accommodates 50-75 passengers of which the maximum range shall be between 1500-2500km.

Reducing the design's environmental footprint is mainly achieved by lowering the climate affects of the product. For aircraft, this is generally split up in three life-cycle phases: the production phase, operational phase and end-of-life phase. Therefore, the project focuses on developing new strategies and design solutions for all these phases, in order to become as sustainable as possible. Aviation contributes to climate change primarily due to the emission of soot particles and greenhouse gasses, like carbon dioxide (CO_2), nitrogen oxides (NO_x), sulfur oxides (SO_x) and water vapor (H_2O) [5]. Since these emissions play a key role throughout the entire life cycle of the aircraft, the lowest possible environmental footprint could therefore be achieved by minimizing the emissions polluted at each life-cycle phase. Furthermore, the social and economical aspects of being sustainable would also potentially lower the environmental footprint of the aircraft. For this exact, lowering the emissions is not the only objective of this project. As the social aspect of the environmental footprint involves the overall impact of the design on human well-being, aircraft noise pollution and emission of harmful particles also affect the environmental footprint of the design.

In short, reducing the environmental footprint involves many different areas. As minimizing the footprint for all of these areas would come at high cost and is very time consuming, a good balance must be found between improving sustainability and cost to ensure competitiveness with the current market.

2.2 Name of the Aircraft

From this section onward, the to-be-designed regional aircraft, that has previously been referred to as "the aircraft", is named "RELIGHT". RELIGHT is short for REgionaL Innovative Green Hydrogen Transport. As the name suggests, hydrogen will be the main source of propulsion, which is considered innovative w.r.t. the current market. The acronym RELIGHT is chosen as it contains the word "LIGHT", which refers to the lightweight application of hydrogen combustion due to its high mass-specific energy density.

2.3 Market Demands

The RELIGHT project aims to bring innovation to the regional aircraft sector. The aircraft makes short frequent trips and are generally less sustainable than large transport jets due to the interplay of fixed costs and a more limited payload carrying capacity. Therefore a reduction in emissions would greatly improve the level of sustainability in this market niche. In order to remain competitive, the purchasing price needs to be comparable to other regional aircraft, as well as the operating cost. The market that was targeted is the one of regional jets with a price tag of 40-60 million. With the aim of being below 50 million USD, to remain attractive to budget airlines.
Growth in aviation is closely tied to economic growth. Regions in Africa, South America and South East Asia will be targeted. In order to gain a foothold in these regions the design considers what important destinations would require a direct connection and aimed to include as many links as possible. A range of approximately 2000km already makes international flights possible, which would make the RELIGHT aircraft of great value to the regional aircraft market. It will be able to service trips such as Rio de Janeiro to Asuncion, Bogota-Belize, Nairobi- Djibouti, Maputo- Cape Town as well as Bangkok- Singapore and Manila- Hong Kong. Therefore clients we aim to interest in with this product, are major regional airlines that cover international flights. Together with airport managements and local governments we aim to set up a collaboration that undertakes the effort to reduce emissions, and possible fuel and trip prices to connect more people and allow

more people to fly in the near future. The aim is to develop a concept hydrogen aircraft to show the feasibility of the fuel source, in order to inspire governments and airport managers to implement changes that will move towards a more sustainable aviation paradigm. Over the course of the long development period, this concept will be further refined to improve efficiency and aesthetics to eventually be able to an attractive, economical and sustainable aircraft to airlines in regions where these developments have been applied.

The development of this aircraft concept is estimated to take between 10-15 years, and as it is heavily dependent on the development of the hydrogen economy and the availability of liquid hydrogen at regional airports, especially in developing economies, the aim is to have the product ready to deliver the first aircraft by 2040.

2.3.1 Strengths & Weaknesses, Opportunities & Threats

The strength of this design, lie primarily in its simplicity, it does not introduce too much innovation at once. Instead it uses a conventional layout that ensures compatibility with already existing norms and methods, focusing instead on the key area. The use of a turbofan engine also allows for high cruise speeds, and the high wing configuration eases the constraint on the bypass ratio for increased fuel savings. On top of the strong savings in emissions hydrogen has another major advantage over kerosene: it is a practically unlimited resource on earth, as long as there is enough water and power available.

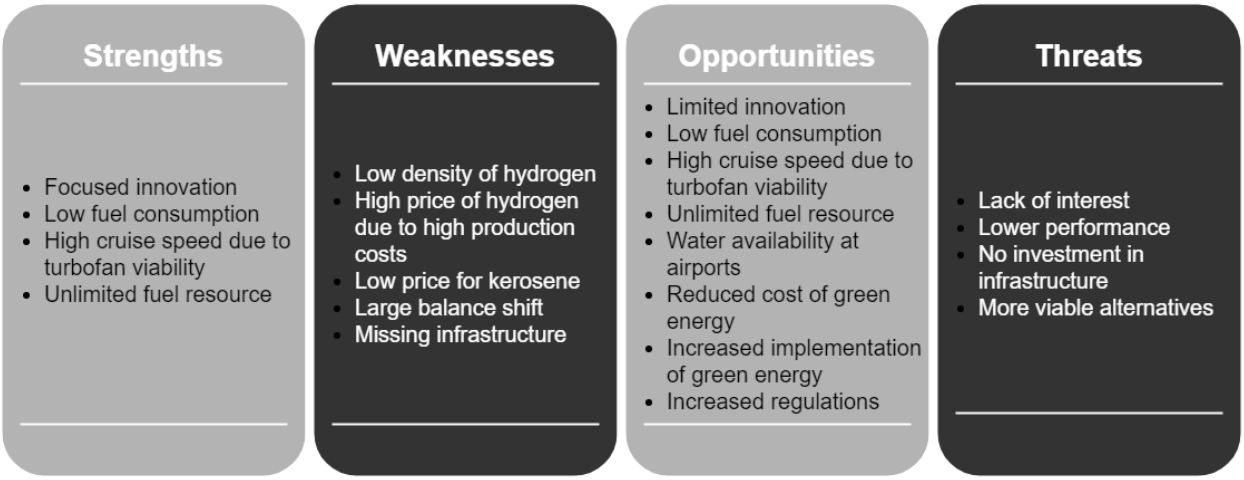

Figure 7: SWOT Analysis

Currently however the price of kerosene is low and on top of that the price of hydrogen quite high. This makes hydrogen usage less attractive in the current market. Whilst the low fuel consumption can compensate for that already, it is really an opportunity for airports that generating hydrogen with their already existing water architecture, to further reduce fuel costs significantly. This opportunity is further promoted by the reduced cost for renewable energies and increased governmental pressure to adopt more sustainable operations.
The success of this project strongly depends on the implementation of a hydrogen infrastructure. Should a lack of interest result in a failure to do so, or should alternatives proof to have a better performance, only then might project not deliver on the value it promises.

3 Mission Characteristics

This section briefly describes RELIGHT's typical mission characteristics. First, the flight profile diagram is shown in Section 3.1, after which the payload-range diagram is discussed in Section 3.2. In addition, typical ground operations and mission logistics are touched upon in Section 3.3. To complete the mission characteristics, a functional analysis is performed in Section 3.4.

3.1 Flight Profile

The flight profile diagram depicted in Figure 8 shows that the mission can be split into 11 different phases. After engine start-up and taxiing to the runway, the aircraft takes off and starts climbing to a cruise altitude of 10km. The aircraft will cruise for approximately 2000km at a cruise speed of 807.6km/h. At the end of the cruise phase, the descent is initiated towards the altitude of the runway on which the aircraft will land. In normal conditions, the aircraft will touch-down, taxi to the gate and shut down the engines. However, in case a diversion is needed, the aircraft will climb again to perform a second cruise. The aircraft will be able to cruise for another 200km at a speed of approximately 646km/h. Then the loitering phase starts, in case the aircraft is put on a holding pattern. As with the second cruise range, the loiter duration is set by CS25 regulations. Hence, the aircraft will have enough reserve fuel to loiter for 45 minutes at a speed of approximately 485 km/h. The mission will then be completed by a second descent and landing.

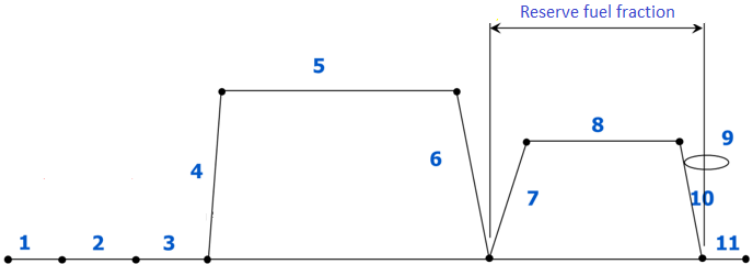

1. Engine start-up
2. Taxi
3. Take-off
4. Climb
5. Cruise
6. Descent
7. 2nd Climb
8. 2nd Cruise
9. Loiter
10. 2nd Descent
11. Landing

Figure 8: Mission flight profile diagram [6]

3.2 Payload-Range Diagram

The payload-range diagram is depicted in Figure 9. It visualizes the achievable range as a function of payload weight taken on board. For conventional aircraft, this diagram consists of three lines: one where the design range is achieved with maximum payload weight, one where payload is exchanged for fuel to increase achievable range and one for the ferry range. However, for RELIGHT, exchanging payload for fuel is not possible as the fuel tanks are designed to the design range of 2000km with maximum payload, including reserve fuel for diversion and loitering. Liquid hydrogen has a low volumetric energy density as compared to kerosene (8600 vs 35000MJ/m^3). Therefore, exchanging passenger for fuel would require an enormous increase in tank volume, which would have negative effects on the overall performance. Exchanging the weight of five passengers would already imply a tank volume increase of 25%. In Section 6.1.8, this is discussed in more detail and possible solutions for this are explored. To conclude, the achievable range will only exceed 2000km if less than the maximum payload weight is taken on board, provided that no extra ballast is needed to ensure a stable and controllable aircraft. In case no payload is carried, a ferry range of 4348km is obtained.

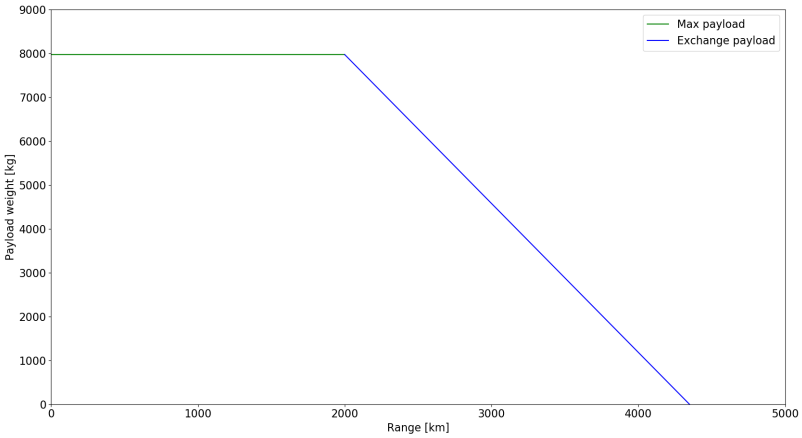

Figure 9: Payload range diagram for a design range of 2000 km

3.3 Operations and Logistics

The schematic presented in Figure 10 shows the ground operations procedure of a typical flight. Starting from the preparation for the next flight, and ending with the necessary post-flight checks. A vast difference from ordinary ground operations seen today is the extra precaution and effort required for the hydrogen propulsion system. The propulsion system requires special care and more frequent inspection. The fuel tank and the fuel pipes will see large temperature differences throughout the flight, As the volume of hydrogen is not constant throughout the flight; it will expand and, as a result, increase in temperature. These large temperature difference will strain the material more than usual, hence frequent and careful inspection is required. Furthermore, during the process of loading the aircraft, the cryogenic hydrogen needs to be safely transported to the aircraft; moreover, refueling has to be performed safely, whilst also minimizing overall temperature increase of the fuel. Lastly, the aircraft will require additional post-flight safety checks before the passengers can disembark.

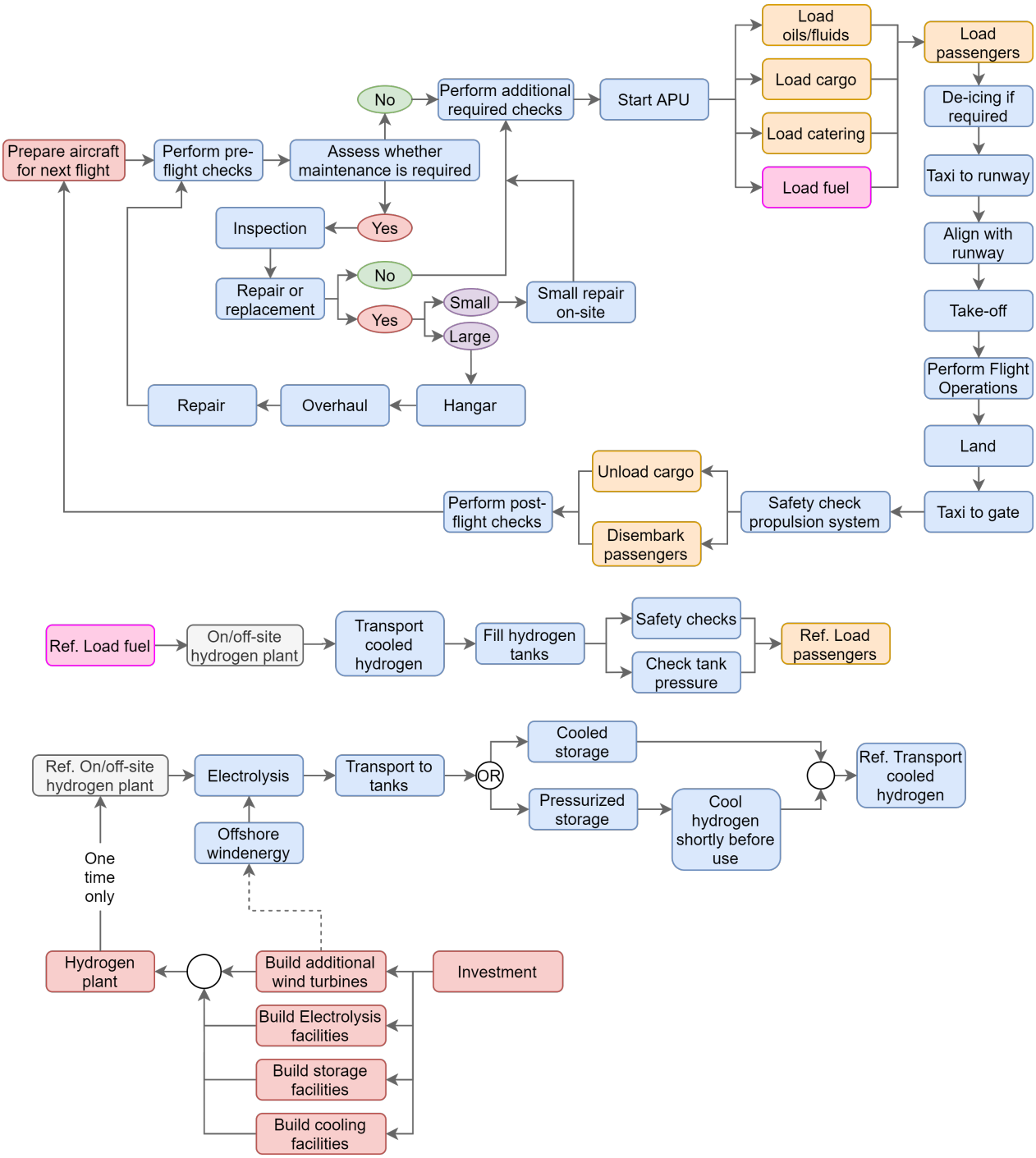

Figure 10: Operations and Logistics Flow Diagram

Generally speaking hydrogen does not produce any CO_2 emissions and has reduced NO_x emissions. That is one of the reasons it was chosen as the fuel source for the aircraft. However, the hydrogen production method can pollute harmful emissions, although this strongly depends on the method used. Advantages of using hydrogen include that the only two resources required are water and energy. Whilst hydrogen can be sourced from splitting methane, this will produce carbon dioxide and is therefore not the preferred method of generation. Hydrogen can also be produced by directly splitting water. Airports already have infrastructure to supply freshwater and electricity, and the project's vision entails the usage of green energy sources to do this splitting directly at airport facilities. This could either be facilitated by general green energy production in a countries economy, or by using wind, solar or geothermal energy if possible at airports, to power the hydrogen generation. In that scenario the production of fuel would be straight forward and no transport costs need to be added. In summary, the required infrastructure consists of green energy production systems, temporal isolated storage units for the cryogenic liquid hydrogen and transport vehicles with safe, insulated tanks. RELIGHT will therefore be limited to land on airports that have the infrastructure required to produce green hydrogen, unless an emergency landing is required. After initial investment costs have been covered, an installation like this will make hydrogen production more environmentally friendly and make the aircraft no longer contribute to the greenhouse effects both directly (during operation) and indirectly (hydrogen production).

The current state of hydrogen production at airports is less developed than required for operation of the RELIGHT aircraft. Though, many initiatives are being investigated and started up around the world, including at airports. Investments are required in a few areas: green energy production, hydrogen electrolysis plants, hydrogen transportation infrastructure, hydrogen storage, hydrogen fuel loading infrastructure. The green energy production is already a hot-topic around the globe, while progressively initiatives are taken up to provide the world with green hydrogen, such as the plans to build a massive 10 gigawatt hydrogen plant in Groningen, by 2040 [2]. The other aspects of flying with hydrogen that need to be developed, are for example the storage of hydrogen, the transportation of hydrogen, and the fueling procedures. Hydrogen is more prone to leaks during transportation and storage than kerosene and is often stored at high pressures, which will imply safety concerns which need to be addressed before entry into service.

3.4 Functional Analysis

Next to the identification of the ground operations, all other functions that the aircraft needs to perform must be acknowledged to facilitate the generation of (sub)system requirements.

3.4.1 Functional Flow Diagram

The Functional Flow Diagram (FFD), of which the initial version was presented in the baseline report [3], has been further adjusted to more accurately describe the chronological order of all system functions. The FFD is provided below, at the end of Section 3. The blue boxes represent the top level functions, after which the one-level-down functions are presented in yellow, followed by the purple functions. Furthermore, the red box '*Assure operative flight*' outlines a separate group of functions. A numbering system is in place to stress the sequential nature. In the diagram the reader can also distinguish '*and*' and '*or*' functions. These stress that some functions are performed together or, that, according to the circumstances, a select number of the functions is to be performed.

Compared to the baseline FFD, a few things have been changed. First of all, new (sub)system function have been identified of which most are related to the use of liquid hydrogen. This for example includes the refueling of liquid hydrogen, which is slightly more complex compared to conventional aircraft. The fuel system is worked out in more detail in Section 6.3. Also monitoring the tank conditions has been added, as these are more likely to change in the external wing tanks due to the passage of airflow, which increases boil-off. Compared to the baseline report, some sub-systems have been worked out in more detail. Although this is not directly implemented in the FFD, schematics of the electrical, hydraulic, data handling, environmental control and APU sub-system can be found in Section 7.

3.4.2 Functional Breakdown Structure

All functions the aircraft is required to perform are presented in the Functional Breakdown Structure (FBS), which is shown at the end of Section 3. The framework for the FBS has been obtained from the baseline

[2] https://nos.nl/artikel/2324772-plannen-voor-het-grootste-europese-waterstofproject-in-groningen.html

report [3]. The basis for the FBS is the FFD, with omission of the chronological aspect, whilst going into more depth on the system functions. The FBS provides the top level functions with subsequent lower level functions, where the lower level functions add additional detail. The top level functions are split into five groups; pre-flight, take-off, cruise, descent and landing, with their respective lower level functions. In order to more clearly visualize the hierarchical nature of the diagram, colors are applied for each specific function level; additionally, a numbering system is in place to indicate at which level the function is.
A careful breakdown of all functions the system is required to perform, was subsequently used to determine system and subsystem requirements. The rigorous approach to the creating of the FFD and FBS ensured no system function was overlooked, and, consequently a very clear and thorough list of requirements was generated.

A Functional Flow Diagram

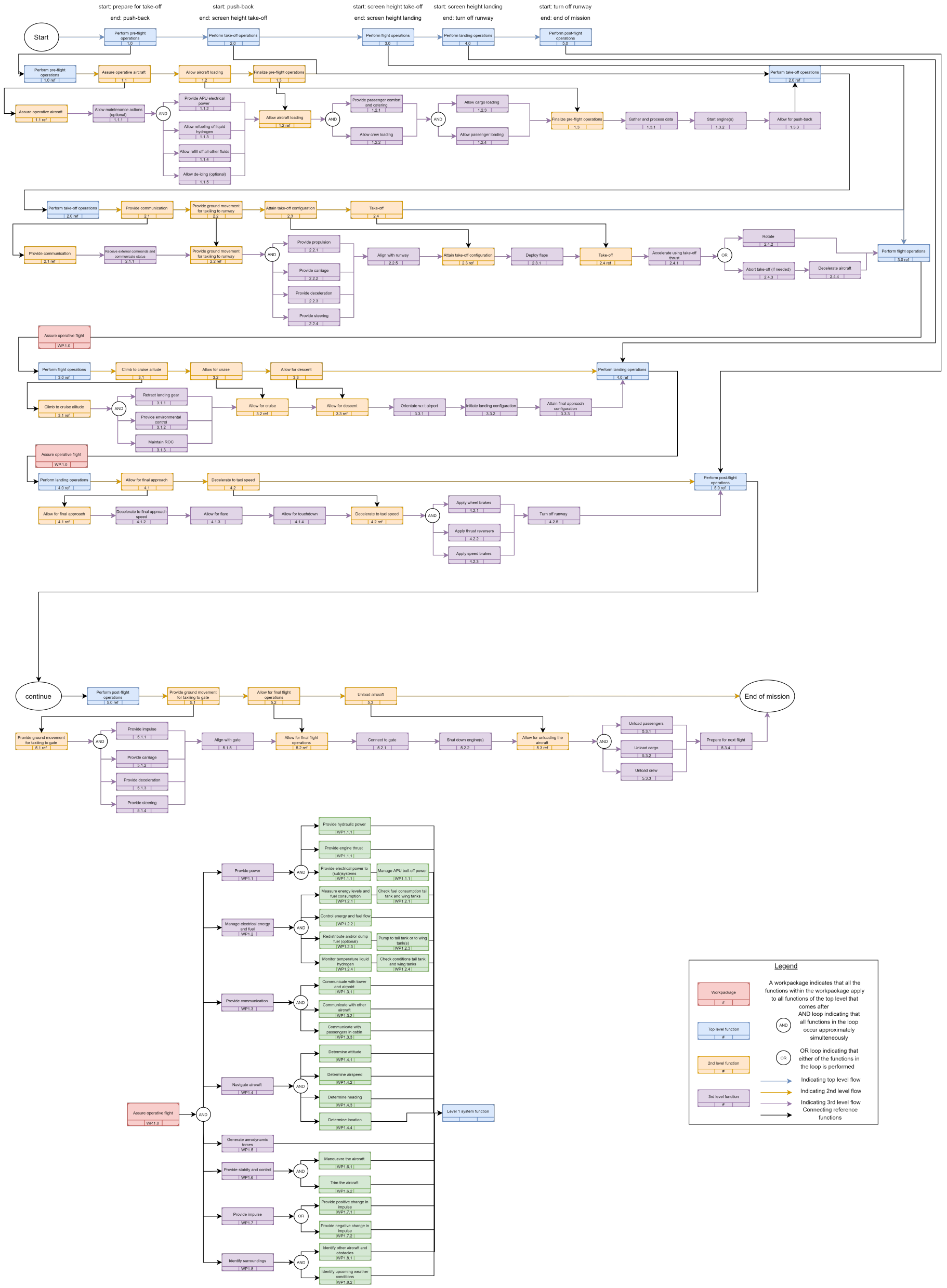

B Functional Breakdown Diagram

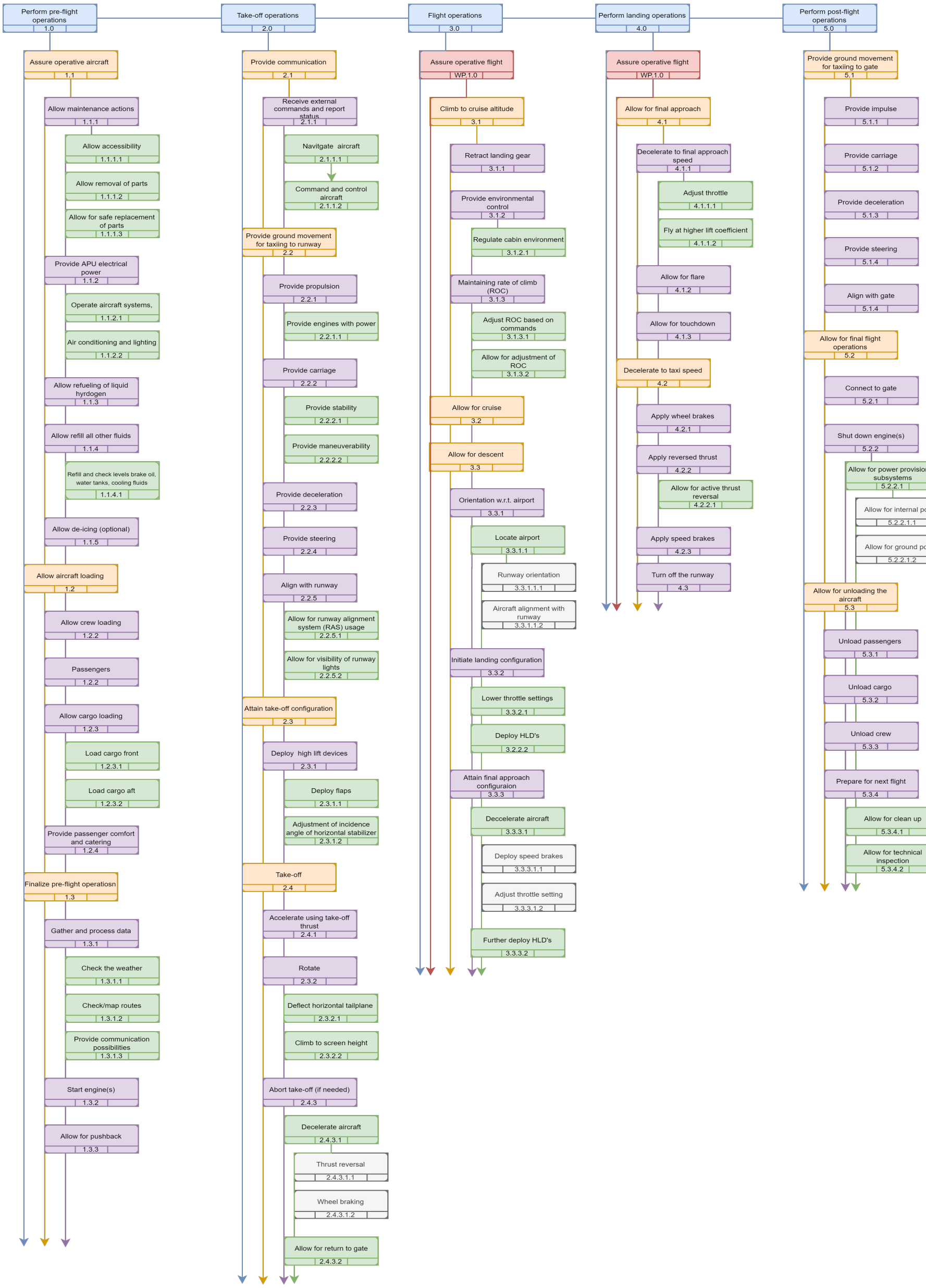

4 Sustainable Development Strategy

This chapter addresses how sustainability is incorporated in RELIGHT's design. First, Section 4.1 dicsusses developments in the aviation industry with respect to sustainability and innovation. After that, an approach towards sustainability is developed in Section 4.2. Finally, Section 4.3 presents the methodology for quantification of sustainability.

4.1 Current Developments

Currently, aviation is one of the most vital facilitators of international transportation and the number of passengers per year keeps growing. Over the course of 2000 to 2018, passenger numbers almost tripled (see Figure 11 [7]), and the IATA predicted passengers numbers to double in 2037, meaning a 3.5 Compound Annual Growth Rate (CAGR) [8][3]. As such, it is evident that air transport facilities will support this growth and keep increasing in size on all scales. However, keeping in mind that the aviation sector takes up about 2% of global emissions [9][4], it is of paramount importance to the environment that these emissions undergo serious measures. If not, then emission could grow by as much as 300% by 2050, as expected by the International Civil Aviation Organization (ICAO) [10][5]. Figure 12 shows, as expected by the IATA, the expected carbon emission growth until 2050 (if no action is taken) together with the goal to reduce carbon emissions by 50% [11].

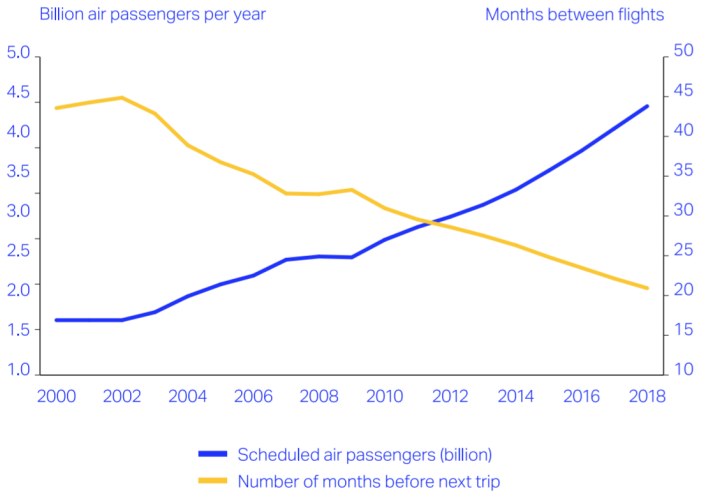

Figure 11: Accessibility of air travel up to 2018

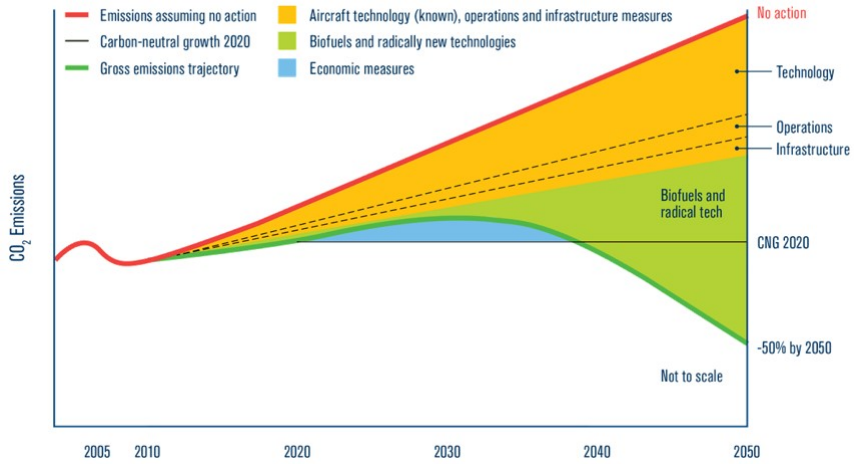

Figure 12: Schematic CO_2 emissions reduction roadmap

[3] https://www.iata.org/en/pressroom/pr/2018-10-24-02/
[4] https://ec.europa.eu/clima/policies/transport/aviation_en#tab-0-0
[5] https://www.icao.int/environmental-protection/Pages/ClimateChange_Trends.aspx

Aside from IATA, the European Comission has dictated the European aviation sector with even more challenging goals by 2050: 75% reduction of CO_2 emissions per passenger kilometer, 90% reduction NO_x per passenger kilometer and 65% noise reduction, with respect to aircraft in 2000. Also, taxiing is to be emission-free, aircraft are to be recyclable and sustainable alternative fuels are to be implemented. Furthermore, air travel should provide accessibility to meet societal and market needs and facilitate 90% of travelers within Europe to arrive at their destination within 4 hours [12]. Hence, the aviation sector is to be improved and innovated on all scales, including regional air travel. As such, small airports and surrounding areas, which are not of utmost importance to mainstream airliners, are addressed as well regarding environmental goals.

4.2 Sustainability Approach

The aim for RELIGHT that arises from the aforementioned reasons, is to be sustainable in the regional aviation sector. Sustainability is in general defined as: 'Meeting the needs of the present without compromising the ability of the future to meet their own needs [13][6]'. As a consequence, in regional aviation, every decision should be carefully taken whilst predicting the corresponding benefits and compromises in the future. Three categories are defined for which these (dis)advantages are addressed: the environment, the economy and society. As such, RELIGHT is seeking to be sustainable in these three fields.

4.2.1 Environmental Sustainability

The first and foremost pillar of sustainability regards the environment. A formal definition is: 'meeting the resource and services needs of current and future generations without compromising the health of the ecosystems that provide them.'[14] Generally, it entails the abatement of the damaging impacts to the planet. Damage is indicating for the future as an adverse effect in meeting their own needs, and mostly comes down to global warming, depletion of resources, pollution and waste creation. One way to indicate these effects is by means of the environmental footprint (EF). The goal for reduction of RELIGHT's EF is only 25% as opposed to the 2050 goals of the European Commission [12]. Hence, RELIGHT is set to come into service much earlier, while being an important step in the right direction.
Before coming into service, RELIGHT is produced and as such the stakeholders and manufactures require sustainability for that as well. Consequently, manufacturing emissions and thereby the production footprint shall both be lowered by at least 25%. More specifically, the manufacturing process is aimed to follow the lean manufacturing method. Also, the total production time for a single unit, which is called the throughput-time, has a limit of six months. The plan for manufacturing is touched upon in Section 9.3.

When RELIGHT's manufacturing is completed, the operational life phase can begin. Most certainly, this is the predominant emission producing phase. Hence, the requirement is to reduce emissions that harm to the environment by at least 25%. Evidently, where possible emissions should be reduced more than that. Another operational requirement is that RELIGHT shall be able to make use of existing facilities at airports. This concerns fueling systems and the fuel (production) itself. If no infrastructure for a sustainable fuel is currently present, it should be developed to ensure future operations at the airport. At least, enough evidence should be obtained that one will exists in the future.

The last phase of RELIGHT's program is called End-of-Life, i.e. the aircraft is taken out of operation. If the aircraft would simply be stored at some deserted location till eternity, environmental sustainability is lost. Therefore, first of all, serviceable subsystems are to be reused in airframes that are either being produced or already in operation. Secondly, the materials used in the airframe should be applicable for recycling as much as possible.

[6] https://www.investopedia.com/terms/s/sustainability.asp

4.2.2 Economical sustainability

Aside from the environment, which is often regarded the most predominant factor in sustainability, the impact on the economy is a crucial factor as well. Being economically sustainable entails that the entire RELIGHT program is profitable and can hence support long-term economic growth [15]. This includes the production program, operation and End-of-Life. Still, the overall costs for the aircraft program are allowed to increase by 25% with respect to reference aircraft. The only cost aspect that shall be similar are the passenger taxes. The other increases in flight crew and cabin costs, operating costs, maintenance costs and purchase costs are allowed to provide a wider design space. As such, there is more room for innovations that would otherwise be unavailable. RELIGHT therefore aims to be as innovative towards sustainability as possible while pushing the costs to this limit. Still, if after careful trade-off a concept arises that is both more sustainable and less costly, it should be selected. Lastly, to avoid unnecessary research costs, components should be selected with a Technology Readiness Level (TRL) higher than 4. Cost performance aspects are discussed in Section 8.4.

4.2.3 Social Sustainability

The third and last pillar of sustainability deals with society. A definition for it is: 'Social sustainability is the enduring, harmonious quality of life of people affected and affecting a project, program, product, or process'[16][7]. Hence, RELIGHT should take into account all people involved. These are first and foremost the stakeholders during development, testing, certification and production. They include employers and employees of the aircraft program and organizations like the European Aviation Safety Agency (EASA) and the Federal Aviation Agency (FAA). An employment structure should be set up that complies with employment law, i.e. the European Labour law [17][8].

During operation another group of stakeholders can be defined; these include the airliners that operate the aircraft, airports and authorities. As such, operational reliability is key for airliners and maintenance operations should be at least similar to current aircraft, which is touched upon in Section 7.4. Also, regarding pilots, aircraft handling, pilot training and automatization systems shall be similar to existing aircraft. Furthermore, compliance with airport and Air-Traffic Control (ATC) requirements is also necessary, which amounts to good communication with ground stations and other aircraft. Also, data relay to ground stations is necessary. Lastly, to be of quality to authorities, regulations have to met; compliance with CS-25 and EASA regulations.

Stakeholders that are affected during operation, but do not have much influence are first of all passengers. Passenger safety is vital, and as such the aircraft shall comply with all safety regulations that are imposed by authorities.Apart from safety, passenger comfort is of utmost importance and should be treated carefully. This includes aspects such as a comfortable cabin environment, comfortable seating, on-board catering and cabin luggage storage similar to current regional airliners. Another portion of this group of stakeholders is taken up by people that live near airports. Aircraft noise should be minimized, since the goal for 2050 is to reduce noise by 65%. Therefore RELIGHT strives to reduce noise by at least 25%. Estimations for noise can be found in Section 8.2.

4.3 Quantification of Sustainability

Sustainability will, as it is composed of three pillars, be measured in terms of the Environmental Footprint, the Economical Footprint and the Social Footprint. The final results of the analysis are presented in Section 8.5.4.

4.3.1 Environmental

To obtain a way of measuring environmental sustainability, the main life phase that is analyzed is operation, as this will take up the largest part. Yet, other aspects such as recyclability, that may be less quantifiable, are discussed in Section 8.5. For the environmental footprint a number of sub-footprints have been investigated. After doing so, two were selected that were regarded most applicable [4]. These are the Carbon Footprint (CF), which describes the carbon equivalent emissions, and the Water Footprint (WF) which incorporates the use of fresh water.

Carbon Footprint The estimation of the CF is included in Section 8.3. For this, emissions of Greenhouse Gases (GHGs) will be analyzed for operation of RELIGHT, expressed as Global Warming Potential (GWP), with a 100 year time horizon [18][19]. The following GHGs were selected: CO_2, H_2O and NO_x. Other GHGs, such as CH_4, N_2O, Unburned-Hydrocarbons (UHCs), Black Carbon (soot) and CO are certainly

[7] https://pages.uncc.edu/inss/blog/2013/08/15/social-sustainability-from-an-engineers-perspective/
[8] https://ec.europa.eu/social/main.jsp?catId=157&langId=en

damaging to the climate, however on a significantly lower scale which makes them not useful here for comparison with reference aircraft. The mass of each GHG emitted per kg of fuel, the Emission Index (EI), is used to obtain kg CO_2-equivalent per passenger kilometer [20]. For instance, $1kg$ of NO_x is equivalent to the impact $28kg$ CO_2.

Water Footprint Fresh water is a quintessential resource on Earth for many processes. For green production of H_2, electrolysis is used, which needs H_2O [21]. Also the production of conventional jet fuel uses H_2O [22]. This H_2O is later emitted as water vapour for both fuels, however water vapour is not directly available as fresh water again. For the production of aircraft, water is needed as well, however the difference between current aircraft and the new concept is not expected to be noteworthy. The WF of current aircraft and the chosen concept will be analyzed and expressed in m^3 water per passenger kilometer. The estimation is discussed in Section 8.5.2.

4.3.2 Economical

To quantify the economical sustainability of RELIGHT, a few estimations on cost are made (see Section 8.4). These estimations include development cost, operating costs regarding fuel, the purchase cost of a single aircraft (unit cost) and a return on investment. The latter requires also an estimation on profit, which is necessary in terms of sustainability. When related to passenger kilometers, all these different cost aspects can be compared to data that is available for reference aircraft. As such an estimation of economical sustainability is done.

4.3.3 Social

For quantification of the social footprint, aspects of RELIGHT are investigated that have impact on people who do not have much influence on the aircraft program. These are for one the people that live near airports and they are affected not only by aircraft noise, but also by pollutants. These pollutants can for instance create smog or have impact on health. As such, two footprint are selected, the Air Pollution Footprint and the Noise Pollution Footprint.

Air Pollution Footprint The Air Pollution Footprint (APF) has to do with effects on human health. It is another aspect of the social pillar of sustainability. Emissions that are harmful to humans are for instance Ozone (O_3) and Particulate matter ($PM_{2.5}$) [23]. $PM_{2.5}$ includes for instance soot. O_3 is also a GHG, but it is not included in the CF as at high altitude O_3 is important for protecting Earth from UV-light [24][9]. Ozone is also not directly emitted from kerosene combustion, but its production is enhanced by emission of NO_x. The APF is be expressed in kg of particles with potential to be harmful to humans, per passenger kilometer, and an estimation is found in Section 8.5.2.

Noise Pollution Footprint Aircraft noise has a adverse impact on society and therefore needs to be reduced as much as possible to be sustainable (social pillar). Therefore, for quantification of the Noise Pollution Footprint (NPF), engine noise and airframe noise are assessed in Section 8.2, and are measured in Sound Pressure Level (SPL), with units dB.

[9] https://www.eia.gov/tools/faqs/faq.php?id=84&t=11

5 Preliminary Concept Description

The purpose of this chapter is to introduce and elaborate on the concepts that the team came up with during the midterm phase of the project. First, a brief summary of the trade-off is given in Section 5.1, after which the most promising concept is worked out in more detail in the remainder of the section. This is done by means of a class I weight estimation and a trade-off to determine the ideal hydrogen and kerosene fuel fractions. Finally, the class II weight estimation framework and the flight envelope are discussed in Section 5.3 and Section 5.5, respectively.

5.1 Preliminary Concept Trade-off Summary

5.1.1 Initial Concepts

At the start of the project, a design option tree was constructed from which the most feasible and promising design solutions were selected. With the project objectives in mind, the team narrowed down the solution space to three concepts, each having a different sustainability driver to significantly lower the environmental footprint. The selected concepts are depicted in Figure 13, in which also the main characteristics can be found.

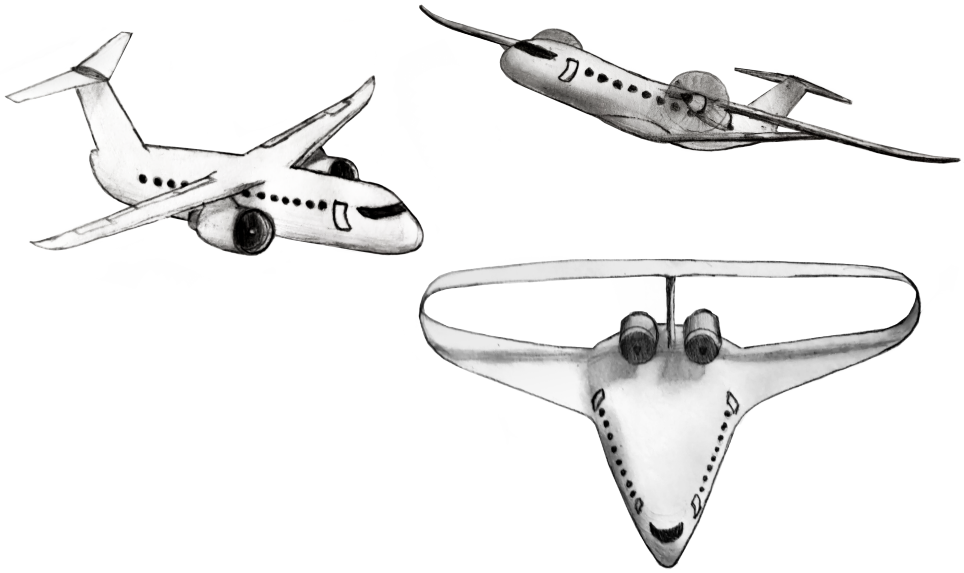

Figure 13: Concept Hybrid Hydrogen (left); hybrid high bypass turbofan engines (kerosene and liquid hydrogen), high wing, T-tail, Concept Strutted Wing (top); high AR strutted high wing, propfan, T-tail and Concept Blended Wing Body (bottom); blended (boxed) wing, high bypass turban, boundary layer ingestion, vertical tail only

.

5.1.2 Trade-off Method

The trade-off enables comparison of the concepts based on six main trade criteria: cost, safety, noise, emissions, ground operations and passenger comfort. The corresponding weights are based on the relative importance to the scope of the design and are mostly derived from top-level requirements and stakeholder requirements. Each main criterion comprises sub-criteria, which are used to assess the concepts at lower levels. The sub-criteria were also given weights based on their importance to the project objectives. For each of the main criteria, the concepts were given scores based on their relative performance to the others. This being either 1, 4, 6 or 9, to make sure the concepts don't end up having similar total scores. In the end, six weighted scores are obtained which indicate how well a certain concepts performs for a sub-criterion. The results are summarized in Table 10. Finally, these weighted scores are weighted once again using the main trade-criteria weights. This resulted in three total scores, one for each concept, the concept with the highest total score is selected.

Table 10: Concept trade-off summary

Criteria	Cost	Safety	Noise	Emissions	Ground operations	Passenger comfort	**Total**
Weights	0.25	0.1	0.1	0.35	0.15	0.05	**1**
Blended Wing Body	4.05	5.9	9	1.3	4.6	5.0	**3.9**
Strutted Wing	6.1	5.0	1	4.2	4.5	5.1	**4.5**
Hybrid Hydrogen	1.9	3.1	4.0	8.2	4.0	5.6	**4.9**

As becomes clear, concept Hybrid Hydrogen came out as winner. The main driver was the remarkable performance in terms of emissions. Although the emissions during the production and end-of-life were similar for all concepts, a significant difference in favor of concept Hybrid Hydrogen was found in the operational emissions due to the lower emissions factors of hydrogen compared to kerosene. Only the emissions factor of water vapor is significantly higher which has a much lower impact on the environmental footprint. [5].

The total score of concept Hybrid Hydrogen was limited due to lower cost and safety performance scores. The latter does not correspond to an unsafe design, but it is indicative of the implications on structural crashworthiness, flammability, emergency evacuation, engine malfunctions and the ability to identify structural faults. Primarily, the use of liquid hydrogen induces additional risk of fuel flammability and a slight decrease in engine reliability due to the application of type of fuel which is relatively new to the aviation industry. The low cost performance is also caused by the innovative characteristics of concept Hybrid Hydrogen. The handling of hydrogen, as well as the availability at airports is more difficult when compared to the kerosene infrastructure. Furthermore, hydrogen is about 2% more expensive in operation than the use of normal jet fuel [25]. Therefore, an increase in operational cost can be expected. Moreover, the research and certification & testing costs will be significantly higher. Liquid hydrogen is chosen over hydrogen gas because the latter requires big, heavy pressurized tanks, which pose even more safety hazards. The larger volume would cause excessive drag and likely requires difficult costly structural engineering in terms of the tanks themselves and/or bubble fuselages. Dealing with cryogenic temperature requires a lot more care than regular fuel and since hydrogen is highly volatile, the cryogenic tank only ensures integrity through rigorous testing. Although this increase in cost might endanger the requirement of being economically competitive, the team believed that this could be suppressed by keeping the development costs in mind whenever a design decision has to be made. Concluding, the concept was chosen which showed the highest potential of minimizing the environmental footprint, whilst still performing sufficiently on key criteria. In the following sections, the Hybrid Hydrogen concept is elaborated further to provide additional insights before the detailed design phase is introduced.

5.2 Hydrogen Hybrid Definition

The hydrogen hybrid concept defines itself as having hybrid consumption of hydrogen and kerosene. At this point it is not yet determined how the hybrid injection will happen (options e.g. are different combustion chambers, combined combustion or different engines). The mass fraction of hydrogen in the combustion injection is the key parameter, which needs to be determined by analyzing its impact on weight, cost, emissions and overall viability. First, a Class I weight estimation method is developed in Python. As input, it takes into account a specified hydrogen mass ratio (the mass of hydrogen compared to the total injected mass). The Class I estimation will be performed for a range of 0 to 100% hydrogen mass fractions, in steps of 1%. This will result in different MTOW, OEW and kerosene/liquid hydrogen fuel weights for different ratios. The Class I weight estimation results and additional parameters (fuel cost, emissions) calculated from them shall be used to determine the final hydrogen mass fraction.

5.3 Class I Weight Estimation

The goal of the Class I weight estimation is to provide preliminary values on the Maximum Take-Off Weight (MTOW), Operational Empty Weight (OEW) and fuel weight. The Roskam [26] method is selected for this. This method will be customized to accommodate hydrogen aircraft elements (i.e. the tanks and hydrogen system weights). The MTOW of the aircraft consists of OEW, payload and fuel weight, shown in Equation 1.

$$MTOW = OEW + W_{Payload} + W_{Fuel} \tag{1}$$

Payload Weight First, the payload mass is determined from requirements. The aircraft shall be able to transport 75 passengers (SRA-STAKE-AL-02, Table 13), assumed to have a mass of $93kg$ each (including cabin luggage), and $1000kg$ of cargo (SRA-PROD-PERF-12, Table 13). This results in a payload weight of $7975kg$.

OEW Then, a MTOW-OEW regression is performed based on reference aircraft. the reference aircraft selected are the Bombardier CRJ100, CRJ550, CRJ700 and CRJ900; Boeing 717-200; DC9-10; Bae RJ70; Fokker F70; Embraer 145. The regression can be seen in Figure 14, as can be the regression formula. An additional weight for the hydrogen system is assumed, as the supporting fuel storage and distribution system weight will be higher than for kerosene. A preliminary weight of 1.5 tons was determined in [27]. This number is multiplied by the hydrogen mass ratio and added up to the OEW. A full hydrogen Class I A/C would thus have an additional 1.5 tons OEW penalty, while a kerosene aircraft would obviously have zero added OEW.

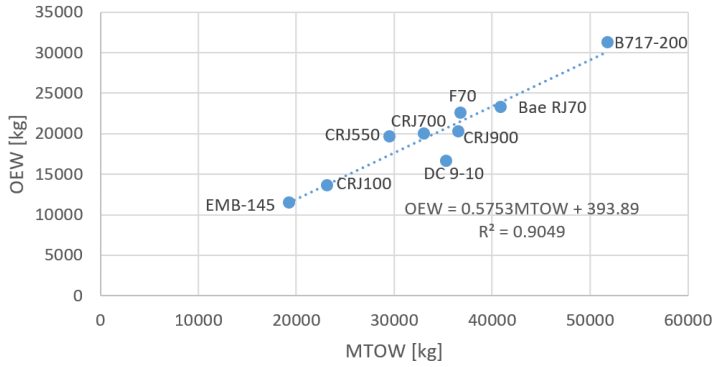

Figure 14: Class I MTOW-OEW regression analysis

Fuel Weight Finally, the amount of fuel to be carried is computed by the fuel fraction method proposed by Roskam [26]. This is done by first defining a mission profile with different phases, then assigning fuel fractions to those phases (W_{end} to W_{begin}), either pre-assumed values (take-off, taxi, shutdown, etc.) from Roskam [26] or calculated using range and loitering equations if applicable. The cruise range is determined to be $2000km$ from requirements, a second cruise diversion range is taken at $200km$, and additionally loitering is allowed for up to 45 minutes. The lift-to-drag ratio of the aircraft is assumed to be 15 [26] in this design stage. Each fuel fraction depends on the weight of the fuel consumed, and as hydrogen and kerosene have different specific energies (shown in Table 11), the total fuel fraction will change over the range of hydrogen mass ratios. To calculate the weight of the consumed fuel, one must determine the Specific Fuel Consumption (SFC) for the cruise and loitering phases. The kerosene SFC is $1.6 \cdot 10^{-5}\ kg/N/s$, slightly lower than the value of $1.9 \cdot 10^{-5}\ kg/N/s$ applicable to the CRJ700's CF34 engine [28][10], as the bypass ratio is higher (this value is comparable to high-bypass engines). First, the hydrogen mass ratio R is defined to indicate the hybrid mixture: this hydrogen mass ratio is $R = \frac{c_h}{c_h + c_k}$. To compute the hybrid SFC, it is assumed that a hydrogen hybrid engine, for a hydrogen mass with equivalent energy to the replaced kerosene mass, will provide the same amount of partial thrust as the replaced kerosene mass did. This involves solving the system of linear equations formed by Equation 2 and Equation 3 with c_h and c_k as unknowns. c_h refers to the hydrogen SFC contribution to the hybrid SFC, c_k to the kerosene SFC contribution, c_{jk} to the full kerosene SFC, e is the symbol for specific energy, and finally R the hydrogen mass ratio. Equation 2 is derived from the assumption that the hybrid configuration requires the same amount of energy as the full kerosene option. Equation 3 is the hydrogen mass ratio $R = \frac{c_h}{c_h + c_k}$ simply rewritten.

$$c_h e_h + c_k e_k = c_{jk} e_k \tag{2}$$

$$(R-1)c_h + Rc_k = 0 \tag{3}$$

[10] https://www.geaviation.com/sites/default/files/datasheet-CF34-8C.pdf

Table 11: Specific energy and mass density of kerosene and liquid hydrogen

Fuel	Specific energy e [MJ/kg]	Mass density ρ [kg/m^3]
Kerosene	42.8	804
Liquid Hydrogen	122.8	70

Adding up the determined c_h and c_k gives the actual hybrid SFC c_j for a certain hydrogen mass ratio. An analogous method is used to compute hybrid second-cruise and loitering SFCs. Also for the assumed fuel fractions a weight reduction correction is implemented w.r.t. the hydrogen mass ratio (as hydrogen weighs less, less mass is consumed in the fuel fraction). Multiplying all fuel fractions results in the final fuel fraction $\frac{W_{end}}{MTOW}$, which expresses the ratio of the end weight to the MTOW. From this, the fuel weight can be derived, i.e. the lost weight equals the consumed fuel weight, as seen in Equation 4. Kerosene and hydrogen masses can be easily calculated by using the hydrogen mass ratio as seen in Equation 5 and Equation 6.

$$M_{fuel} = (1 - \frac{W_{end}}{MTOW}) \cdot MTOW \tag{4}$$

$$M_h = R \cdot M_{fuel} \tag{5}$$

$$M_k = (1 - R) \cdot M_{fuel} \tag{6}$$

5.3.1 Results Discussion

In Figure 15, the Class I results are shown. For each hydrogen mass fraction percentage (0%-100%) the Class I weight estimation was performed, with MTOW and OEW visible in the top left graph, and fuel weight visible in the top right. In the other graphs, derived values which are helpful in selecting the right fraction are shown.

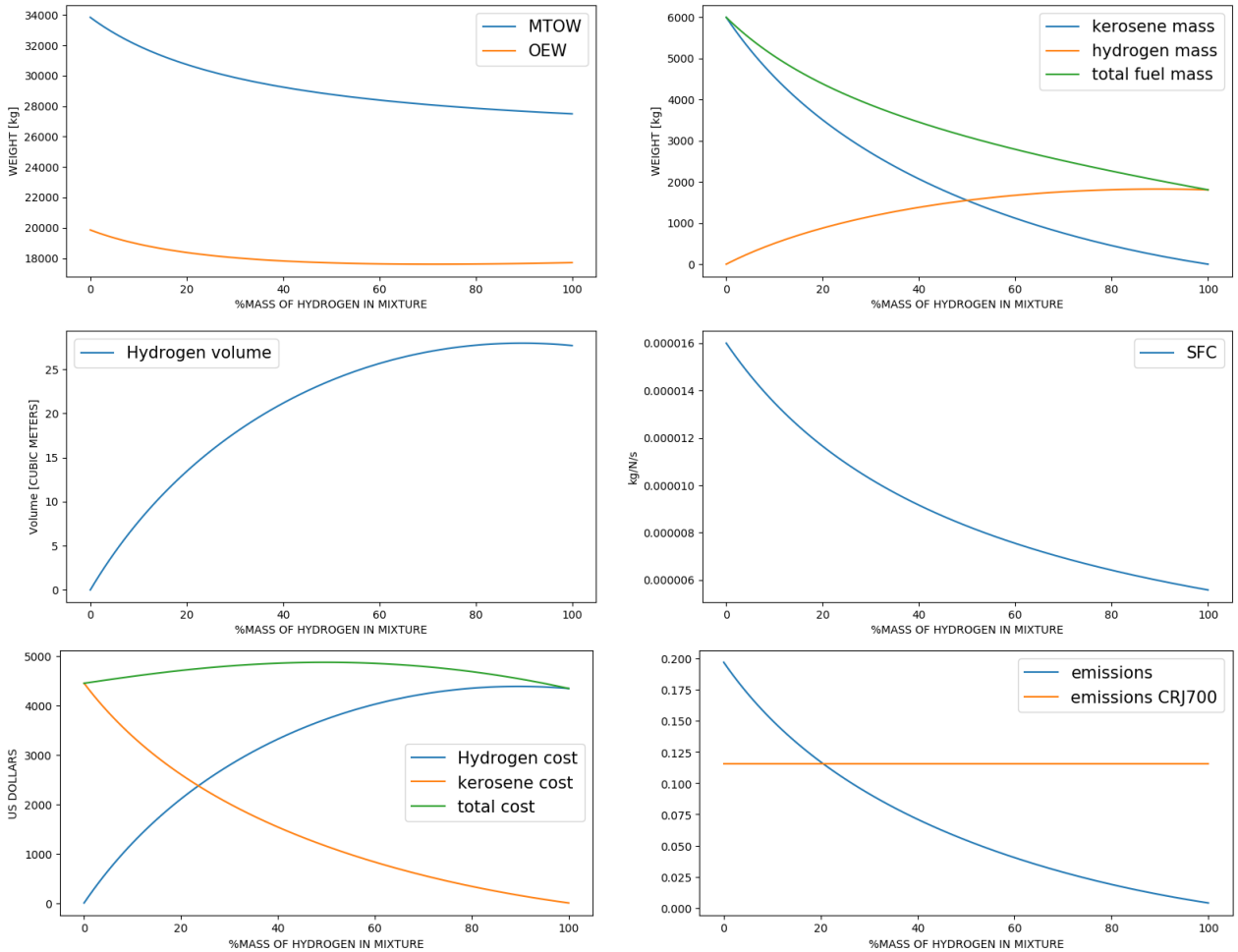

Figure 15: Hybrid fraction trade-off

MTOW/OEW/Fuel The OEW of the aircraft decreases with increasing hydrogen mass fraction. The reason for this is the fact that the hydrogen has a specific energy which is three times as high. This is reflected in the fuel weight in the top right graph. As this fuel weight decreases, MTOW decreases and thus structural loads also decrease, allowing for a lower OEW. The OEW curve flattens at 40% hydrogen fraction due to the hydrogen system mass taking effect (bringing along a 1.5 tonne penalty at full hydrogen). Less weight means less induced drag (so less fuel consumption) and less airframe production costs. A full hydrogen concept would be beneficial from a weight perspective, bringing the MTOW from 34 tonnes to 28 tonnes, which reduces the OEW from 20 tonnes to 18 tonnes.

Hydrogen Volume As the density of hydrogen is approximately ten times as low while only having a specific energy of 3 times as high w.r.t. kerosene (Table 11), the required tank volume is important to consider. A full hydrogen aircraft would require a tank size of $27m^3$. A 40% hydrogen aircraft would require $20m^3$. Thus solutions should be found in the form of top tanks above the cabin, external wing tanks beneath the wing, additional fuselage compartments or a combination of the solutions listed. All solutions increase drag, structural complexity and potentially cause control/stability issues. The assumed hydrogen density is $70kg/m^3$. The hydrogen volume shown is enlarged by 7.2% as suggested by Colozza [29] to create space for boil-off hydrogen gases.

Specific Fuel Consumption (SFC) The SFC strongly decreases with increasing hydrogen mass fraction. This is logical as hydrogen has a higher specific energy, roughly by a factor 3. Thus the fuel injected in the full hydrogen configuration is roughly three times as low. This results verifies the SFC calculation. It also shows again how light hydrogen is as compared to kerosene.

Fuel Cost If the fuel weights are known, an analysis can be made on their emissions and cost. The cost for kerosene is assumed to be 0.6$ per liter (0.75$ per kg), with the cost of green liquid hydrogen assumed to be 2.4$ per kg in the future [30][11]. The kerosene price of 0.75$ per kg is considerably lower than the 2.4$ per kg of green liquid hydrogen. However, as hydrogen has three times the specific energy this effect is negated and both fuel options end up costing about the same, thus the total cost line will not vary wildly. In fact, cost savings will be present because hydrogen weighs less, which leads to a snowball effect, leading to less fuel and less cost. Fuel prices can heavily vary in the future. This is also under the assumption that the hydrogen is produced locally (with green energy), otherwise, additional transport costs will be in place. If the cost of green hydrogen is still higher than kerosene in the future, one can partially use cheaper grey hydrogen (not produced by renewable energy) as long as the emissions target is met, or accept the additional costs as a risk.

Emissions A Carbon Footprint analysis is also performed. This entails the calculation of CO_2-equivalent emission mass per passenger kilometer (see Section 8.3 for a more details). The CF of the Bombardier CRJ700 was also calculated. Requirement SRA-STAKE-ENV-01.1 (Table 71) stated that RELIGHT should be below 75% of the CRJ700 emissions. As such, emission data is obtained for each hydrogen mass ratio. The requirement is already met at roughly 35% hydrogen mass fraction. At 100%, the emissions are very low. However, this particular part of the trade-off did not take into account the effects of hydrogen production, distribution, and hydrogen parts manufacturing into account.

5.3.2 Concept Selection

In the end it was decided to go for the full hydrogen configuration (hydrogen mass fraction is at 100%). The emission savings are key to this project and a full hydrogen configuration scores exceptionally well in this regard, while the cost would be the same in 2040. The added volume does not pose a significant threat. Also the complexity of a hybrid configuration (two tank types, two fuel systems, two or combined combustion chambers) pushes the design towards a single fuel solution (of which hydrogen is the best).

5.4 Class II Weight Estimation

The Class II weight estimation was created to provide a framework for the iteration of the aircraft design. The weight estimation is based on the Roskam method [31], with the functions used specifically belonging to jet transport aircraft and the Torenbeek method. Occasionally the Torenbeek methods were verified with the GD methods [31]. The equations used for the weight estimation of each component will be elaborated throughout Section 6. The code that was written to perform the Class II weight estimation takes a wide range of aircraft

[11] https://www.rolandberger.com/en/Publications/Hydrogen-A-future-fuel-of-aviation.html

Table 12: Summary table for Class-II estimation

Component	RL [kg]	C.G.[m]	F28 [kg]	737-200 [kg]	RL fraction [-]	F28[-]	737 [-]
MTOM	28083.0	14.5074	29483.5	52389.9	1.000	1.000	1.000
OEM	18275.6	14.5858	14160.7	27310.8	0.650	0.480	0.521
Zero fuel mass	26249.5	14.237	20683.4	42184.1	0.934	0.702	0.805
Max fuel mass	1847.7	None	7861.2	15776.4	0.066	0.267	0.301
Max payload	7975.0	None	6522.7	15780.5	0.284	0.221	0.301
Wing group	2349.5	15.5029	3324.8	4814.0	0.084	0.113	0.092
Empennage	769.8	29.2592	740.3	1232.9	0.027	0.025	0.024
Fuselage	3948.2	14	3194.7	5492.1	0.141	0.108	0.105
Nacelle	803.6	13.2426	378.3	631.4	0.029	0.013	0.012
Landing gear	1234.4	None	1251.5	1974.9	0.044	0.042	0.038
Main LG	1017.2	15.4	None	None	0.036	None	None
Nose LG	217.3	3.835	None	None	0.008	None	None
Total structural	9105.5	None	8889.5	14145.3	0.324	0.302	0.270
Engines	2328.1	13.2426	2038.9	2820.0	0.083	0.069	0.054
Exhaust	None	None	57.6	456.8	None	0.002	0.009
Kerosene system	0.0	None	247.2	260.8	0.000	0.008	0.005
Hydrogen tanks	279.0	15.7025	None	None	0.010	None	None
Power controls	136.3	13.2426	97.5	171.5	0.005	0.003	0.003
Total propulsion	2743.4	None	2441.2	3709.0	0.098	0.083	0.071
Electrical systems	1342.8	13.2426	858.2	917.2	0.048	0.029	0.018
Instruments	382.1	2.3889	137.0	283.5	0.014	0.005	0.005
Flight controls	613.5	14.9608	794.2	1461.0	0.022	0.027	0.028
APU	210.7	27.2	156.9	379.2	0.008	0.005	0.007
Air conditioning	611.3	14	487.2	642.3	0.022	0.017	0.012
Furnishing	3028.5	14	1828.0	3013.2	0.108	0.062	0.058
Cargo handling	111.3	16.6667	None	None	0.004	None	None
Miscellanous/paint	126.4	14	None	56.2	0.005	None	0.001
Total fixed equipment	6426.7	None	4261.5	6752.6	0.229	0.145	0.129

parameters as input, and works in such a way that a new weight estimation can be obtained every time a parameter is changed. The code iterates the Class I and Class II weight estimations until the results of the two converge to within 1%. A graph has been made of the OEM converging, which can be seen in Figure 17. The Class II estimation returns a value for the OEW, which can be used by the Class I code to find a new MTOW, which is cycled through the Class II estimation again. The data flow of the elements used in the Class I & Class II weight estimations is shown in Figure 16. The component weights computed in the estimation have been divided in three categories, namely structural weight, power system weight and equipment weight. In Table 12 rows 5 to 13 make up the structural weight, rows 14 to 19 make up the power system weight and the rows from 20 to the end include all the fixed equipment. For comparison, data about the weight and weight fractions of components from two similar aircraft are also shown [31]. A pie chart overview of the weight fractions making up the overview is also given in Figure 47. Note that for layout purposes, RELIGHT has been abbreviated to RL. Furthermore, the C.G. of certain components is also given in the table. These will be used in Section 6.4.2.

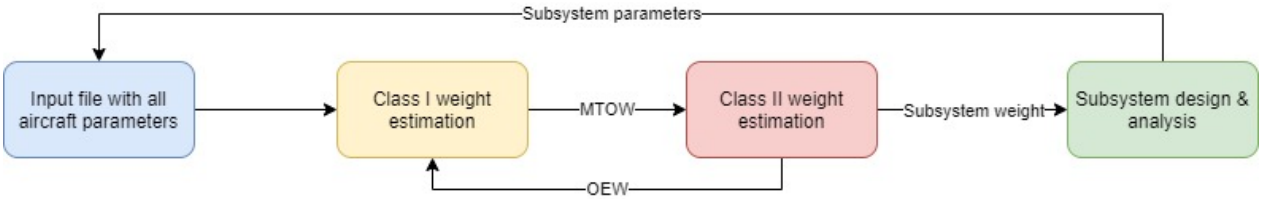

Figure 16: Data flow for weight estimations

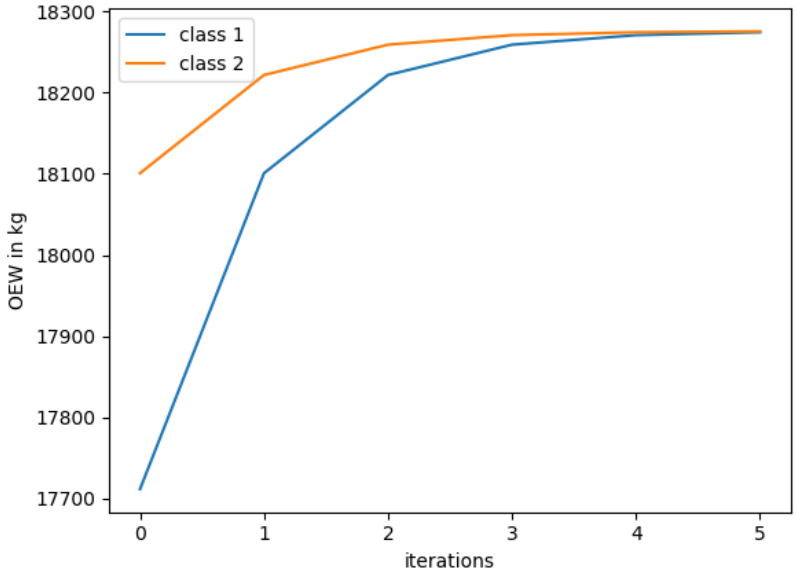

Figure 17: Convergence of Class I and Class II weight estimations

Verification & Validation All of the equations used to calculate the component masses have been verified with an hand calculation, directly from [31]. One very important note that must be kept in mind, is that the equations from [31] are all in imperial units. In the implementation of the Class II weight estimation, great care was taken to convert all units properly. Each and every parameter has been checked to be in the appropriate units at least twice to avoid mistakes. The results of the Class II weight estimation have all been displayed in kilograms to avoid confusion during the design of the multitude of subsystems of RELIGHT.

To Validate the results, the component masses have been compared to two reference aircraft. Both the absolute masses and the fraction with respect to MTOM have been compared. It can be noted that the OEM fraction of RELIGHT is relatively large, which can be attributed to the use of hydrogen. The rest of the components are in the same order of magnitude, with some components weighing relatively more than in the comparison aircraft. This is due to the use of hydrogen, lowering the MTOM, and advances in technology placing more emphasis on electronic systems. This will increase the APU and electrical system mass, while reducing the flight control mass.

5.5 Flight Envelope

The flight envelope is, along with the Class II weight estimation, the primary base upon which the entire preliminary design is built. It dictates the graphical region in the airspeed-load factor relation at which the aircraft is allowed to operate in. That is, for certain Class I output values, the flight envelope predicts operational speed values and load factors, for which the aircraft will perform its designated mission to the maximum of its potential, but also safely. Regardless of operational mission, all aircraft entail such a process in the design face, but obviously generate a different set of output limits, and allowable regions of operation.

The calculation is split in two branches. Initially the flight manoeuvre diagram is calculated, during which the load factors and design speeds are calculated solely for the aircraft's performance. Then, the plotting of

the gust manoeuvre diagram follows, with designed load factors and speeds for wind gusts and generally for unpredictable ambient conditions. Broadly for both, the rule that can be seen from the plots is that for higher speeds higher load factors are visible, and the closer the speed is to zero, so is the factor.

$$V_S = \sqrt{\frac{2 \cdot \frac{GW}{S}}{\rho \cdot C_{N_{max}}}} \quad (7) \qquad n_{lim_{pos}} = 2.1 + \frac{24,000}{GW + 10,000} \quad (8) \qquad C_{N_{max}} = 1.1 \cdot C_{L_{max}} \quad (9)$$

Initially, the starting values to be obtained are the stall speed and the positive limit load factor. The latter, shown above depends solely on the Gross Weight, which is the maximum take-off weight together with the fuel weight for taxiing, and is estimated as $\frac{MTOW}{0.99}$. The value is also limited from the relation below due to empirical data. The stall speed, here V_S, is by definition the minimum airspeed at which the aircraft is controllable, and so it is found first at a load factor of +1g. It is dependent upon the gross wing loading, the cruise density, and the maximum normal force coefficient, empirically estimated at 1.1 times the $C_{L_{max}}$ requirement (which is determined to be 1.8), shown in Equation 9.

$$2.5 < n_{lim_{pos}} < 3.8$$

Therefore, it is determined that if the value is calculated to be below 2.5 it should be automatically be 2.5, and similarly above 3.8. Furthermore, the cruise speed is obtained with Equation 10 and is also dependent upon the gross wing loading and k_c, a constant that varied with wing loading values for utility aircraft, and therefore here is 26.5. Furthermore, one can also get the value for V_A, the design manoeuvering speed, using Equation 11 with the output values of the to equations above.

$$V_C = k_c \cdot \sqrt{\frac{GW}{S}} \quad (10) \qquad V_A = V_S \cdot \sqrt{n_{lim}} \quad (11)$$

Moreover, the above values of the different speeds will become the slopes in the gust loading diagram of Figure 18b, forming the gust lines that start from the loading value of +1g. Lastly, the negative values for the manoeuvering load diagram source from statistics of similar aircraft. For the envelope procedures and loading calculation, the major distinction of aircraft is made between normal category, which is the category under which the RELIGHT belongs, utility category, with minor acrobatic allowance, and acrobatic category, for large range of motion possibility, usually seen in military aircraft. For normal category aircraft, the negative limit load factor is suggested to be -1g, and the stall speed value is henceforth calculated according to this reduction.

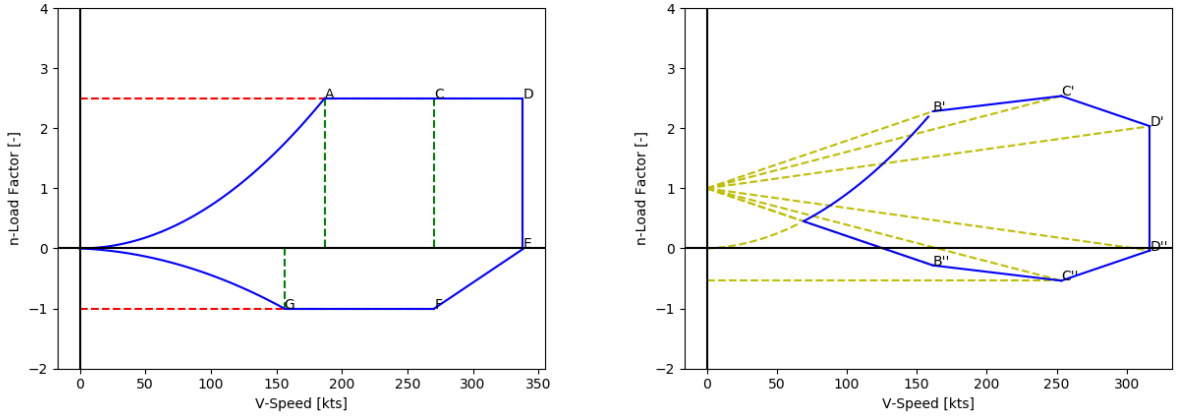

(a) Flight Manoeuvre Diagram

(b) Flight Gust Diagram

Figure 18

The sole purposes of the flight envelope are vehicle safety and a successful flight mission. The above two resulting diagrams, the manoeuvre diagram and gust diagram, take into account all possible phases and sub-phases of the aircraft's flight, from taxiing before take-off to taxiing after landing. Any manoeuvre and any gust and wind condition for which it has operational clearance is accounted for. This is also the reason the

two diagrams do not diverge much in values of load factor or speed. It is now time to merge them and obtain the resulting envelope. The overlap is visible in Figure 19a, and after clearing out the unnecesary lines, the obtained final envelope diagram by the calculation process can be seen in Figure 19b.

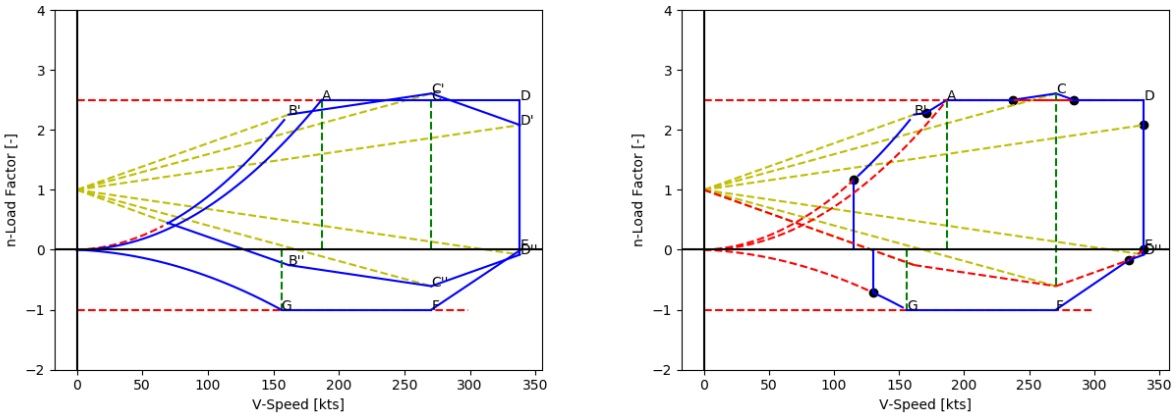

(a) Merged Diagram

(b) Resulting Envelope

Figure 19

To give the reader a clear understanding of the overall result, looking at the merged diagram the governing outline is the one that remains. That is, if any of the blue lines has another blue line further to the outside, then it is neglected, and displayed as a dotted line, to still give the idea of the structure behind it. It should also be noted, in case it has not been clear, that for all 4 plots, the blue lines represent the outlines for the limiting region, that is led by the aforementioned equations of the flight envelope procedure. Lastly, the envelope is limited by the stall speed, both the one in the positive and the one in the negative region, and does not include the part of the convergence towards zero even if it existed previously. That is because realistically, at speeds below the stall speed, there occurs events such as flow separation on the wing surface and the plot behavior cannot be predicted by classic aerodynamics, and so it is intentionally left out of the result.

6 Subsystem Development

This chapter outlines the detailed design phase of designing the individual subsystems. First, the fuselage and tank layout is discussed in Section 6.1. This is followed by the design of the wing planform, propulsion system, empennage and landing gear in Section 6.2, Section 6.3 and Section 6.4, respectively. The section is closed off with Section 6.5, in which a structural analysis of the wing box, fuselage and fuel tank is performed along with the selection of materials. Each of the aforementioned subsections follows a common structure. First, the subsystem requirements are tabulated in which also the compliance is shown. A '✓' indicates compliance, '✗' means a requirement has not been met and '✓/ ✗' implies that either the requirement is partially met or shows a high potential of being met after more detailed analysis. Then the technical work is presented, followed verification of the codes uses and validation of the code results obtained. Next, a sensitivity analysis is performed to check the behavior of the results with the uncertainties present in the inputs. In this way, more insight is gained in the sensitivity of certain design parameters, which might endanger compliance with certain requirements. Finally, the compliance with the requirements are discussed. In some cases, recommendations are stated to facilitate the discussion on the compliance with requirements.

6.1 Fuselage and Tank Layout Design

The fuselage provides space for the cockpit, galleys, passengers and cargo. In the case of RELIGHT, liquid hydrogen must very likely be stored in the fuselage as well because of its limited volumetric energy density. The fuselage also provides mounting for the wings, empennage and landing gear.

6.1.1 Preliminary Requirements

The fuselage design and tank placement are subject to several requirements, presented in Table 13. The green boxes indicate driving requirements. Compliance will be checked after design, in Section 6.1.7.

Table 13: Internal layout requirements

Requirement Identifier	Requirement	Compliance
SRA-STAKE-AL-02	The aircraft shall accommodate 65 to 75 passengers in an economy class setting.	✓
SRA-PROD-PERF-12	The aircraft shall be capable of carrying all passenger cabin luggage plus 1000 kg extra cargo.	✓
SRA-STAKE-AP-03	The aircraft shall not require stairs from the airport to embark/disembark.	✓
SRA-STAKE-AP-06	The aircraft shall allow for safe loading of cargo and baggage with available equipment at regional airports.	✓
SRA-STAKE-PSG-02	The aircraft shall provide for comfortable seating.	✓
SRA-STAKE-PSG-03	The aircraft shall enable on-board food catering.	✓
SRA-STAKE-PSG-04	The aircraft shall feature a similar amount of cabin luggage storage as the reference aircraft, the Bombardier CRJ700 series.	✓
SRA-PROD-PERF-08	The aircraft shall have enough fuel reserves to fly an additional 45 minutes at cruise speed and altitude.	✓
SRA-SYS-FG-05	The fuselage shall allow for natural light to enter.	✗
SRA-SYS-FG-03	The fuselage shall be able to accommodate aircraft systems.	✓

6.1.2 Passenger Compartment Cross Section

The first step consists of defining the number of seats per row, seat pitch and other relevant cabin dimensions. Aircraft of similar seating capacity tend to have 4 (Bombardier CRJ700) or 5 (Antonov An-148) seats abreast. A 5 seats abreast configuration results in a shorter but wider fuselage. This is advantageous for top tanks (as in a fuselage double bubble) and aft tanks. This is because in the volume calculation of a cylinder, the radius is squared, whereas the length is not, resulting in a more efficient tank shape for wider fuselages. Thus, 5 seats on a row are chosen. Data on cross section dimensions are given in Table 14 and are derived from

both values given by Roskam [32] and similar aircraft (Airbus A220, Bombardier CRJ700) cross-sections to develop realistic dimensions for an economy class configuration. After the internals are drawn, the smallest circle possible is drawn around them. Then, a wall thickness (consisting of insulation, structural elements and skin) of $100mm$ is assumed. This results in a final diameter of $3.486m$ as can be seen in Figure 20. In this figure a 60x40cm bag is included to show that it is possible to store such a bag on one side of the cabin in the overhead storage bins. The other side can be used for smaller bags. Cargo space is also provided, the cargo hold is $0.9m$ high.

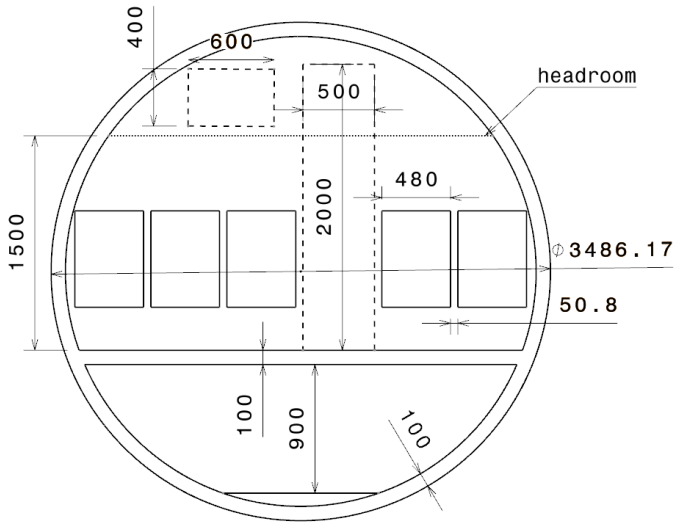

Figure 20: Cabin cross-section

Table 14: Cabin cross-section

	[inches]	[m]
seat width	18.9	0.48
armrest width	2	0.508
clearance	0.4	0.01
aisle width	19.7	0.5
aisle height	78.5	2
headroom height	59	1.5
floor thickness	3.9	0.1
wall thickness	3.9	0.1

6.1.3 Cabin Layout

The width of the cabin has been determined in the previous section, with 5 seats per row. Now, the cabin-layout is developed, with the end result shown in Figure 21. As the aircraft must be able to transport 75 passengers, this implies that 15 rows must be installed. The seat pitch is assumed to be 32 inches ($0.81m$), an industry standard for economy class for many airlines. The seat length is 22 inches ($0.56m$). Starting at the front, a cockpit length of $3.6m$ is assumed, then a front galley is installed, with a length of $2.5m$, including a lavatory, closet, the galley itself, and crew jump-seats. The front galley is split by the main entrance, being $0.8m$ wide, resulting in a combined $3.3m$. Then, the passenger section starts. Complying with EASA regulations [33], a type B exit and a type III exit are installed at each side of the fuselage. A type B exit minimally measures 32 by 72 inches, and corner radii not bigger than 6 inches ($0.81m$ by $1.83\ m$ and radii of $0.15m$). Type III exits must be at least 20 by 36 inches with corner radii not bigger than 7 inches ($0.51m$ by $0.91m$ with radii of $0.18m$) [33]. There are 7 rows in front of the type III exit, and the remaining 8 are placed behind the exit. An additional 10 inches ($0.25m$) of emergency clearance space is added to the seat pitch between seat row 7 and 8. With an assumed seat length of 22 inches ($0.56m$), this leaves 20 inches ($0.51m$) of emergency aisle width. An aft galley of $1.5m$ is also installed. This is followed by half a meter of space for hydrogen support systems and bulkhead (this tail tank was placed according to Section 6.1.5. The tail cone is $6.91m$ in length. The overall fuselage length (nose to aft) is $28m$. It is seen that the front galley is rather large. Further research can be done into alternative lay-outs, so a customer has the possibility to shorten it to allow for an extra row, but with fewer amenities.

6.1.4 Cargo

RELIGHT is required to carry $1000kg$ of cargo in its hold. Two cargo holds are used: a front hold (C.G. assumed at $6m$ from nose onward) and an aft hold (C.G. at $19m$). The aft hold will carry 2/3 of the cargo. The front hold will carry 1/3. It is more centered towards the back to limit CG excursion, but this will have an impact on control and stability. From reference aircraft, the density of cargo is assumed at $150 kg/m^3$. The frontal area of the cargo hold is assumed to be $1.8m^2$. The front cargo hold must then be $1.24m$ long, the aft hold $2.47m$. Better distribution and impact on control and stability could be researched.

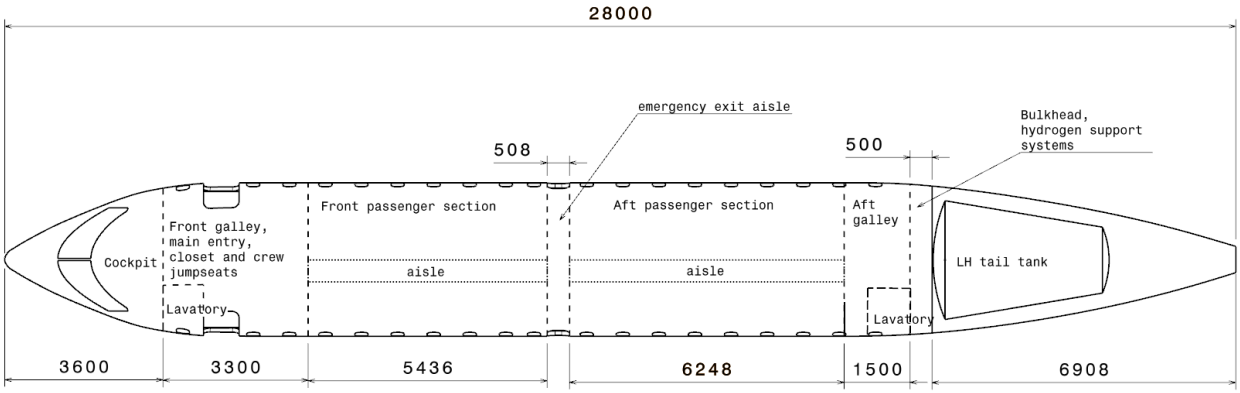

Figure 21: Top view of fuselage

6.1.5 Tank Placement

The energy density of hydrogen is $122.8 MJ/kg$, with a density of $70 kg/m^3$, this results in a volumetric energy density of only $8.6 MJ/liter$. For kerosene, this number approaches $34.5 MJ/liter$. Thus, for the same amount of energy, 4 times the volume is needed. On top of this, a 7.2% boil-off volume is added [29]. The Class II weight estimation (in combination with Class I weight estimation iterations) found a required fuel weight of $1847 kg$. This results in a total tank volume of $28.3 m^3$. Solutions to store all of this volume can be in the form of a top tank (a bubble added on top of the fuselage), a cylinder tank (placed in an extension of the cylindrical fuselage), a tail tank (placed in tail cone), external wing tanks or a combination of the previously mentioned solutions. Tanks in the aircraft belly are discarded, as this would compromise crash safety and limit cargo space. The tank placement will heavily influence aerodynamics, control and stability, and safety. A cylinder tank or tail tank seem more favorable for aerodynamics, but negatively impact control and stability. A trade-off is done to select the best tank placement configuration possible. It was decided beforehand that a tail tank is preferred over a cylindrical aft tank, to reduce the fuselage length (less drag, less weight and less cost for manufacturing). Preliminary geometrical checks in CATIA indicated that the tail cone can at most store half of the required volume, as space for the APU and other systems must be provided. The rest of the fuselage fuel (if not stored in external wing tanks) must be put in an aft cylindrical tank (placed between cabin and aft tank).

Trade-off Top vs Wing Tank First, a trade-off is done between top tank or external wing tanks. Two configurations are considered, those being a top tank with tail tank, and external wing tanks with tail tank. the top tank is split in two tanks. Python code was developed to size tanks according to thermodynamic (boil-off) and structural considerations in Section 6.3 and Section 6.5. The code takes as input the required hydrogen volume, the fraction one wishes to put in the tail, and either tank length (for top tank: $17.5 m$, for pod tank: $5 m$) or tank radius (for tail tank, an oblique truncated cone modeled as a cylinder). It outputs the other dimension (so radius for length and vice versa, by using Equation 16 and Equation 17), thickness and tank weights. The fraction in the tail was varied from 0 to the maximum of 0.5.

Drag For each case a drag model (during cruise) is set up. In the case of a top tank, the fuselage drag will increase. The Torenbeek method found in [34] was applied to calculate this drag force, seen in Equation 12. P is the fuselage perimeter, which was calculated by adding the perimeter of the top tank, to the perimeter of the cabin cross-section. l_F is the fuselage length ($28 m$). λ_f is the fineness ratio of l_F over the height of the fuselage.

$$S_{wet,F} = \pi \cdot \frac{P}{\pi} \cdot l_F \cdot \left(1 - \frac{2}{\lambda_F}\right)^{2/3} \left(1 + \frac{1}{\lambda_F^2}\right) \tag{12}$$

For the pod configuration, the added drag from the pods has to be computed. The drag calculation from the component drag build up method is used [34]. C_{fpod} is the skin friction coefficient for turbulent flow. FF_{pod} is the form factor of the object, giving its pressure drag contribution. For the pod, the nacelle formula is used, where λ is the fineness ratio (length over diameter). The diameter is added to the length to account for the cones. The wetted area of the pod is easily computed. In this stage of the design, the reference area S_{ref} is taken from the CRJ700 ($62.5 m^2$) as the actual wing area is not known yet, this is reasonable as this is used

just for trade-off purposes. IF is the interference factor caused by the proximity of the wing. It is 1.3 [34] for items less than a pod diameter away, which is the assumed distance range here.

$$C_{D_{pods}} = \frac{1}{S_{ref}} \cdot C_{f_c} \cdot FF_c \cdot IF_c \cdot S_{wet_c} \tag{13}$$

$$C_{fpod} = \frac{0.455}{log_{10}(Re)^{2.58}}(1 + 0.144M_{cruise}^{0.65}) \qquad FF_{pod} = 1 + \frac{0.35}{\lambda} \qquad \lambda = \frac{l_{pod} + D_{pod}}{D_{pod}} \tag{14}$$

$$IF_{pod} = 1.3 \qquad S_{wet_{pod}} = \pi D_{pod} l_{pod} + \pi D_{pod}^2 + 2h_{pylon} l_{pylon} \tag{15}$$

It can be seen in Figure 22 that the podded option is the clear winner. It has less drag (the drag is fuselage drag and pod drag added) than the top tank configuration. Less drag will lead to less fuel consumption, and savings in operational cost. It is also less difficult to design and implement, from both a structural and aerodynamic point of view. It is assumed a that the tail can hold at most 50% of the fuel, this explains the shift seen in the left graph at a wing/top tank fraction of 0.5. If the wing/top tank fraction is higher, the drag will increase, up to a point where pod drag becomes higher than the top tank drag. External wing tanks also have a structural advantage, they provide bending relief and do not impose the complicated structural design of a double bubble. As the hydrogen is carried outboard it is also safer. It is thus advantageous to go for external wing tanks, but to make them as small as possible to minimize drag. However, mass and balance constraints will determine how low the mass actually can be. The actual fraction chosen in the end will depend on the mass and balance analysis.

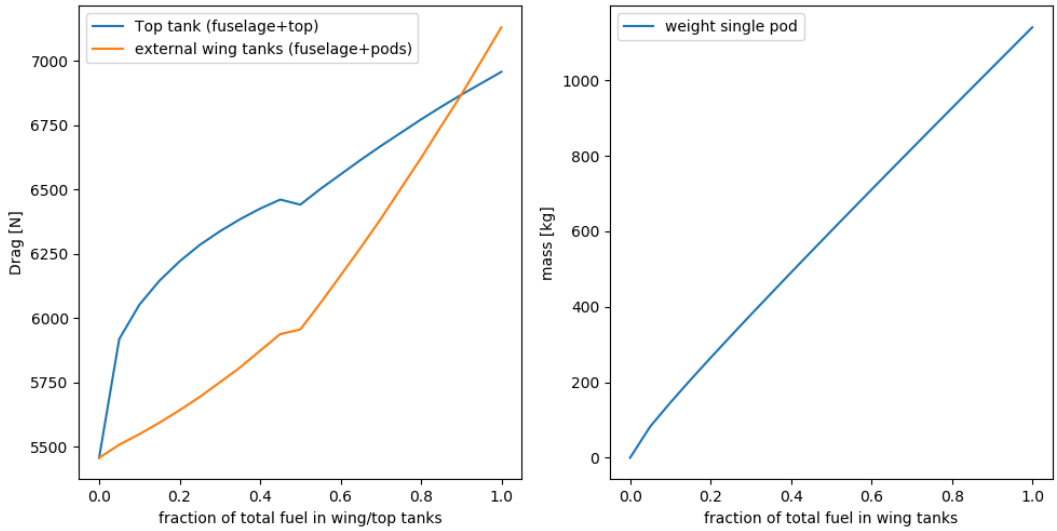

Figure 22: Top tanks vs wing tanks

Mass and Balance The tail tank/wing tank ratio will have a large impact on the control and stability of the RELIGHT design. The code returns tank weight, and fuel weight can be easily determined by evaluating the needed volume. The distances of the tank CG from the nose onward is straightforward in case of the tail tank, and the external wing tank CG is assumed to be placed at the leading edge of the MAC for balance calculations. In reality however, this can change according to the area ruling. Extensive stability and control codes were written in Section 6.4. Those can be used to generate CG excursions (as % of MAC) and tail sizes (derived from scissor plots). This was done for an aircraft where the fuel is placed completely aft (so both cylinder and tail tanks), and for an aircraft where half of the fuel is stored in the external wing tanks. For the completely aft filled aircraft, a CG excursion of 28% was found, with a horizontal tail area ratio $\frac{S_h}{S}$ of 0.43. When half of the fuel is placed in external wing tanks, the CG excursion reduces to 14%, and the

horizontal tail area ratio decreases to a more reasonable 0.36. This indicates that putting half of the fuel in the external wing tanks is very advantageous for control and stability. Adding even more would be even more advantageous, but this would come at the cost of more drag (Figure 22), and structural loads on the wing. Also, as the tank diameter increases and the tanks are placed $7.44m$ from the center-line (determined by aileron and flap placement), ground clearance might become an issue. Also the boil-off is bigger in the outside tanks. Therefore, the decision is made to store half of the fuel in the wing tanks, and the other half in the tail tank, as tail size and CG excursion are low enough.

Sizing $1847kg$ of LH is needed to fulfill the mission requirements, diversion range and loitering included. Accounting for boil-off volume, this means a hydrogen volume of $28.28m^3$ must be provided. $14.14m^3$ must be stored in the tail, $14.14m^3$ in the external wing tanks (so $7.07m^3$ per tank). For the external wing tanks, it is decided to have cylindrical pods with end caps, with a total estimated length of $5m$, including caps, not aerodynamic cones. The end caps have a height equal to halve the radius. The volume of one such tank is then given by Equation 16. The formula is solved for R by iteration.

$$V = (5 - 2h_{cap})\pi R^2 + 2\pi\frac{h_{cap}}{6}(3R^2 + h_{cap}^2) \tag{16}$$

A diameter of $1.39m$ is found. For the tail tank, an oblique truncated cone is assumed (to make it fit into the tail section). The end caps are assumed to have a height of one fifth of the radius of the cone end they are placed on. The formula for a truncated oblique cone is given in Equation 17, taking into account end caps, with d the depth, R the big radius, and r the small radius. However, to simplify thermodynamic and structural calculations, the tank is modeled in the Python programs as a cylinder with the same volume in Section 6.5 and Section 6.3.

$$V_{t.o.cone} = \frac{\pi}{3}length(r^2 + rR + R^2) + \frac{\pi}{6}(3(\frac{r}{5})^2 + r^2) + \frac{\pi}{6}(3(\frac{R}{5})^2 + R^2) \tag{17}$$

For the cone, r, R and d are free variables. An analysis in CATIA found that a cone with R equal to $1.35m$, r equal to $0.75m$ and d equal to $3.58m$ would fit inside the tail while respecting the 14.14 volume constraint, as well as staying outside of the $100mm$ structural wall thickness limit. The structural elements supporting the tank can be integrated with the fuselage structural elements. The anti boil-off insulation still needs to be added, but it is assumed that this can be integrated within the structures surrounding the tank. The insulation and structural sizing is done in Section 6.3 and Section 6.5 respectively. In the latter, the final tank weights are given. In Figure 23, a render illustrating the tank placement is shown. Again, one can see the tail tank structure must be properly incorporated into the fuselage structure (e.g. the vertical tail structure).

Figure 23: External wing tank and tail cone tank

6.1.6 Verification and Validation

Verification A Python code was developed to calculate the length of the cabin, this was checked by hand. This means adding all dimensions (cockpit, 14 seat pitches, etc.) and comparing this to the code output. The entire configuration was drawn in CATIA in order to verify the design. It was compared against cabin plans from reference aircraft to assess if the dimensions allow for a spacious and useful cabin. Also drag calculations were checked by hand, to make sure the formulas are correctly implemented into the code. The dimensions on external wing tanks were given by the code, but were calculated manually again to make sure they corresponded to the right volume.

Validation It is clear that the fuselage and tanks are able to serve their intended purpose. The fuselage is able to carry 75 passengers, crew, and provides them with the necessary amenities, as well as luggage and cargo space. The tank volume offers the required amount of LH necessary for the mission.

6.1.7 Requirements Compliance

RELIGHT is able to transport 75 passengers in economy class, fulfilling SRA-STAKE-AL-02. Under the floor of the cabin and cockpit, the aircraft will feature plenty of space for the required aircraft systems and cargo, satisfying SRA-PROD-PERF-03 and SRA-PROD-PERF-12. If a stair is built into the front door (and the front door folds downwards), SRA-STAKE-AP-03 is also met. SRA-STAKE-AP-03 is met as cargo doors are well positioned. SRA-STAKE-PSG-02, SRA-STAKE-PSG-03 and SRA-STAKE-PSG-04 are all met, as is SRA-PROD-PERF-08 (enough tank volume has been secured). SRA-SYS-FG-05 is not met yet, as the large engines developed in Section 6.3 obstruct light and solutions must yet be researched in Section 6.1.8.

6.1.8 Fuselage and Tank Layout Recommendations

Configuration Changes Further research may be done in alternative seating configurations. Examples are including a business class, having a 30 inch seat pitch and/or shortening the front galley to include more seats. If more passengers are added, either the carried fuel or luggage/cargo must be reduced. The first one reduces range by a great amount. As LH has a low volumetric energy density, a lot of energy (and thus range) must be sacrificed. If a passenger and their cabin luggage weigh $93kg$ in total, $465kg$ of tank capacity cannot be used if an extra row is added. If the 45 minutes loitering time and diversion range of $200km$ stay in place, the operational range would drop to $1000km$ according to the equations used in the Class I weight estimation. If the customer wishes to fly at the same range with more seats, cargo hold weight must be sacrificed. Seating configurations with a row less (by e.g. including a business class) could take more cargo. As the fuel tanks are already fully filled for the mission range of 2000 km, to save on drag and volume, it might be an idea to develop a version of RELIGHT with larger external wing tanks which allows this kind of flexibility. The tail tank reached its maximum capacity. The external wing tank should be enlarged by 50%, from $7.1m^3$ to $10.6m^3$, for a hydrogen increase of $465kg$ (5 passengers). The diameter needs to increase by 20%. All of this brings extra drag, structural loads on the wing so more research is needed on enlarging the external wing tanks to essentially allow for more flexibility in the payload-range relation. This does not only hold for a configuration with 70 passengers, but also for a configuration with 75 passengers where only 70 passengers are flying. The range could be enlarged to $3000km$ with taking 5 passengers less and enlarging the external wing tanks by 50%.

Cabin Natural Light The turbofan engines developed in Section 6.3 have a high bypass, leading to a large nacelle. Combined with a top wing, this might obstruct natural light from coming in, and obstruct the view. It is recommended to research the impact and provide solutions like extra lighting, or enlarged windows in the affected area.

Cargo It is assumed 1/3 of the cargo goes in the front, 2/3 in the back. This ratio can be altered in the further analysis, to see if it improves control and stability.

6.2 Wing Planform Design

At the current stage of the design, aerodynamics becomes a vital section to focus on in detail. The airflow behavior around the wing, fuselage and tail is paramount and directly affects the structure and flight performance, which then directly affect sustainability, the primary goal. This section displays the general wing planform layout, in Section 6.2.3. Then, in Section 6.2.4, the process of the airfoil selection is described, as well as the final choice, and its characteristics. Lastly, the sizing of the high-lift devices and ailerons is

presented, as well as the general lift and drag characteristics.

6.2.1 Preliminary Requirements

The methodology and procedure for the aerodynamic analysis and the wing planform sizing uses certain preliminary requirements as guidelines that generate further, sub-requirements. The top level ones are therefore presented inTable 15, the highlighted boxes in green being the critical ones, along with a general compliance checks that will be elaborated in Section 6.2.9.

Table 15: Wing Planform System requirements

Requirement Identifier	Requirement	Compliance
	Wing Planform System	
SRA-SYS-WAero-01	The wing shall be able to provide a maximum lift coefficient of 2.25	✓
SRA-SYS-WAero-02	The wing shall be able to provide a C_{Lmax} of 1.8 in clean configuration and 2.25 in landing configuration.	✓
SRA-SYS-WAero-03	The wing shall allow for the cruise Mach number	✓
SRA-SYS-WAero-04	The wingspan shall fall within 15-23.99 m.	✓
SRA-SYS-LG-06	The landing gear shall not account for more than 15% of the total drag	✓

6.2.2 Methodology

To obtain the aerodynamic characteristics, first the ones that regard creating lift are addressed. The dimensions of the wing planform are determined and an airfoil is selected from a trade-off. The trade-off yields the airfoil that performs best with respect to the aforementioned requirements and some other important criteria. With the selected airfoil, the maximum lift coefficient can be derived, and the need for additional lift creating surfaces, high-lift devices, is determined. The reason for this is that more lift is needed during take-off and landing than during cruise. Without high-lift devices, the wing would be over designed in cruise, adding additional drag. Then, after the the necessary aileron surface is determined for rolling requirements, the high-lift devices are placed on the wing keeping in mind the ailerons.

With the lift characteristics being covered, the overall drag of RELIGHT is determined. For each and every component the zero-lift drag is analyzed, which is influenced by skin friction, the overall exposed ('wetted') area, the specific shape and interference with other components. To obtain the total drag, the lift-induced drag is added, which is influenced by the wing planform characteristics. Then, after determining the drag polar, the curve with possible lift-to-drag ratios is obtained.

6.2.3 Wing Planform

The wing area S is derived from the wing loading, which is determined by the design point in the thrust and wing loading diagram. Also, the AR is chosen to be 8 to increase aerodynamic efficiency by lowering the lift-induced drag. $C_{L_{max}}$ is taken to equal 1.8 as a first estimate. During airfoil selection it will become apparent if this is feasible.

Using Equation 18 and Equation 19, the characteristics for the tapered trapezoidal wing planform are determined. The span b, the root chord c_r, the tip chord c_t and the mean aerodynamic chord c_{MAC} follow from simple geometrical equations. The sweep at quarter chord is obtained from drag divergence considerations. The relation in Equation 18 follows from statistics on transport aircraft. A technology factor $M^\dagger$ for supercritical airfoils is assumed, for which the reason is explained in Section 6.2.4. Taper is selected to obtain as much as possible an elliptical lift distribution, which minimizes induced drag [6]. Then the limiting thickness-to-chord ratio t/c is either 0.18 or lower, depending on the sweep , the technology factor for supercritical airfoils $M^\dagger$, the drag-divergence Mach number M_{dd} and the cruise lift coefficient $\hat{C_L}$. Also, note that sweep is not included yet, as this parameter is dependent on the critical Mach number M_{cr} which is determined during airfoil selection (see Section 6.2.4).

$$b = \sqrt{S \cdot AR} \qquad \Lambda_{c/4} = cos^{-1}\left(0.75\frac{M^\dagger}{M_{dd}}\right) \qquad \lambda = 0.2 * (2 - \Lambda_{c/4}) \tag{18}$$

$$c_r = \frac{2S}{b * (1+\lambda)} \qquad c_t = \lambda \cdot c_r \qquad MAC = \frac{2}{3}c_r\frac{1+\lambda+\lambda^2}{1+\lambda} \tag{19}$$

$$t/c = min\left(\frac{(cos\ \Lambda_{c/2})^3(M^\dagger - M_{dd}\ cos\ \Lambda_{c/2}) - 0.115\ \hat{C_L}^{1.5}}{(cos\ \Lambda_{c/2})^2},\ 0.18\right) \tag{20}$$

$$M^\dagger = 0.935 \qquad M_{dd} = M_{cruise} + 0.03 \qquad \hat{C_L} = \frac{MTOW}{\frac{1}{2}\ \gamma\ p\ M_{cruise}^2\ S} \tag{21}$$

Table 16 summarizes the wing planform characteristics. Note that the dihedral angle Γ is important for lateral stability, for instance to damp the Dutch roll motion. Γ is affected by the sweep Λ and vertical wing placement. In Figure 24, an oversight is provided, including the engine and fuel pods.

Table 16: Wing planform characteristics

Parameter	**Value**	**Unit**
Wing area - S	62.248	m^2
AR	8	–
Span b	22.316	m
Taper ratio λ	0.310	–
Root chord c_r	4.259	m
Tip chord c_t	1.320	m
Mean aerodynamic chord MAC	3.048	m
Thickness-to-chord ratio t/c	0.14	–
Dihedral Γ	-1	deg

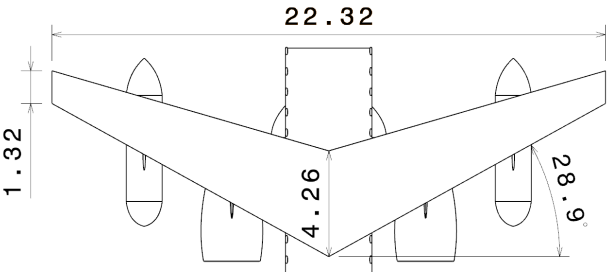

Figure 24: Wing planform and mountings

6.2.4 Airfoil Selection

The driving parameter in airfoil selection is the $C_{L_{des}}$, the design lift coefficient during cruise. The airfoil should be chosen such that drag is minimal at $C_{L_{des}}$ and is determined as follows:

$$C_{L_{des}} = \frac{1.1}{q}\left(\frac{1}{2}\left[\left(\frac{W}{S}\right)_{start,cruise} + \left(\frac{W}{S}\right)_{end,cruise}\right]\right) \tag{22}$$

Note that Equation 22 determines the design lift coefficient for the entire wing. However this needs to be translated to the airfoil design lift coefficient $C_{l_{des}}$ by taking into account the sweep angle Λ. Furthermore, $C_{l_{des}}$ needs to be corrected for compressibility effects as the cruise Mach number M_{cruise} is 0.75 and it was now calculated for stationary flow ($M = 0$). This is done by the Prandtl-Glauert correction. Both corrections are shown in Equation 23.

$$C_{l_{des}} = \frac{C_{L,des}}{cos^2\ \Lambda} \qquad C_{l_{des,M=0}} = C_{l_{des}}\ \sqrt{1 - M_{cr}^2} \tag{23}$$

To select a number of suitable airfoils for the wing, some parameters that are favorable were set up. These criteria are as follows:

- Wide drag bucket at $C_{l_{des}}$
- Large $C_{l_{max}}$
- No steep drop in C_l after stall
- Low C_m at $C_{l_{des}}$
- Large t/c
- High M_{cr}
- Large C_l / C_d at $C_{l_{des}}$

The criteria come forth from the desire to have a large lift-to-drag ratio at multiple angles of attack and speeds are the wide drag bucket, a large $C_{l_{max}}$, no steep drop in C_l after stall, a high M_{cr} and noticeably a large C_l / C_d at $C_{l_{des}}$. To have better airfoil stability, a C_m

As the cruise Mach is in the transonic region ($M_{cruise} = 0.75$) , airfoils are preferred that minimize heavy shock wave behavior and therefore drag. These airfoils are called supercritical. This causes supersonic flow to have a more constant pressure coefficient C_p along the topside. Hence, no large drop in pressure back to subsonic flow occurs.

5 airfoils were selected, of which 4 are supercritical. They were modeled in XFLR5, which is airfoil analysis software. In this program the C_p-distribution along the airfoil, the lift curve, the lift-drag curve, the $C_l - C_m$ curve and the $C_l/C_d - C_l$ curve could be visualized. The program takes as input the Reynolds number, which is calculated as follows:

$$Re = \frac{\rho \, V_{TAS_{cruise}} \, MAC}{\mu} \tag{24}$$

All criteria except for M_{cr} are taken from XFLR5 directly. M_{cr} is determined by taking the minimum C_p at $\alpha = 0$ (visible in Figure 25), and is then corrected for compressibility, such that $C_{p,0}$ at the cruise Mach is obtained. For this the Prandtl-Glauert correction from Equation 25 is used. Then, $C_{p,0_{M_{cruise}}}$ is set equal to $C_{p_{cr}}$ and with Equation 26 the critical Mach number is calculated.

$$C_{p,0_{M_{cruise}}} = \frac{C_{p,0_{M=0}}}{\sqrt{1 - M_{cruise}^2}} \tag{25}$$

$$C_{p,0_{M_{cruise}}} = C_{p_{cr}} = \frac{2}{\gamma \, M_{cr}^2} \left[\left(\frac{1 + \frac{\gamma-1}{2} M_{cr}^2}{1 + \frac{\gamma-1}{2}} \right)^{\frac{\gamma}{\gamma-1}} - 1 \right] \tag{26}$$

The criteria that were used and corresponding weights and scores for each airfoil are summarized in Table 17. The weights are determined by relative importance and scoring is done qualitatively on a 1,4,6,9 basis. All airfoils are analyzed at a Reynolds number of $20 \cdot 10^6$, which corresponds to cruise conditions. However the software is inaccurate for compressible flow and therefore comparison is done for stationary flow ($M = 0$). Because of this, values like $C_{l_{max}}$ will be overestimated but can still be used for comparison.

Table 17: Airfoil trade-off

Airfoil	Wideness of drag bucket	$C_{l_{max}}$	Stall behaviour	C_m @ $C_{l_{des}}$	t/c	M_{cr}	C_l / C_d @ $C_{l_{des}}$	
Weight	0.1	0.25	0.2	0.05	0.05	0.2	0.15	**Total**
NASA SC (2) 0714	9	9	1	9	4	4	4	4.8
NASA SC (2) 0614	9	6	4	6	4	6	6	**4.9**
NASA SC (2) 0518	1	6	6	4	9	6	4	4.65
DFVLR R-4	9	4	4	4	1	9	9	4.75
NACA 63(3)-618	4	1	9	4	9	6	4	4.3

The resulting airfoil from the procedure is visibly, the NACA-SC(2)0614 supercritical airfoil. Although this airfoil scores average in most criteria, it still outperforms the others. The airfoil together with the pressure distribution at zero angle of attack is shown. Figure 26 shows the lift curve of the airfoil.

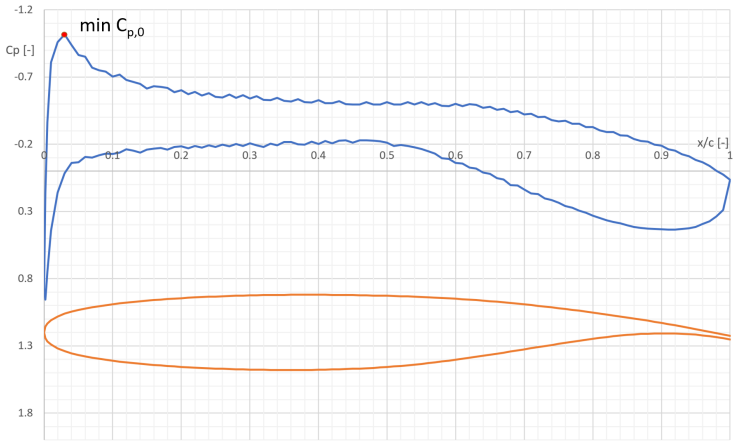

Figure 25: The pressure distribution along the NACA-SC(2)0614 supercritical airfoil at $Re = 20113773$, $M = 0$ and $\alpha = 0$. The minimum pressure point is denoted by $C_{p,0}$

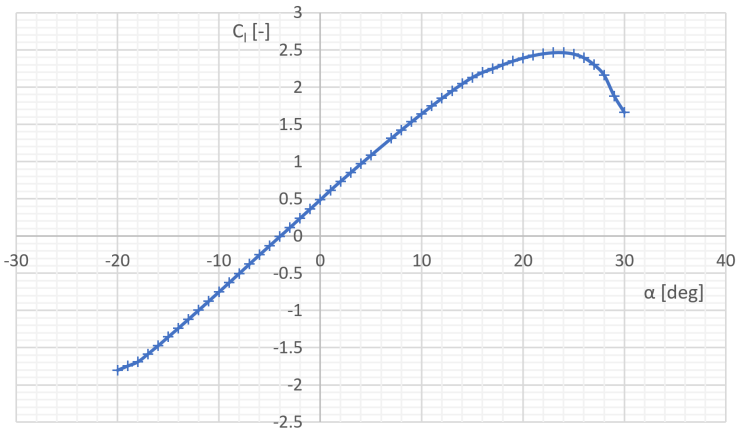

Figure 26: Lift curve of the NACA-SC(2)0614 airfoil at $Re = 20113773$ and $M = 0$

6.2.5 High-lift Devices

Sizing One of the key and most vital steps in aerodynamic analyses of airborne vehicles is high lift devices sizing. The airfoil along with its characteristics in clean configuration are presented before, in Section 6.2.4. After CL_{des} estimation and equivalent wing-to-airfoil conversion, the required CLmax values emerge for all three configurations, shown in Table 18. Consequently, the desirable flap device is chosen using Table 19. As is highlighted, the plain flap was proven to be ideal in the specific case of the aircraft design, and so the mechanism along with the deflection angles in take-off and landing conditions are shown in Table 27.

Table 18: $C_{L_{max}}$ requirement for the three configurations

Configuration	$C_{L_{max}}$
Clean	1.8
Take-off	2.1
Landing	2.25

Table 19: Contribution of ΔCL_{max} for different high-lift devices [35]

High-Lift device	ΔCL_{max}
TE devices	
Plain & Split	0.9
Slotted	1.3
Fowler	1.3c'/c
Double Slotted	1.6c'/c
Triple Slotted	1.9c'/c
LE devices	
Fixed Slot	0.2
LE Flap	0.3
Kruger Flap	0.3
Slat	0.4c'/c

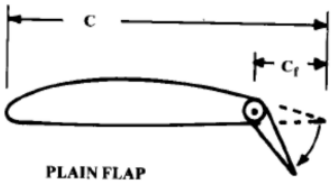

Typical deflection angles	
Take off	Landing
20 deg	60 deg

Figure 27: Plain flap formation [35]

It should be mentioned that increasing the maximum lift coefficient is not the only result of adding flaps, but so is a steeper slope, and hence a different Cl-α relation. In fact, the entire graph is translated both vertically and horizontally resulting in both a higher Cl_{max} and a $\alpha_{Cl=0}$ translated to the left. Figure 28 portrays the resulting lift curve. Having gone through the selection process for high lift devices, the team then moves forward towards the application and sizing of it in the three-dimensional wing planform.

$$\Delta C_{L_{max}} = 0.9 \cdot \Delta C_{l_{max}} \cdot \frac{Swf}{S} \cdot \cos \Lambda_{hingeline} \tag{27}$$

$$\Delta\alpha_{CL=0} = (\Delta\alpha_{CL=0})_{airfoil} \cdot \frac{Swf}{S} \cdot \cos\Lambda_{hingeline} \tag{28}$$

The high-lift devices are applied on the hingeline of the wing, which in the airfoil cross-section is the spar face, and is at a chordwise location $0.25\bar{c}$ from the trailing edge, as is the conventional setup [35]. Equation 27, and Equation 27 are the next step in the procedure, where all is now known and one solves for Swf. The unknown represents the wing area occupied by the high-lift device. It should not be mistaken for the area of the device itself, as it is the whole wing area, from trailing edge to leading edge, in which a device is present. Hence, knowing the chordwise flaps range from literature as mentioned above, and now the spanwise flaps range from the above calculation, the high-lift devices are now sized to an actual covered area of 24.3 m^2. At this milestone, the aerodynamic analysis now checks the effect of the high lift devices to the lift curve of the wing, referring to Figure 28.

$$C_{L_{\alpha_{flapped}}} = C_{L_{\alpha_{clean}}} \tag{29}$$

Firstly, all 3 graphs have parallel slopes, the indicator of identical C_{L_α} derivative. This is a result of Equation 29, which states the new slope is unchanged to the clean one, and is because the flaps are non-expandable. If the flaps were in Fowler formation for example, upon deployment the area also increases since a layer expands further to the back.

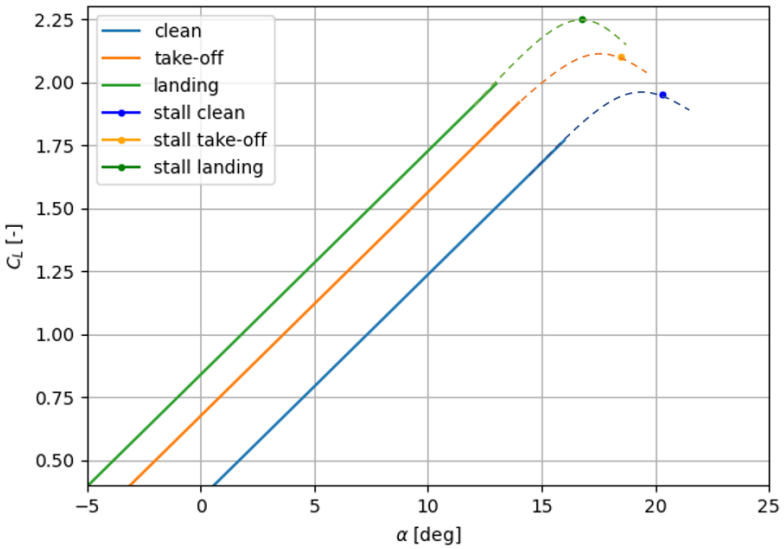

Figure 28: Wing lift curves for clean, take-off and landing configuration

Then, with respect to the plot, the lowermost lift curve represents the clean configuration performance RELIGHT. One will notice, though, that it is slightly altered from the one in Figure 26. This is the result from the conversion of airfoil to wing geometry, which is dictated by the DATCOM method [35]. Following that, are the two adjacent graphs in the plot. The one in the middle and the one directly above it represent the take-off and landing configuration respectively. Since both top curves represent configurations with flaps deployed, there is still margin between them because the topmost one representing the landing configuration occurs at a larger flap deflection than during take-off. The margin between curves is also not linear with flap deflection since the difference between take-off and landing condition flap angles is larger than between take-off and clean condition but the opposite is true for the margins between the curves in Figure 28. One will notice that no leading edge high lift devices were considered. For this decision the effects of the different devices are considered. Trailing edge devices significantly alter the lift, by their lowering, and the creation of a new chord line, that leads to a higher virtual angle of attack. Leading edge devices delay the stall angle of attack, which affect lift at a lower level and is mostly applicable for the manipulation of the stall condition. Since the maximum lift coefficient reached a desirable value with the current flaps design and the high-lift airfoil selection, no slats were needed for lift contribution and most importantly, looking at Figure 28, one notices

a stall angle shift that did not prove drastic or abrupt upon flap deployment. Hence slats were also deemed unnecessary for stall condition improvement.

Clearance After sizing and placing the high lift devices along the planform, certain considerations take place, regarding their integration with the surrounding systems. Section 6.2.3, portrays the high lift devices set up as sized in Section 6.2.5. In the wing, however, also are mounted engines, and external wing tanks. This layout generates further clearance check. Should there need to be a split of the flap in two parts by the external wing tanks for example, the clearance causes a decrease in ΔCL_{max}, which will consequently call for compensation in the form or slats or other devices, for which there is still space. From documentation of the Hercules C-130 aircraft [12], and the Boeing 777 aircraft [13], it is determined that the flaps on the planform can remain hinged and functioning behind both the engines and the external wing tanks either in the current form, or in the form of flaperons for additional roll rate. The reader should note that those vehicles are not of equivalent wing planform dimensions or mission as RELIGHT but their structural layout suggests that podded tank placement does not require a gap in high-lift devices behind them and this is that conclusion of this section.

6.2.6 Drag Characteristics

Then, with all lift characteristics done, the drag characteristics of RELIGHT are evaluated. The drag polar consists of two terms, the zero-lift drag C_{D_0} and the lift-induced drag and is calculated by using Equation 30, which also includes the AR and the oswald efficiency factor e.

$$C_D = C_{D_0} + \frac{C_L^2}{\pi\ AR\ e} \tag{30}$$

Zero-Lift Drag The zero-lift drag of the aircraft consists of a number of terms and is evaluated by using the component drag build up method. For this the following equation is established [35]:

$$C_{D_0} = \frac{1}{S_{ref}} \sum_c C_{f_c} \cdot FF_c \cdot IF_c \cdot S_{wet_c} + C_{D_{misc}} \tag{31}$$

In Equation 31 the first sum includes for different components c the skin friction coefficient C_{f_c}, the form factor c, the Interference Factor IF and the wetted area S_{wet}. Components that are evaluated using the component build up method from Raymer (1999) are the main wing, the tail wings and the fuselage [36]. As for the engine nacelle, its wetted area was estimated with the method from Torenbeek (1973) [37], but the other factors were also taken from Raymer. Evidently, the drag increment of the fuselage pods is of main interest. The pods have a cylindrical shape with cones on the ends, assumed to have the surface area of a hemisphere. Its componental factors are:

$$C_{f\,pod} = \frac{0.455}{log_{10}(Re)^{2.58}}(1 + 0.144M_{cruise}^{0.65}) \qquad FF_{pod} = 1 + \frac{0.35}{\lambda} \qquad \lambda = \frac{l_{pod} + Diam_{pod}}{D_{pod}} \tag{32}$$

$$IF_{pod} = 1.3 \qquad S_{wet_{pod}} = \pi Diam_{pod} l_{pod} + \pi Diam_{pod}^2 + 2h_{pylon} l_{pylon} \tag{33}$$

After similar calculations for the other main components, the total sum is then divided by the reference wing area S_{ref}, and a term for miscellaneous drag components is added. Some miscellaneous terms are added as seen in Equation 34: the drag due to fuselage tail upsweep $C_{D_{upsweep}}$, the wave drag $C_{D_{wave}}$ and drag due to excrescence and leakage $C_{D_{leakage}}$[35][36].

$$C_{D_{misc}} = C_{D_{upsweep}} + C_{D_{wave}} + C_{D_{leakage,excresence}} \tag{34}$$

Both wave drag and leakage/excrescence increments were calculated using the methods from ADSEE II [35][36]. The wave drag calculation resulted in M_{cruise} not being larger than M_{dd}, the drag divergence Mach number. Consequently, this lowers the drag. The leakage and excrescence factor was taken as a $1.02 \cdot C_{D_0}$,

[12] https://www.lockheedmartin.com/content/dam/lockheed-martin/aero/documents/C-130J/C130

[13] https://www.flightglobal.com/boeing-777-aircraft-profile/76641.article

but could be as high as 1.05. Concerning the upsweep, after some research, it was found to be quite different for different sources. In the end the following approach was taken [38][14]:

$$C_{D_{upsweep}} = 0.075\ (h/l)_{.75l_t} = 0.075\ \frac{0.75\frac{D_{fus}}{2}}{l_{fus}} \tag{35}$$

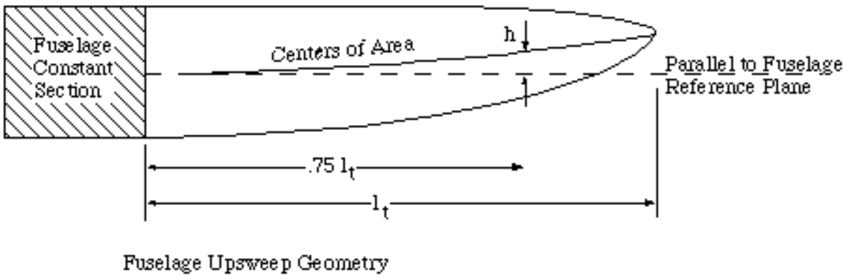

Figure 29: Paramaters used for the upsweep drag [38]

Finally, estimations were done fore landing and take-off configurations, to see how these increase the drag. When the landing gear is deployed, quite some drag is added. This is calculated as follows [35][36]:

$$C_{D_{gear}} = \frac{n_{wheels}\ (D/q)_{front}\ S_{ref_{gear}} + (D/q)_{strut}\ S_{ref_{strut}}}{S} \tag{36}$$

To clarify Equation 36, D/q is the drag area, S_{ref} is the reference frontal area, i.e. a box is drawn around the gear. S is simply the main wing area.
The second drag addition in take-off and landing comes from flap deployment and it is estimated as follows:

$$C_{D_{flap}} = 0.0144\ (S_{flap}/S_{ref})(\delta_{flap} - 10) \tag{37}$$

The results of the component build up method for C_{D_0} are summarized in Table 20. Note how first C_{D_0} is shown and then the percentage of the total zero lift drag. Also note how in take-off and landing the deployed gear and especially flaps take up a considerable portion. Figure 30 shows the zero-lift drag component build up during cruise.

Table 20: Component build up of C_{D_0}

Component	C_{D_0}	% **of total**	**Miscellaneous**	**CD0**	% **of total**
Wing	0.00523	22.80	Upsweep	0.00350	15.26
Horizontal tail	0.00201	8.76	Wave drag	0.00054	0.0377
Vertical tail	0.00114	4.98	**Additional**	**CD0**	% **of total**
Engine nacelle	0.00271	11.79	Landing gear	0.00354	13.40
Fuselage	0.00624	27.20	Flaps at take-off	0.05625	67.223
Pod fuel tanks	0.00112	4.88	Flaps at landing	0.28124	91.11

[14] http://aerodesign.stanford.edu/aircraftdesign/drag/upsweepdrag.html

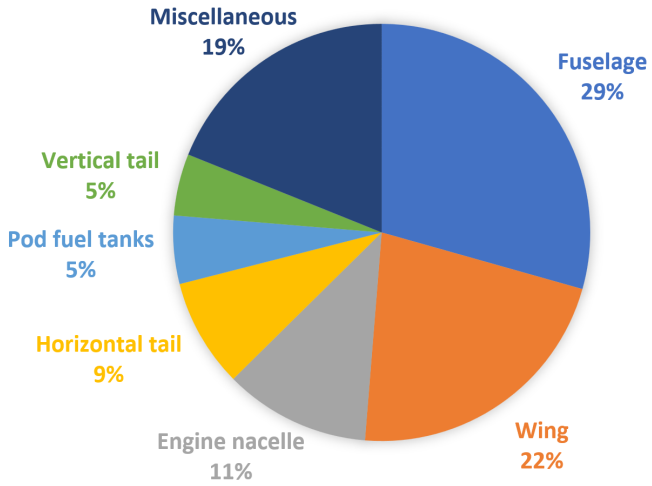

Figure 30: RELIGHT's zero-lift drag component build up for cruise

Lift-induced Drag The Oswald efficiency factor, being a vital factor to the lift induced drag calculation, has different approaches to obtaining it. Namely, the DATCOM method [39], that is shown in Equation 38, and the two other equations, retrieved from TU Delft Aerospace Engineering material [35], Equation 39, and Equation 39. Equation 38, depends on the C_{L_α} slope, the AR and the ratio labeled R, which physically represents the leading edge suction acquired over the one theoretically possible [39]. The latter can be obtained graphically from empirical data of Reynolds numbers. Unfortunately, for this specific aircraft design, the Reynolds number is too high compared to the available range so the DATCOM method, although the most accurate, cannot be used here.

$$e = \frac{1.1 \cdot (C_{L_\alpha}/A)}{R \cdot (C_{L_\alpha}/A) + (1 - R) \cdot \pi} \tag{38}$$

Hence, the estimation proceeds with Equation 39 and Equation 40, shown below. They are dependent upon AR and sweep angle of the leading edge. Equation 40 concerns swept wings and this specifically refers to sweep angles larger than 30 degrees. Therefore, the designed wing is applicable to Equation 39. One therefore, obtains an estimate for the factor in clean configuration. After that, the effect of flap deflection is considered, with adding Δe from Equation 41 to Equation 39. As a result, the factor is also obtained for both the take-off configuration with deflection angle 20 degrees, and landing configuration with deflection angle of 60 degrees, and all are listed in Table 21.

$$e = 1.78 \cdot (1 - 0.045 \cdot A^{0.68}) - 0.64 \tag{39}$$

$$e = 4.61 \cdot (1 - 0.045 \cdot A^{0.68}) \cdot (\cos(\Lambda_{LE}))^{0.15} - 3.1 \tag{40}$$

$$\Delta e = 0.0046 \cdot \delta f \tag{41}$$

Table 21: Oswald factor per configuration

	e
Clean	0.811
Take-off	0.812
Landing	0.815

Drag Polar Finally, the drag polar is obtained as being:

$$C_D = 0.0238 + 0.0491 \ (C_L - C_{L,Dmin})^2 \tag{42}$$

Equation 42 takes into account a translation in the drag curve that occurs due to the wing lift coefficient at minimum drag $C_{L,Dmin}$. This effect is caused by camber, i.e. the larger the airfoil camber the larger $C_{L,Dmin}$. The airfoil that was selected has a camber of 2.1%, however the $C_{L,Dmin}$ calculation for this is very extensive [40]. Therefore known $C_{L,Dmin}$ data for an airfoil with 3.2is taken and translated to the selected airfoil [41]. This results in $C_{L,Dmin} = 0.1273$. Figure 31a and Figure 31b show, for the entire aircraft, the drag polar and lift-to-drag ratios at each lift coefficient, respectively. Note however that the lift-to-drag ratio is not maximal

at the design lift coefficient ($C_{L_{des}} = 0.4567$). Instead, $L/D_{max} = 17.51$. This occurs at $C_L = 0.71$, which would either result in a lower cruise speed or a higher altitude. Therefore it is chosen to remain at the design lift coefficient and hence $L/D_{cruise} = 15.6371$.

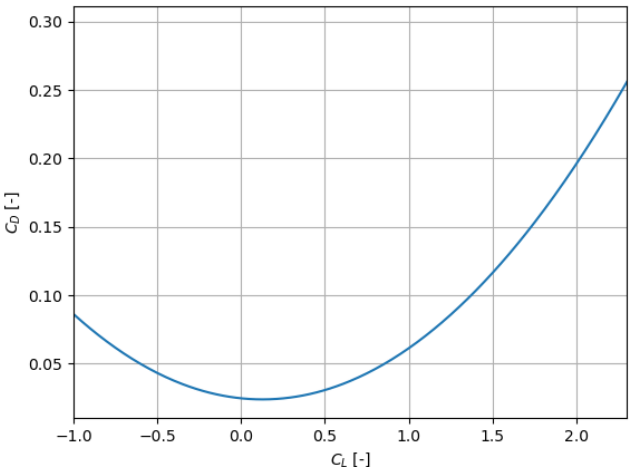

(a) Drag polar of RELIGHT

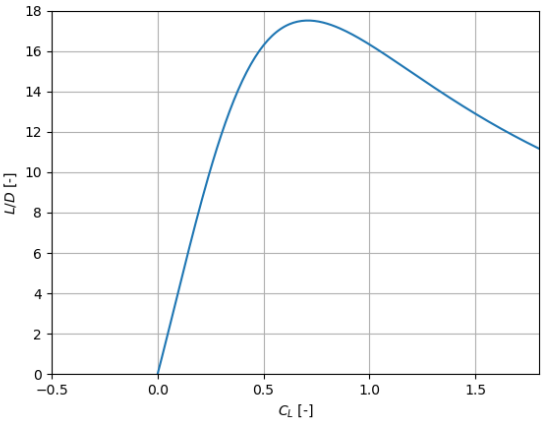

(b) RELIGHT's lift to drag ratio versus C_L

6.2.7 Aerodynamic Verification & Validation

To verify both the lift and drag calculations, several input variables are increased and the effect is estimated. If the result is as expected, a Pass is given. Otherwise, in case of a Fail, the code is revised. The verification is summarized in Table 22. Note how the expected results represent the lift, drag, airfoil and HLD parameters.

Table 22: Verification of the wing sizing calculations

Function	Action	Expected result	Pass/Fail
Wing design			
	increase $MTOW$	L/D decreases, C_{D_0} increases	Pass
	increase S	L/D increases, C_{D_0} decreases	Pass
	increase sweep	t/c increases, S_{wf}/S decreases	Pass
	increase AR	L/D increases, C_{D_0} increases	Pass
	increase D_{fus}	L/D decreases, C_{D_0} increases	Pass

To validate the lift and drag characteristics, a look is taken at reference aircraft. First of all, the L/D_{max} for the Bombardier CRJ200-ER is about 17.5 [42]. The design range of the CRJ200 is only 491 km more than RELIGHT's and has slightly less passengers than the CRJ700 (50 instead of 78), but is shape-wise very similar to the CRJ700. Therefore this validates RELIGHTS L/D_{max} of 17.51. Concerning the drag polar, for RELIGHT, C_{D_0} is about 0.024 and the k-value ($1/\pi ARe$) is about 0.05. Taking a look at statistics, ranging from the A320 to the B737, usually the zero-lift drag coefficient is in the range from 0.02 to 0.03, which validated RELIGHT's value [43]. As for k, it seems to be somewhat larger than the reference (which is about 0.045 at most), however RELIGHT's AR is even larger than the A388 ($AR = 7.5$) [43], and hence the value is validated.

6.2.8 Aerodynamic Sensitivity Analysis

To test how an increase in certain inputs influences the outputs of the lift and drag calculations, a sensitivity analysis is carried out. The main parameters for which the sensitivity is tested in every technical department are changes in MTOW, Thrust. As a the cg location is only determined after the wing is sized, it does not have a direct influence, only through the snowball effect. The whole point of the sensitivity analysis is to neglect this effect and search for direct influence only. As extra parameters, a change in AR and M_{cruise} are investigated, as they have a significant impact on lift and drag characteristics. Also, these values are estimated, even though the estimation might be well-substantiated. The sensitivity will be reflected through parameters that follow from the wing requirements. As requirements SRA-SYS-WAero-01 and SRA-SYS-WAero-02 already dictate the airfoil selection, which is done in Section 6.2.4, they are not mentioned here.

However, following from the remaining requirements, compliance is tested for: the Mach drag divergence number (M_{dd}), the wing span and the landing gear drag partition. For M_{dd} it will be checked if M_{cruise} does not surpassed, as drag is increase massively. As can be seen in Table 23, no inputs are marked red and hence all alterations comply with the requirements. Also, some alterations have no effect at all.

Table 23: Sensitivity analysis results for the aerodynamic calculations

Parameter	**value**	MTOW +10%	MTOW - 10%	Thrust +10%	Thrust -10%	AR +10%	AR -10%	M_{cruise} +10%	M_{cruise} -10%
b	22.316	-	-	-	-	+ 4.88	-5.13	-	-
M_{dd}	0.803	-0.78	+0.78%	-	-	-	-	+ 7.41%	-8.06%
$C_{D_{0,gear}}\%$	12.938 %	-0.18%	+0.16%	-0.001%	+0.027%	-0.35%	+0.38%	-0.10%	- 0.25%

6.2.9 Requirements Compliance

Earlier, in Section 6.2.1 the top level requirements were listed with the critical ones highlighted in green. Having approximated the design lift coefficient using the wing loading, the transformation to the equivalent airfoil value is made, as well as the correction for compressibility using Equation 23. The result is then the primary factor for the airfoil selection. Section 6.2.5 then gives a step-by-step thought process behind the airfoil selection and the resulting $\Delta C_{L_{max}}$ value obtained for the different configuration. The obtained lift curves showed in Figure 28, portray the success in achieving a C_{Lmax} of 2.25, which fulfills SRA-SYS-WAero-01. Similarly, the same plot gives the $C_{L_{max}}$ for the other two configurations, and so it is also visible that the value of 1.8 in clean configuration is achieved, which deems SRA-SYS-WAero-02 fulfilled. Furthermore, estimating the wingspan and obtaining the cruise speed requirement from the envelope, also gets requirements SRA-SYS-WAero-03, and SRA-SYS-WAero-04 met. After this sizing process Section 6.2.6 takes place, obtaining the drag characteristics and thus finalizing the aerodynamic analysis which, in turn makes available the outputs of $C_{L_{des}}$, $C_{L_{max}}$, C_{d_0}, C_{L_a}, and L/D. The last requirement that is complied with, is SRA-SYS-LG-06, between the primary requirements in the beginning of this section. From the drag characteristics, and specifically from Table 20, the additional segment mentions a landing gear drag contribution of 13.4%, coming at just under 15%. Hence, all top-level requirements that guided the wing planform sizing procedure and the aerodynamic analysis are met.

6.2.10 Component Weight Estimation

Having completed the development of the wing planform subsystem, the sizing is placed in queue, using the Class II weight estimation algorithm. Referring to Table 12, the aerodynamics department has obtained an overall wing group mass of 2349.5kg, occupying 8.4% of the maximum take-off weight. The result sources from both the detailed sizing of this section, taking into account sweep, flaps, hinges, and ailerons, but also from the structural analysis of the design.

6.2.11 Aerodynamic Recommendations

First of all, although the chosen L/D ratio for cruise is near the one predicted in the Class I weight estimation, the maximum L/D ratio possible is much larger. This implies that the wing has been oversized. This thought also arises from the high-lift device sizing, where large flaps and slats were not required. If the L/D ratio is increased to the maximum, the angle of attack increases to as much as $\alpha = 4.06\ deg$. Also the lift coefficient increases by almost 100% changing either the cruise speed or altitude and other characteristics with it. Therefore it is recommended that a more advanced analysis on lift and drag is done. However still, a benefit is that the payload-range diagram shows a larger margin for the design range, which lowers the fuel burn per passenger kilometer, which is important for both environmental and economical sustainability.

As mentioned before, no large high-lift devices are needed. About 40% for the wing had to be occupied by trailing-edge devices, whereas most aircraft today make use of flaps and slats along a larger part of the span. For that reason, the most simple flaps available were chosen, to not overdesign the wing and to drive the cost down. However, by only selecting plain flaps, the stall angle is lowered and the drag is increased substantially (see Table 20). Therefore, investigation into leading edge slats should be done to increase to the desired stall angle. Also, flaps should be designed to not increase the drag during landing by a significant amount.

The under-wing fuel pod tanks feature a cylinder-shaped design with hemispheres on both ends. Even though

the drag portion is only 5.27%, this could be lowered. It should be investigated whether use of drag lowering and/or anti-shock bodies (Küchemann bodies) would be advantageous. Also, the interference drag with the wing should be assessed. Furthermore , the pod tanks' contribution to both lift and lift-induced drag is recommended to be investigated. Also, more data could be found on podded fuel tank aircraft to verify the estimation.

Few high wing aircraft feature winglets, which would suggest that it has little advantages. However the lift-induced drag decrease should be investigated. Also, the effects of twist on the lift distribution as well as making use of different airfoils, could be beneficial and should be researched

6.3 Propulsion System Design

The propulsion system contains the fuel tanks, fuel system and engines. The main purpose of this system is to deliver the required thrust force during the different flight phases. The engine design is given in Section 6.3.3. Then the hydrogen tanks are configured in Section 6.3.4 and, finally, the fuel distribution is given in Section 6.3.5.

6.3.1 Guiding System Considerations

The aim of the propulsion system design is to generate a component configuration that delivers the required thrust whilst minimizing weight, emissions and fuel cost.

In Section 5.3 it was decided to go for a 100% liquid hydrogen aircraft. This means the hydrogen will need to be stored as a cryogenic liquid ($20K$). This will change the propulsion/power systems design considerably as liquid hydrogen has different properties to the conventional kerosene jet fuel. Liquid hydrogen is highly flammable, needs to be stored at very low temperatures (thus a heat exchanger is required before combustion) and is highly volatile. The specific energy is roughly three times as high, while the mass density as roughly a tenth of kerosene, resulting in a hydrogen mass required which is a third of kerosene, but at the same time having more than three times the volume.

6.3.2 Preliminary Requirements

The initial set of requirements for the propulsion system was established during the earlier stages of the project. They are presented in the table below. It can be seen that these are the top level requirements guiding the system behavior. he driving requirements are highlighted in green.

Table 24: Propulsion System requirements

Requirement Identifier	Requirement	Compliance
	Propulsion System	
SRA-SYS-PROP-01	The propulsion system shall provide enough thrust to achieve steady, level flight at cruise altitude.	✓
SRA-SYS-PROP-02	The propulsion system shall provide enough thrust to achieve take-off for a runway length of 1500 m.	✓
SRA-SYS-ENY-02	The energy system shall be able to be replenished up to capacity between flights.	✓
SRA-SYS-ENY-03	The energy system shall provide the required energy for propulsion.	✓
SRA-SYS-ENY-04	The energy system shall at least have one redundant distribution subsystem.	✓
SRA-SYS-PROP-03	The propulsion system shall allow for controlling the amount of impulse delivered.	✓
SRA-SYS-ENY-01	The energy system shall control the flow of energy throughout the operation of the aircraft.	✓

6.3.3 Engine

A high wing configuration was chosen which allows for high bypass turbofans, increasing the propulsive efficiency. In design, the hydrogen turbofan shows large similarities to its conventional counterpart, with inlet, compressors, combustion chambers, turbines and core versus bypass flows. Significant differences exist in the lower Turbine Entry Temperature (TET), the addition of a heat ex-changer, and the specific fuel consumption.

Previously the team has decided to opt for a full hydrogen turbofan design to propel the aircraft [4]. This has several implications that factor into the considerations required to achieve the subsystem's aims. First of all the thrust can be achieved in a multitude of ways, strongly influenced by the bypass ratio that determines how the work extracted by the turbine is distributed between the core jet and the fan. More core thrust implies lower fuel efficiency at a more compact design and lower frontal intake area. This influences the total size of the engine and therefore the weight. Minimizing weight is important as this parameter will influence all other subsystems and their size. This can lead to a snowball effect that may result in building an overly large system. This results in failing to achieve the other aims, by requiring more thrust and therefore a higher fuel flow rate. Since the aircraft concept is going with a high wing design, considerations involving engine clearance and therefore size constraints were not taken into consideration.

Keeping emissions as low as possible is one of the key aspects to consider, as this is one of the driving requirements for the aircraft design in general. Propulsion plays a key role in this aspect, as the combustion chamber is where such emissions would be generated. Emissions strongly depend on the type of fuel used and the amount of fuel consumed. The amount of fuel consumed clearly has a strong influence on the cost of operation, therefore emissions and fuel cost are closely linked. With the team's decision to go for a fuel hydrogen configuration, emissions are reduced significantly, however this only holds true if the hydrogen consumed is produced without emissions. As this will not always be the case it is still advisable to reduce the consumption of hydrogen in the engine to as low as possible, helping reduce the fuel expenses also. Therefore the aim to minimize emissions and operational costs can be expressed by trying to maximize the fuel efficiency of the resultant engine design. This efficiency can be expressed as specific fuel consumption, which has the units of g/kN.
Specific fuel consumption is strongly influenced by several design parameters. A high bypass ratio increases the efficiency through generating a larger proportion of the total thrust by the fan, which is more efficient. However this means that the fan requires more energy from the turbine as well as generally increasing the size of the engine and therefore weight of the subsystem. A high combustion temperature will require a higher fuel consumption, on the other hand it makes more energy available to be extracted by the turbine. The total mass flow going through the engine has a major influence on the thrust produced as well as the total fuel consumption. Generally speaking it is therefore desirable to produce as much thrust as possible with the fan, through a high bypass ratio, ensuring that the combustion temperature is high enough to provide enough energy to power it, whilst keeping the total mass flow as low as possible.

Engine Requirements The engine design is based on a set of requirements that need to be satisfied to ensure successful mission execution. The required thrust at take-off, based on the Class II parameters and the updated power loading diagram, a thrust of $121000N$ is needed. This means for a two-engine configuration each engine needs to produce a thrust of $60.5kN$. If this requirement is met, then the aircraft would be able to satisfy the top level requirement of having a take-off distance lower than $1500m$ at a runway altitude of $1500m$. In case on one engine failing, the thrust generated by one engine should be enough to continue the mission and perform landing. Table 25 showcases the more precisely specified engine requirements as derived from the top level requirements.

Table 25: Propulsion System Requirements

Requirement Identifier	Requirement	Compliance
	Concept Requirements	
SRA-PSR-1	The system shall be a turbofan engine.	✓
SRA-PSR-2	The system shall use cryogenic hydrogen as fuel source.	✓
	Driving Requirements	
PSDR-1	The system shall deliver 65 kN of thrust at 1500 m altitude.	✓
PSDR-2	The bypass ratio shall not be greater than 12. [15]	✓
PSDR-3	The emissions produced by the system shall be at least 25% lower than the engines used by the CRJ700.	✓
PSDR-3.1	The system shall produce not less than 50% of total net thrust through the fan.	✓
PSDR-3.1.1	The system shall have a bypass ratio of at least 10.	✓
PSDR-3.2	The system shall burn as little fuel as possible.	✓

Table 26: Engine component requirements

Requirement Identifier	Requirement	Compliance
	Component Requirements	
PSCR-1	The inlet efficiency shall not be lower than 0.97	✓
PSCR- 2.1	The fan efficiency shall not be lower than 0.85	✓
PSCR- 2.2	The fan compression ratio shall be 1.4	✓
PSCR- 3.1	The low pressure compressor (LPC) efficiency shall not be lower than 0.9	✓
PSCR- 3.2	The low pressure compression ratio shall be 2	✓
PSCR- 4.1	The high pressure compressor (HPC) efficiency shall not be lower than 0.87	✓
PSCR- 4.2	The high pressure compression ratio shall be 10	✓
PSCR- 5.1	The combustor efficiency shall not be lower than 0.99	✓
PSCR- 5.2	The combustor pressure loss shall not be higher than 4%	✓
PSCR- 6	The mechanical efficiency shall not be lower than 0.99	✓
PSCR- 7	The gear box efficiency shall not be lower than 0.95	✓
PSCR- 8	The low pressure turbine (LPT) efficiency shall not be lower than 0.89	✓
PSCR- 9	The high pressure turbine (HPT) efficiency shall not be lower than 0.89	✓
PSCR- 10	The efficiency of the nozzel shall not be lower than 0.98	✓

Engine Modeling Procedure and Sizing The engine was modeled analytically using conventional thermodynamic relations to find the total temperature and pressure at various stations through the turbofan. The model allows for alteration of engine configuration, conveniently allowing real time updated values at all stations when changing a parameter.

This approach ensured that engine performance could quickly be assessed at different stages during the mission profile. The two main stages considered were at $1500m$, just after take-off (just abbreviated as take-off) and top of the climb (abbreviated as simply cruise condition). Table 27 shows typical inputs. The temperature, pressure and speed follow from the investigated speed and altitude. For the cruise condition the mach number was exchanged for the speed, where the other value would be calculated from the respective input.

Table 27: Inputs for take-off at 1500m altitude

Inputs for Take-off (1500 m altitude)		
Flight inputs		
T	278.4	K
P	84556	Pa
V	69.3	m/s
Design Inputs		
BPR	10	-
T04 (Combustion Temperature)	1200	K
Inlet Diameter	2.285	m

The design inputs were varied greatly in the modeling process as they confound the amount of thrust produced, as well as the specific fuel consumption. The inlet diameter determines the total mass flow through the engines and both thrust and size could be altered this way. The burning temperature had a large impact on SFC, and initially it seemed that ensuring the turbines were able to extract sufficient energy was the only constraint set on the minimum temperature. More on this will be presented later. The mass flow into the engine was determined with the following equation:

$$\dot{m} = \rho V A \tag{43}$$

After setting up all relevant inputs, the stations were modeled with the according equations. First the intensive state variables were assessed at the inlet for this following equation was used:

$$p_{0,inlet} = p_0 \left(1 + \eta_{eff} \frac{\gamma - 1}{2} M^2\right)^{\frac{\gamma}{\gamma - 1}} \tag{44}$$

In order to accommodate for disparities between theoretical thermodynamic cycles and real cycles, efficiencies were introduced to account for losses. These efficiencies were chosen based on conventional values and set as requirements to ensure that the engine design would be achievable with conventional components.

After this the compressor stages were computed. Since the pressure ratios were set by the requirements (1.4 for the fan, 2 for the low pressure compressor and 10 for the high pressure compressor), only the temperature needed to be calculated, as the pressures after the stages follow straight forwardly from the pressure ratios. The temperature was calculated with the following equation.

$$\frac{T_2}{T_1} = 1 + \frac{1}{\eta_{is}} \left[\left(\frac{p_2}{p_1} \right)^{\left(\frac{\gamma - 1}{\gamma}\right)} - 1 \right] \tag{45}$$

Knowing the temperature rise over the compressors, the work required for every stage can be calculated with the following equation:

$$\dot{W} = (\dot{m}_{core}\{+\dot{m}_{fuel}\}) \cdot c_{p,a/g} \cdot (T_{0,end} - T_{0,start}) \tag{46}$$

In order to determine the fuel mass flow the following equation can be used:

$$\dot{m}_{air} \cdot c_{pg} \cdot \Delta T_{cc} = \eta_{cc} \cdot \dot{m}_{hydr} \cdot LHV_{hydr} \tag{47}$$

With this $\dot{m}_{hydr}$ can be determined based on the lower heating value of hydrogen, the difference in temperature between the combustion temperature and the inlet temperature as well as the combustion efficiency. Here the specific heat capacity for hot combustion gases was determined based on a weighted average of hydrogen and air with respect to their approximate proportions in the mixture.

Dividing the work for the individual stages by the mechanical efficiency determines the work for the turbine. Together with the predetermined combustion temperature the work can be plugged into the work equation again to find the temperature after the turbine stages. As indicated with the curly brackets, the fuel mass flow

needs to be added to the core mass flow. The change of specific heat capacity at constant pressure needs to be taken into account as well.

After this the temperature and pressure ratios can be calculated using the expansion equation given below:

$$\frac{T_2}{T_1} = 1 - \eta_{is}\left[1 - \left(\frac{p_2}{p_1}\right)^{\left(\frac{\gamma-1}{\gamma}\right)}\right] \tag{48}$$

In order to calculate thrust it needs to be checked whether the nozzle flow is choked or not. If it is, the required area of the nozzle needs to be determined to be able to calculate the force of the excess pressure in order to be able to add it to the thrust term. This needs to be done for both the core stream as well as the bypass stream. The formula for the critical pressure ratio is given below. For the bypass the specific heat capacity of air and for the core stream the specific heat capacity of hot combustion gasses needs to be used respectively.

$$\varepsilon_{cr} = p_1/p_2 = \left[\frac{1}{\left(1 - \left(\frac{1}{\eta_j}\right)\cdot\left(\frac{\gamma_g-1}{\gamma_g+1}\right)\right)^{\frac{\gamma_g}{\gamma_g-1}}}\right] \tag{49}$$

The pressure in an not completely expanded jet stream can be found by dividing the pressure after the turbine by this ratio. The temperature can be found similarly by dividing the temperature after the turbine by $\frac{(\gamma+1)}{2}$. Using this temperature the exhaust velocity can be calculated.

$$A_{jet} = \frac{\dot{m}RT_{jet}}{p_{jet}v_{jet}} \tag{50}$$

$$Thrust = \left(\dot{m}_{core} + \dot{m}_{fuel}\right)\left(v_{jet} - v_0\right) + A_{jet}\left(p_{jet} - p_0\right) \tag{51}$$

For complete expansion the pressure in the nozzle is equal to the static pressure of the surrounding air. Using the following formulas the thrust can be calculated for complete expansion:

$$T_{0,LPT} - T_{jet} = T_{0,LPT}\cdot\eta_{is,noz}\left[1 - \left(\frac{p_0}{p_{0,LPT}}\right)^{(\gamma_g-1)/\gamma_g}\right] \tag{52}$$

$$v_{jet} = \sqrt{2c_{p,g}\left(T_{0,LPT} - T_{jet}\right)} \tag{53}$$

$$Thrust = (\dot{m}_{core} + \dot{m}_{fuel})n\cdot(v_{jet} - v_0) \tag{54}$$

Values were adjusted until the desired thrust level was reached. The specific fuel consumption was calculated by dividing the fuel mass flow by the total thrust achieved. This was taken as the main measure of performance.

Further Considerations Initially it was found that a very low specific fuel consumption could be achieved at very low combustion temperatures ($1200K$), these seemed unreasonable and the equations were verified, however no mistake was found. It could be argued that as long as the temperature drop across the turbine stages is sufficient to produce the required work, the specific fuel consumption could be decreased by decreasing the burner temperature, which decreases the thrust of the core, increasing the contribution of fan thrust to total thrust. This seems problematic as it is physically infeasible to take out all kinetic energy out of the core stream. Later it was reasoned that as long as the exhaust pressure ratio did not fall below unity the temperature could be reduced. However this still resulted in unrealistically low values for the specific fuel consumption. Ultimately this conundrum made it necessary to use an external tool to validate the analysis.

Engine Design and Parameters The model that was created covers all the intermediate stations that a turbofan has, starting with the free stream conditions and finishing with the exhaust conditions. The parameters at the different stations along the engines are presented in Table 28, with their respective locations shown in Figure 32, for a take-off at an airport located at $1500m$ altitude as this was decided for the highest airport the aircraft shall be able to operate from.

Table 28: Values of different parameters along the engine (take-off)

Station	Total Temperature (K)	Total Pressure (Pa)
0	280.79	87124.53
1	314.12	121865.35
2	390.57	243730.7
3	808.38	2437307.1
4	1200	2339814.81
5	864.22	849671.3
6	508.1	160179.1
7	402.61	84556 (static)
Work needed to be delivered to:		**Unit**
Fan	10022693,1	W
LPC	2089464	W
HPC	11420588,7	W

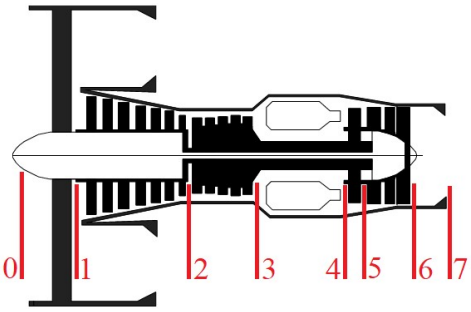

Figure 32: Location of different stations along the engine

Verification In order to verify the right use of equations as well as the correctness of the equations in the modeling process, a comparable theoretical turbofan engine was used. For this engine all parameters were available including the total temperature and pressure at every station, the total thrust, mass flows, pressure ratios, efficiencies, work extracted and generated. This engine was modeled with the equations used to size and the resultant values were compared to given values to ensure the correctness of the implementation of the equations. Since the equations take their inputs from subsequent steps in the thermodynamic analysis, the correct application of the equations themselves were also verified using this approach.

Validation In order to validate whether the engine model provides realistic results, a simulation tool was used to check the engine in the desired settings, to see how the simulations results correspond to the analytically determined values.

The simulation tool used was the *EngineSim Version 1.8a* developed by the Glenn Research Center of the National Aeronautics and Space Administration[16]. The use of this tool showed that the modeling process used does not accurately assess the pressure drop over the turbine, as this was the only disparity found when validating the results. According to the simulation the combustion temperature must be at least around $1500K$, whilst in the model used it was found that $1200K$ would be sufficient. The temperature drop across the turbine however stayed the same, implying that the modeling process did not accurately assess the pressure drop. The result of this was a lower amount of energy required to have a functioning core stream after the turbine. After this finding, the combustion temperature was increased.

The first iteration of the simulation software showed that $1431K$ was the minimum necessary temperature to produce thrust. At this temperature the engine produced $98.7kN$ of thrust for the same input values. This resulted in a core flow of $47kg/s$ and a fuel flow of $0.3kg/s$. For the same combustion temperature the model calculations resulted in a core mass flow of $27kg/s$ and a fuel mass flow around $0.165kg/s$, approximately half of the simulation. However the model calculations only resulted in $65kN$ of thrust.
This clearly shows that there are large discrepancies between the model and the simulation.

Subsequently the inlet diameter was reduced to $1.79m$ in the simulation to achieve $61kN$ of thrust. This resulted in a core mass flow of $29kg/s$ and a fuel flow of $0.18kg/s$. A lot closer result when compared to the model. However when reducing the model intake area, the thrust decreased significantly. This could be due to discrepancies in the methods used to determine actual mass flow through the engine.
What has to be taken into consideration is that the engine configuration modeled, places the fan and low pressure compressor on the same spool, whilst keeping the high pressure compressor on a separate spool. These are powered by a low pressure turbine and a high pressure turbine respectively. In the simulation only

[16] https://www.grc.nasa.gov/WWW/K-12/airplane/ngnsim.html

overall pressure ratio and efficiency should be input for the compressors and only the efficiency for the turbine. It was not possible to simulate multiple spools, this could also be a cause of the difference in results between the simulation and the model.

Results & Final Design This section presents the results obtain from the analysis of the model. In Table 29 the most important output parameters of the engine are given. It can be seen that the thrust the engine produces satisfies the take-off thrust requirement. The hydrogen fuel flow rates are $0.1036 kg/s$ and $0.1623 kg/s$ per engine for the take-off and cruise, respectively.

Table 29: Thrust values of a single engine at different mission stages

	Core Thrust (N)	**Fan Thrust (N)**	**Total Thrust (N)**	**Specific Fuel Consumption (g/kN/s)**
Take-off	12154.66	48596.55	60751.20	1.706
Cruise	13435.90	31190.16	44626.06	3.637

Compliance with Requirements After the design is complete, the engine needs to be checked whether it complies with the requirements formulated in the begining. Having a max cruise thrust of 89.2 kN and a drag of 18.87 kN it can be said that SRA-SYS-PROP-01 is satisfied. This is also satisfied in case one engine fails and all the cruise thrust is produced by only one engine. To fulfill SRA-SYS-PROP-02 the thrust required for the take-off condition is calculated, this stems into requirement PSDR-1, which according to Table 29 is met. The max cruise thrust is almost five times the drag experienced during cruise, the throttle can be used to reduce this thrust, thus satisfying the requirement that the propulsion system shall allow for impulse control (SRA-SYS-PROP-03). The requirements presented in Table 25 can easily be verified, except for PSDR-3, which is hard to quantify, meaning further analysis is needed in the future. Finally, the component requirements in Table 26 need to be satisfied by the supplier of the engine parts. This can be checked by tests and analysis of the parts to ensure the engine is going to work as intended.

Recommendations for further Engine Improvements The engine sizing analysis has so far not included a thorough combustion analysis or stoichiometric calculations. This would be the first thing that would need to be analyzed to ensure that no combustion instabilities occur. This would go hand in hand with flow analysis. After that several engine improvements can be considered. Considering the use of cryogenic hydrogen recuperation would bring a major increase in efficiency. Additionally the ideal combustion temperature could be investigated further, should it turn out that increasing combustor temperature results in a large decrease in core mass flow and therefore in fuel consumption, active cooling could be applied to achieve higher burner and turbine temperatures whilst continuing to use non-exotic materials. Recuperation could also applied to make the best use of wasted heat to increase efficiency. Finally through a thorough study it could be assessed whether a decrease in engine efficiency but an increase in overall power would benefit the entire aircraft system due to potential weight savings. The complexity of including all these factors in the analysis is too time consuming but is highly recommended for future iterations.

6.3.4 Hydrogen Tanks

The tail tank will serve as storage tank. From here, pumps send the hydrogen to the feed tanks, which are the external wing tanks below the wing. Structural design of the tanks can be found in Section 6.5.3. An important issue which needs to be addressed is the boil-off of the liquid hydrogen. No cooling system is installed as this increases complexity. Instead, insulation is used around the tank. Thermodynamic analysis must be performed in order to calculate the required insulation thickness. Tank dimensions can be found in Section 6.1.5.

Boil-off Issues Hydrogen is stored as a cryogenic liquid at $20K$, but due to a heat flux with the outside, it heats up and boils off as a gas. This gas is relieved when necessary, and pressure should be kept below 1.45 bars, low enough to limit structural tank weight, but high enough to provide over-pressure and keep air out (which introduces combustion danger if mixed with hydrogen). The additional boil-off volume in a full tank is 7.2% (that is, the required mission hydrogen volume multiplied by 1.072) [29]. This extra 7.2% is assumed to be directly filled with gaseous hydrogen after fueling (due to refueling discrepancies, remaining gases and possible pre-cooling or purge gases). Depending on the insulation thickness and thermodynamic properties,

the tank has a certain boil-off rate $[kg/s]$. It is decided that enough insulation should be provided to limit the boil-off to 1% over a maximum span of 10 hours. This includes 6 hours of the aircraft being grounded with full tanks (due to technical defects, airport delays or other factors) and 4 hours of flight. The reason that boil-off is only taken at 1%, is that this boil-off needs to be either relieved, or burnt off by the Auxiliary Power Unit (APU). Relieving of boil-off gas poses a big hazard during grounded conditions, and burning it through the APU during grounded conditions should be minimized as a running APU must be avoided during unexpected technical repairs (A. Rao, personal communication, 10/06/2020).

Thermodynamic Principles The hydrogen heats up because of a heat flux with the hotter outside environment. The surround temperature T_∞ on ground is assumed to be 37 degrees Celsius ($310K$). In the air, the podded tanks are exposed to temperatures of -68 degrees Celsius ($205K$). The tail tank is placed after the bulkhead so it also experiences a decrease in temperature, and a temperature of $220K$ is assumed here. First, the outside surface temperature of the insulation T_s must be found [29]. The insulation receives convection and radiation heat flow from the outside ($Q_{\text{convection}}$ and $Q_{\text{radiation}}$), and has a conduction heat flow $Q_{\text{conduction}}$ going out of the wall, and into the hydrogen. The heat flows and their calculation are given in Equation 55 and Equation 56 [29]. The in-going heat-flow and out-going heat-flow need to be equal. This depends on the surface temperature T_s, the value is raised in an iterative process until the heat flows are equal.

$$Q_{\text{in}} = Q_{\text{convection}} + Q_{\text{radiation}} = h\left(T_\infty - T_s\right) + \varepsilon\sigma\left(T_\infty^4 - T_s^4\right) \tag{55}$$

$$Q_{\text{out}} = Q_{\text{conduction}} = K\left(T_s - T_{LH2}\right)/L \tag{56}$$

ϵ is the emissivity coefficient of the insulation and σ is the Stefan-Boltzmann constant ($5 \cdot 10^{-8} W/m^2/K^4$). h is the convection coefficient, given by Equation 57 and K is the insulation thermal conductivity. The convection coefficient is for a cylinder in static air. This is the case when grounded, and for the tail tank sitting inside the pressurized fuselage. However, the external wing tanks are exposed to airflow during flight. This effect has not been researched and is included the recommendations. The insulation thickness will very likely increase. Insulation is very light-weight and the added thickness is likely in the order of centimeters so the current discrepancy is judged as allowable.

$$h = N_{UD} K_g / D \tag{57}$$

In Equation 57, D is the tank diameter, N_{UD} is the Nusselt number and K_g is the thermal conductivity of the air, assumed to be $0.024 W/m/K$. For a cylinder, the Nusselt number can be computed via Equation 58 [29]. All tanks are assumed to be cylindrical, although this is not the case for the tail tank, which is an oblique truncated cone. PR is the Prandtl number ($\frac{\upsilon}{\alpha}$), equal to 0.71, R_{ad} is the Rayleigh number given in Equation 59 [29]. υ is the air viscosity and α is the air diffusivity, given by Equation 60 and Equation 61 respectively. β is the inverse of T_∞ [29].

$$\mathrm{N_{UD}} = \left[0.60 + 0.387\mathrm{R_{ad}^{1/6}} / \left[1 + (0.559/\mathrm{PR})^{9/16}\right]^{8/27}\right]^2 \tag{58}$$

$$R_{\text{ad}} = g\beta\left(T_\infty - T_s\right) D^3/(\upsilon\alpha) \tag{59}$$

$$\upsilon = -2.08 \cdot 10^{-6} + 2.78 \cdot 10^{-8}\mathrm{T_\infty} + 1.08 \cdot 10^{-10}\mathrm{T_\infty^2} \tag{60}$$

$$\alpha = -3.12 \cdot 10^{-6} + 3.54 \cdot 10^{-8}\mathrm{T_\infty} + 1.68 \cdot 10^{-10}\mathrm{T_\infty^2} \tag{61}$$

Q_{in} and Q_{out} should be equal to each other, this way the surface temperature T_s can be computed. This is done iteratively. This way, the heat flow can be obtained, and thus, a boil-off balance is set up via Equation 62. T_{LH} is the temperature of the liquid hydrogen ($20K$), A is the surface area of the tank (trivial computation), L is the thickness of the insulation, K is the insulation thermal conductivity, and h_{fg} is the latent vaporization heat of hydrogen ($446592 J/kg$). M is the boil-off rate in kg/s [29]. M is easily extracted from Equation 62. Multiplying this by the mission duration the total boil-off is obtained, which must be less than 1% of the total fuel mass.

$$\mathrm{KA\left(T_s - T_{LH}\right)/L = Mh_{fg}} \tag{62}$$

Insulation Thickness calculation The goal of losing less than 1% in boil-off must be met by adding enough insulation. A Python program was developed combining all thermodynamic formulae. The first step calculates the boil-off for zero thickness, then, the thickness is increased by 1 millimeter each step until the boil-off is less than one percent. The program takes into account the difference between external wing tank and tail tank dimensions, and ground temperature vs flight temperature (although the tail tank is assumed to be a cylinder, and the in-flight convection coefficient for the external wing tank is calculated as if the tanks were isolated from airflow). The insulation material selected is rigid closed cell polymethacrylimide, with a density of $35.3 kg/m^3$ and thermal conductivity K of $0.0096 W/m/K$ [29]. The thicknesses computed are $3.5 cm$ for the external wing tank, and $2.8 cm$ for the aft fuselage tank.

Verification and Validation on Insulation Thickness Once the iterative process of finding the right surface temperature is completed, the heat flow balance was checked by hand. Then, the program must indicate the insulation thickness where boil-off drops below 1%. Calculations were done by hand with the equations, to check if the boil-off indeed stayed below 1%. The found thicknesses lie in the range of a couple of centimeters. This is the same range as the insulation thicknesses reported for space cryogenic tanks [44].

External wing tanks placement The external wing tanks need to be placed on the wing. As the engines are also wing-mounted, the lateral location of the tanks need to be determined as such to limit the interference between the two. The aircraft is cruising at Mach of 0.75. To minimize the drag at transonic and maybe sonic speed the aircraft may experience the area rule can be used, which is a technique that minimizes the drag [45]. The cross sectional area of the aircraft needs to follow a gradual transition. This means that if the tanks are placed on the same longitudinal position as the engines there will be a large increase in cross sectional area, which has a negative effect. To combat that the external wing tanks are placed on the back of the wing with some part of them sticking out of the trailing edge. That way the area transition after the wing's longitudinal position is smoothened instead of having the the cross-sectional area drop abruptly after the wing. The last thing left to do is to determine the lateral position of the tanks. As they are extending past the trailing edge, possible connection can disturb the flaps or the ailerons. This means the only place the tank pylon can be situated is at the space between the flaps and aileron. This results in a position of 66.6% of the half span or $7.44 m$ from the centerline.

6.3.5 Fuel Distribution

The fuel distribution system of the hydrogen aircraft will show both similarities and differences compared with conventional kerosene aircraft. The extra challenges faced in designing a cryogenic hydrogen fuel system are storage of liquid hydrogen, difference in storage vs required injection temperature, boil-off and the extremely low cryogenic temperature itself. In Figure 33 the fuel system schematic can be seen. The fuel system design is largely based on a concept study by different European contributors coordinated by Airbus Deutschland GmbH [27]. The system shall store its fuel in the liquid hydrogen storage tank (passive tail tank) and from here it shall pump the fuel into the wing feed tanks (active external wing tanks). The wing tanks do also serve as storage tanks and are full after refueling. It is assumed the pumps will fit within the wing-box. The external wing tanks serve as feed tanks. The feed tanks pass the fuel to the engine. A total of seven subdivisions can be identified within the fuel system in Figure 33, being:

- Refueling: Allows for refueling of the tanks via a refueling inlet.
- Dumping: In case of emergency the liquid hydrogen can be drained from all tanks. A two-valves-in-parallel configuration is used for redundancy in case one valve malfunctions. This can also be used to drain the tank if a filled aircraft remains unexpectedly grounded. This is done by ground equipment.
- Transfer: The transfer system includes the main storage tanks which flow into the feed tanks. The fuel is extracted by a jet pump and then it is pumped to the feed tanks by a low pressure transfer pump.
- Engine: The engines are fed from the feed tank. A jet pump retrieves the fuel and a low pressure pump pushes the fuel to the engines high pressure pump, mounted to the shaft. Then the cryogenic hydrogen is sent through a heat exchanger (or heater) and finally it is combusted. A return line is placed to prevent cavities and keep the flow rates low [27].

- APU: The APU can work on the boil-off gases provided by the relief system [27]. If this is not available, it can work on liquid hydrogen, provided by the passive storage tank (which turns active for the APU). The APU provides electric power to the Electrical Power System (EPS) and the compressed air to start the main engines. In the case of the hydrogen aircraft it also can burn boil-off hydrogen.
- Relief: As no cooling is used, the hydrogen tanks will gradually heat up and boil off will occur. This gases can either be redirected to the APU, or simply be vented.
- Purge: The purge system cleans the fuel system of hydrogen at shutdown or air at startup, as oxygen and hydrogen together give rise to safety concerns involving flammability and explosion.

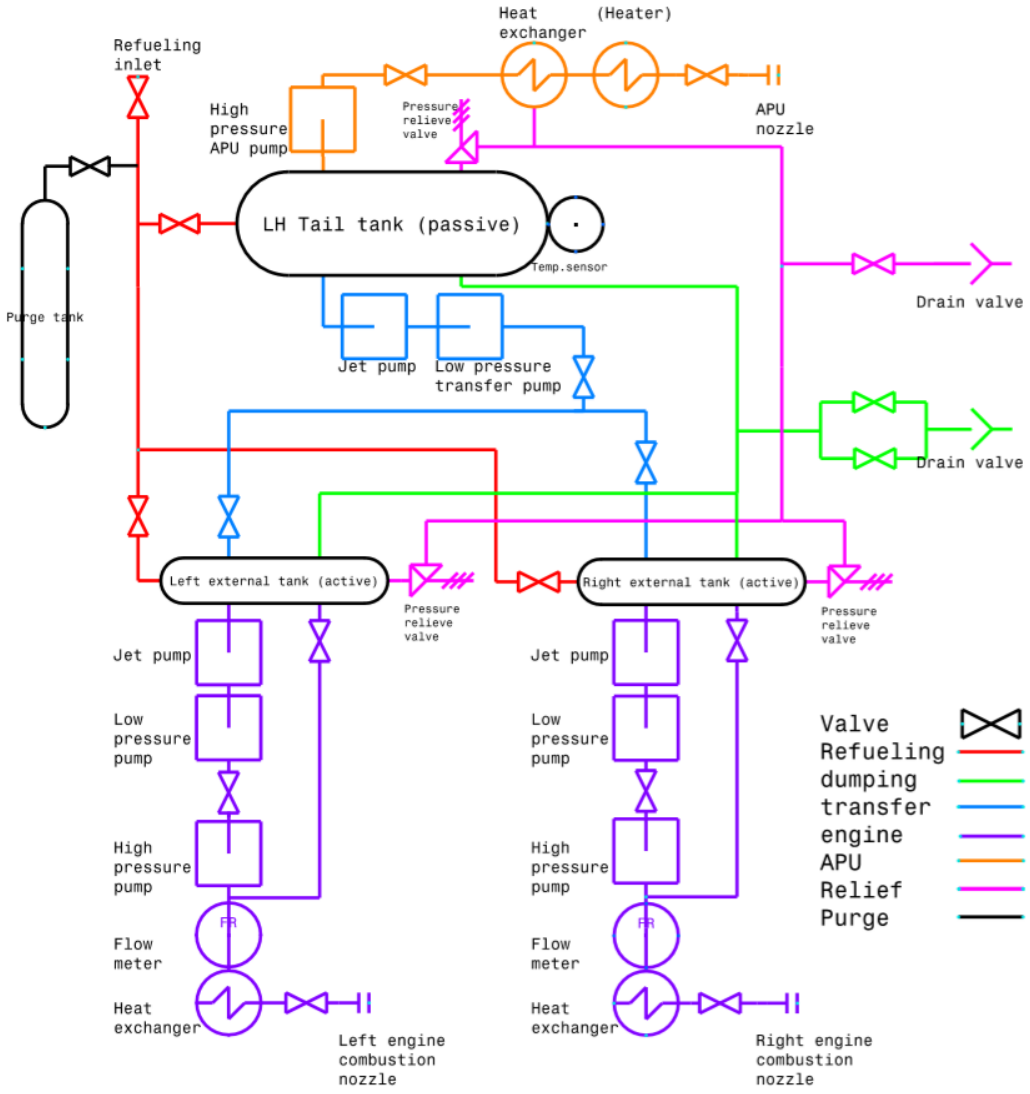

Figure 33: Fuel system diagram

Hydrogen Pipes The liquid hydrogen is transported in the aircraft by the means of fuel pipes. These pipes have to resist the cryogenic temperatures and seep through of hydrogen. composite pipes can be used with radiation shielding in order to reduce the axial and radial thermal energy transfer [27]. A Carbon Fibre Reinforced Polymer (CFRP) using XU 3508 is selected, with metallic coating to prevent hydrogen seep through, this use of CFRP over steel pipes introduces a weight saving of 60% [46][17]. Additionally the pipes should be cooled at startup as reported by [27], which should be done by circulation of a cold inert gas, prior to fueling. This can be the purging gas if it is applied from the outside. The pipes itself must allow for expansion and

[17] http://www.jeccomposites.com/knowledge/international-composites-news/carbon-fibre-reinforced-polymer-cryogeni

contraction due to the encountered temperature differences, this can be done by providing bends in the shape of an Ω.

Pumps Three types of pump are used as seen in Figure 33.

- Jet pump: it assures that the liquid is extracted from the tank, into the other pumps [27].
- Low pressure pump: this pump makes sure that enough fuel is sent into the high pressure pump. It is electrically driven [27].
- High pressure pump: This pump is mechanically driven via a gear on the engine shaft and pumps high pressure liquid hydrogen into the heat exchanger [27].

The number of pumps is doubled to provide redundancy.

Valves The valves should shut off and regulate the fuel flow. Two separate valves can be included to improve reliability, one for shut off and one for flow regulation, it is chosen to combine them together into one valve to save weight. The valves are powered by electric actuators. This power is provided by the EPS. Also back up power is of paramount importance and thus the EPS should provide this as well. The combined valve-actuator system is estimated to have a mass of $6kg$ per piece [27].

Heat Exchanger and Heater The liquid hydrogen must be heated from 20K to a gaseous condition of 150-250K before it can bfuelinjected in the combustion chamber. This is done by putting the LH through a heat ex-changer tube wrapped around the jet pipe exhaust as proposed in studies by SNECMA (an industry partner in [27]). The lower exhaust temperature has negligible effects on thrust decrease. The fuel lines should be carefully constructed in this region, as leakage near a hot area (e.g. combustion chamber) can lead to leak explosion [47]. Also for the APU a heat ex-changer is installed. At startup, the engine exhaust will not be warm enough to provide heat to the heat ex-changer, which in turn cannot convert the liquid hydrogen to a gas. An electric heater is installed as proposed by Khandelwal et al. [47]. This electric heater is also used in the APU. The heaters shall be powered by the EPS.

Purge System As hydrogen is highly flammable in combination with oxygen, no air can be present in the fuel system. At startup (or refueling), the air must be purged after which hydrogen comes in. After shutdown the hydrogen should be purged after which air is allowed in. This can be done by an inert gas such as helium, nitrogen or carbon dioxide. Purging gas can come from an external supply on the ground, and be cold to pre-cool the pipes, but is also carried on-board if such system is not available during shutdown.

Final Considerations The additional weight of the hydrogen system compared to a kerosene system is roughly estimated to be 1.5 tonnes [27]. This weight needs to be added to the OEW in the very first loop of the Class I weight estimation (performed in Section 5.3).

Fuel System Recommendations

- The thermodynamic modeling of the external wing tanks need to be reconsidered, as they are exposed to the free-stream flow. Also forming of ice must be investigated (as the tank is cryogenic), and de-icing measures may be taken due to otherwise increased drag.
- boil-off gases only might not be sufficient for the APU, so the tail storage tank in the back must sacrifice some fuel. The influence of the extra needed fuel on the mission fuel mass must be considered.

The thermodynamic modeling of the external wing tanks need to be reconsidered, as they are exposed to the free-stream flow.

6.3.6 Propulsion System Sensitivity Analysis

Several tests can be performed to assess the behavior of the propulsion system design based on changing some of the input parameters.

The minimum thrust that is required stems from the MTOW of the airplane. This means that a change in the MTOW will require a direct change of thrust in order to fulfill the take-off thrust requirement. The T/W fraction remains equal to 0.44 as it is not influenced by MTOW. Changing the MTOW by $+/-10\%$ will

change the required thrust by 4.4%, or make it 109058-$133293N$, respectively.

Another parameter that can be altered is the combustion chamber temperature. Currently it is set to $1200K$ and it allows for the work required to be extracted from the flow. During a consultation with a propulsion expert[18] it was stated that this temperature is too low. To see what what the effects of this the temperature was increased to $1600K$. This results in the engine requiring more than twice the hydrogen flow to achieve this burning temperature. The flow now contains a lot more energy, so after the turbines the pressure is still very high, needing a shockwave at the nozzle to allow the flow to exit. This configuration delivers $68500N$ per engine, which is just 12% higher than the current design while requiring twice the amount of fuel.

In order to further investigate the effect of varying parameters, several design parameters were varied independently by 10%. A more thorough analysis would require to extensively test the sensitivity of confounding factors, however varying the parameters independently gives a decent estimate for their effect on the engine performance.

Table 30: Effect of varying design parameters by 10%

	Effect on Thrust		Effect on SFC	
Parameter	$\times 1.1$	$\times 0.9$	$\times 1.1$	$\times 0.9$
T04	66346.93 (+9.2%)	48836.22 (-19.6%)	2.04 (+19.6%)	1,47 (-13.7%)
Fan Π	0 (-100%)	55627.1 (-8.4%)	∞	1.99 (+17%)
LPC Π	59992.67 (-1.2%)	61450.31 (+1.2%)	1.62 (-5%)	1.8 (+5.5%)
HPC Π	60035.88 (-1.2%)	61410.27 (+1.1%)	1.62 (-5%)	1.79 (+5.4%)
BPR	58061.63 (-4.4%)	63587.73 (+4.7%)	1.64 (-4.1%)	1.79 (+5.1%)
In take diameter	73508.96 (+21%)	49208.48 (-19%)	1.71 (0%)	1.71 (0%)
LNG Fuel		64358.93 (+5.9%)		4.29 (+252%)

As can be seen varying the combustion temperature has a major effect on engine performance. An increase produces more thrust, as it strongly effects the energy in the core stream after the turbine, however this also has a significant impact on the specific fuel consumption, the largest of all parameters, since more fuel needs to be burned to achieve the increased combustion temperature. For this reason the aim was to keep the combustion temperature as low as possible.

Generally speaking increasing the compression ratios of the compressors decreases thrust by a small amount. This is due to increased turbine work required, that leaves the core stream with less energy after the turbine, therefore producing less jet thrust. However it also has a significant effect on the specific fuel consumption and can therefore be a useful parameter in reducing the fuel consumption of the engine.

Varying the fan compression ratio has a significant impact on the engine performance. Increasing the compression ratio requires too much turbine work for the core stream to remain intact. So not enough energy can be extracted from the flow, making it go to zero. Decreasing the compression ratio greatly decreases thrust and produces a large increase in specific fuel consumption. Therefore, ceteris paribus, a variation in fan compression ratio is detrimental to performance.

The effect of varying the bypass ratio was not as profound as expected. an increase in bypass ratio decreases thrust without significantly decreasing the specific fuel consumption, and a decrease in bypass ratio increases thrust, due to a larger jet component, but also increases the specific fuel consumption.

Changing intake parameter has a large effect on engine performance as it determines the overall mass flow through the engine. However it also increases system weight. It did not have any effect on the specific fuel consumption and for this reason the intake diameter was varied and changed until the engine achieved the design thrust. More specifically the intake diameter was increased and the combustion temperature decreased in an attempt to achieve more thrust at lower fuel flow. Further analysis might find an optimum as the high

[18](A. Rao, personal communication, 10/06/2020)

wing configuration does not place a tight constraint on engine size.

When changing the fuel source to liquid natural gas, the thrust increases and the specific fuel consumption does by a factor of 2.5. This is due to the fact that hydrogen is more than 2.5 times more energetic than Liquefied Natural Gas (LNG). Using LNG is definitely possible, however less economical. Possible advantageous could include an increased range, due to lower density of fuel and therefore more tank capacity, however more thorough analysis would be required to make such conclusions.

6.4 Stability and Control

Stability and controllability are discussed in this section, establishing the center of gravity and sizing control surfaces.

6.4.1 Requirements

Table 31: Control, stability and landing gear requirements

Requirement Identifier	Requirement	Compliance
	Control System	
SRA-SYS-CNTR-01	The control system shall provide directional control in all axes.	✓
SRA-SYS-CNTR-02	The control system shall provide rotational control in all axes.	✓
SRA-SYS-CNTR-03	The control system shall provide static stability in all axes.	✓
SRA-SYS-CNTR-04	Trim drag shall be less than 10% of the total aircraft drag.	✓
SRA-SYS-CNTR-05	Max stick control force shall satisfy the requirements from CS 25.143.	✓
SRA-SYS-CNTR-06	The control system shall be able to rotate the aircraft during take-off with the most forward center of gravity.	✓
SRA-SYS-CNTR-07	The control system shall allow for a roll angle of 45 degrees in 1.45 seconds at stall velocity.	✓
SRA-SYS-CNTR-08	The control system shall provide lateral control in one engine inoperative conditions.	✓
	Landing Gear System	
SRA-SYS-LG-01	The landing gear shall withstand the weight of the aircraft.	✓
SRA-SYS-LG-02	The landing gear shall provide for directional control during taxiing.	✓
SRA-STAKE-AP-05	The aircraft shall allow for maneuvering and taxiing on the ground.	✓
SRA-SYS-LG-03	The landing gear shall provide for deceleration during landing and taxiing.	✓
SRA-SYS-LG-04	The landing gear shall withstand for acceleration during take-off.	✓ / ✗
SRA-SYS-LG-05	The landing gear shall withstand the impact of touchdown.	✓
SRA-SYS-LG-07	The landing gear shall be able to function on regional airport runways under wet conditions.	✓ /✗
SRA-PROD-PERF-18	The aircraft shall not tip over in any direction at any time during ground operations.	✓
SRA-PROD-PERF-17	The aircraft shall satisfy all ground clearances.	✓
	Other	
SRA-PROD-CG-01	The center of gravity shall stay within the specified range while the checked-in luggage is being loaded.	✓

6.4.2 Weight and Balance

To size the horizontal tail and the longitudinal position of the wing and landing gear, the C.G. range of the aircraft must be determined, which will be done in the coming paragraphs.

OEW Center of Gravity To to determine the C.G. range during operation, the C.G. of the empty aircraft must be determined. This is done using the component weights from [31] and Equation 63. The process of obtaining the component weights is automated using Python, with most component C.G. estimations being based on reference points in the fuselage or wing. The final component masses can be found in Table 12 which is situated in Section 5.4, with their respective estimated C.G. locations.

$$x_{cg} = \frac{\sum_i M_i \cdot x_{cg_i}}{\sum_i M_i} \tag{63}$$

Aircraft Loading The operational C.G. range must be computed to determine the required tail size, and landing gear position. Equation 64 is used to calculate the C.G. location and mass for each load scenario. The resulting loading diagram is given in Figure 34. The method used to the generate the loading diagram was taken from [48]. The diagram shows a loading sequence, in which the cargo is loaded first, after which the passengers are loaded, and finally the fuel. Each part of the loading sequence can be performed from the front of the aircraft, or from the back of the aircraft. The forward and aft C.G. limits have been indicated by the bright green and pink vertical lines. Both include a 3% margin with respect to the most extreme C.G. locations that may occur in flight. When the aircraft is operated, the C.G. must remain between these two limits without the added 3% margin during the entire flight. During loading and unloading, the C.G. is allowed to shift further forward or backward. The top red passenger loading therefore does not influence the most forward C.G., while the external tank does influence the most forward C.G. limit. The passenger and cargo loading sequence, as indicated by window, middle and aisle seats as well as cargo in Figure 34 are shown to indicate the C.G. location during loading, which is used to determine if the aircraft will not tip back during loading. The forward and aft limits during loading are not indicated in this figure. The aft C.G. during loading is allowed to come near the main landing gear, which is at 70% of the Mean Aerodynamic Chord (MAC), while forward it is allowed to reach 0% of the MAC. In the loading diagram, it can be seen that the fuel is loaded in two parts. This is due to the aircraft having two hydrogen tanks available, as explained in Section 6.1.5. Additionally, it can be noted that the aircraft will not be allowed to take-off when only carrying fuel. This would shift the C.G. is aft of the pink line. The operator shall carry ballast in the front of the aircraft to counteract the C.G. being too far aft.

$$x_{cg_{new}} = \frac{x_{cg_{old}} \cdot M_{old} + \sum_i x_{cg_i} \cdot M_i}{M_{old} + \sum_i M_i} \tag{64}$$

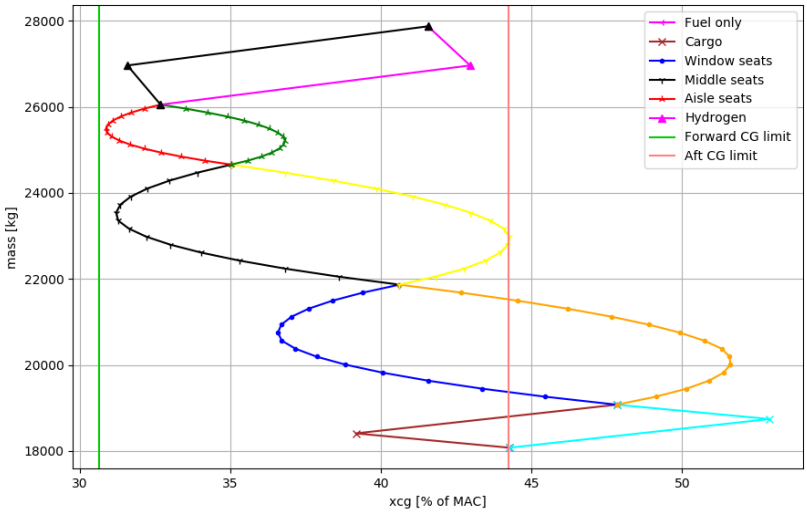

Figure 34: Loading diagram

Table 32: Input and output parameters of the loading diagram

Parameter	Value [unit]	Source
Input		
Passenger mass	93 [kg]	[26]
OEM	18275.6 [kg]	Class-II weight estimation
Forward cargo mass	333 [kg]	Requirement
Aft cargo mass	667 [kg]	Requirement
Passenger seat location	varying, spread through the cabin	Cabin design
Forward cargo C.G.	6 m	Estimate
Aft cargo C.G.	19 m	Estimate
External tank fuel mass	916 kg	Tank design and Class-I
Tail tank fuel mass	916 kg	Tank design and Class-I
External tank C.G.	13.2 m	Estimate
Tail tank C.G.	23.4 m	Estimate
C.G. margin	3% m	Estimate
Output		
C.G. aft limit	43.9 % MAC	Equation 64
C.G. fwd limit	30.3 % MAC	Equation 64

6.4.3 Roll Control Sizing

According to CS.25 regulations, Class II aircraft shall achieve a roll angle of 45 degrees in 1.45 seconds, i.e. a roll rate of 31.0 degrees per second [49]. As a regional jet aircraft falls under Class II, the ailerons must be sized for this roll rate at stall velocity, as is the critical condition for rolling. This is done using the approach mentioned in [50]. The aileron roll rate follows from Equation 65. In order to calculate the roll rate, the aileron control derivative, roll damping coefficient and average maximum deflection angle must be known. The former two are calculated by Equation 66 and Equation 67, respectively. The chord length along the span, c(y), follows from Equation 68. The resulting aileron geometry, along with some input parameters used, are summarized in Table 33.

$$P = -\frac{C_{l_{\delta a}}}{C_{l_p}} \delta a \left(\frac{2V}{b} \right) \tag{65}$$

$$C_{l_{\delta a}} = \frac{2C_{l_{\alpha_{al}}} \tau}{S_{ref} b} \int_{b1}^{b2} c(y) y dy \equiv \frac{2C_{l_{\alpha_{al}}} \tau}{S_{ref} b} \left[\frac{1}{2} C_r (b_2^2 - b_1^2) + \frac{2(C_r - C_t)}{3b} (b_1^3 - b_2^3) \right] \tag{66}$$

$$C_{l_p} = -\frac{4(C_{l_{\alpha_{al}}} + C_{d_{0_{al}}})}{S_{ref} b^2} \int_0^{\frac{b}{2}} y^2 c(y) dy \equiv -4 \frac{(C_{l_{\alpha_{al}}} + C_{d_{0_{al}}})}{S_{ref} b^2} \left[\frac{C_r b^3}{24} - \frac{b^3 (C_r - C_t)}{32} \right] \tag{67}$$

$$c(y) = C_r - \frac{C_r - C_t}{b/2} y \tag{68}$$

Table 33: Input and output parameters for aileron sizing

Parameter	Value [unit]	Source
Input		
$C_{l_{\alpha_{al}}}$	6.48 [1/rad]	Derived from airfoil simulation
$C_{d_{0_{al}}}$	0.007 [-]	Derived from airfoil simulation
τ	0.5 [-]	Determined graphically using c_a/c [50]
S_{ref}	47.4 [m^2]	Approximated by $S - C_r D_{fus}$
δ_{up}	25 [deg]	Derived from reference aircraft
δ_{down}	18.8 [deg]	Taken 0.75 δ_{up} to reduce adverse yaw
Output		
b1	7.6 [m]	Optimal configuration to meet roll rate requirement
b2	10.3 [m]	Optimal configuration to meet roll rate requirement
c_a/c	0.25 [-]	Based on reference aircraft and rear spar location
$C_{l_{\delta a}}$	0.28 [1/rad]	Calculated with Equation 66
C_{l_p}	-1.05 [-]	Calculated with Equation 67
P	31.4 [rad/s]	Calculated with Equation 65

Since a configuration with only outboard ailerons satisfies the roll rate requirement, less deflection is required compared to inboard ailerons due to the bigger moment arm. Along with the design of the flaps, efficient use is made of the space available on the wing trailing edge.

6.4.4 Vertical Tail Sizing

Vertical Tail Parameters When designing the vertical tail, the AR , taper ratio and the sweep angle have to be determined. A conventional value of the aspect ratio A_v is between 1 and 2. For the taper ratio λ_v, a nominal value lies between 0.3 and 0.7. When choosing the sweep of the vertical tail it is important that is is both larger than the wing sweep and, since it is a jet aircraft, it is smaller than 50 degrees [6]; postponing compressibility effects and increasing the stall angle of attack. The AR, taper ratio and sweep have to be chosen by the designers. The positive effect of sweep angle on C.G. moment arm, the positive effect of the AR on the tail plane effectiveness, and an absence of adverse effects of the taper ratio on the effectiveness, lead to the selection of an AR of 1.7, together with a taper ratio of 0.6 and a sweep angle of 35 degrees.

Vertical Tail Area Estimate Preliminary sizing of the vertical tail plane area is done by collecting statistical data on reference aircraft; the selection is succeeded by averaging the parameters, in order to come up with an accurate estimate, as suggested in Roskam [2]. Below, in Table 34, the aircraft that have been used as reference aircraft for sizing the vertical tail are tabulated, together with their respective vertical tail volume $\bar{V}_v$ and ratio of rudder area to vertical tail area $S_r/\bar{S}_v$.

Table 34: Reference Aircraft Used to Determine Vertical Tail Volume and Rudder Area

Airplane type:	F-28	Bae 146-200	Tu-154	DC-9-MD80	DC-9-50	B767	B737-200	B737-300	B727-200	**Average**
$\bar{V}_v$	0.085	0.12	0.055	0.062	0.079	0.067	0.1	0.1	0.11	0.086
$S_r/\bar{S}_v$	0.16	0.44	0.27	0.39	0.41	0.35	0.24	0.31	0.16	0.303

Averaging the statistical data yielded a value of 0.303 for the ratio of rudder to vertical tail area and 0.086 for the vertical tail volume; a definition of the vertical tail volume is provided in Equation 69. These values have subsequently been used in Equation 70 and Equation 71, in order to obtain the initial values for the vertical tail and rudder area; which resulted in $9.014m^2$ and $2.731m^2$ for the vertical tail area S_v and rudder area S_r, respectively, which are relatively small estimates.

$$\bar{V}_v = l_v S_v/(Sb) \quad (69) \qquad S_v = \bar{V}_v Sb/x_v \quad (70) \qquad S_r = S_r/\bar{V}_v \cdot \bar{V}_v \quad (71)$$

Airfoil selection When it comes to selecting an airfoil for the vertical tail, two geometrical properties are of importance. First and foremost, the airfoil needs to be symmetrical, to be able to provide lateral control

in both directions. Additionally, a blunt leading edge is desirable, since it delays leading edge vortices [51]. The formation of leading edge vortices occur at higher angles of attack; a large yaw angle can therefore have drastic effects on the airfoil efficiency, especially if it has a sharp leading edge. For the airfoil used in the vertical tail there were two options considered, the joukovsky 0009-jf and the NACA 0012, which both have a blunt leading edge. Their most notable difference is, aside from a slightly different lift curve slope, their difference in the thickness-over-chord ratio t/c. Later, when sizing the rudder, the influence of the t/c ratio will be elaborated on, and the airfoil will subsequently be selected.

Vertical Tail Sizing for One Engine Inoperative The vertical stabilizer must be designed in such a way that it can provide lateral control during all possible scenarios in the operational life of the aircraft. The most critical scenario is during take-off, with One Engine Inoperative (OEI); the asymmetric thrust causes a large yawing moment which is to be counteracted by the vertical stabilizer. In order to produce a counteracting yawing moment, the rudder has to be deflected; furthermore, the rudder deflection should not exceed 25 degrees in absolute sense [31]. The reader is, for all equations, figures and variables used in this paragraph, referred to Roskam books II [2] and VI [31] on empennage design and lateral control.

$$\delta_r = ((1+N_D)N_{t_{crit}}) \,/\, (\bar{q}_{mc} S b C_{n_{\delta_r}}) \qquad \bar{q}_{mc} = \frac{1}{2}\rho_{to} V_{mc}^2 \qquad V_{mc} = 1.2\, V_{min} \qquad N_{t_{crit}} = T_{TO_e}\, y_t \tag{72}$$

With Equation 72 the deflection of the rudder is calculated for a specific value of the vertical tail area, rudder to vertical tail chord ratio and control derivative $C_{n_{\delta_r}}$. It is assumed that the rudder vertical tail area ratio is the same as the ratio of rudder-chord and chord c_f/c of the vertical tail. The equations used to determine the control derivative are Equation 73 through Equation 77. The only parameter in Equation 72 that is dependent on S_v and c_f/c is the control derivative $C_{n_{\delta_r}}$; although this is not directly apparent, as c_f/c is used to determine the values for k', $\alpha_{\delta_{cl}}$ and $cl_{\delta_{theory}}$.

$$C_{n_{\delta_r}} = -C_{y_{\delta_r}} (l_v cos\alpha + z_v sin\alpha)/b \tag{73}$$

$$C_{y_{\delta_r}} = (C_{L_{\alpha_v}} \,/\, c_{l_{\alpha_v}})\,(k'\,K_b)\{(\alpha_\delta)_{C_L} \,/(\alpha_\delta)_{c_l}\}\,(C_{l_\delta} \,/\, c_{l_{\delta_{theory}}})\, c_{l_{\delta_{theory}}} (S_v/S) \tag{74}$$

$$C_{L_{\alpha_v}} = 2\pi A_{v_{eff}} / [2 + \{(A_{v_{eff}}^2 \beta^2 k^2)\,(1 + tan^2 \Lambda_{c/2}/\beta^2) + 4\}^{1/2}] \tag{75}$$

$$A_{v_{eff}} = (A_{v(f)}/A_v)\, A_v \,\{1 + K_{vh}\{(A_{v(hf)}/A_{v(f)}) - 1\}\} \tag{76}$$

$$\beta = (1 - M_{to}^2)^{1/2} \qquad k = (c_{l_\alpha})_{M_{to}} \,/\, (2\pi/\beta) \qquad A_v = (b_v)^2/S_v \tag{77}$$

Using the previously established rudder area estimations, the required rudder deflection is determined for the respective vertical tail area. Through iteration, the minimum vertical tail area is determined, whilst keeping the magnitude of the rudder deflection below 25 degrees, and, at the same time, also manually adjusting the coefficients which have been obtained from graphs in [52]. The values that are subjected to change with vertical tail area are: K_{vh} and the ratios of $A_{v(f)}/A_v$ and $A_{v(hf)}/A_v$. Lastly, it should be noted that the NACA 0012 airfoil has been chosen for the vertical tail design for the reason of a higher t/c ratio, which decreased the vertical tail area required. The parameter $c_{l_{\delta_{theory}}}$ is strongly influenced by the t/c ratio; the smaller t/c of the joukovsky 0009-jf results in an increase in vertical tail area of almost 3%.

In Figure 35 the relationship between the vertical tail area S_v and the associated required rudder deflection to counteract the EOI yawing moment has been depicted on the right; on the left, the relationship between the control derivative and the required rudder deflection can be seen. As can be seen in the figure, an increase in vertical tail area will logically result in a decrease in required rudder area; similarly, an increase in magnitude of the control derivative will too result in a decrease in required deflection of the rudder. Furthermore, from Equation 73 and Equation 74 it becomes apparent that an increase in vertical tail area increases the effectiveness of the rudder.

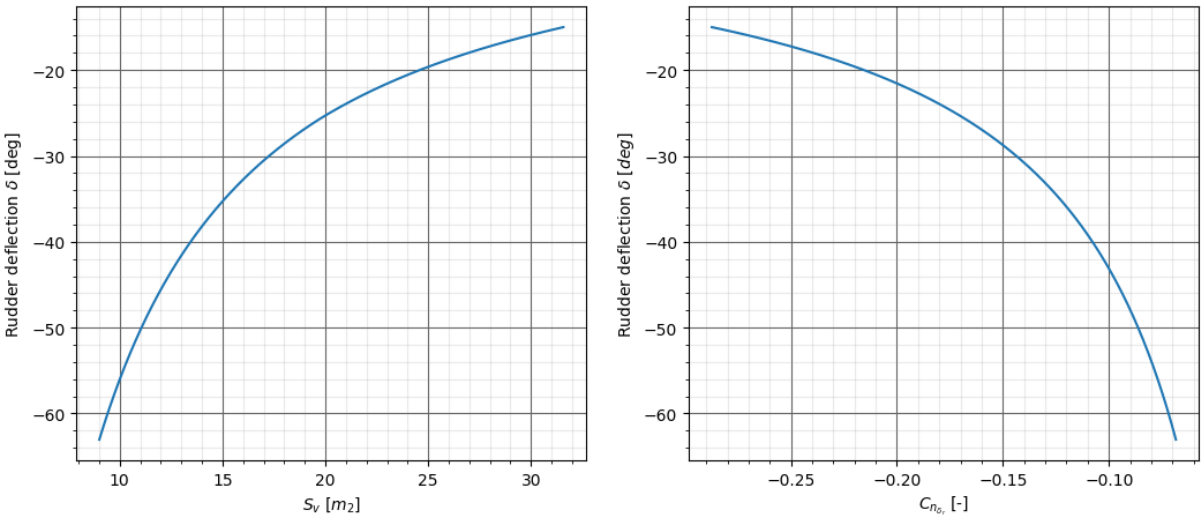

Figure 35: δ [deg] plotted against S_v [m^2] (l) and δ [deg] against $C_{n_{\delta_r}}$ [-] (r)

After the design was finalized, it was noted that the vertical tail area was too large. Therefore, as suggested in Roskam [2], the rudder will get a double hinge line. This means it has variable camber, which allows for further deflection of the rudder, up to 40 degrees. It should be noted that the author mentions it will require further research and possibly wind tunnel testing. It is however, assumed that it is possible to make use of the double hinge line rudder, and that is has been, as the author suggests, validated. Below, in Table 35, all relevant dimensions of the vertical tail are tabulated, which have been obtained based on the OEI rudder design.

Table 35: Vertical tail dimensions

Vertical tail area S_v/S [-]	Vertical tail span b_v/b [-]	Vertical tail AR A_v [-]	Vertical tail taper ratio λ_v [-]	Rudder area S_r/S_v [-]	Vertical tail volume $\bar{V}_v$ [-]	Distance aerodynamic center to nose A/C ac_v [m]	Distance aerodynamic center to A/C C.G. l_v [m]
0.224	0.207	1.7	0.6	0.303	0.117	26.20	11.71

Recommendations and Requirements Compliance The ratio of the vertical tail to wing area equals 0.325; the vertical tail has a significant size compared to the wing area. The reason for this is the high take-off thrust, required for taking off at an altitude of 1500m. The thrust will, in case of an engine malfunction, cause a large yawing moment, hence the relatively large required vertical tail area.

An improvement in rudder performance can be made by, instead of taking a simple flap, doing further aerodynamic research on the the rudder with a double hinge line. It is also recommended to do further research on the effect of increasing or decreasing c_f/c. Furthermore, when modeling the control derivative $C_{n_{\delta_r}}$, a lot of parameters are read off from graphics presented in Roskam. Modeling these coefficients with software would not only speed up the process, but would also make it more accurate.

The requirements that influence the vertical tail and rudder design are requirement SRA-SYS-CNTR-01, SRA-SYS-CNTR-02, SRA-SYS-CNTR-03 and SRA-SYS-CNTR-08. Of these requirements, SRA-SYS-CNTR-08, is of most interest for the vertical tail of the empennage. The required S_v to counteract the moment caused by an inoperative engine has been determined in this section; to this end the vertical tail was designed. The design therefore complies with the set requirements. Furthermore, regarding the other requirements, the rudder will allow for pitch and yaw control and stability.

Sensitivity Analysis In order to prove the solidity of the design, a sensitivity analysis is performed. The effect of a change on the MTOW, thrust and c_f/c ratio has been evaluated and tabulated in Table 36. Although at first glance the effect of an increased MTOW might seem counter intuitive, however, the MTOW determines the

minimum control speed; a higher MTOW makes it so the minimum control speed V_{mc} increases, resulting in a decreased required vertical tail area. The effect of thrust is straight forward, a higher thrust causes a higher yawing moment resulting in a larger tail. Lastly, it should be noted that for both an increase and decrease in ratio of C_f/c the required vertical tail area increases, although the former has a stronger influence. This therefore shows that the value for S_r/S_v obtained from statics has proven to be a good estimate.

Table 36: Sensitivity analysis of the vertical tail design

Parameter	**value**	MTOW +10%	MTOW - 10%	Thrust +10%	Thrust -10%	c_f/c + 0.1	c_f/c - 0.1
S_v/S	13.23 [m^2]	-8.0 %	+ 9.6 %	+ 8.6 %	-9.82 %	+ 10.2 %	+ 1.4 %
S_r	4.50 [m^2]	-8.0 %	+ 9.6 %	+ 8.6 %	-9.82 %	+ 10.2 %	+ 1.4 %
$\bar{V}_v$	0.117 [-]	-9.8 %	+ 10.7 %	+ 9.7 %	- 9.85 %	+ 11.4 %	+ 1.6 %

The columns in red show for which differences in the design it is required to redesign the vertical tail. Requirements that will no longer be met due to this required increase in vertical tail area are: SRA-SYS-CNTR-08, SRA-SYS-CNTR-01, SRA-SYS-CNTR-02 and SRA-SYS-CNTR-03. The effects of decreasing c_f/c by 0.1 should be studied further.

6.4.5 Horizontal Tail

The horizontal tail must comply with several requirements. Each of the following paragraphs will make sure that the requirements that apply to the horizontal tail are met. The final input and output parameters are given in Table 37.

Stability The requirement of static longitudinal stability of the aircraft, SRA-SYS-CNTR-03, will be satisfied by placing the neutral point aft of the C.G. The most aft C.G. location is a function of the aerodynamic center x_{ac}, the lift slope of the horizontal tail $C_{L\alpha_h}$, the tailless aircraft lift slope $C_{L\alpha_{A-h}}$, downwash $\frac{d\epsilon}{d\alpha}$, tail arm l_h, Mean Aerodynamic Chord $\bar{c}$, tail speed ratio $\frac{V_h}{V_\infty}$, tail to wing ratio $\frac{S_h}{S}$ and the stability margin $S.M.$. The function is given in Equation 78. Since the aerodynamic center shifts forward as the mach number of the aircraft increases, and the nose down moment caused by the flaps is not present, the most critical flight condition for stability is during cruise. The location of the aerodynamic center has been determined using the method from [48]. This includes calculating the aerodynamic center shift due to several aircraft components; fuselage, nacelles, wing. The horizontal tail lift slope is estimated using the DATCOM method [48], as shown in Equation 79. In this equation, β is the Prandtl-Glauert correction.

$$x_{cg} = x_{ac} - \frac{C_{L\alpha_h}}{C_{L\alpha_{A-H}}}\left(1 - \frac{d\epsilon}{d\alpha}\right)\frac{l_h}{MAC}\left(\frac{Vh}{V}\right)^2\frac{Sh}{S} - S.M. \tag{78}$$

$$C_{L\alpha} = \frac{2\pi AR}{2 + \sqrt{4 + (\frac{AR\beta}{\eta})^2 + \frac{tan^2\Lambda_{0.5c}}{\beta^2}}} \tag{79}$$

The tailless aircraft lift coefficient was given by Equation 80, with $C_{L\alpha_w}$ being estimated using Equation 79. b_f is the width of the fuselage, while S_{net} is the area of the wing not inside of the fuselage. The downwash of the wing is not of a large effect on the tail, as a T-tail configuration is used. Though, it is still taken into account. The speedratio between the free stream and the tail due to the wing wake is taken to be 1, due to the T-tail configuration[48]. The stability margin is taken to be 5% of the mean aerodynamic chord, as suggested in [48]. The tail arm length and tail area are to be optimized.

$$C_{L_{\alpha_{A-h}}} = C_{L\alpha_w}(1 + 2.15\frac{b_f}{b})\frac{S_{net}}{S} + \frac{\pi}{2}\frac{b_f^2}{S} \tag{80}$$

Control During the entire flight, the aircraft must remain controllable, according to SRA-SYS-CNTR-01 and SRA-SYS-CNTR-02. The control limit is given by Equation 81 [53]. Once again, it is a function of the location of the aerodynamic center, tail arm, speed ratio of the tail and the ratio of the horizontal stabilizer with respect to the wing. In this equation, the moment coefficient around the aerodynamic center $c_{m_{ac}}$ is required. Furthermore, the lift coefficient of the tail and of the tailless aircraft are used. The most critical condition for control is during approach, as the flaps contribute a lot to the moment coefficient around the

aerodynamic center. The moment coefficient was determined once again by matter of summing up moment coefficients caused by several aircraft components, as suggested in [53]. Note that all of the parameters required in Equation 81 were recalculated for the lower mach number. Finally, the $C_{L_{H_{max}}}$ is dictated by the tail type. In this design, a adjustable tail is chosen, as it is cheaper than a full moving tail, while still having the advantages of achieving a high lift coefficient of 0.8. Additionally, it is widespread in aircraft of similar size and function.

$$x_{cg} = x_{ac} + \frac{C_{m_{ac}}}{C_{L_{A-H}}} + \frac{C_{L_{H_{max}}}}{C_{L_{A-H}}} \frac{l_h}{MAC} \left(\frac{Vh}{V}\right)^2 \frac{Sh}{S} \tag{81}$$

Scissor Plot and Wing Placement The equations that were used in Section 6.4.5 have been combined into a single figure, as a function of $\frac{S_h}{S}$, to form the scissor plot. In this plot, the C.G. with respect to the mean aerodynamic chord is shown on the x-axis, while the ratio between the horizontal tail area and wing area is given on the y-axis. The C.G. of the aircraft must be to the right of the control limit, and to the left of the stability limit.

As this plot changes for each wing position, an iterative program was created to find the wing position with the lowest $\frac{S_h}{S}$ possible. For each wing position, the C.G. was recalculated, as well as the control and stability limits. The iteration found the tail area to be lowest at the wing root placed at $10.m$, measured from the nose. The tail size it yields, with a 5% margin for both control and stability, is 0.155. The figure can be seen in Figure 36. Note that this horizontal tail size is very low when compared to other aircraft. In further subsections it will change.

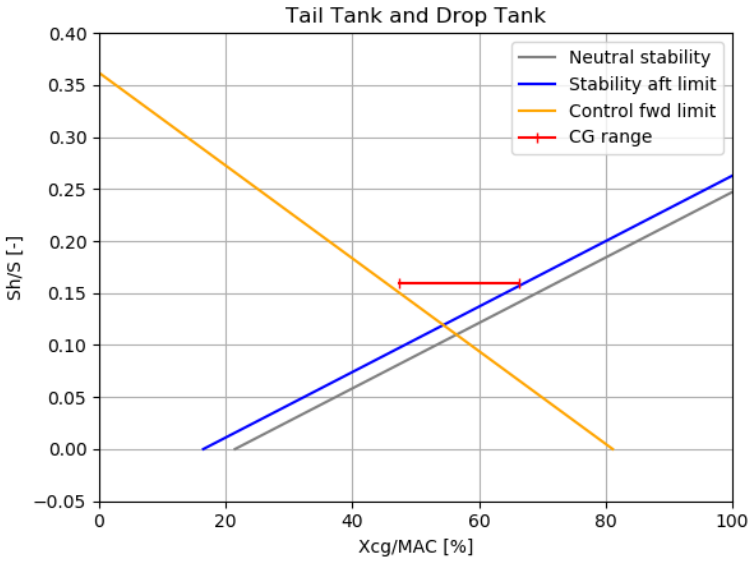

Figure 36: Scissor plot determining tail size

Rotation Another requirement for the horizontal stabilizer, is that it shall be able to provide enough downforce to rotate the aircraft when taking off, as specified in SRA-SYS-CNTR-06. All calculations were done with values during take-off in mind. The most critical case is when the C.G. is furthest forward, as this creates a large nose-down moment around the landing gear. To aid the rotation of the aircraft, the distance between the wing and landing gear should be maximal, as the lift of the wing creates an upward moment around the landing gear. This implies that the wing must be placed as far forward as possible. Again, for each wing position, the minimum horizontal tail size was calculated iteratively, using Equation 85, which receives inputs from Equation 82, Equation 83 and Equation 84. The results for the stability and control, and the rotation requirement were combined. For each wing placement, the maximum of the two tail sizes was taken, to fulfill both requirements. Note that the landing gear location is calculated in Equation 6.4.6. The result of the minimum tail size according to rotation is that the C.G. would be extremely far aft relative to the wing. This would cause enormous trim drag, or even make it impossible to fly. It was therefore chosen to include the rotation requirement as a green line in the final scissor plot in Figure 37. The sizing according to trim drag is

discussed further in the next paragraph.

$$M_{weight} = W_{aircraft} \cdot (x_{mainLG} - x_{cg}) \quad (82) \qquad M_{lift} = \frac{1}{2}\rho \cdot V_{TO}^2 \cdot S \cdot C_{L_0} \cdot (x_{mainLG} - x_{ac}) \quad (83)$$

$$M_{aerodynamiccenter} = C_{m_{ac}} \cdot \frac{1}{2}\rho \cdot V_{TO}^2 \cdot S \cdot MAC \quad (84) \qquad S_h = \frac{(M_{weight} - M_{lift} - M_{ac})}{\frac{1}{2}\rho \cdot V_{TO}^2 \cdot C_{L_{H_{max}}} \cdot (x_{ac_{tail}} - x_{mainLG})} \quad (85)$$

Trim The final criteria to which the horizontal tail must be sized to, is the trim drag, as specified in SRA-SYS-CNTR-04. The trim drag consists of the induced drag, caused by the lift of the tail. It increases with a larger tail lift coefficient. The equation is given in Equation 86. To trim the aircraft, the moment coefficient C_m must be zero. This can be satisfied by changing the incidence angle of the horizontal stabilizer, thus changing C_{L_h}. The required tail lift coefficient can be calculated using Equation 87, with the drag calculation following that in Equation 86.

$$D_{trim} = \frac{1}{2}\frac{\rho V^2 S_h C_{L_h}}{\pi A R_h e} \quad (86) \qquad C_{L_h} = \frac{Cm_{ac} S \cdot MAC}{S_h l_h} + C_{L_{A-h}} S(x_{cg} - x_{ac}) \quad (87)$$

If the tail size and C.G. location is taken from Figure 6.4.5, the lift coefficient of the tail becomes too large. Thus the tail requires a more forward C.G.. This implies that the wing must be placed more aft, while the tail size according to the rotation requirement must increase. A point was chosen, in which the tail size would not be more than 20% larger than the reference aircraft (CRJ700), while the trim drag during cruise remains below 10% of the total aircraft drag. The scissor plot according to this selection is shown in Figure 37. A planform drawing is shown in Figure 38.

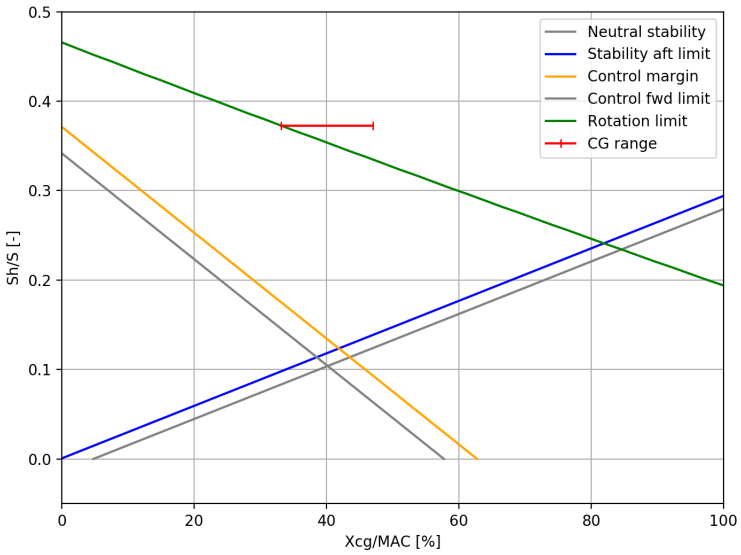

Figure 37: Scissor plot including rotation requirement

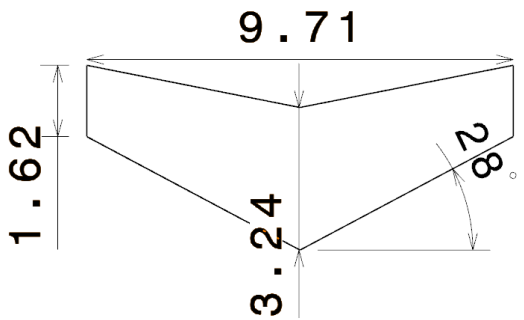

Figure 38: horizontal tail planform $[m]$

Table 37: Input and output parameters for sizing the horizontal stabilizer

Parameter	Value [unit]	Source
Stability		
x_{ac}	4.7 [%]	Calculated [48]
$C_{L_{\alpha_H}}$	4.36 [-]	DATCOM
$C_{L_{\alpha_{A-H}}}$	5.86 [-/rad]	Calculated[48]
$\frac{d\epsilon}{d\alpha}$	0.08[-]	Estimated [48]
l_h	15.2 [m]	Geometric estimation
MAC (wing)	3.05 [m]	Wing sizing
$\frac{V_h}{V}$	1 [-]	[48]
β	0.66 [-]	Prandtl-Glauert
$C_{L_{\alpha_w}}$	5.46 [-/rad]	DATCOM
b_f	3.486 [m]	Cabin layout
b	22.3 [m]	Wing sizing
$\frac{S_{net}}{S}$	0.76 [-]	Geometric estimation
S.M.	5 [%]	[48]
Control		
x_{ac}	-3.5 [%]	Calculated [48]
$C_{m_{ac}}$	-1.45 [-]	Calculated [53]
$C_{L_{A-H}}$	2.36 [-]	Wing sizing
Rotation		
$W_{aircraft}$	256266 [N]	$M_{zfw} \cdot g$
x_{mainLG}	15.44 [m]	Section 6.4.6
x_{cg}	14.56 [m]	Section 6.4.2

Parameter	Value [unit]	Source
Rotation		
ρ	1.225 [kg/m^3]	ISA SL
V_{TO}	59 [m/s]	
S	62.248 [m^2]	Wing sizing
C_{L_0}	0.96 [-]	Approximation
x_{ac}	-0.035 [-]	Calculated [53]
$C_{m_{ac}}$	-0.61 [-]	Calculated [53]
AR_h	4 [-]	Decided upon
C_{L_h}	Varying	Calculation
e	0.85[-]	[48]
$C_{L_{H_{max}}}$	-0.8 [-]	adjustable tail[53]
Results		**Notes**
$x_{rootchord}$	10.7 [m]	
x_{lemac}	13.14 [m]	
S_h	23.58 [m^2]	
$\frac{S_h}{S}$	0.3788 [-]	
$x_{ac_{tail}}$	28.9 [m]	
D_{trim}	2272 [N]	Approach/TO, max
D_{trim}	45 [N]	Cruise, max
b_h	9.7 [m]	
MAC_h	2.52 [m]	
$_{0.5c}$	25 [deg.]	

Recommendations As the horizontal tail meets each appropriate requirement given in Table 31, no specific recommendations will be given to achieve the requirements. Though, a few recommendations following the results of the tail sizing can be made. First of all, the horizontal tail size is relatively large when compared to other aircraft. The main factor that influences this result is the rotation requirement, and the forward C.G. location. The recommendation is to investigate in what way other aircraft achieve rotation at their most forward C.G., to possibly further reduce the horizontal tail size. Moving the gear further forward could also be investigated. The C.G. range of RELIGHT is similar to other aircraft, while the horizontal tail size is relatively large. Furthermore, the dynamic stability of the aircraft must be researched.

Table 38: Sensitivity analysis horizontal tail

Parameter	**value**	MTOW+10%	MTOW-10%	x_{cg}+10%	x_{cg}-10%	C_{L_H}+10%	C_{L_H}-10%	$C_{m_{ac}}$+10%	$C_{m_{ac}}$-10%
$\frac{S_h}{S}$	0.3788	+8.6%	-10 %	-6.1%	+5.6%	-9.1%	+11%	+11%	-6.1%
D_{trim}	45 [N]	-4%	+13 %	+202%	-70%	+13%	-8.9%	-33%	+51%

Sensitivity Analysis In Table 38 the results of the sensitivity analysis of the horizontal tail is given. In the sensitivity analysis, the wing root was kept at the same location, while only the shown input parameters were adapted. The largest direct influence is the tail lift coefficient, C_{L_H}. If it can be increased, the tail area can be reduced drastically. Note that the decrease in take-off weight also decreases the horizontal tail size relative to the wing area. This is due to the large influence the weight has on the rotation requirement. If the MTOW or $C_{m_{ac}}$ is increased, SRA-SYS-CNTR-06 will not be met without a larger horizontal tail. This also holds for a C.G. shift forward, or a reduction in maximum tail lift coefficient. Note that the increase or decrease in trim drag is percentually very large, while the absolute differences are relatively insignificant. This ensures the compliance with SRA-SYS-CNTR-04.

6.4.6 Landing Gear Sizing

In this section, all parameters, unless specified otherwise, have either been directly obtained from, or have been calculated using methods presented in Roskam part IV [52], which treats the design of landing gear.

Lastly, it is important to note that several times in this sections units are given in United States customary units; this facilitates reproducibility of the sizing procedure.

Determining Number of Struts and Wheels per Strut Due to the high wing configuration, wing-mounted landing gear is no option, instead the retractable landing gear is mounted on the fuselage. The number of main landing gear wheels is determined based on the W_{TO} in newtons. Using Equation 88, which is valid for regional jets, the obtained value for N_{mw} is to be rounded to the nearest multiple of 4, with a minimum of 4, and the number of nose wheels equals 2 for al CS25 aircraft [6]. The same source suggests that if the total number of wheels is below or equal to 12, the number of main landing gear struts is equal to 2. The aircraft will have 1 nose gear strut with 2 wheels, and 2 main gear struts, both with 2 wheels.

$$N_{mw} = W_{TO}/120,000 \tag{88}$$

Longitudinal and Vertical Position of the Nose and Main Landing Gear The location of the main landing gear X_{LG} with respect to the nose of the aircraft is determined based on the clearance angle θ and the angle β, which are both defined in Figure 39; the angle β is the angle the line through the most aft C.G. and the contact point of the main landing gear with the ground at lift-off makes with the line normal to the lift-off ground line. The clearance angle equals 15 degrees, which is a nominal value for aircraft [6]. It is required that the angle β is strictly larger than θ; by iterating the height of the landing gear Z_{CG} and setting the constraints on both angles, the exact longitudinal and vertical location of the landing gear are determined.

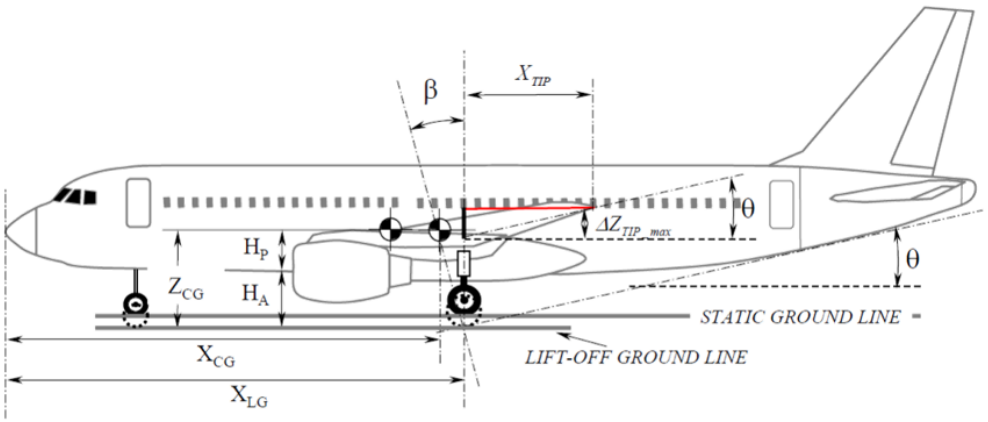

Figure 39: Pitch angle limit [48]

$$X_{LG} = X_{CG_{aft}} + Z_{CG} \cdot tan\beta \tag{89}$$

In a similar fashion, the location of the nose landing gear can be determined. However, it is required, for adequate steering, that the load on the nose gear is not less than 0.08 times the weight at take-off [52], nor larger than 0.15 times the take-off weight [6]; this holds for the most forward and most aft C.G. location the aircraft has whilst still being operable. If, for example, the aircraft has just landed after burning all fuel, the C.G. location has, as can be seen in Figure 34, moved forward. This causes the nose gear to be loaded more excessively; the loading on the nose gear should not be too excessive to cause partial or complete failure. Likewise, when the aircraft flies with only cargo and is filled with fuel, the aircraft C.G. is more aft, which is allowable as long as the nose gear is sufficiently loaded for steering. The set location of the main landing gear allows for a small design space in which the nose gear can be placed; consequently, the nose gear is placed such that it has the smallest normal force acting on it as possible, whilst being in compliance with aforementioned requirements. Table 39 provides all relevant distances and locations of the main and nose landing gear.

Lateral Position of the Main Landing Gear The lateral position of the main landing gear Y_{LG} is constrained by the turn over angle, as it shall not exceed 55 degrees [48]. The definition of the turn over angle Ψ can be seen in Figure 40.

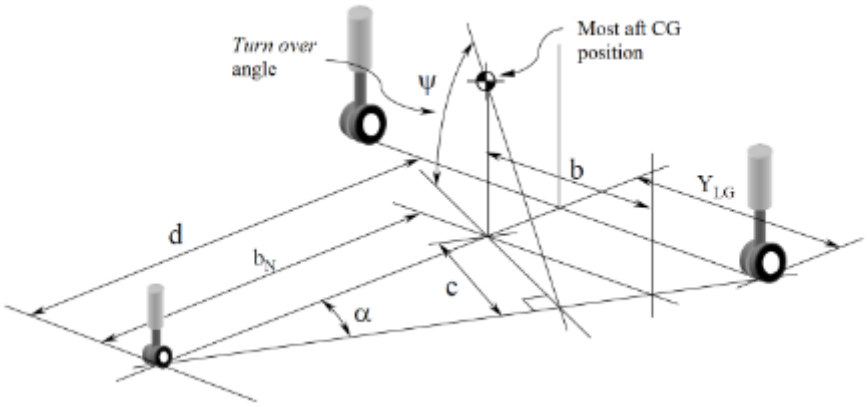

Figure 40: Sizing lateral position of the main landing gear [48]

$$\alpha = arctan\left(\frac{Y_{CG}}{d}\right) \qquad c = b_N sin\alpha \qquad \Psi = arctan\left(\frac{Z_{CG}}{c}\right) \tag{90}$$

Through iteration the smallest lateral distance of the main landing gear is determined. Furthermore, it is assumed that this location, that is to say the theoretical minimal lateral distance, is located between the main landing gear tires. As the aircraft has only one main gear strut, the nose gear lies on the symmetry plane of the aircraft.

Landing Gear Location Overview Table 39 provides an overview of the landing gear placement. In the right-most column the relative loading of the main and nose gear is given, which indeed shows that the aircraft does indeed exerts a sufficiently large normal force on the nose gear strut to be able to steer the aircraft.

Table 39: Landing gear location

Landing gear	Longitudinal position w.r.t. A/C nose [m]	Vertical position from ground w.r.t. Z_{cg} [m]	Lateral position Y_{LG} w.r.t. A/C symmetry plane [m]	Loading relative to W_{TO} [-]
Main	15.4311	3.203	2.295	0.9118
Nose	3.84	3.203	-	0.0882

Tire Pressure An important aspect of the design of the landing gear is a careful selection of the right tires and a careful assessment on the allowable wheel load per landing gear strut. To avoid surface damage of the runway due to landing, the load exerted by each tire should not be too high. Therefore the LCN (Load Classification Number) method, established by the ICAO, is used. The lower the LCN, the less impact the aircraft will have on the runway [6][52]. In order to assess the LCN, the Equivalent Single Wheel Load (ESWL) is to be determined. For dual wheel layouts, the ESWL is determined using Equation 92 and Equation 91, where P_m and P_n, the load on the main and nose landing gear respectively, is the load per strut; both the load on the nose and main landing gear are in Newtons.

Using Equation 91, Equation 92 and Equation 93, together with relevant figures obtained from Torenbeek [54], the LCN and required tire pressure can be determined. Although having a low as possible LCN is favorable in terms of landing possibilities on different airports, it does have adverse effects on the wheel size; a higher value of the LCN allows for a higher tire pressure, thus resulting in smaller and lighter tires.

$$ESWL_{mw} = P_m/1.33/g \quad (91) \qquad ESWL_{nw} = P_n/1.33/g \quad (92) \qquad p = 430ln(LCN) - 680 \quad (93)$$

It is determined that, based on the equivalent single wheel loading, the tires will operate at an LCN of 40, at a pressure of $906.22kPa$, which is 8.5% lower than the CRJ700 tire pressure[19].

[19]The CRJ700 tires operate at $1060kPa$

Tire Sizing and Selection Procedure When sizing for the main gear tires, the maximum static load, at the weight/C.G. location which results in the highest load per tire, is the most critical loading scenario. Nose wheel tires are, on the contrary, designed for the maximum dynamic loads. The maximum dynamic load experienced by the nose gear tire is determined from Equation 94, with a_x/g, the braking coefficient for dry concrete, taken for that of simple brakes. Lastly, in order to proceed to selecting the right tires, the tire speed is to be calculated, using Equation 95; the highest value is taken as the maximum tire speed.

$$P_{n_{dyn_t}} = W_{TO}\{l_m + a_x/g(h_{cg})\}/n_t(l_m + l_n) \quad (94) \qquad V_{tire/max} = 1.2\, V_{s_L} \quad V_{tire/max} = 1.1\, V_{s_{TO}} \quad (95)$$

The tire selection is confined to tires made by Dunlop, who have also supplied the CRJ700 aircraft tires. For the tires, a selection is made from the Goodyear tire catalogue[20].

Some of the tires have a 'H' before the first dimension, denoting a 5% bead taper; beads are layers of steel wires embedded in the rubber, providing a firm fit for the wheel [52]. Tires are often inflated to a lower pressure than the rated inflation pressure specified in the tire manufacturer catalogue; if this is the case, pressures are linearly reduced with the loads [55]. The CRJ700 reference aircraft is equipped with Dunlop H36x12.0-18 tires on the main wheels, and 20.5x6.75-10 nose tires[21], which respectively have a 1220 and 1241 PSI rated inflation pressure. However, the main tires only operate at roughly 85% of this pressure[22]. Note that tire dimensions are given in Outer diameter x Width - Inner diameter in inches.

When selecting the tires for RELIGHT, several parameters are looked at. First, whether the tires can sustain the applied loads; second, whether they are made to allow for the maximum calculated tire speed; furthermore, their required inflation pressure should not be too much above the calculated tire pressure, as the load it can bear will also decrease. With these requirements in mind, a similar selection procedure has been performed as is suggested in [52]. The selected tires are tabulated in Table 40 below. The tires will operate, as calculated with Equation 93, at 906.22kPa.

Table 40: Selection of viable Dunlop tires for the main gear of the aircraft

	Size Dxb−d (in)	**Ply Rating**	**Rated Speed (MPH)**	**Rated Load (lbs)**	**Rated Inflation (PSI)**	**Part Number**
Main gear tire	34x9.25-16	18	210	17800	190	348F83-2
Nose gear tire	17.5x5.75-8	12	210	5000	180	178K23-5

Wheel brakes are implemented in the wheels to allow for slowing down the aircraft, help steering, running up of the engines, and holding it in place during loading or unloading. It should be noted that a detailed design of the brakes is left for future design.

Shock absorber design At the moment of touchdown, the total total kinetic energy of the aircraft has to be absorbed. The tires absorb some of this kinetic energy, whilst the remainder is to be absorbed by a built in shock absorption mechanism; to this end, oleo-pneumatic shock absorbers are used, as they have a high energy absorption efficiency [52]. Equation 96 is used to determine the total kinetic energy, with which, after having selected the correct tires, the shock absorber stroke length of the main and nose landing gear, and the diameter can be calculated using Equation 97, Equation 98 and Equation 99, respectively. Table 41 provides the results of the shock absorber design; it lists the stroke length including the required diameter of the oleo-pneumatic absorber. At last, the effect of fuselage mounted gear should be mentioned: Since the load on the main gear will not be an axial load, but more of an oblique load, the structure of the main landing gear will have to be stronger to absorb the oblique load. However, following from the equations below, the stock stroke will not become longer, as the multiplication factor this would introduce is found both in the denominator and in the numerator.

$$E_t = 0.5(W_L)(w_t)^2/g = W_L N_g(\eta_{tire} s_t - \eta_s s_s) \quad with \quad W_L = n_s P_m \quad (96)$$

[20] https://www.goodyearaviation.com/resources/pdf/tire-specifications-6-2018.pdf
[21] https://www.dunlopaircrafttyres.co.uk/aircraft/bombardier-crj-700-900-tires/
[22] https://tc.gc.ca/media/documents/ca-opssvs/dec_list.pdf

$$s_s = \{(0.5(W_L/g)(w_t^2)/(n_s P_m N_g)) - \eta_{tire} s_t\}/\eta_s + 1 \quad with \quad s_t = D_o - 2(loaded\ radius) \tag{97}$$

$$s_{s_{nose}} = \{(0.5(P_n/g)(w_t^2)/(n_t P_{n_{dyn_t}} N_g)) - \eta_{tire} s_{t_{nose}}\}/\eta_s + 1 \ with \ s_{t_{nose}} = (D_o - 2(loaded radius))_{nose} \tag{98}$$

$$d_s = 0.041 + 0.0025\ (P_m)^{1/2} \tag{99}$$

Table 41: Relevant Shock Absorber Dimensions

Shock absorber	Stroke length $[m]$	Diameter $[m]$
Main gear	0.341	0.146
Nose gear	0.324	0.077

Recommendations and Requirement Compliance The location of the nose landing gear is, when compared to other aircraft, quite far aft. An explanation for this is that it is due to the nature of the C.G. excursion, as can be seen in Figure 34. As the passengers take up a large part of the payload weight, the loading diagram strongly tilts to the left, that is to say: it causes a large C.G. shift forward. On the contrary, the extreme loading case, when seen relative to the OEW C.G. location, does not move the c.g. that far aft. Therefore, the main landing gear is located relatively close to the C.G. of the aircraft. As explained in Equation 6.4.6, the nose landing gear is constrained by steering requirements; it therefore can not be located too far away from the main landing gear, hence the aft location.

The recommendation for the design of the landing gear is to further study the structural design, as well as conducting studies on the effect of adding multiple plies on the tires. Also, a detailed look into landing gear breaks is advised. Moreover, new technologies should be considered to improve the shock absorptive efficiency of the landing gear.

All landing gear requirements mentioned in Table 31 have been met, except for requirements SRA-SYS-LG-04 and SRA-SYS-LG-07, which have partially been met. Regarding the latter, the effects of using normal tires, instead of anti-skid, with respect to the required landing distance has not been studied; it is therefore recommended take this into account in further considerations. Regarding the take-off acceleration: if the landing gears are capable of absorbing the landing shock, whilst also being able to brake after landing, it will also provide structural integrity to cope with take-off accelerations. For all other requirements has compliance been proven; the landing gear is capable of absorbing shocks, providing steering, as well as providing deceleration during taxiing.

Sensitivity Analysis In this paragraph a short overview of the performed sensitivity analysis is given, of which the results are found in Table 42. Interestingly, as can also be deduced from aforementioned equations, an increase of MTOW has no effect on the shock absorber stroke; only the diameter becomes larger. The position of the landing gear did, expected, not change, as it is merely dependent on the C.G. excursion. By shifting the entire C.G. excursion by $\pm$ 1 meter, the landing gear location does change. The location of the nose landing gear is very sensitive to the C.G. location; largely due to the fact that it is constrained by steering requirements. Lastly, the required shock absorber stroke length s_s is only influenced by the differing touchdown rate. If RELIGHT was to have a higher touchdown rate, the shock absorbs should be significantly longer; however, a value of 10 is a nominal value for transporters [52], and it is therefore unlikely the aircraft will experience a higher touchdown rate.

Table 42: Sensitivity analysis landing gear

Parameter	**value**	MTOW +10%	MTOW - 10%	X_{XG} + 1m	X_{XG} - 1 m	w_t + 1 fps	w_t - 1 fps
Main X_{LG}	15.43 $[m]$	+ 0 %	+ 0 %	+ 0.94 m	- 0.931 m	+ 0 %	+ 0 %
Nose X_{LG}	3.84 $[m]$	+ 0 %	+ 0 %	+ 1.80 m	- 1.78 m	+ 0 %	+ 0 %
Main Y_{LG}	2.295 $[m]$	+ 0 %	+ 0 %	- 0.173 m	+ 0.172 m	+ 0 %	+ 0 %
Z_{LG}	3.203 $[m]$	+ 0 %	+ 0 %	- 0.24 m	+ 0.238 m	+ 0 %	+ 0 %
Main s_s	13.42 $[in]$	+ 0 %	+ 0 %	+ 0%	+ 0 %	+ 25.7 %	- 23.2 %
Main d_s	5.736 $[in]$	+ 4.3 %	- 4.86 %	- 0.012 %	- 0.00155 %	+ 0 %	+ 0 %

The cells in red in above table indicate the infeasibility of the design, should an increase in MTOW or touch-down rate occur. The requirement SRA-SYS-LG-05 will then no longer be satisfied. Furthermore, the design should be checked with requirement SRS-SYS-LG-01, to determine whether the landing gear can still provide carriage.

6.4.7 Verification and Validation

The verification procedures of the Stability and Control section are specified in Table 43. The specific verification and validation procedures will also be elaborated below the table.

Table 43: Verification of the stability and control calculations

Function	Action	Expected result	Pass/Fail
OEW calculation			
	increase mass of forward situated component	OEW increases CG location moves forward	Pass
	move component further aft	CG location moves aft	Pass
	hand calculation of adding single component	Common result of CG and OEW between program and hand calculation	Pass
	hand calculation of sum of each component	match of OEW results	Pass
Loading Diagram			
	visual inspection of diagram	Increase in mass as loading increases	Pass
	visual inspection of diagram	Component masses and MTOM mass equal with program	Pass
Roll Control			
	unit check integral in Equation 66	[1/rad]	Pass
	unit check integral in Equation 67	[-]	Pass
	decrease τ	$C_{l_{\delta a}}$ and P decrease, C_{l_p} unchanged	Pass
	double δ_a	$C_{l_{\delta a}}$ and C_{l_p} unchanged, P doubled	Pass
	decrease aileron span width	$C_{l_{\delta a}}$ and P decrease, C_{l_p} unchanged	Pass
S_r & S_v design			
	increase S_v	$C_{n_{\delta_r}}$ increases, δ_r decreases	Pass
	increase S_h	S_v, $C_{n_{deltar}}$ increase, δ_r decreases	Pass
	adjust values obtained from tables	Correct change in S_v	Pass
	decrease l_v	increase in S_v	Pass
	lower S_r/S_v	larger required S_v	Pass
	lower A_v	require larger S_v	Pass
	increase y_t	increased δ_r, increased required S_v	Pass
	hand calculation and unit check	equal results and correct units	Pass
Horizontal tail			
	Verify formula's in code	Formula's agree with [48]	Pass
	Calculate each step by hand following [48], [53]	Values agree within small margin	Pass
	Compare scissor plot to [53] plot	Similar shape similar values	Pass

	Compare input and intermediate variables with known variables of other aircraft	same order of magnitude similar values	Pass
LG location			
	increase aft C.G. position	X_{LG} moves aft, $X_{LG_{nose}}$ forward	Pass
	increase Z_{CG}	X_{LG} moves aft, β, θ stay constant Y_{LG} increases, $X_{LG_{nose}}$ moves forward	Pass
	Increase θ	β increases, Y_{LG} increases, X_{LG} moves aft, $X_{LG_{nose}}$ moves forward,	Pass
LG loading			
	Increase MTOW value	P_{mw}, P_{nw}, $ESWL_{mw}$ and $ESWL_{nw}$, $P_{n_{dyn_t}}$ increase	Pass
	Move LG apart	Increased P_{mw} and $P_{n_{dyn_t}}$, P_{nw} decreases	Pass
Shock absorber			
	Increase P_{mw}	s_s, d_s increase, $s_{s_{nose}}$, $d_{s_{nose}}$ decrease	Pass
Landing gear code			
	hand calculation and unit check	equal results and correct units	Pass

Weight and Balance As the loading diagram method is adapted from [48], the validation procedure is not extensive. The results obtained will be the most forward and aft C.G. locations during flight. If the aircraft is loaded in a different order, the C.G. does not change, and stays within limits.

Roll Control Sizing The aileron sizing is validated by comparing the aileron with existing class II, as a these aircraft have similar rol rate requirements. To take the CRJ700 as example, it has outboard ailerons only, just like RELIGHT. Furthermore, the ailerons spans about $2.25m$ each, whereas it is $2.7m$ for RELIGHT. As this, together with the data from other reference aircraft, fall within the expected range, the roll control sizing is validated.

Vertical Tail A good way of validating the obtained results, is by comparison with other aircraft. Table 44 shows the consider aircraft with their respective tail volumes. The data was obtained from [2]. Compared to several aircraft of different sizes shows it is in the correct order of magnitude. The reason the vertical tail volume is on the high side is due to the high trust in combination with a relatively short aircraft; this significantly decreases l_v, which in turn reduces the effectiveness of the vertical tail. When comparing the vertical tail area over the wing area S_v/S, it can be seen that RELIGHT has a nominal value, right in between the other aircraft. This suggest it is not only proportionally accurate, but also correctly sized.

Table 44: Validation of the vertical tail volume

Aircraft	B727-200	B737-200	B737-300	A300-B4	A310	F-28-4000	Bae 146-200	**RELIGHT**
$\bar{V}_v$	0.110	0.100	0.100	0.094	0.098	0.085	0.12	0.117
S_v/S	0.248	0.238	0.214	0.174	0.207	0.185	0.269	0.223

Horizontal Tail To validate the results of the horizontal tail calculations, a comparison was made between this aircraft, and the CRJ700. The horizontal stabilizer of the CRJ700 is 15.91 m^2, while $\frac{S_h}{S}$ is 0.225 [56]. In comparison to RELIGHT, the horizontal stabilizer is relatively small. The larger RELIGHT stabilizer is likely due to the aft tail tank filled with hydrogen at take-off, causing a large C.G. shift during flight. The requirement that then increases the horizontal tail size is the rotation requirement. A further look should be taken if the RELIGHT aircraft can rotate with a smaller horizontal tail in further design.

Landing Gear In Table 43, the unit tests to verify the landing gear code and calculations are tabulated. Below, in Figure 41, the shock absorber stroke of several aircraft are given. It can be seen that heavier aircraft

with an equal touchdown rate (10 fps), have a slightly larger shock stroke. Although this is not dependent on the MTOW, as proven in the sensitivity analysis of the LG design, it is dependent on the type of wheels that have been selected, which could cause minor differences in shock stroke length. As previously discussed, a higher touchdown rate will increase the required shock stroke length.

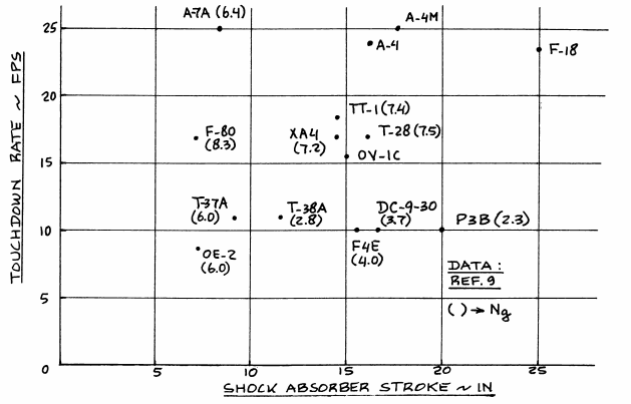

Figure 41: Shock absorber stroke [52]

In order to validate the locations of the landing gear, it is compared is compared to the CRJ700. Of course, the exact location is heavily dependent on the C.G. range. However, methods presented in [48] have carefully been followed. Furthermore, the main landing gear are behind the C.G. location; the lateral position is below the wing, 'sticking out' of the fuselage, which is the same for the CRJ700. When it comes to the nose gear location, there is a striking difference. RELIGHT'S nose landing gear is a lot more forward. This is due to the C.G. range, as the main landing gear are relatively close to the C.G., which results in a more forward location of the nose gear. Hence, the results are validated.

6.4.8 Component Weight Estimation

The following formula's were used to calculate the weight of the components that were discussed in this section. Note that Z_h in Equation 101 is the vertical placement of the horizontal stabilizer along the vertical stabilizer. This was approximated at 95% of the vertical stabilizers' span. The resulting weights are reported in Table 45.

$$M_{vertical} = K_v \cdot S_h \cdot \frac{3.81 \cdot S_h^{0.2} \cdot V_{dive}}{1000 \cdot cos(\Lambda_{0.5c})^{0.5} - 0.287} \tag{100}$$

$$K_v = 1 + \frac{0.15 \cdot S_h \cdot Z_h}{S_v \cdot b_v} \tag{101}$$

$$M_{horizontal} = 1.1 \cdot S_h \cdot \frac{3.81 \cdot S_h^{0.2} \cdot V_{dive}}{1000 \cdot cos(\Lambda_{0.5c})^{0.5} - 0.287} \tag{102}$$

$$M_{mainLG} = 1.08 \cdot \left(40 + 0.16 \cdot MTOW^{0.75} + 0.019 \cdot MTOW + 0.000015 \cdot MTOW^{1.5}\right) \tag{103}$$

$$M_{noseLG} = 1.08 \cdot \left(20 + 0.10 \cdot MTOW^{0.75} + 0.000002 \cdot MTOW^{1.5}\right) \tag{104}$$

Table 45

Vertical tail [kg]	Horizontal tail [kg]	Main landing gear [kg]	Nose landing gear [kg]
329.2	440.6	1017.2	217.3

6.5 Materials and Structural Design

In this section the design of the main structures of the aircraft, as well as material choices for said structures, are discussed. The section starts with the wing box, followed by the fuselage structure and concluding with the tanks, that due to the fuel choice, require special attention.

6.5.1 Wing Box Design

Table 46: Wing system requirements

Requirement Identifier	Requirement	Compliance
Wing System		
SRA-SYS-WAero-01	The wing shall be capable of bearing all loads at n_{ult}	✓
SRA-SYS-WAero-03	The wing shall be able to withstand the loads created by aerodynamic forces without yielding or buckling	✓/✗
SRA-SYS-FG-01	The fuselage shall withstand the pressure difference between the cabin and environment at service ceiling.	✓
SRA-SYS-FG-04	The fuselage shall not fail/yield or buckle during operations.	✓/✗

The main structural purpose of a wing box is to carry the bending, shear and torsional loads that act on the wing during the mission. The wing box must be designed for the most critical load cases, which is when the load factor is at its ultimate level n_{ult} = 3.8. The first step in the wing box design process was to identify all the loads that act on the wing. These can be seen in the free-body diagram below:

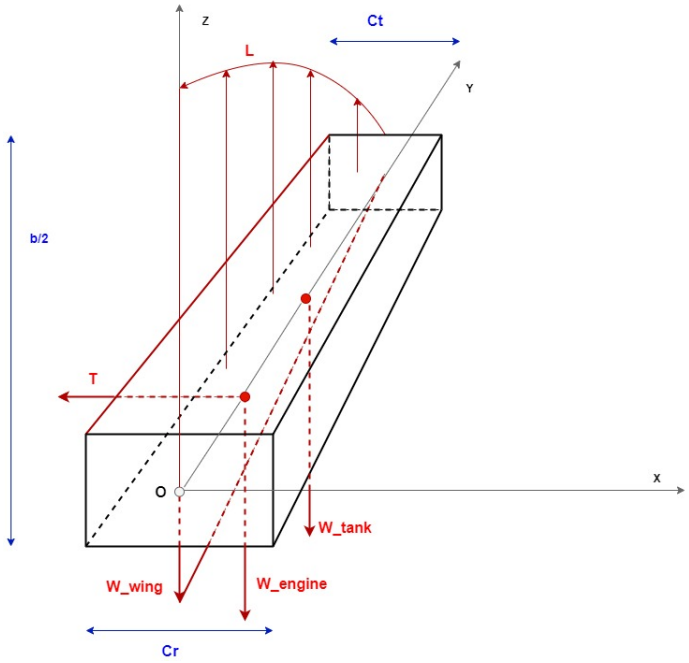

Figure 42: Wing box FBD

Loads and Loading Diagrams The lift distribution used for the calculation is elliptical, which is an accurate approximation for wings with taper in the 0.3-0.4 range [add reference]. Integrated over the wing span, the lift distribution amounts to half the MTOW times the ultimate load factor. The distribution of the weight varies linearly along the span. Finally, the distance of the engine from the wing root is approximated to be one third of the length of the wing while the wing-mounted tank is placed 7.74m away from the root. The fact that only one peak is present is due to the fact that there only one load-carrying spar is present.
The reaction forces at the root could then be found, allowing for the creation of 5 loading diagrams, describing the bending moment around the x and z axes, the torque and the shear forces in the x and z directions.

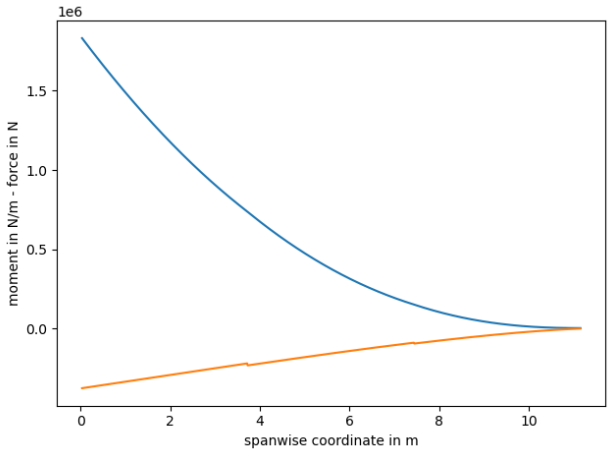

(a) Bending moment about x axis (blue) & Shear force in z direction (orange)

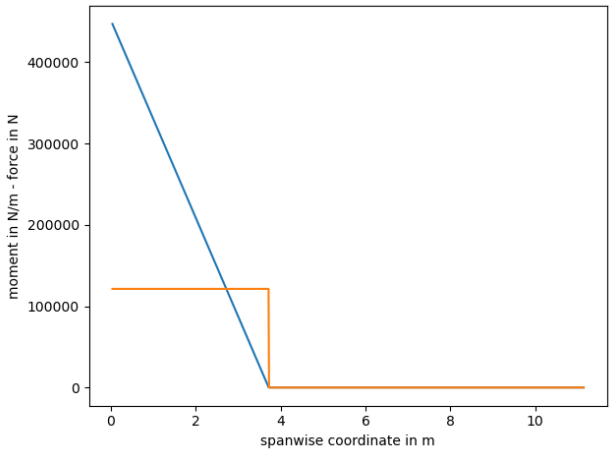

(b) Bending moment about z axis (blue) & Shear in x direction (orange)

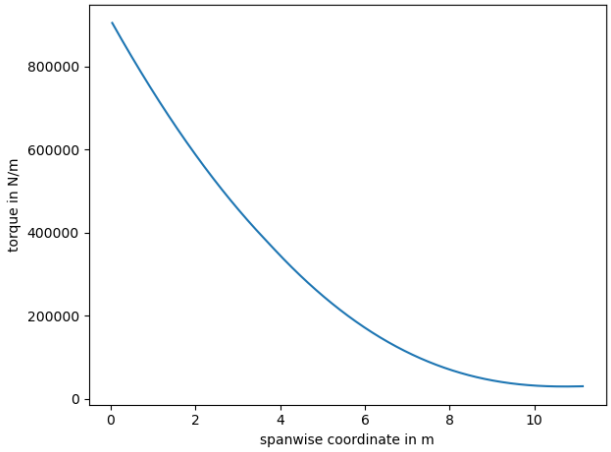

Figure 44: Wing torque

Stress Calculations and Design At this point the sizing of the wing box could start. The first iteration of the design was a simple square 4-panel rectangular box with no stringers attached, which was then improved to a wing box whose cross-section shape matches that of the airfoil. Finally, stringers were added to help with bending stresses. While refining the wing box design, a number of assumptions were made in order to make calculations possible:

- The structure is assumed to be thin-walled
- The shape of the cross section, while still closely resembling and fitting inside that of the airfoil, has been made symmetrical
- The stresses were calculated using the principle of structural idealization: the mass of the skin is grouped to that of the nearest stringer.

Also, the ways in which the wing box could fail had to be identified:

- Bending yield failure: normal stresses exceed σ_{yield}
- Shear failure: the Tresca failure criterion for shear has been used, meaning that the maximum shear stress in the cross section shall not exceed $\frac{\sigma_{yield}}{2}$

Rather than computing the needed moment of inertia needed for the cross section, a more versatile approach has been devised. Code has been written that calculates the internal loading and cross section dimensions at

any point along the wing span. Then, the user may add any amount of stringers with variable cross section area. Also, the thickness may be modified Finally, the program calculates the bending and shear stresses acting on the cross section based on these parameters. The bending stress (Equation 105) is entirely due to the internal bending moment while the shear stress (Equation 106) is a combination of shear due to internal shear force and shear due to the applied torque.

$$\sigma = \frac{M_x}{I_{xx}} z + \frac{M_z}{I_{zz}} x \tag{105}$$

$$\tau = \frac{VQ}{I_{xx} t} + \frac{T}{2A_{enclosed} t} \tag{106}$$

In other words, the corresponding stresses for a given combination of skin thickness, number of stringers and stringers cross section could be determined. This allowed the team to experiment with various combinations in order to find the optimal one. Obviously, these combinations differ for every possible material taken into consideration.

Material Choice Different materials were considered for the manufacturing of the wing box, which parameters can be seen in Table 47.

Table 47: Properties of candidates for material selection

Material	Al 2024-T351	T304 Steel	Epoxy / Carbon fiber reinforced composite	Aramid fibers
Yield Strength (Mpa)	324 (100 actual)	215	945	2800
Young Modulus (Mpa)	73100	200000	69900	62000
Density g/cm3	2.78	8.0	1.40	1.44
Specific Cost €/kg	8.77	1.75	20.0	33.64

The main factor in deciding the material for the wing box was cost rather than performance. The aircraft is likely to meet the emissions requirements just by implementing hydrogen propulsion, which is also expected to drive up the cost. In order to offset this, materials who prioritize cost must be selected. However, the weight penalty that would result from implementing a steel wing box was deemed excessive. Thus, aluminum 2024-T351 was selected as a compromise that would allow sufficient performance while keeping the weight low.

Once the material was selected, the optimal combination of stringers, stringer area and skin thickness could be found by iterative design. For a wing box with 34 equally spaced stringers with an area of $0.0015 m^2$ each and a skin thickness of $6.5 mm$, the resulting stresses along the wingspan are shown in Figure 45. The stresses in the figure represent the maximum value in the cross section at a certain point in the span. For bending stresses, the maximum magnitude occurs at the furthest distance from the cross-section neutral line while the maximum value for the shear stress occurs at the neutral line. The maximum magnitudes for bending and shear stress are $93.81 MPa$ and $27.18 MPa$ respectively, and they satisfy the yield failure and Tresca failure criteria for the chosen material, Aluminum 2024-T351.

Table 48: Wing box parameters

Material	**# Stringers**	**Stringer area**	**Skin thickness**	**Max I_{xx}**
Aluminum 2024-T351	34	0.0015 m^2	6.5 mm	0.00558 m^4

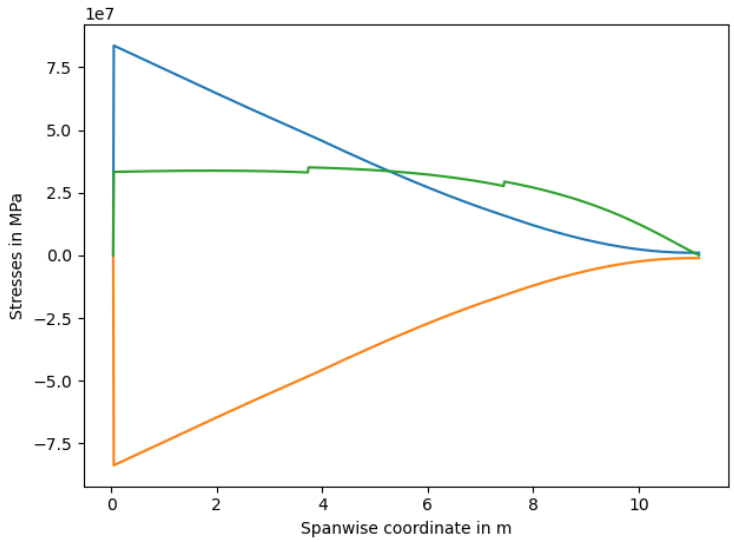

Figure 45: Top (orange) and bottom (blue) bending stresses + shear stress (green) relative to spanwise location

Sensitivity Analysis The sensitivity analysis was carried out on the design of the wing structure by varying the weights of the components that have the highest amount of uncertainty. Since the engine weight, external wing tank weight, and MTOW weight are all computed using the Class II weight estimation the numbers contain a significant uncertainty to them. We therefore vary these parameters with by +/- 10% and see how that affects the design of the structure. The wing span is also varied +/- 10% in case any adjustments need to be made. Due to the relative weight of the engine and podded tanks with that of the lift which is equivalent to the MTOW, a +/- 10% in these components have a minimal change to the stresses induced in the aircraft structure, and therefore are not reported. On the other hand +/- 10% changes in the MTOW and the wingspan, have significant implications on the structure of the aircraft. The changes are reported in table Table 49.

Table 49: Effect of changes in MTOW and wingspan on the wing box

Parameter	MTOW +10%	MTOW -10%	b +10%	b -10%
Max bending stress	+7.302 MPa (+8.70%)	-11.788 MPa (-14.05%)	+3.112 MPa (+3.71%)	-13.05 MPa (-15.56%)
Max shear stress	+3.085 MPa (+8.79%)	-4.74 MPa (-13.50%)	+0.38 MPa (+1.08%)	-3.32 MPa (-9.46%)

The design is most sensitive to a decrease in MTOW and wingspan. But when looking at the structural design these changes in stresses don't result in very large variations in the overall design so the variation in the uncertain parameters won't have disastrous results.

Verification and Validation Verification is carried out to ensure that the code created to size the wing box is turning out reasonable results. The functions used in the code were unit tested and their implementation was also checked and compared to hand calculations. For validating, a different analytical approach was used to quickly assess the stresses at the root, courtesy of Ir. Jos Sinke. The lift of the wing will equate have the MTOW. Next the loading points is assumed to be at a 1/3 of the wing span from the root, this is at $3.7m$. The bending moment is $1.85m$ x MTOW. Following this the load factor used in the code is used. The moment is divided by the wing thickness at the root used in the code, to obtain the skin load. Finally, the stresses are found by dividing the skin loads by the cross section of the upper/lower skins, thereby resulting in stresses. The values obtained where within 10% of those that code provided.

Recommendations Drag has not been taken into account while calculating the internal loads acting on the wing box. Taking drag into account might actually make the structure lighter, since it would relieve some of the lateral shear force and moment that is generated by the thrust. Modes of failure that still need to be further investigated are those of buckling, fatigue, creep, deflection, and fracture. Currently, the wing box has been designed around the loads at the wing root. Further away from the root these loads become increasingly smaller, meaning that some weight could be saved by changing the thickness and/or number of stringers along the span. Also, using multiple load-carrying spars could lower the intensity of the peaks in the moment and shear loading diagrams, although this will make the design more complex as well.

In order to ensure that skin buckling does not occur either enough skin thickness is required or stringers have to be placed close enough to each other. The buckling stress can be found using Equation 107:

$$\sigma_{cr} = \frac{\pi^2 k_c E}{12\left(1-v^2\right)}\left(\frac{t}{b}\right)^2 \tag{107}$$

Ribs have not yet investigated and need to be further investigated. Ribs have to be investigated in the structure since they fulfill several roles, they maintain the shape of the desired aerodynamic cross section, and contribute to preventing column buckling of stiffeners and plate buckling of skin panels. The placement of ribs has to be investigated to ensure that the stringers do not fail due to column buckling. The key is to strike a balance if the ribs are spaced too far apart and the force in the stringers is too high the structure will buckle, on the other hand if the ribs are spaced too close to each other it will add unnecessary structural weight. First the force that the stringers experience has to be computed from Equation 108:

$$F_{stringers} = \frac{A_{stringer}}{A_{skin} + A_{stringer}} \cdot F_{total} \tag{108}$$

With Equation 109 the distance between ribs can be computed.

$$F_{cr} = \frac{\pi^2 EI}{L^2} \tag{109}$$

The buckling do to shear also has to be accounted for as well and this can be done using Equation 110.

$$\tau_{cr} = \frac{\pi^2 k_s E}{12\left(1-v^2\right)}\left(\frac{t}{b}\right)^2 \tag{110}$$

6.5.2 Fuselage Design

The fuselage of the aircraft is affected by loads due to lift on the wing and on the horizontal tailplane, weight distribution, rudder force and pressurization. For the sake of simplicity the weight of the aircraft is assumed to be uniformly distributed along the length of the aircraft. This assumption leads to designing structures stronger than needed as the increased weight around the area of the wing would decrease the internal moments and shears caused by the wing lift, which is the cause of peak stresses. The lift is applied at the wing aerodynamic center and the torque due to the rudder force is treated as a pure torque. Also, the fuselage is initially assumed to be a cylindrical thin-walled tube. These loads are translated into the bending moment about the y-axis and the shear force in the z direction in Section 6.5.2.

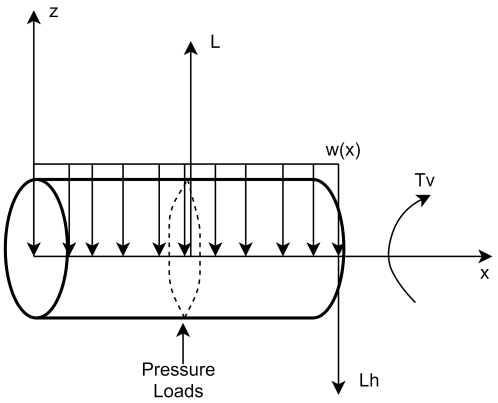

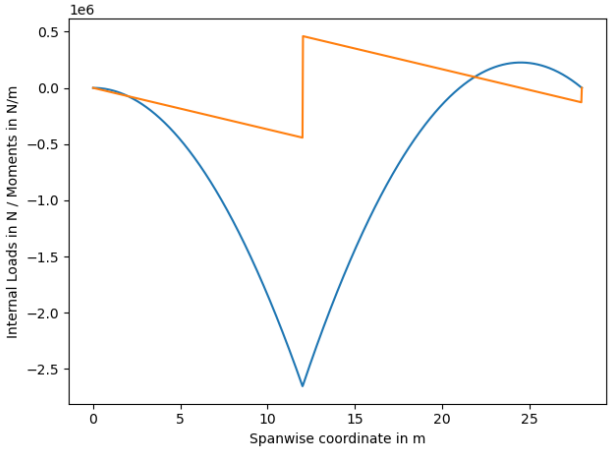

Material Choice and Stresses The material selection process was performed along that of the wing box and it led to the same result. For the time being a fuselage entirely made of Aluminum 2024-T351 has been chosen for the same reason it was chosen for the wing box, namely that it is the best compromise between cost and performance. The calculations for stress are also identical since the type of internal loading is identical (normal stress due to bending and pressurization (constant) and shear stress due to shear force and torsion). Again, the optimal combination of number of stringers, stringer area and skin thickness has been determined

and is shown in Table 50. The major difference is that due to the simplicity of the fuselage cross-section with respect to that of the wing box, the thickness of the fuselage varies along the span to save weight.

Table 50: Fuselage parameters

	For x<8m and x>16	**For x between 8 and 16m**
Material	Aluminum 2024 T351	Aluminum 2024 T351
Skin thickness	1.5mm	3mm
Stringer area	0.0001 m^2	0.0001 m^2
Number of stringers	55	55

Sensitivity Analysis The sensitivity analysis for the fuselage is carried out to determine how sensitive the fuselage design is to its most uncertain parameters. For this analysis the MTOW is varied +/- 10% due to its uncertainty, since it is computed using the Class II estimation. Varying other load components is not very useful since their impact on the stress will be very small.

Table 51: Effect of changes in MTOW on the fuselage

Parameter	MTOW +10%	MTOW -10%
Max bending stress	+7.11 MPa (+8.25%)	-7.11 MPa (-8.25%)
Max shear stress	+2.81 MPa (+9.96%)	-2.81 MPa (-9.96%)

The stress change due to the MTOW is minimal, and leads to a very small variation in the structural design, therefore the overall design is not over sensitive to the uncertain parameter.

Verification and Validation All calculations for the internal loading diagrams and bending/shear stresses were checked by hand. The model used to determine the stresses in the fuselage has been validated against that used in [57] and it has been found that it is consistent.

Recommendations The interaction of the fuselage and wing group as well as that of fuselage and empennage have not been considered in detail from the structural point of view. It is very likely that the points of junction between the different structural group will be critical from the loading and stresses perspective, so it is important to look into reinforcements at those points.

In order to save weight, the different panels for the fuselage skin could be designed differently based on the local stresses. The number of stringers and/or the local thickness could be changed to save weight. It is also possible to use different materials. While this could lead to significant weight savings, the interactions at the boundaries and joining methods could raise some complications.

6.5.3 Hydrogen Tanks

The cryogenic temperature of liquid hydrogen, its permeability, low energy density and the presence of boil-off gases result in a radically different structural tank design compared to conventional kerosene tanks. First, this section explains the design methodology used. Then, a trade-off is done between three different materials. Finally, a material is selected and possible consequences of that choice are discussed.

Design Procedure Two different tank types are used in the aircraft: a cylindrical tank for the external wing tanks, and a truncated oblique cone for the tail tank. However, to simplify the preliminary structural calculations, the latter will also be modeled as a cylinder. The stresses occurring are the circumferential and longitudinal stresses due to pressure build-up, and thermal stresses due to the extreme temperature differences ($20K$ for full cryogenic liquid hydrogen tanks and $310K$ for empty ground conditions). Circumferential and longitudinal stresses can be calculated by Equation 111 and Equation 112 respectively. p is the pressure, which is 1.45 bars [29], R is the radius of the tank, t the thickness and FoS is a safety factor, set equal to 2. Thermal stress can be computed via Equation 113, with E being the Young's modulus, α the coefficient of thermal expansion and T_{des} the design temperature where thermal stress is zero. T is the actual temperature. Also the fuel load is considered: the weight of the hydrogen in the tank, multiplied by an ultimate load factor n_{ult} of 3.8, divided by the upper view cross section (found by multiplying thickness t and perimeter P), gives the resulting stress. This is given in Equation 114.

$$\sigma_{circ} = \frac{FoS \cdot p \cdot R}{t} \quad (111) \qquad \sigma_{th} = FoS \cdot E \cdot \alpha \cdot (T - T_{des}) \quad (113)$$

$$\sigma_{long} = \frac{FoS \cdot p \cdot R}{2t} \quad (112) \qquad \sigma_f = \frac{M_f \cdot g \cdot n_{ult}}{t \cdot P} \quad (114)$$

Different loading cases will exist for different scenarios. Four loading cases are analyzed:

- cold pressurized tank: the fuel is in the tank, tank is cooled down and gases are present. Includes fuel load.
- hot pressurized tank: The tank is 'hot' but purge gases/initial refueling gases are present. Fuel load is not present.
- hot unpressurized tank: the tank is empty and hot. Fuel load is not present.
- cold unpressurized tank: fuel is in the tank but relief system just vented all gases. Fuel load is present.

For the first two loading cases, which are pressurized, a thickness can be computed based on yield stress. This thicknesses are given by Equation 115 and Equation 116, which superimpose longitudinal stress and thermal stress, and circumferential and thermal stress and fuel load respectively (fuel load stress is assumed to be pointing in the vertical direction of the tank). The absolute value of the denominator should be taken. The thickest option overall is chosen (over the two load cases and over the two long./circ. stress case, one is selected). If a unidirectional CFRP is investigated, it is assumed filament winding is used with an angle of 55 degrees. This is the optimum angle according to Geng et al. [58]. Then, the yield stress in the longitudinal thickness formula must be multiplied by $\cos(55^o)$, in the circumferential thickness calculation by $\sin(55^0)$. Then the thicknesses need to be summed up. This is given in Equation 117 and Equation 118. This is not the case for a metal or quasi-isotropic crossply CFRP, the thickest thickness provides enough strength in the other direction as well. The last two loading cases do not involve pressurization, and thus no thickness is calculated here, but the thermal stress must not exceed the yield stress of the material. The thermal stress here will depend on the design temperature. This temperature is taken at $155K$, half of the maximum temperature, to limit thermal stresses for both cold and hot tank conditions, thus lowering fatigue.

$$t = \frac{pR}{2abs(\sigma_{yield}/FoS - \sigma_{th})} \quad (115) \qquad t = \frac{pR}{2abs(\sigma_{yield}cos(55^o)/FoS - \sigma_{th})} \quad (117)$$

$$t = \frac{pR + n_{ult}M_f g/P}{abs(\sigma_{yield}/FoS - \sigma_{th})} \quad (116) \qquad t = \frac{pR + n_{ult}M_f g/P}{abs(\sigma_{yield}sin(55^o)/FoS - \sigma_{th})} \quad (118)$$

Material Trade-off Three materials are considered: aluminium, titanium and CFRP. All are known to be light weight aerospace materials. Special alloys/CFRP types should be selected for cryogenic conditions. For aluminium, the Al 2014 T6 alloy is selected, as the 2014 series is known for its performance at cryogenic temperatures as reported by Kendall [59]. Properties of Al2014T6 are taken from [60] [23]. For titanium, the Ti-5Al-2.5Sn alloy is selected, because of it being one of the best Ti alloys for cryogenic applications as stated by [59]. Its mechanical properties are taken from [61] [24]. As a CFRP, the Hexply 8552 with Hexcel IM7 is selected [62] [25]. This CFRP was previously used in different cryogenic space applications[63]. The company (Hexcel) reports it to be suitable for filament winding [62]. This will be done at an angle of 55 degrees.

Table 52: Material Properties

	Al 2014	Ti-5Al-2.5Sn	Hexply 8552
E [GPa]	72.4	110	164
α [μm/m/K]	23	9.4	-0.64
σ_y [MPa]	414	827	2723
ρ [kg/m^3]	2800	4480	1780

[23] http://asm.matweb.com/search/SpecificMaterial.asp?bassnum=MA2014T6
[24] http://asm.matweb.com/search/SpecificMaterial.asp?bassnum=MTA520
[25] https://www.hexcel.com/user_area/content_media/raw/IM7_HexTow_DataSheet.pdf

For each material, the minimum thickness is calculated according to the load cases, and a check is performed if the thermal stress does not exceed the yield stress (which is divided by a Factor of Safety of two). The design temperature T_{des} for CFRP is set at $300K$ instead of $155K$. This is because CFRP expands when cooled down, so tensile stress occurs. If the design temperature is $155K$, the CFRP will shrink and endure compressive stresses, which should be avoided for this type of material. For the trade-off, the total tank volume is set at $28m^3$. Half of it is in the tail tank, the other half is in the pod tanks. The pod length is assumed to be $5m$, and the tail tank radius is assumed to be the median of 1.35 and $0.75m$, which is $1.05m$. Those values can be different from the final design values of the aircraft, but this calculation is only used for a trade-off and thus is valid. Total tank mass and thicknesses are computed, and are the trade-off parameters. Baffles are included to prevent sloshing and are assumed to double the tank weight. They also stiffen the tank. The baffles reduce the magnitude of the forces and increase the damping therefore increasing the speed at which the forces die out, which would otherwise lead to stability issues.

Trade-off Result and Consequences The results shown in Table 53 indicate that CFRP is the best solution for the tanks from a weight perspective, the weight difference is extremely significant. Another advantage of using CFRP is that is does not experience hydrogen embrittlement unlike metals. The thicknesses of the CFRP are below one millimeter. Manufacturing such thickness in CFRP filament winding is possible [26].

Table 53: Trade-off results

	Al 2014	Ti-5Al-2.5Sn	Hexply 8552
$t_{ext.}$ [mm]	2.2	0.42	0.2
t_{tail} [mm]	3.3	0.63	0.24
$m_{ext.}$ (one) [kg]	351.6	176.9	112
m_{tail}[kg]	557.7	207.1	76.8
m_{total} [kg]	1260.9	560.9	300.7
σ_{th}	exceeded	pass	pass

A drawback of using CFRP's is the fact that they are permeable the hydrogen molecules. This is not the case for metals. A non-permeable liner should be applied at the inside of the tank. A polyamide liner can be applied for CFRP vessels, which is installed via a blow molding technique developed by Kautex Maschinenbau [64][27].

Implementation of Hydrogen Tank To recap, the tail tank is an oblique truncated cone (but modeled as a cylinder) which is integrated in the tail cone of the aircraft. It features a liner, a CFRP pressure shell, baffles and insulation. The tail tank itself is supported by the fuselage structural parts. The external wing tanks also have a CFRP shell, baffles, and insulation. It will need an additional fairing and nose cones. This has not been developed yet in detail. The fairing will also add extra mass. A preliminary calculation, assuming a pod length of $5m$, puts the fairing weight per pod at $40kg$ per millimeter of aluminum, and $25kg$ for CFRP (Hexply 8552). As this has not been properly researched yet, the tank weight of the CFRP is still taken at $300kg$. This does not match exactly to the 280 kg given in the class II weight estimation due to a late slight change in input parameters.

Verification and Validation Stresses calculated by the code were printed and manually checked. This was done in unit tests for the thermal stress, load stress and pressure stress separately. One should also be able to notice weight savings for CFRP, which is the case. To validate the procedure, the results can be compared to the ones obtained by Colozza [29]. Colozza reports that tank mass (insulation, boil-off and structural) for a tank the size of the tail tank is about $200kg$. This is the case for titanium. Colozza did not mention the material used.

Sensitivity analysis The structural design of the hydrogen tanks will mostly depend on changes in the required volume. The volume was both increased and decreased by 20% in Table 54.

[26](J. Sinke, personal communication, 17/06/2020)

[27]https://www.kautex-group.com/en/about-us/company/hydrogen-liner.html

Table 54: Sensitivity analysis hydrogen tank structure

Volume	Al 2014	Ti-5Al-2.5Sn	Hexply 8552
17[m^3]	1490 [kg]	650[kg]	340 [kg]
11.3[m^3]	1027[kg]	468[kg]	260[kg]

Recommendations The baffle placement and weight need to be examined in more detail. The fairing and cones for external wing tanks need to be researched, as do their masses. More research can be done in filament winding, load cases and CFRP behavior. The exact details of how to support the tail tank and external wing tank must also be considered. For now it is assumed that the aft fuselage structure also serves as aft tail support. The external wing tank is attached to the wing via a fairing and pylon. The weight of this fairing must be accurately determined for control and stability reasons, as well as for the wing structure. Also bird strikes and ground collision cases must be researched and designed for.

6.6 Final Design

The individual subsystems described in the previous subsections are integrated to form the final design. The external wing tanks and the engines are mounted onto the wings, which in turn are connected to the fuselage. The horizontal tail is jointed with the vertical and the whole assembly is assembled with the fuselage. Lastly, the landing gear is integrated on the lower side of the fuselage. The final design can be seen in Figure 46.

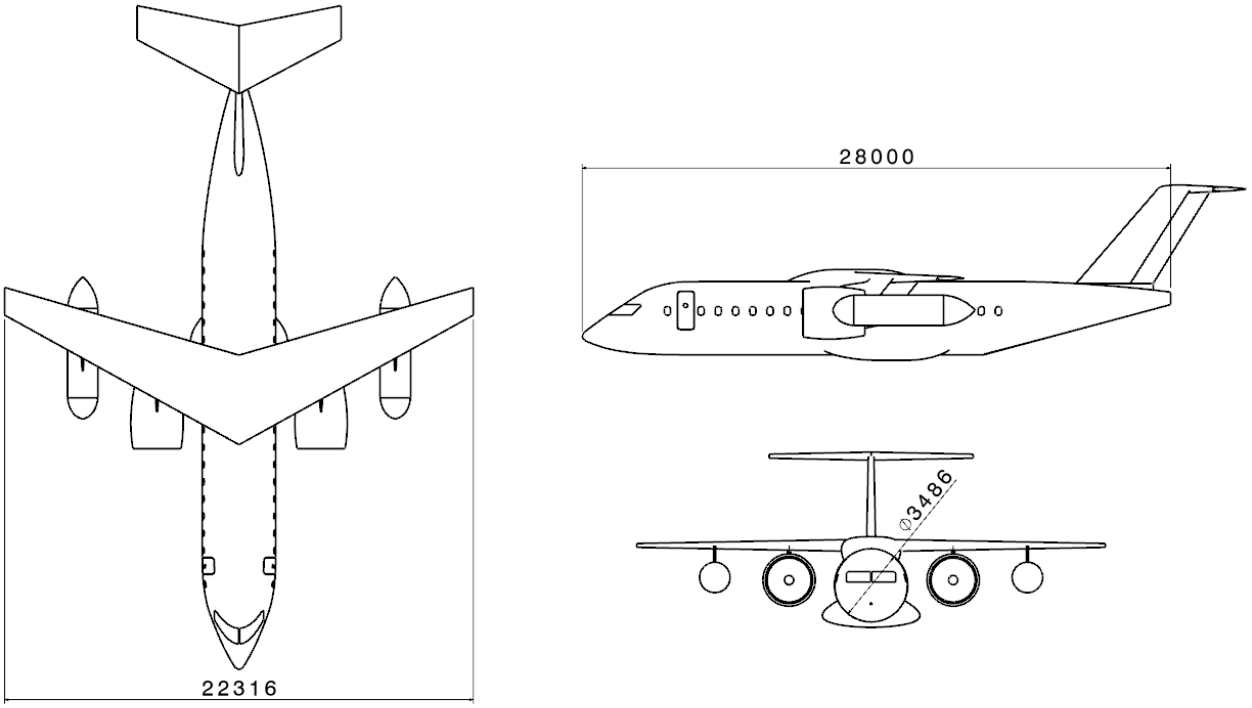

Figure 46: Three view drawing of RELIGHT

7 Final Design Characteristics

This chapter describes main features of the resulting end product that are unrelated to the main subsystem design results. First in Section 7.1 stake holder requirements, that the aircraft needs to fulfill to be certified and capable of performing its mission profiles, are discussed as well as the level to which they have been achieved. This section is followed by the mass breakdown and resource allocation in Section 7.2, that summarizes the final masses as calculated for various subsystems, as well as determining fuel weights, range, take off length, emissions and more and scores them using a performance index. After concluding that the chapter delves into various other subsystems and the plan for their implementation, before concluding with the RAMS characteristics in Section 7.4, that discusses reliability, availability, maintainability and safety aspects of RELIGHT's final configuration.

7.1 Requirements

Table 55: General final design requirements

Requirement Identifier	Requirement	Compliance
SRA-STAKE-AP-04	The aircraft shall be able to use existing facilities at regional airports (availability information found in [65]).	✓
SRA-STAKE-PIL-02	The aircraft shall require similar pilot training as the reference aircraft, the Bombardier CRJ700 series.	✓/✗
SRA-STAKE-AUT-01	The aircraft program shall comply with CS-25 regulations.	✓/✗
SRA-STAKE-AUT-02	The aircraft program shall comply with regulations issued by EASA.	✓/✗
SRA-PROD-PERF-04	The aircraft shall be able to withstand adverse weather conditions.	✓
SRA-PROD-PERF-09	The aircraft shall have an operational lifetime of 28000 cycles or 20 years.	✓
SRA-PROD-PERF-15	The aircraft shall allow for a turnaround time (on ground) of a maximum of 30 minutes.	✓

In Table 55 several more requirements are shown which have not yet been discussed. The SRA-STAKE-AP-04 requirement concerning the use of existing facilities at regional airports has been met, as the aircraft remains in the EASA class B gate category. The class B gate category specifies that the wingspan of the aircraft must remain below 24m. Furthermore, the width of the main landing gear must remain below 6m. Both requirements are met, thus the aircraft will be able to fit in class B gates. The requirement is relevant, as the aircraft is able to park at any gate the CRJ700 does, thus remaining flexible and able to service any airport the CRJ700 does. Furthermore, the aircraft has been developed with the regional facilities in mind. The choice of a high-wing aircraft helps with boarding, while the large engines will provide enough thrust to be able to take-off from short runways. At this time, the pilot training requirement SRA-STAKE-PIL-02 cannot be investigated in depth, as this requires an in-depth study into cockpit design. Though, the development of the aircraft until this point has not violated the requirement. The same holds for SRA-STAKE-AUT-01 and SRA-STAKE-AUT-02. The main regulations have been taken into account, making the design compliant up to this point. However, an in-depth study is required to make sure that every regulation will be met. This also returns in the SRA-PROD-PERF-04 requirement. The gust velocities during flight have been determined in Section 5.5, which the aircraft will be designed for. This causes the design to be compliant with this requirement. SRA-PROD-PERF-09 and SRA-PROD-PERF-15 have been taken into account during the design of RELIGHT, while they also need further investigation during future design. These requirements can be met with proper design decisions in the future.

7.2 Resource Allocation / Budget Breakdown

As the project develops, the design is faced with less uncertainties; this results in an increase in resource spending, which can significantly alter the design and drive up costs. To keep this from happening a contingency plan has been created, together with a mass budget. The contingencies constrain the design of the system, requiring design choices to be made accordingly; therefore the system has be below, or equal to, the specified value said system will be designed for, when the contingency is included.

In Figure 47 both a mass breakdown of the OEW of the aircraft and a mass breakdown of the mass of the whole aircraft relative to the MTOW are given, both at the current design state.

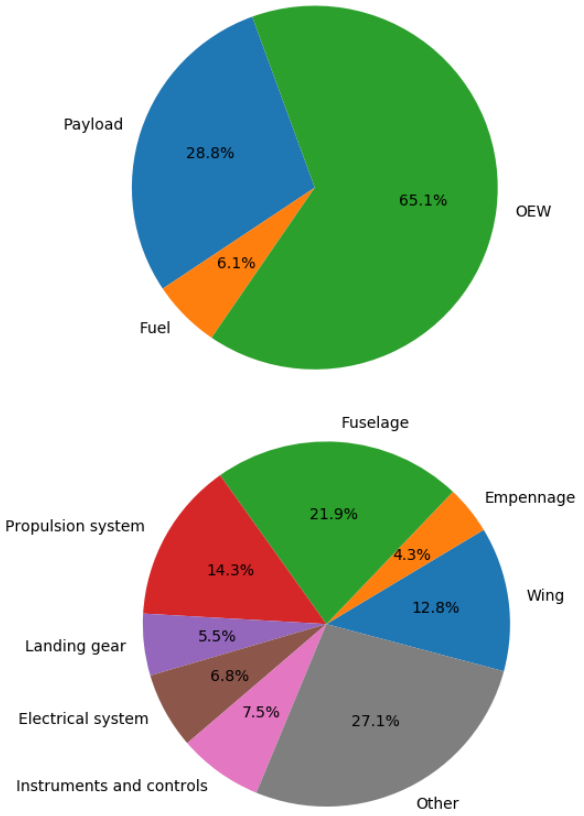

Figure 47: Pie chart mass breakdown of the entire system relative to MTOW (top) and of the OEW (bottom)

Table 56: Mass budget final design

System/Group	Mass [kg]
MTOW	28083
Fuel	1847.7
Payload	7975
OEW	18275.6
Structural weight	9105.5
Wing	2349.5
Empennage	769.8
Fuselage	3948.2
Nacelles	803.6
Landing gear	1234.4
Propulsion system	2743.4
Engines	2328.1.6
Power controls	136.3
Hydrogen tanks	279
Electrical system	1342.8
Instruments and controls	995.6
Instruments	382.1
Flight controls	613.5
Other	4088.2

To ensure that the final design parameters will be within the bounds specified at the start of the design process, a contingency plan was created. During different design stages parameters are designed for values lower than what was allocated from the technical budget. Table 57 below was first constructed during the conceptual phase of the project [3]; it is now updated to take into account the current design state of the project with its respective contingencies. For some of the parameters the contingency values remain the same as previously determined, while some of them are set to zero. This is the case for the take-off length and passengers as their final value is already known so they are not expected to change in the future. For the emissions a quite extensive analysis was performed meaning they are already known with great certainty thus reducing the contingency for this parameter.

Table 57: Contingency Factor Table [%]

	MTOW	**Range**	**Take-off Length**	**Emissions**	**Cost**	**Passengers**
Conceptual	46	50	20	75	85	40
Preliminary	20	40	15	30	65	40
Detailed Design	10	15	10	20	20	0
Manufacturing	5	5	2	5	10	0
Flight Test	2	0	0	5	0	0
Production	0	0	0	0	0	0
Current design	**10**	**10**	**0**	**5**	**20**	**0**
Relative Importance	25	10	10	25	20	10

In order to quantify the technical performance, the Performance Index PI, as given in Equation 7.2 is used. PI is a measure of the relative difference in design, including its contingency, at the current state, and the design goal. It is a measure of uncertainty, which, logically, will decrease as the design progresses. This relative distance will decrease till the design fully converges, as is depicted in Figure 48; the performance

index is depicted during the different design phases. Currently, during the detailed design, it can be seen that the PI has overshoot the goal. This can be justified by the fact that many of the systems are now known with a greater degree of certainty than it was expected, meaning their parameters will have minor changes during the remaining design phases. This will result in the same target values being reached.

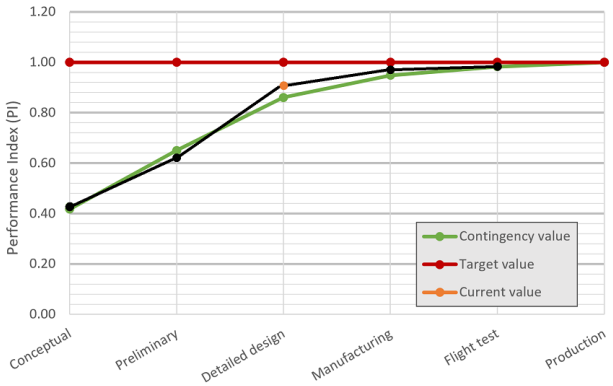

Figure 48: Design phase performance parameter

$$PI = \sum contingency \cdot relative\ importance \tag{119}$$

7.3 Aircraft Systems

In this section, an overview of a few operation critical systems will be given. These systems are all vital for the operation for the aircraft, while not being investigated into detail at this time. First, the pneumatic system will shortly be discussed in Section 7.3.2. The next systems that will be described are the electric system in Section 7.3.3, the hydraulic system in Section 7.3.4, while the data handling system is covered in Section 7.3.5. Finally the environmental control system is discussed in Section 7.3.6.

7.3.1 Aircraft System Requirements

Table 58: Aircraft system requirements

Requirement Identifier	Requirement	Compliance
SRA-STAKE-PIL-01	The aircraft shall have similar handling characteristics to existing airliners.	✓
SRA-STAKE-PIL-03	The aircraft shall feature similar or more automation systems as the reference aircraft, the Bombardier CRJ700 series.	✓/✗
SRA-STAKE-PSG-01	The aircraft shall feature a cabin altitude lower than 2500m.	✓
SRA-STAKE-ATC-01	The aircraft shall be capable of communicating with ground stations.	✓
SRA-STAKE-ATC-02	The aircraft shall be capable of communicating with other aircraft.	✓
SRA-STAKE-ATC-03	The aircraft shall be capable of relaying data to ground stations.	✓
SRA-PROD-PERF-02	The aircraft shall be navigable using existing technologies and infrastructure during cruise.	✓
SRA-PROD-PERF-03	The aircraft shall be able to communicate using existing technologies and infrastructure during cruise.	✓
SRA-SYS-EPS-01	The EPS shall provide TBD power to aircraft instrumentation.	✓/✗
SRA-SYS-EPS-02	The EPS shall at least have one redundant energy source.	✓
SRA-SYS-COM-01	The navigation system shall be able to collect data from primary flight instruments.	✓
SRA-SYS-COM-02	The navigation system shall provide navigational data to the pilots.	✓
SRA-SYS-COM-03	There shall be one level of redundancy for critical flight instruments.	✓

The handling characteristics of RELIGHT have not been investigated in depth. However, due to the application of fly-by-wire systems as will be discussed in Section 7.3.5, and the layout of control surfaces being very similar to existing aircraft, the layout of the controls will be very similar in the cockpit, while the operation will not be much different. The automation systems in the aircraft have not been investigated, causing the compliance with requirement SRA-STAKE-PIL-03 to be unknown. The environmental system discussed in Section 7.3.6 will ensure compliance with SRA-STAKE-PSG-01. The communication will be handled by a to be designed communication system. This is present in all modern aircraft, and has not been investigated at this stage of the design. Though, it can be said with certainty that the requirements SRA-STAKE-ATC-01, -02, -03, SRA-PROD-PERF-02 and -03 will be met with the -to be designed- communication and navigation systems.

7.3.2 Pneumatic System

One of the main aircraft systems is the pneumatic system. In most passenger airliners, the pneumatic system is used for the pressurization of the cabin, anti-ice systems on the aircraft, and to start the engines. Usually, high pressure and temperature air is taken from the turbine in the aircraft's' engine or APU. In this aircraft, some changes will be made concerning the pneumatic system. To save weight and complexity, the pneumatic system will not be installed on the engines, will not be installed in the APU, and will not be used in anti-ice systems. Instead, only the cabin will be pressurized using an environmental control system as described in Section 7.3.6.

All of the power extraction will be done by electric generator/starter motors, from both engines and the APU. It is estimated that the amount of power extraction required is up to 35% lower than when using a pneumatic system [66][28]. The reduction in fuel burn could be up to 3% due to the reduction in power extraction and reduction in weight. The reduced complexity will allow for easier, lower cost, and less frequent maintenance, while reliability will become higher [66]. Furthermore, the production costs will also be lower.

7.3.3 Electrical System

Figure 49 shows an overview of the electrical system of the aircraft. As an highly advanced airliner, the main power system is the electrical system. The system has two central power controllers, one forward and one aft. These will be similar in size, while providing power to different systems. Furthermore, the controllers themselves will be redundant, minimizing the chance of failure of either of the systems. The forward controller is mainly to power the forward part of the aircraft; the instruments and systems in the cockpit. It will provide an unknown amount of power to the instrumentation, as specified in SRA-SYS-EPS-01. Further investigation into the power requirement is necessary. The aft system will power more aft systems, such as the fuel system. Both will be linked to a relatively large battery, to be able to provide high peak-power. Both engines, the APU and the Ram Air Turbine (RAT) will feature two generator/starter motor systems. They will be able to provide electricity to both power systems for redundancy, while requiring power during start of the respective system. This satisfies requirement SRA-SYS-EPS-02. Furthermore, the power controllers will be able to send power to the other power controller during peak demand. It is not possible to fully use this as a back-up in the event of a power controller failure. This is due to the faulty power controller not being able to control the flow of electricity, thus not being able to provide power to critical systems in the aircraft. If the situation would occur that one or two of the generators would not function, this link would be able to provide electricity to the other power controller. To be able to provide power to critical flight systems in the event of a complete power controller failure, there are two backup systems in place; one backup from the forward power controller, and one from the aft power controller. Both power each others' safety critical systems during contingencies with the systems' primary power controller. This backup system is shown as yellow arrows.

The result of two smaller power systems is a reduction in weight and complexity. The total amount of wiring will be much lower, as in most aircraft a single power system powers the entire aircraft, with the systems in the front of the aircraft. Another difference in comparison to the mainstay of airliners, is that the hydraulic pumps will also be driven electrically, and not by the aircraft's engines or APU. This will cause a much smaller hydraulic system, which can be much more local, with a lower complexity. This will reduce weight,

[28] http://www.boeing.com/commercial/aeromagazine/articles/qtr_4_07/AERO_Q407_article2.pdf

maintenance time and cost.

Another large change is that the engines of the aircraft will be started up using the generator/starter motors, while in most aircraft, they are rotated for engine start using the pneumatic system. The use of the generators as starter motors again reduces weight and complexity, and makes the engine start more reliable.

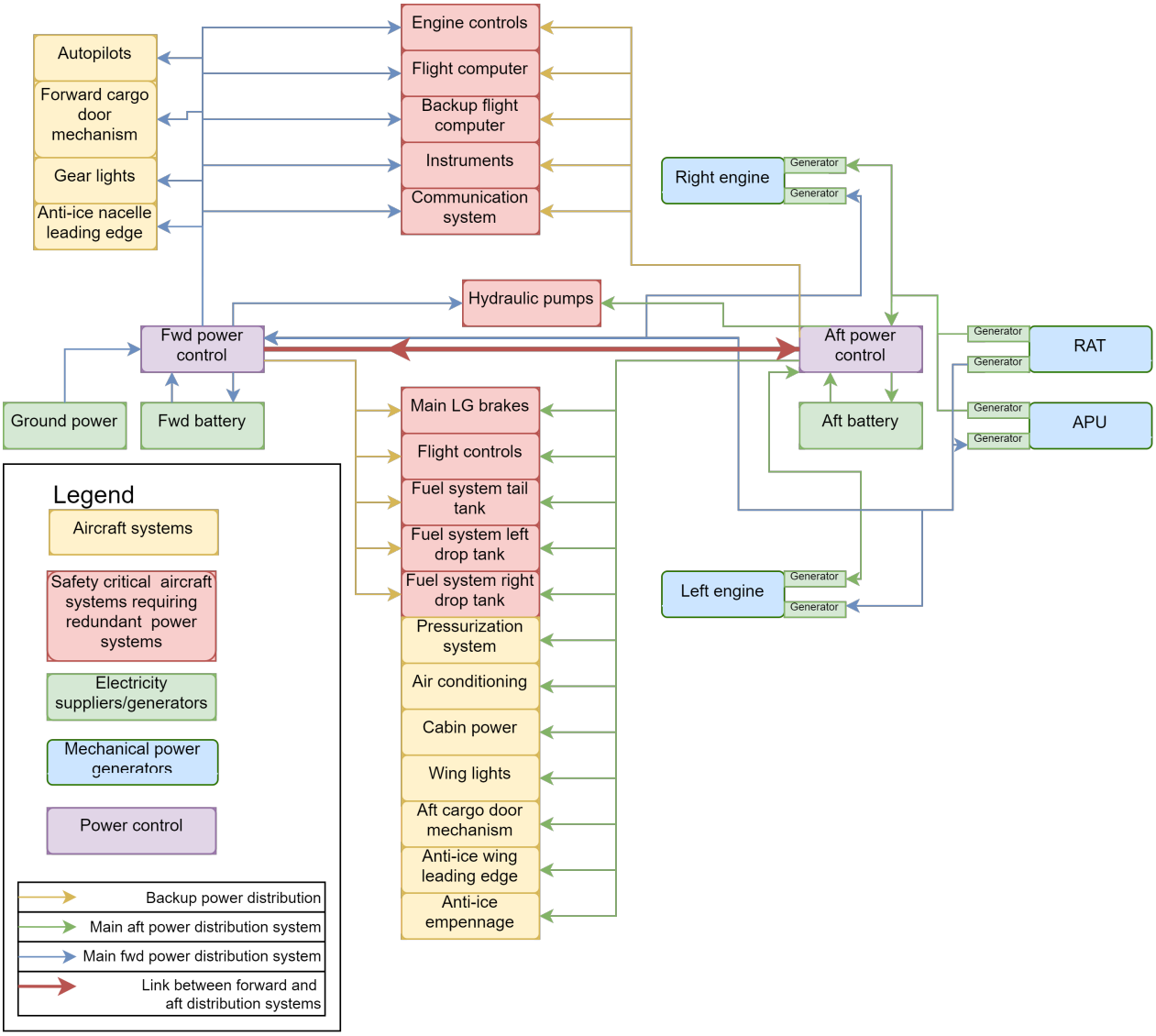

Figure 49: Electrical system schematic

7.3.4 Hydraulic System

The hydraulic system will consist of four systems: red, green, blue and yellow (backup). A schematic overview can be seen in Figure 50. The yellow system will be able to power the primary flight controls (rudder, elevators, ailerons) as a back-up during contingencies with the primary systems. The blue system will effectively be the system for the tail, providing power to the rudder and elevators. Next, the green system will control the main landing gear, outboard spoilers, flaps and thrust reversers. This system will require very little power during the cruise phase. The red system will power the inboard spoilers, ailerons during regular operation, and the nosewheel retraction and steering mechanisms. Note that the landing gears will not be powered by the backup system, as the gear can be lowered by gravity if the hydraulic systems are inoperative.

Each hydraulic system has two hydraulic pumps: one connected to the forward electrical system, and one connected to the aft electrical system. During operation of a lot of systems, such as during taxi, approach and after landing, the combination of pumps will ensure that enough hydraulic power is available. If any of

the pumps becomes inoperative, the hydraulic capability of that system will decrease. Proper warning signals from the aircraft during this contingency shall warn the pilots, causing a different operation procedure, ensuring that the aircraft remains controllable, and all required systems are able to operate, albeit at lower power. Note that the hydraulic systems in this aircraft will be much more local than the hydraulic systems in widespread aircraft. The advantage is a much smaller hydraulic system overall. The local systems reduce the amount of hydraulic lines, reducing pressure loss, reducing required power and lowering the total amount of hydraulic fluid. The more local systems are a direct cause of the switch to fully electric hydraulic pumps. Another advantage is that the electrically powered hydraulic pumps can be very easily throttled when compared to their mechanic counterparts.

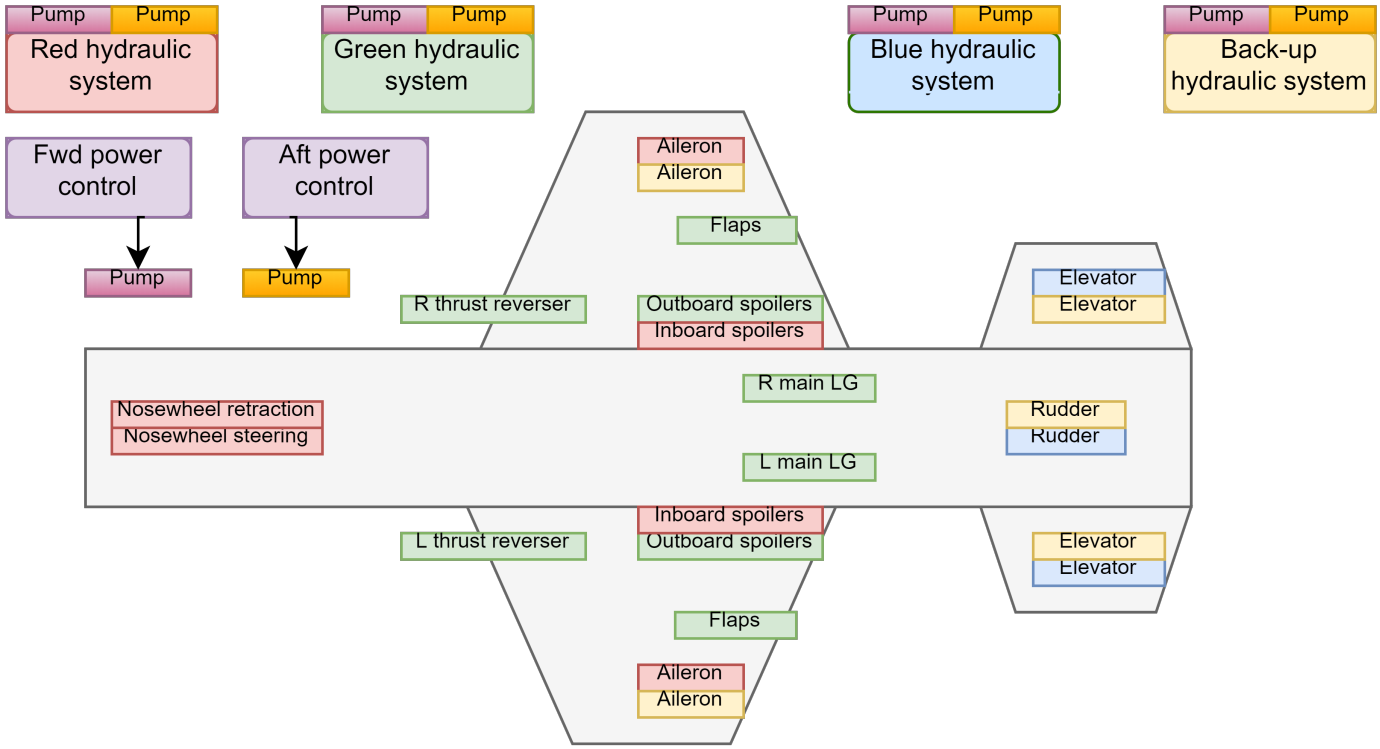

Figure 50: Hydraulic system schematic

7.3.5 Data Handling System

Similarly to the previous schematics, a visual representation has been made of the data handling and data transferring processes within aircraft electronics. Figure 51, portrays that with the appropriate accuracy and helps the reader understand the gathering of all data and how it is manipulated to the aircraft operator's benefit. On the top left all the data input is listed. The network is split between the data transfer within the system (top) and the interaction with the human component (bottom), separated by the dashed line. All sensor readings that are imported in the form of data sets are included in the list, such as heading, airspeed, altitude and more. After sorted, the data is transferred at high rate to the queue awaiting to enter the processing unit. The watchdog timer interferes at this point and checks for malfunctions and for available space before allowing new data to enter the processing device. In parallel the memory and mass storage components handle the pre-existing data and inform on available space. After interaction with the logic unit, and decision making on the location desired for each output, the data is sent out of the CPU, also at a high rate.

The output of interest to the operator, is either in digital form, in the displays visible to the pilot, or in mechanic form, in the throttle feedback. For each form, the pilot interacts with the output and generates different inputs dependent on the outcome, which can be viewed as two different feedback loops in the lower part of the schematic. Notably, the pilot-display loop is assisted by the Fly-By-Wire systems. Those are a part of modern recent aircraft control, and convert the pilots inputs into electrical inputs, that then trigger the actuators to the desired output. This is a significant novelty since the pilot system interaction data transfer rate is naturally minuscule compared to the one within the system components. Hence, now this system integration not only

increases it but now the outcome is also much more accurate and quickly correctable, fact that allows the flight control of even unstable vehicles like the X-29 aircraft or a majority of helicopters. It will also further ensure compliance with handling characteristic requirements, such as SRA-STAKE-PIL-01.

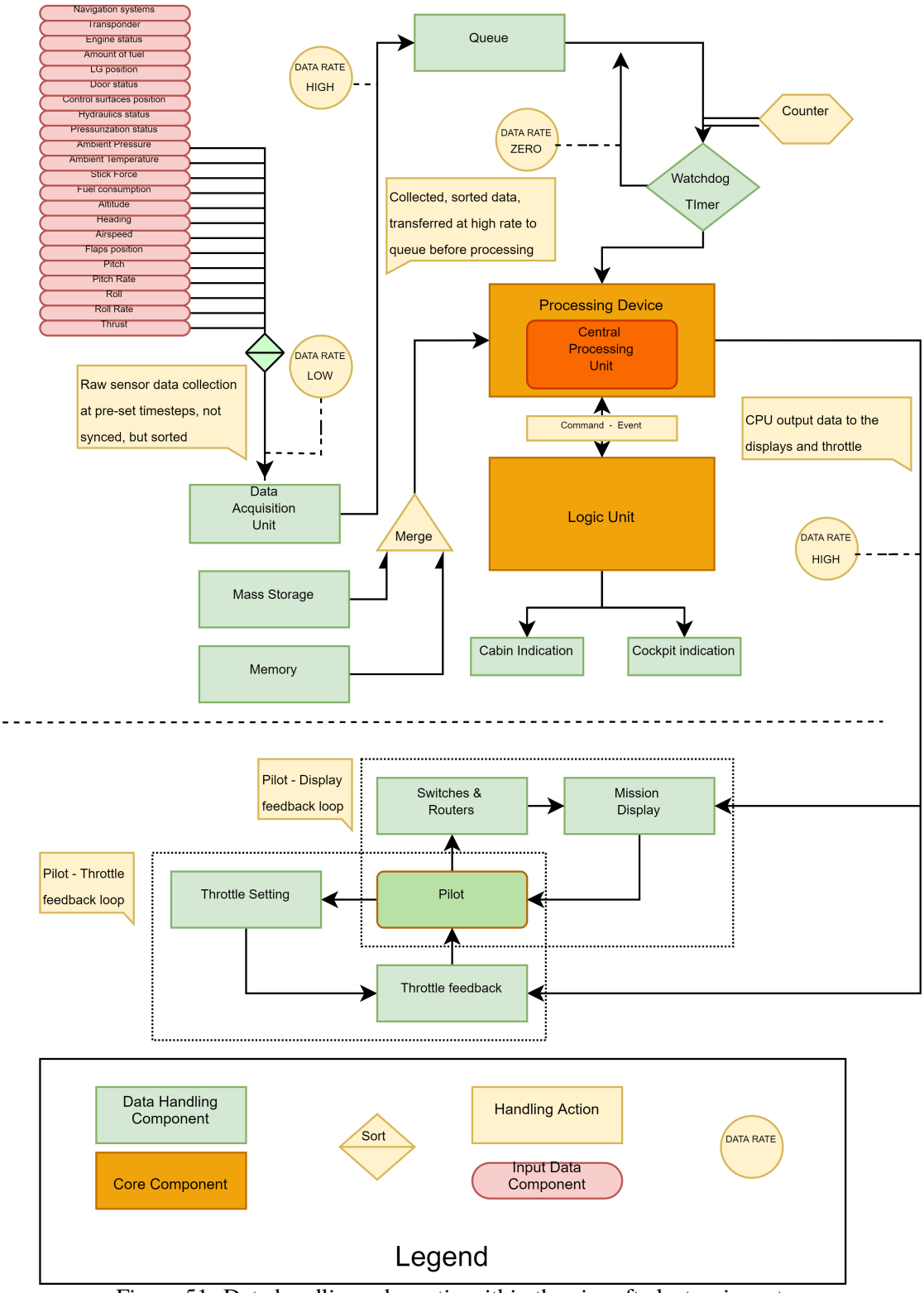

Figure 51: Data handling schematic within the aircraft electronic systems

7.3.6 Environmental Control System

Lastly, the network under analysis is that of environmental control. That is, the group also has interest in accurately designing the exchange of air with the ambient of the aircraft during operation phase. Figure 52

gives the overview of such exchange from the intake until release back out. Air is initially received from the ram air intake, part of which is compressed and heated or cooled while the rest of it remains uncompressed in order to assist heat exchange. The mixer then gets both the newly taken air and air flowing out of the cabin and blends them before filtering for partly renewing the cabin air. After going through the filter, the air enters the cabin and cargo area, with connecting ducts to obtain equilibrium. Overall, the green boxes of the diagram in Figure 52 represent flow controlling devices such as ducts, valves and pumps. The target areas for the environmentally controlled air are the cabin and cargo area, displayed in dark pink, and finally, the light blue boxes all represent machinery, that electrically or passively operate, to make the process successful.

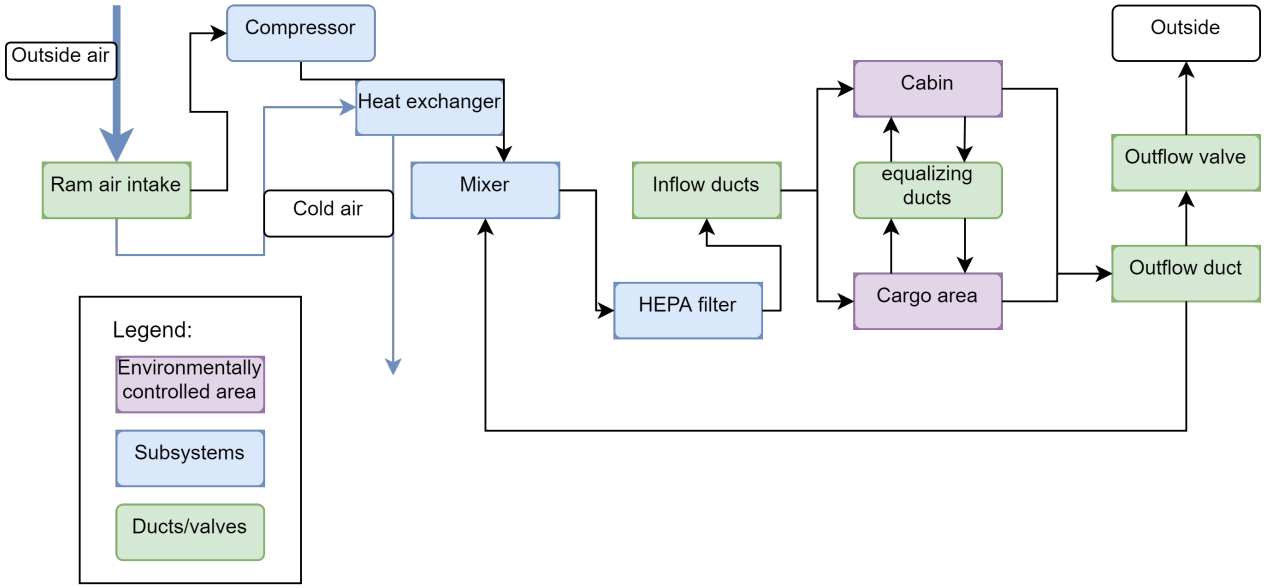

Figure 52: Environmental control system schematic

7.3.7 APU

To power all systems in the aircraft when the engines are switched off, an APU will be installed in the rear of the aircraft. As RELIGHT will require a similar amount of power for its' systems as the CRJ700, the same APU is used as a baseline. The Honeywell RE220 is reliable, tested, and adaptable to hydrogen. The RE220 provides $45kW$ of electrical power, with bleed systems installed. Removing the bleed systems and installing more capable generators will allow the electrical output to increase up to $224kW$, allowing for enough power throughout the aircraft [29].

7.3.8 Hardware- and Software Block diagrams

In Figure 53 a pictorial representation is given of both the hardware block diagram and the software block diagram, as well as the interaction between each other. In green the software blocks are visible, those namely being between four main categories; Avionics, Electrical Power System, Environmental Control System, and Data Acquisition software. The two latter, have already been discussed in Figure 52, and Figure 51 respectively. The Environmental Control System software lists and gives a division of the tasks that are to be carried out by the hardware components of Figure 52. On the other hand the branch of Data Acquisition is ultimately a summary of the data handling procedure presented in detail in Figure 51. Furthermore, the link of the software part of the systems to the hardware part is the Electrical Power System software and Flight Control System link. The control positional data is the information given from the hardware to the software, which is directly processed and a new command is given from software to hardware.

The hardware tree of Figure 53 is the one placed at the top part, in light blue. Most information for its arrangement is drawn from the team's N2 systems interface definition created in the midterm report [4] by the systems engineering department. The main system blocks, (labeled with S. for system and a number) are closely interconnected, with the latter ones (higher label number) branching from the earlier ones (lower

[29] https://aerospace.honeywell.com/en/learn/products/auxiliary-power-units/re220-apu

label number) through a decision series. For example, starting from the Flight Control System, input values for the control surfaces are fed, which in turn, triggers the Hydraulics System. Consequently, the decision or command to deflect causes the action of the control surfaces. The overall importance of the H/W - S/W diagram is large as it does not just portray the interaction between different hardware and software components, as did the systems interface chart [4], but gives a flow of the actions step by step, somewhat like a manual to someone who would want to end up in one of the system actions shown.

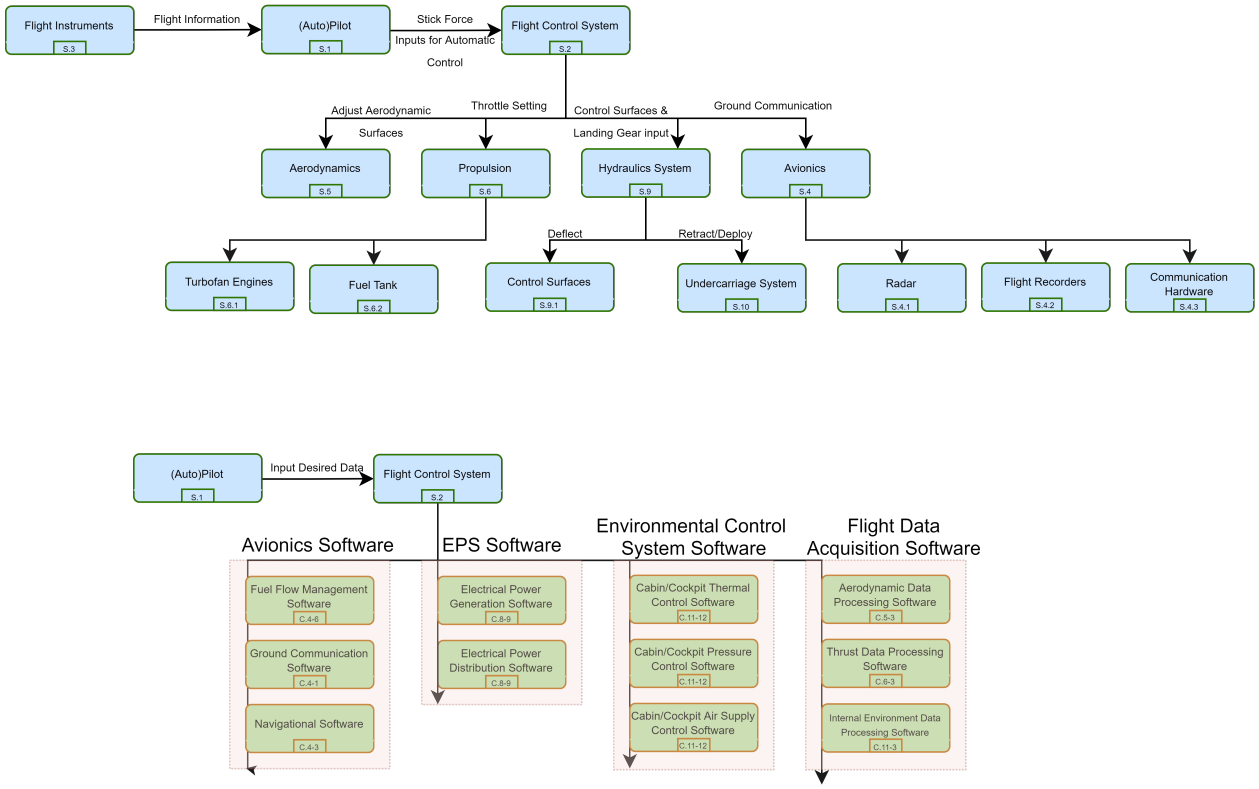

Figure 53: H/W - S/W

7.4 RAMS characteristics

This section discusses reliability, availability, maintainability and safety aspects of the final design, as well as relate these to the requirements.

7.4.1 Requirements

Table 59: Sustainability requirements

Requirement Identifier	Requirement	Compliance
SRA-STAKE-AL-08	The aircraft shall have a similar operational reliability with respect to the reference aircraft, the Bombardier CRJ700 series.	✓
SRA-STAKE-AL-09	Maintenance operations shall be similar to those performed for aircraft of the same category.	✓/✗

As the preliminary design approaches the final decisions, the Reliability, Maintainability, Availability and Safety (RAMS) characteristics take place. They are carried out by a certification officer in the form of inspections and give a "green light" to the manufacturer to begin along with the assembly plan drafted by the team. These were also discussed in the midterm report [4], and now, since the preliminary design is explored, the need for a deeper look into those characteristics is called for.

7.4.2 Reliability

In general, the reliability of an aircraft is the probability that it will perform in a satisfactory manner for a given period of time when used under specified operating conditions [67]. The reliability of the concept aircraft shall be similar to aircraft in operations. Naturally, the reliability of all components and systems used in the aircraft have to be up to par with today's standards. he main difference with existing aircraft is the

hydrogen propulsion system. The other components are already widely used in the aerospace industry so it is assumed that the reliability of these aircraft components is the same as the industry average. This includes the turbofan engine, which requires little modification to make it run on hydrogen.

A more detailed look in the propulsion system reliability is needed. Starting with the hydrogen storage analysis, it can be said that hydrogen is very flammable and its storage is quite challenging. Although it has only be done experimentally on aircraft, hydrogen tanks can be seen in ground-based industries such as hydrogen cars and energy storage. As these applications are not bounded by the weight of the storage system as much as the aircraft is meaning that possibly a compromise with the reliability systems needs to be made to make the tanks suitable for aircraft.

Additionally, the aircraft has three fuel tanks, one in the back and two external wing tanks in the wings. Cross-feed between the tanks is possible, so when fuel gets used the remaining can be distributed among the tanks, to ensure there is fuel in all the tanks in case one fails. Thus there is a redundancy in the system meaning the reliability is also increased as the chance for all the three tanks failing during the same flight mission is greatly reduced.

The fuel transfer system uses multiple pumps in parallel to allow for redundancy. Also allows for feeding the engines from different fuel tanks in case there is a problem in one of them. These measures decrease the likelihood of leaving an engine without access to fuel, thus increasing the reliability of the propulsion system. It can be concluded that RELIGHT will likely meet SRA-STAKE-AL-8, although further investigation in the future is necessary to keep ensuring compliance.

7.4.3 Availability

The availability characteristic concerns replacements frequency, staff presence and maintenance budgets which call for assurance. Specifically concerning the hydrogen refueling, it should once again be mentioned that the assumption of hydrogen availability in regional airports will have happened by the time the aircraft becomes operational. That is, it has been assumed that in the years to come, an acceptable amount of regional airports will include storage of hydrogen in cryogenic state, to assist aircraft in terms of refueling.

The midterm report has already explored inherent, achieved and operational availability [4]. Those, collectively rely on Mean Time Between Maintenance (MTBM), Mean Time To Repair (MTTR), and Mean Time To Maintain (MTTM). Since only in preliminary phase, the design will need to advance to manufacturing, certification, and on to the flight testing to obtain a - still - vague picture of the aforementioned values. More specifically, the hydrogen concept entails a significant amount of novelty, which mostly proves vital for the general view, but provides large uncertainty in need for replacement or inspection of aircraft subsystems. Just like for maintainability, after the flight test phase that will follow manufacturing and assembly, the Mean Times above will be of certainty, and availability will be a well-calculated characteristic, but it cannot be possible to be accurate about it at the preliminary design phase. Furthermore, accessibility to certain regional airports needs to be analyzed, before finally creating a networking plan, of the regional airports, in which the level of availability is stated, as well as distance to major cities and depots for the possibility of replacements shipping.

7.4.4 Maintainability

As it has been previously mentioned, maintainability is the ability of the aircraft structure to perform all its operations at minimum maintenance, that being scheduled and unscheduled [4]. Having made detailed sizing for the different subsystems, maintenance planning is more specialized for the group's resulting design. Notably, the integration of external wing tanks assists maintainability, since they are mechanically removable with ease by design for refueling. Upon removal, quick inspection and unscheduled maintenance is also done with ease due to the simplistic and aerodynamic shape. Similarly, the aircraft design entails a high wing configuration for which maintainability is also at desirable levels. Should there occur small non-hazardous structural faults on the wing, even in the root of it, the configuration makes it accessible to maintenance

without scheduling as well.

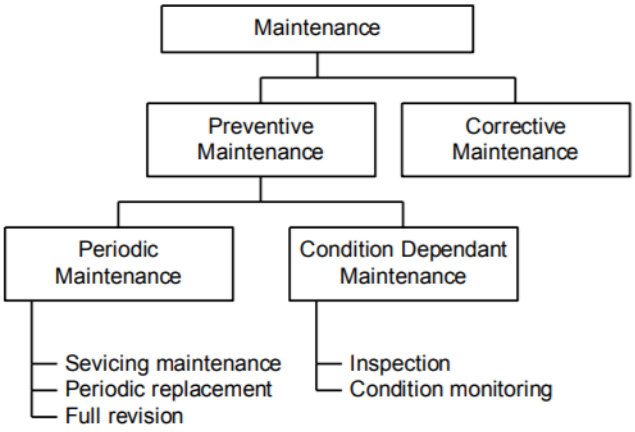

Figure 54: Maintenance breakdown [4]

To optimize the maintainability for this aircraft further, the team revisits the maintenance breakdown, portrayed in Figure 54. Preventive is compared to corrective maintenance since both have positive aspects to offer. Among preventive maintenance events, all are scheduled, which calls for predicted time cost. In association with reliability and the aspects mentioned inSection 7.4.2, this cost will be factoring against maintainability, but still factors in favor of a more reliable and safe structure, a desirable outcome. On the matter of inspection, not much is changed in relation to conventional aircraft. Inspection processes are specifically created with methods to accommodate most aircraft. However, periodic maintenance will show changes for the current design.

Following the above considerations of maintainability and the breakdown of maintenance specified for the new design under preliminary phase, planning for the specific characteristics shall be under way. That is, a form of scheduled maintenance will be drafted by the Quality Control officer, specific for this particular aircraft, will be sent for approval of the certification officer, and then will be filled and mailed to the directors of repair hangars, before arrival for the previous procedures. The same line of events will be followed for inspections and condition monitoring, while now it will be filled and mailed by the certification party to the airline.

7.4.5 Safety

The safety aspect of the aircraft is of upmost importance. During every mission human lives are at stake, so it needs to be ensured that the risk is low, meaning safety needs to be high, because even a single emergency/crash can shatter the reputation of the aircraft.

The biggest concern regarding safety in the aircraft is connected with the hydrogen storage and transfer. Hydrogen is stored in the tanks in cryogenic temperatures. If the tank insulation is damaged the temperature will start to rise, meaning the liquid hydrogen will start to evaporate which will increase the pressure in the tank. This can lead to an explosion. To prevent this, a pressure relieve valve is present, which discharges hydrogen into the atmosphere once a pressure of $1.45bar$ is reached within the tank.

The fuel transfer system has multiple safety valves which can be used to restrict flow to pipes when there is a problem. Additional safety concerns come from the combustion chamber of the engines. Steady combustion needs to be ensured, which can be a problem when heated air is mixed with cold liquid hydrogen. To combat that, a heat exchanger is placed in the system to warm up the hydrogen and reduce the temperature difference between the combustion ingredients.

Another place safety concerns may arise is the manufacturing process. Manufacturers should follow the specific guidelines like material quality and clearances. This can be checked by performing tests and inspection of samples from batches.

8 Aircraft Performance Analysis

With the completion of the design of the subsystems and overall design characteristics, a closer look can be taken at the performance of the aircraft. First, the take-off, climb cruise, turning and landing performance is discussed in Section 8.1. These performance parameters are a measure of RELIGHT's in-flight maneuverability and capabilities. Next, a closer look it taken at the noise pollution in Section 8.2. Section 8.3 quantifies the emissions polluted during operation. Furthermore, a cost analysis is performed in Section 8.4, in which also the return on investment is derived. Finally, all sustainability aspects that have not yet been mentioned, are discussed in Section 8.5.

8.1 Take-off, Climb, Cruise, Turning and Landing Performance

8.1.1 Requirements

Table 60: Take-off, landing, cruise and turning requirements

Requirement Identifier	Requirement	Compliance
SRA-STAKE-AL-01	The maximum range at maximum payload shall be between 1500 km and 2500 km.	✓
SRA-STAKE-AP-01	The aircraft shall be able to take-off from a 1500 m runway at MTOW at both sea level and 1500 m altitude	✓/✗
SRA-STAKE-AP-02	The aircraft shall be able to land on a 1500 m runway at MLW.	✓
SRA-STAKE-AP-07	The aircraft shall be capable of operating from the same class of runways as the reference aircraft, the Bombardier CRJ700 series.	✓
SRA-PROD-CG-02	The cruise altitude of the aircraft shall be below 12000 m.	✓
SRA-PROD-PERF-01	The cruise Mach number of the aircraft shall fall between Mach 0.65 - 0.90.	✓
SRA-PROD-PERF-07	The aircraft shall cover max range distance at max payload in under 3.5 hours.	✓
SRA-PROD-PERF-13	The aircraft shall have a minimum rate of climb at sea level of 10 m/s.	✓
SRA-PROD-PERF-14	The aircraft shall be able to perform a rate one turn at sea level, with a bank angle lower than 25 degrees.	✓

8.1.2 Airfield Performance

To check the compliance with the runway requirements, the take-off and landing airfield performance must be quantified. The take-off airfield performance is expressed in terms of ground run distance $(x_{gr_{to}})$, lift-off speed (V_{lof}), transition distance (x_{tr}) and climb-out distance (x_{cl}). The screen height is set equal to 50 ft, as specified by CS-25 regulations [49]. The take-off distance required is then obtained by adding the ground run distance and the airborne distance, as specified in Equation 120. Landing airfield performance is expressed in similar quantities, such as approach distance (x_{ap}), flair distance (x_{fl}), rotation distance (x_{rot}) and braking distance (x_{br}). The Required Field Length (RFL) then follows straightforwardly from the total ground run distance during landing as can be seen in Equation 121.The reader must note that the presented results are valid for a condition with no ground effect, a non-inclined runway and no wind. Hence, if the runway is non-inclined, the actual performance will slightly increase compared to what is presented below due to the ground effect.

Since the aircraft must be able to take-off from and land at an elevated runway at $1500m$ of altitude, airfield performance is both quantified for sea level conditions and conditions on a hot day at $1500m$ of altitude ($\rho = 0.974$). The results are summarized in Table 61. The climb-out distance turned out to be zero, which implies that the aircraft already reaches screen height during the transition phase.

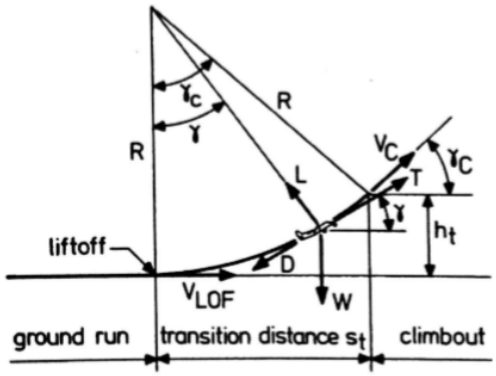

Figure 55: Take-off airfield performance free body diagram [68]

$$
\begin{aligned}
x_{gr_{to}} &= \frac{V_{lof}^2}{\frac{2g}{W}(\overline{T} - \overline{D}(\overline{V}_{to}) - \mu(W - \overline{L}(\overline{V}_{to}))} \\
V_{lof} &= 1.05 V_{min} \ , \ \overline{V}_{to} = \frac{V_{lof}}{\sqrt{2}} \ , \ \overline{T} = \frac{T_{to}}{\sqrt{2}} \\
x_{air_{to}} &= x_{tr} + x_{cl} = \frac{V_{lof}^2}{(n_{to} - 1)g} \sin\gamma_{cl} + \frac{h_{sc} - (1 - \cos\gamma_{cl})\frac{V_{lof}^2}{(n_{to}-1)g}}{\tan\gamma_{cl}} \\
x_{to} &= x_{gr_{to}} + x_{air_{to}}
\end{aligned}
\tag{120}
$$

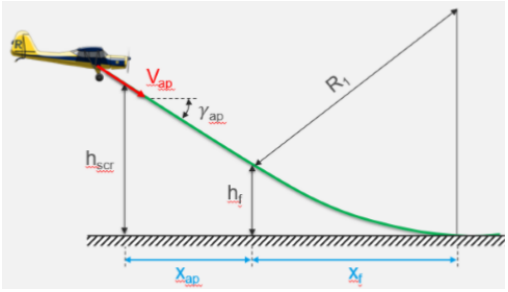

Figure 56: Landing airfield performance specification [68]

$$
\begin{aligned}
R_{la} &= 1.3^2 \frac{\frac{W}{S}\frac{2}{\rho}\frac{1}{C_{L_{max}}}}{\Delta n_{la} \cdot g} \\
x_{air_{la}} &= x_{ap} + x_{fl} = R\sin\gamma_{ap} + \frac{h_{sc} - (1 - \cos\gamma_{ap})R}{\tan\gamma_{ap}} \\
x_{br} &= \frac{W^2}{gS}\frac{1}{\rho}\frac{1.3^2}{C_{L_{max}}}\frac{1}{\overline{T}_{rev} - \overline{D}(\overline{V}_{la}) - \mu_{br}(W - \overline{L}(\overline{V}_{la}))} \\
\overline{V}_{la} &= \frac{V_{ap}}{\sqrt{2}} \ , \ x_{rot} = 2.6 V_{min} \\
x_{gr_{la}} &= x_{br} + x_{rot} \ , \ x_{la} = x_{air_{la}} + x_{gr_{la}} \ ,
\end{aligned}
\tag{121}
$$

During the airfield performance analysis, it became clear that the take-off requirement at 1500m altitude was the driving factor for determining the required thrust. In sea level conditions, the aircraft already complies with the requirement SRA-STAKE-AP-01 at a thrust-to-weight ratio of 0.31, whereas the equivalent sea level thrust-to-weight ratio for the condition at 1500m is 0.44. From this, the conclusion can be drawn that the thrust required is very sensitive to this requirement. In the case the aircraft is only operated at sea level conditions, the propulsion system will be over designed.This also explains the relatively low values obtained for the airfield performance quantities at sea level conditions.

Table 61: Airfield performance at sea level and at 1500m altitude for a reverse thrust of 50% at sea level and 100 % at 1500m; all distances reported in [m] and all velocities in [m/s]

	$x_{gr_{to}}$	V_{lof}	x_{tr}	x_{cl}	x_{to}	R_{la}	x_{ap}	x_{fl}	V_{ap}	x_{rot}	x_{br}	$x_{gr_{la}}$	x_{la}
sea level	737.4	59.5	293.2	0	1030.6	5532.4	289.5	146.1	73.7	147.3	901.4	1048.7	1484.4
1500m	1160.1	66.7	368.8	0	1528.9	6958.1	364.2	108.8	82.6	165.2	842.1	1007.3	1480.3

8.1.3 Climb Performance

In order to climb, the available engine power must be converted into potential energy. However, as part of the engine power is wasted on drag, one must make sure that the available power is greater than the required power for counteracting drag. The performance diagrams, that visualize the engine excess power, are shown in Figure 57 for both sea level climb and climb at 1500m altitude. For this, Equation 122 is used. The thrust at altitude is approximated by converting the sea level thrust with Equation 123, whereas the thrust is assumed independent of airspeed [68].

$$
D = CD_0\frac{1}{2}\rho V^2 S + \frac{2W^2}{\pi A e \rho V^2 S} \qquad P_a = T \cdot V \qquad P_{req} = D \cdot V \tag{122}
$$

$$
T = T_0\left(\frac{\rho}{\rho_0}\right)^{3/4} \tag{123}
$$

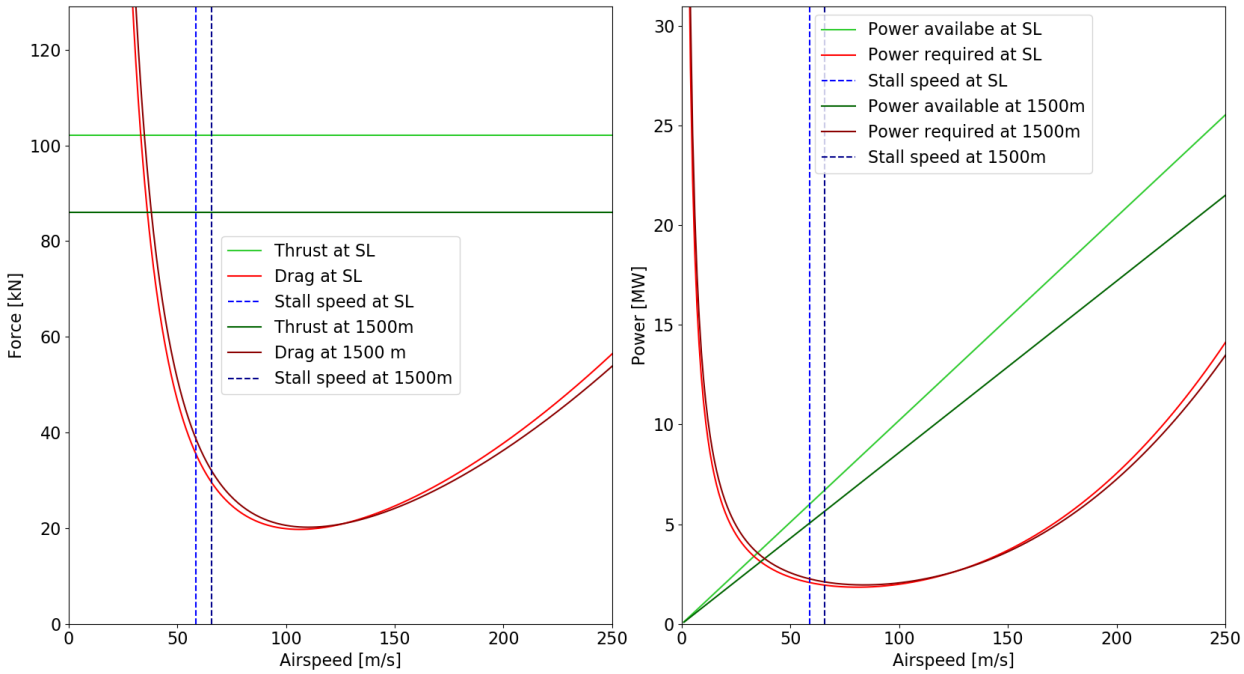

Figure 57: Performance diagrams; left: Thrust against V, right: Power against V

It becomes clear that, in both conditions, the power available is greater than the power required. The achievable steady rate of climb then follows from Equation 124. The maximum rate of climb is achieved where the difference between the power available (P_a) and power required (P_r) is the greatest. Since this condition changes with altitude, the maximum achievable rate of climb is shown in Figure 58 as a function of altitude. The corresponding airspeed at which the maximum rate of climb is achieved is also shown in this figure. From this, the maximum climb angle at each altitude is computed using Equation 125

$$ROC_s = \frac{P_a - P_r}{W} \qquad (124)$$

$$\gamma_{cl_{max}} = \sin^{-1}\left(\frac{ROC_{s_{max}}}{V_{ROC_s = ROC_{s_{max}}}}\right) \qquad (125)$$

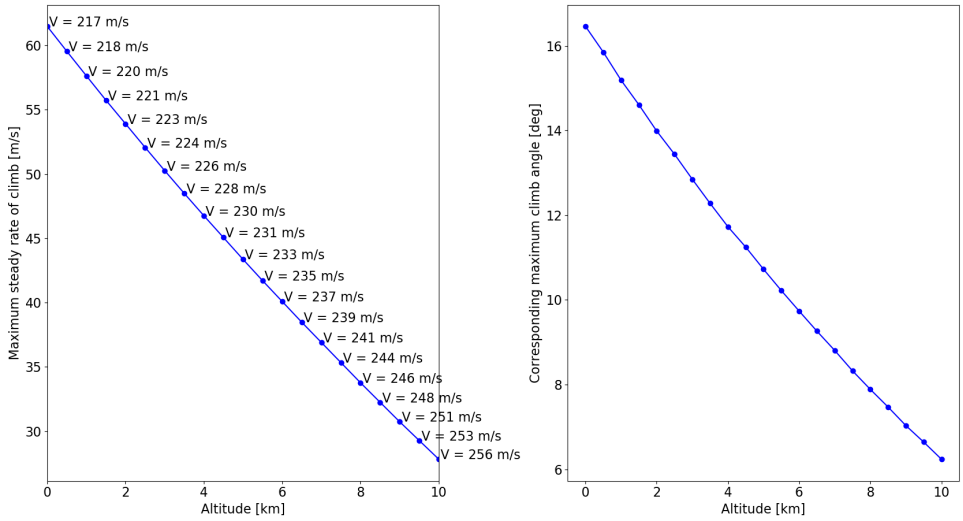

Figure 58: Maximum achievable steady rate of climb as function of altitude (left) and corresponding maximum climb angle (right)

8.1.4 Cruise Performance

An important parameter for cruise performance is V/F, where V is the velocity and F is the fuel flow, defined as $c_T T$; the thrust specific fuel consumption multiplied by the thrust. The parameter V/F, called the specific range, will, when maximized, result in the maximum range. The specific range can be determined as follows: Looking at Figure 59, and drawing a line from the origin crossing the intersection of the drag curve and the

cruise speed. The angle this line makes with the horizontal is the angle β; a smaller β results in a larger range [69]. The theoretical maximum V/F is achieved when the line is tangent to the graph, where the aircraft will fly at the optimal velocity, with the respective C_D and C_L. However, the optimal velocity is higher than the limit velocity; hence Equation 126 is used, where the both C_L and C_D have increased [69].

$$V_i = \sqrt{\frac{W_i}{S}\frac{2}{\rho}\frac{1}{C_L}} \qquad C_L = \sqrt{C_{D_0}\pi Ae} \qquad C_D = 2C_{D_0} \tag{126}$$

$$R_{max_{alt}} = \frac{2}{c_t C_D}\sqrt{\frac{1}{S}\frac{2}{\rho}C_L}(\sqrt{W_1} - \sqrt{W_2}) \tag{127}$$

$$R_{max_v} = \frac{V}{c_T}\frac{C_L}{C_D} ln\left(\frac{W_1}{W_2}\right) \tag{128}$$

$$V_2 = \sqrt{\frac{W_2}{S}\frac{2}{\rho_2}\frac{1}{C_L}} = \sqrt{\frac{W_1}{S}\frac{2}{\rho_1}\frac{1}{C_L}} = V_1 \tag{129}$$

$$\rho_2 = \frac{W_2}{W_1}\rho_1 \tag{130}$$

During cruise, in order to fly at a constant velocity, the aircraft is required to gradually climb as it loses weight through burning fuel. From Equation 130 the density at the end of cruise (when $W = W_2$) is determined. Whereas the drag is proportional to the weight, the velocity is proportional to the square root of the weight. This will cause the drag curve in Figure 59 to move down and to the left; it moves more downward than left [69]. The grey dashed line for the drag curve at an altitude of $12379m$ has a lower slope for the drag curve at the higher altitude, which has been obtained from the new density calculated with Equation 129 and Equation 130, which equates to a larger specific range. It should be noted that this cruise behavior is generally not allowed by the ATC. Furthermore, due to the regulations on emissions, the aircraft is required to stay below $10000m$. On top of that, requirement SRA-PROD-CG-02 prohibits flying above $12000m$. Therefore the altitude at which RELIGHT flies, is taken to be constant for cruise analysis. If the altitude is fixed, the maximum range is determined using Equation 127. The altitude being fixed, causes the velocity to change over the cruise flight. From Equation 126 it becomes clear that the velocity decreases with decreasing aircraft weight. The subscript i denotes the weight at a given point during cruise.

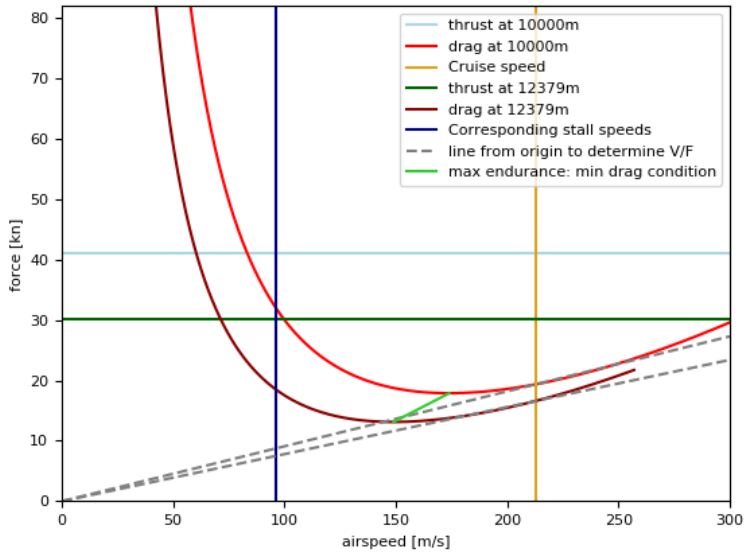

Figure 59: Altitude effect on cruise when flying at constant speed

Endurance, the maximum time the aircraft can spend in the air, is obtained by flying at the minimum D/V condition [69]. This is at the lowest point on the drag curve in Figure 59. The green line indicates at which drag and velocity condition the pilot is supposed to fly, when climbing during cruise, to maximize the endurance. The higher the aircraft flies, the lower the speed will be for the minimum D/V condition. Endurance is calculated using Equation 131

Below, in Table 62, the maximum range, ferry range and maximum endurance are provided.

$$E = \frac{1}{c_T}\frac{C_L}{C_D} ln\left(\frac{W1}{W2}\right) \tag{131}$$

Table 62: Maximum range, ferry range and maximum endurance

Maximum range $[km]$	Maximum ferry range $[km]$	Maximum endurance $[hh:mm:ss]$
2159.3	4318.73	03 : 26 : 30

The range turns out higher than it was initially designed for. The most prominent reason for this, is the low SFC obtained during the sizing procedure of the engines (Section 6.3. This causes the fuel flow to be lower than expected (since $F = T \cdot c_T$), therefore increasing the cruise distance with the same amount of fuel.

8.1.5 Turning Performance

Turning performance is expressed in terms of the steepest turn, minimum turn radius and minimum time to turn. The reader must note that the presented results only apply to steady level turns without the presence of wind gusts. This implies that the load factor stays constant throughout the turn. The load factor is defined as stated in Equation 132.

$$n \equiv \frac{L}{W} = \frac{L}{Lcos\phi} = \frac{1}{cos\phi} \tag{132}$$

Load Factor Analysis Turning performance is dictated by the maximum attainable load factor. Since this condition varies with airspeed and altitude, the turning performance will mainly be visualized graphically for three different altitudes: sea level, $1500m$ and cruise altitude. The range of airspeed for which turning performance is quantified at each of these altitudes, depends on stall limits and the balance between power available (P_a) and power required (P_r). In order to perform a steady level turn, the load factor must be greater than one. As this changes the $P_a - P_r$ balance, the load factor lines must be included in the performance diagrams. On the left side of Figure 60, these lines are shown for load factors up until the maximum load factor n_{max} at sea level. Similar diagrams are made for $1500m$ altitude and cruise condition, of which the latter is shown in Figure 61. Then, at each load factor, the operable airspeed range is computed. The minimum airspeed is always determined by the stall limits, as the starting points (from the left) of the drag lines are below the thrust available. The upper airspeed constraint is due to the power required exceeding the power available. From this, the so-called $n_{max} - V$ diagram is derived as shown on the right side of Figure 60 and Figure 61.

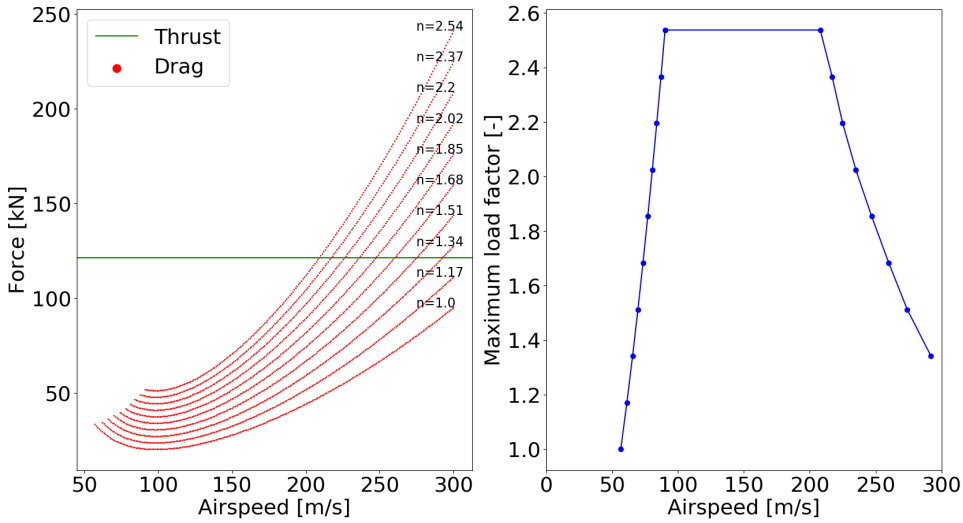

Figure 60: Left: performance diagram for varying load factor at sea level; right: maximum load factor as function of airspeed at sea level

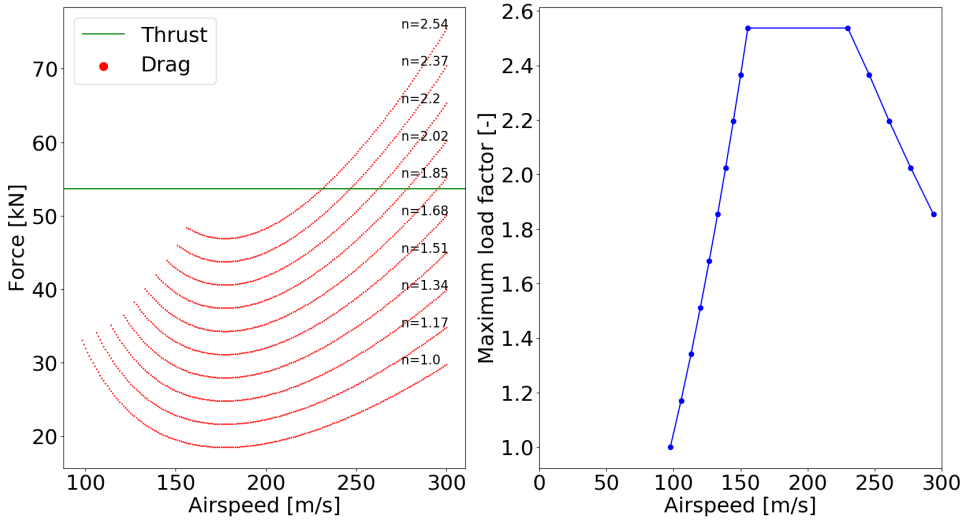

Figure 61: Left: performance diagram for varying load factor at cruise; right: maximum load factor as function of airspeed at cruise

Minimum Turn Radius and Minimum Time to Turn With the $n_{max} - V$ diagram being constructed for each flight condition, the minimum turn radius and minimum time to turn can be computed as function of airspeed by using Equation 133. For each airspeed in the operable flight regime for turning, the corresponding maximum load factor should be taken as found from the $n_{max} - V$ diagrams. The results are depicted in Figure 62 in which the blue, green and red lines represent sea level, 1500m and cruise conditions, respectively. Furthermore, the rate 1 turn performance for a bank angle of 25 degrees is shown to enable assessment of requirement SRA-PROD-PERF-14.

$$R = \frac{V^2}{g\sqrt{n^2 - 1}} \qquad T_{2\pi} = \frac{2\pi V}{R} \tag{133}$$

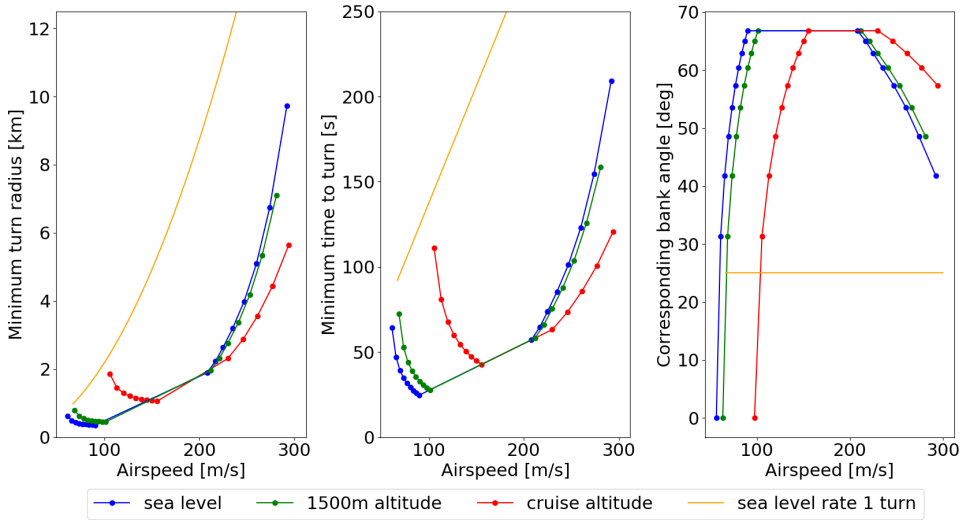

Figure 62: Minimum turn radius, minimum time to turn and corresponding bank angle for sea level, 1500 m and cruise conditions

Steepest Turn The steepest turn is characterized by the maximum attainable load factor, in this case 2.54. The corresponding maximum bank angle is 66.8 degrees. The range of airspeed that can be achieved at this load factor, without exceeding the maximum load factor, is derived from the horizontal line segments in the $n_{max} - V$ diagrams. The resulting steepest turn radius and turn time are computed with Equation 133 and plotted in Figure 63 for sea level, 1500m and cruise conditions.

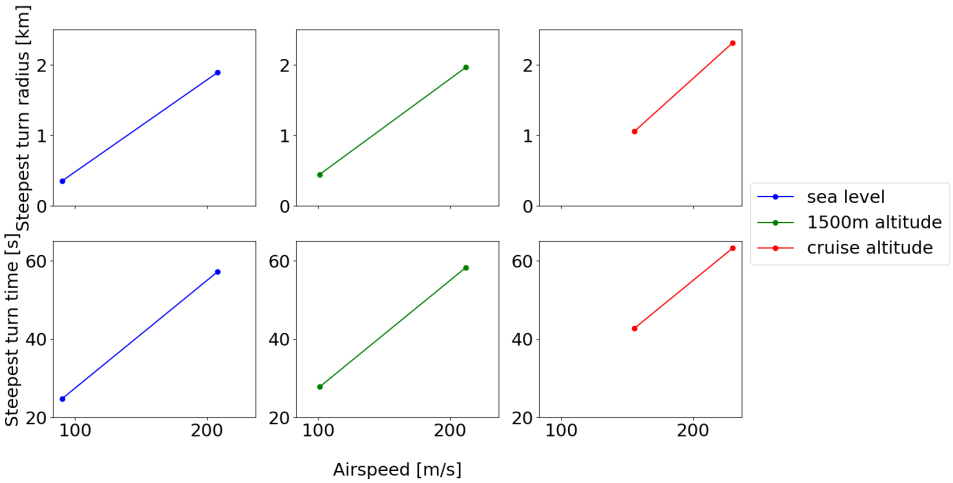

Figure 63: Steepest turn characteristics; top: turn radius; bottom: turn time

8.1.6 Verification and Validation

The airfield, climb, cruise, turning and landing performance calculations have been verified through a number of unit tests, as specified in Table 63.

Table 63: Performed unit tests to facilitate verification of the flight performance functions

Function	Action	Expected result	Pass/Fail
Performance diagrams	decrease ρ	T, D, P_a and P_{req} decrease, $V_{T=D}$ increases	Pass
	increase W	D and P_{req} increase, T and P_a unchanged, $V_{T=D}$ decrease	Pass
	decrease T	T, P_a and $V_{T=D}$ decrease, D and P_r unchanged	Pass
	double n	D increased by factor 2, V_{min} increased by factor $\sqrt{2}$	Pass
Max steady ROC	decrease ρ	max steady ROC decreases, $V_{ROC=max}$ decreases	Pass
	decrease T	max steady ROC decreases, $V_{ROC=max}$ increases	Pass
	decrease W	max steady ROC increases, $V_{ROC=max}$ decreases	Pass
Take-off distances	increase W	$x_{gr_{to}}$, $x_{air_{to}}$ and x_{to} increases	Pass
	increase T_{to}	$x_{gr_{to}}$ and x_{to} decrease, $x_{air_{to}}$ unchanged	Pass
	increase μ	$x_{gr_{to}}$ and x_{to} increase, $x_{air_{to}}$ unchanged	Pass
	decrease γ_{cl}	$x_{gr_{to}}$ unchanged, $x_{air_{to}}$ and x_{to} increase	Pass
Landing distances	increase W	$x_{air_{la}}$, $x_{gr_{la}}$ and x_{la} increases	Pass
	increase $\overline{T}_{to}$	$x_{air_{la}}$ unchanged, $x_{gr_{la}}$ and x_{la} decrease	Pass
	decrease μ_{br}	$x_{air_{la}}$ unchanged, $x_{gr_{la}}$ and x_{la}increase	Pass
	increase γ_{ap}	$x_{air_{la}}$ and x_{la} decrease, $x_{gr_{la}}$ unchanged	Pass
$n_{max} - V$ diagrams	increase altitude	required airspeed increases, velocity range at n_{max} decreases	Pass
	lower T	increasing number of T=D intersections at lower load factors, more upper airspeed constraints	Pass
	n = 0	D = 0, only stall airspeed constraints	Pass
Turn radius and turn time	increase altitude	minimum and steepest turn radius, speed at minimum turn radius and minimum and steepest turn time increase (graphs shift upward and to the right)	Pass
	n = 1	minimum and steepest turn radius, minimum and steepest turn time and corresponding bank angle are zero	Pass

Maximum cruise range	decrease W	$Range_{max}$ decreases, V_1, V_2 and η_t decrease	Pass
	increase ρ	$Range_{max}$, $V_{1,2}$, η_t increase	Pass
	increase T	nothing changes	Pass
	increase SFC c_T	$Range_{max}$ decreases, $V_{1,2}$ unchanged	Pass
Maximum endurance	decrease ρ	no effect	Pass
	increase T	endurance decreases	Pass
	increase SFC c_T	endurance decreases	Pass
	increase W	no effect	Pass
	increase C_{D_0}	endurance decreases	Pass
	increase C_L	endurance increases	Pass
All functions	Hand calculations and unit checks	Similar results	Pass

The maximum rate of climb calculations are validated by comparing the climb angle, associated with the maximum rate of climb, with existing aircraft over a range of altitudes from sea level until cruise altitude. From Figure 58, it was found that the climb angle ranged from 16.5 degrees at sea level to 6.2 degrees at cruise altitude. This falls within the expected range of maximum climb angles, hence the calculations are validated.

The turning performance is validated by comparing the turning characteristics with the ones from the Cessna Citation, as data could be found for this specific aircraft. Looking at Table 88, some interesting remarks can be made. First of all, the range of airspeed at which the maximum load factor can be achieved is high, compared to reference aircraft. Normally, this condition is obtained where the thrust intersects the minimum drag condition. However, as can be seen in the performance diagrams, the minimum drag does not exceed the available thrust for all possible load factors. This is due to a combination of high available thrust and a low value for CD0, which is derived in Section 6.2. This has the following implications on turning performance:

1. The minimum turn radius is relatively short since only stall speed is limiting at low values of airspeed and not the power available.

2. The minimum time to turn is relatively short due to the same reasoning as point 1. In addition, the minimum time to turn at maximum load factor is even decreased further due to the high airspeed that can be attained (right limit of the horizontal line segment in Figure 62).

This explains why both the minimum turn radius and minimum time to turn were lower than expected, also when compared to the Cessna Citation and compared to the turn radius of category D aircraft[70]. Furthermore, the Cessna Citation data is used as input and yielded similar turning performance. Hence, the turning performance module is validated.

Table 64: Turning performance comparison at 7000m altitude

	n_{max}	$V_{n_{max}}$	R_{min}	$V_{R_{min}}$	T_{min}	$V_{T_{min}}$
Cessna Citation	2.34	150	675	110	40	115
RELIGHT	2.54	90-210	924	145	40	145

Validation of the cruise performance can partially be done by looking at the CRJ700 payload range diagram. It is observed that the ratio of maximum range to ferry range of RELIGHT is similar to that of the CRJ700. Generally, with hydrogen aircraft the maximum payload capabilities are not that great as there is, due to the presence of fuel tanks in the fuselage, a limited storage space for payload [71]. As it is very difficult to find a proper reference aircraft, with equal range, passengers and fuel system, the obtained values are validated against the results of the payload range estimation presented in Section 3. The payload range estimation has

been verified and validated, therefore serving as an appropriate validation model to analyze the design. With the validation of the range performance, endurance is automatically validated; endurance is calculated using the same equations, but optimized for different parameters.

8.1.7 Sensitivity Analysis

A sensitivity analysis is performed to check the compliance with the flight performance requirements due to the variations in the MTOW, take-off thrust and zero drag coefficient. As the red-colored cells in Table 65 indicate, the take-off and landing requirement at 1500m altitude would be exceeded if MTOW increases by 10% or the take-off thrust decreases by 10%. On the other hand, the compliance with the take-off requirement would improve if opposite changes occur. The other parameters of interest, like maximum rate of climb and minimum turn radius and turn time would not be endangered for the introduced uncertainties. Therefore, it is recommended to reconsider the take-off and landing configuration of the aircraft to reduce the sensitivity of total take-off and landing distance with MTOW and take-off thrust.

Table 65: Sensitivity analysis for critical flight performance parameters

Parameter	**value**	MTOW +10%	MTOW - 10%	Thrust +10%	Thrust -10%	CD_0 +10%	CD_0 -10%
x_{to} at 1500m [m]	1528.9	+21.2%	-19.0%	-9.2%	+11.4%	+0.013%	-0.52%
x_{la} at 1500m [m]	1480.3	+11.2/%	-10.9%	-3.5%	+3.8%	-0.25%	+0.047%
maximum sea level ROC [m/s]	61.5	-9.6%	+11.7%	+15.9%	-15.1%	-4.9%	+5.7%
minimum sea level turn radius [m]	356	+10.1%	-9.9%	-	-	-	-
minimum sea level time to turn [s]	24.8	+4.8%	-5.2%	-	-	-	-
Maximum range [km]	2159.3	+4.88%	-4.42%	-	-	-6.31%	+8.2%
Endurance [s]	12390	-	-	-	-	-4.67%	+ 5.41%

For calculating the endurance, a slight inconsistency with reality should be noted. The mass fractions have been taken from the Class I weight estimation. Although in reality the maximum endurance does change with a change in MTOW, it does not in the model as it is based on statistics.

8.1.8 Compliance with Requirements

Airfield Performance As shown in Table 61, the total take-off distance required at sea level and 1500m is 1030.6 and 1528.9m, respectively. The latter theoretically violates the requirements SRA-STAKE-AP-01 and SRA-SYS-PROP-02. However, as previously stated, this might not be the case in case the ground effect is taken into account, as this will cause a significant reduction in induced drag of 25% [72]. This will result in a decrease in take-off length of approximately 100m, which would imply compliance with the take-off requirement. Therefore, it is recommend to investigate the influence of the ground effect on the take-off distance required. Both runway requirements SRA-STAKE-AP-02 and SRA-STAKE-AP-07 are met, as the landing distance are below 1500m and the sea level one is below the required sea level take-off and landing field length for the CRJ700 of 1605 and 1540m, respectively [73][30].

Climb Performance The maximum achievable rate of climb at sea level is deduced from Figure 58. Since this is found to be approximately 61 m/s, requirement SRA-PROD-PERF-13 is met.

Turn Performance In order to comply with requirement SRA-PROD-PERF-14, a rate one turn must be achieved with a bank angle lower than 25 degrees. Figure 62 depicts such turning condition. All three subplots show compliance with this requirement: the most left plot proves that this turn would not exceed the minimum turn radius at each airspeed, the middle plot proves the same for the minimum time to turn. Finally, the most right plot shows that the corresponding load factor will remain below the maximum load factor, regardless of airspeed.

[30] https://mhirj.com/themes/bca/pdf/Bombardier_CRJ_Series_Brochure.pdf

Cruise Requirement SRA-PROD-PERF-07 requires the that range is covered in less than three and a half hours. When flying at $10000m$ altitude the maximum range is covered in 03:19:59, therefore complying with the requirement. Requirement SRA-STAKE-AL-01 is also satisfied, as the maximum range is $2159km$, which is within the specified range.

8.2 Aircraft Noise

As the noise polluted by RELIGHT will affect the environmental footprint, a detailed noise analysis is required to quantify the contribution to sustainability. Before the noise analysis, a closer look is taken at the noise requirements set by the ICAO.

8.2.1 Noise Requirements

Table 66: Noise requirements

Requirement Identifier	Requirement	Compliance
SRA-STAKE-ENV-02	The noise footprint of the aircraft shall be reduced by at least 25% with respect to the reference aircraft, the Bombardier CRJ700.	✓/✗
SRA-PROD-PERF-10	The aircraft shall fall into the ICAO stage-5 noise level category.	✓/✗
SRA-PROD-PERF-11	The cabin noise during cruise flight shall not exceed 82 dB and 110 dB during take-off.	✓/✗

SRA_PROD_PERF-10 implies that the flyover noise, approach noise, lateral noise and cumulative noise shall be limited to 86, 95, 91 and $264dB$, respectively [74]. As the distance from the noise source to observer affects the noise level perceived, fixed points exist at which the three noise levels are measured, as depicted in Figure 64. Also the directional characteristics of a noise source, i.e. directivity, will affect the perceived noise levels. The directivity is described by two angles: polar directivity angle (θ) and azimuthal directivity angle (ϕ). The definition of both angles is shown in Figure 65 [75]. For simplicity sake, θ and ϕ are set constant and equal to 90 and 10 degrees, respectively. Although this would introduce minor discrepancies with the real world noise levels, the performed noise analysis will be sufficient to check the compliance with the noise requirements at the current state of the design.

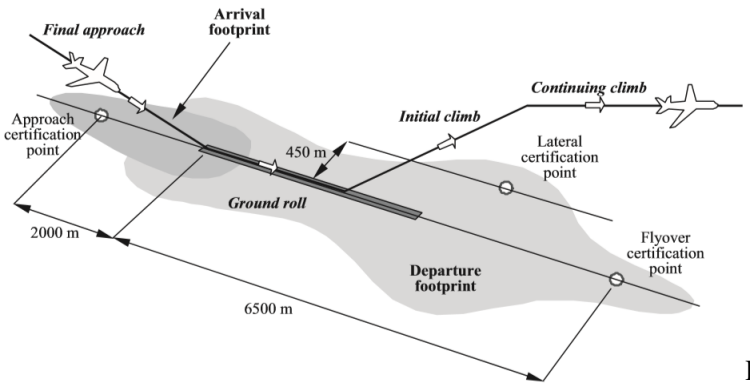

Figure 64: Certification procedure for measuring flyover, approach and lateral noise levels [76]

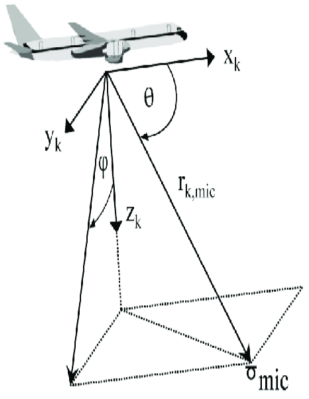

Figure 65: Definition of polar directivity angle (θ) and azimuthal directivity $\angle$ (ϕ) [76]

8.2.2 Analysis Methodology

The noise pollution is quantified according to empirical methods specified in [77]. A distinction is made between engine noise and airframe noise. Both noise sources are further split into their main contributors. Engine noise consists of fan noise, combustion noise, turbine noise and jet noise. Aircraft noise can be split into engine noise and airframe noise. Jet shock cell noise is not considered, as the fully expanded jet mach number does not exceed one. Regarding airframe noise sources, the clean wing, horizontal tail, vertical tail, flaps, nose landing gear and main landing gear are considered.

For each considered noise source, the far-field mean-square acoustic pressure $\langle p^2 \rangle^*$ is computed, where the superscript $*$ denotes a normalized quantity. As the computation of acoustics pressures requires many constants derived from empirical data, only the most important ones have been reported. To fully understand the source of all these constants, please consider the approach specified in [77]. Other input parameters were derived from the designed propulsion system, as discussed in Section 6.3. After obtaining the required inputs, the acoustic pressure is converted to a Sound Pressure Level (SPL), measured in decibels (dB) and using a reference acoustic pressure of 2E-5Pa (threshold of human hearing). The sound spectrum is computed for each frequency ranging from 100 to 10000Hz. The reader must note that these frequencies represent central frequencies of the corresponding 1/3 Octave Band. In case of tonal noise sources, all pure tones that fall within a 1/3 Octave Band are added. The tones that fall within each band (n) is computed using Equation 134. Since noise is produced in-flight, the effect of forward velocity on acoustic power must be taken into account. A so-called "Doppler factor" is computed for each central frequency, as stated in Equation 135.

$$n_l = int[10^{-1/20}\eta] + 1 \quad n_u = int[10^{1/20}\eta] \quad n = n_u - n_l + 1 \quad (134) \qquad \eta = (1 - M_\infty \cos\theta)\frac{f}{f_b} \quad (135)$$

8.2.3 Engine Noise

The engine noise is predicted using various empirical methods. Since the empirical data is gathered from kerosene-fueled aircraft, the affects of combustion of liquid hydrogen on the noise pollution is not taken into account.

Fan Noise Fan noise is predicted using an empirical method developed by Heidman [78] and is obtained by summing up six contributors: inlet- and discharge broadband noise, inlet- and discharge rotor-stator interaction tones and inlet flow distortion tones. Broadband noise is caused by turbulence flow passing the fan blades, rotor-stator interaction tones by lift variations on rotor or stator blades. The fan noise SPL is obtained by converting the far field mean-square acoustic pressure computed by Equation 136 using Equation 137. These equations are also valid for combustion noise and turbine noise. The acoustic power of all engine noise sources, that is needed to compute the acoustic pressures, is summarized in Table 68. The sound spectrum functions and the directivity of each noise component can be found in Table 67. The resulting sound spectrum for a single engine is shown in Figure 66 for a distance between noise source and observer (r_s) of 104.81m, the distance used for certification of approach noise. The maximum fan noise SPL turned out to be 96.9dB.

$$\langle p^2_{fan} \rangle^* = \frac{A^* \Pi^*}{4\pi (r_s^*)^2} \frac{D(\theta) S(\eta)}{(1 - M_\infty \cos\theta)^4} \quad (136) \qquad SPL_{fan} = 10 \log_{10} \langle p^2_{fan} \rangle^* + 20 \log_{10} \frac{\rho_\infty c^2_\infty}{P_{ref}} \quad (137)$$

Combustion Noise Combustion noise is predicted using an empirical method of Matta [77]. With a maximum SPL of 69.3dB, significantly less combustion noise is polluted compared to the other engine noise sources.

Turbine Noise Turbine noise is predicted using an empirical method of the General Electric Company [79]. The maximum turbine noise SPL turned out to be 92.5dB.

Jet Noise Jet mixing noise, resulting from shock-free circular nozzles is predicted by a slightly different empirical method [77]. The jet acoustic pressure and SPL are obtained by Equation 138 and Equation 139, respectively. The spectrum shape is now contained in the parameter F, instead of S, and is a function of the corrected Strouhal number S_c as defined in Equation 140. The analysis resulted in a maximum jet noise SPL of 94.7dB.

$$\langle p^2_{jet} \rangle^* = \frac{A^*_j \Pi^*}{4\pi (r_s^*)^2} \frac{D(\theta, V_j^*)}{1 - M_\infty} \frac{F(S_c, \theta, V_j^*, T_j^*)}{\cos(\theta - \delta)} \left(\frac{V_j^* - M_\infty}{V_j^*} \right)^{m(\theta)} \quad (138)$$

$$SPL_{jet} = 10 \log_{10} \langle p^2_{jet} \rangle^* + 10 \log_{10} \frac{\rho^2_\infty c^4_\infty}{P^2_{ref}} \quad (139) \qquad S_c = \frac{f * d_j^*}{\xi V_j^*} \quad (140)$$

Now the SPL of each engine component is derived, the total engine noise polluted can be computed using

Equation 141. This turned out to be 99.0dB for a single engine and 101.7dB for both engines.

$$SPL_{tot} = 10\log_{10}\sum_{i=1}^{N_{comp}} 10^{2PL_i/10} \tag{141}$$

Table 67: Spectrum function and relevant constants for various engine noise components

Noise component	**Spectrum function $S(\eta)$** or F($S_c, \theta, V_j^*, T_j^*$)	**K** [−]	**$\log_{10}$** D(θ)[−]
Fan			
Inlet broadband	$0.116e^{-0.5[\frac{ln(\eta/2.5)}{ln(2.2)}]^2}$	1.552E-4	-0.87
Inlet rotor-stator	$\sum_{n=n_l}^{n_u} S(n,i,j)$	2.683E-4	-0.85
Inlet flow distortion	$9\sum_{n=n_l}^{n_u} 10^{-n}$	1.488E-4	-0.85
Discharge broadband	same as inlet broadband	3.206E-4	-0.04
Discharge rotor-stator	same as inlet rotor-stator	2.643E-4	-0.05
Combustor	see empirical data in [77]	9.85E-7	-0.16
Turbine			
Broadband	see empirical data in [77]		
Pure tone	$0.6838 \cdot 10^{-(n-1)/2}$	8.589E-5	
Jet	see empirical data in [77]	6.67E-5	

Table 68: Acoustic power of various engine noise components

Source	**Acoustic Power Π^***
Fan	$\text{KG(i,j)(s}^*)^{-a(k,l)} M_m^b(\dot{m}^*/A^*)\cdot (\Delta T^*)^2 F(M_r, M_m)$
Comb.	$K\frac{\dot{m}_i^*}{A^*}\left(\frac{T_j^*-T_i^*}{T_i^*}\right)^2 (p_{t,i}^*)^2(\Delta T_{des}^*)^{-4}$
Turbine	$K\left(\frac{h_{t,i}^*-h_{s,j}^*}{h_{t,i}^*}\right)^a (U_{T^*})^b$
Jet	$K(\rho_j^*)^\omega (V_j^*)^8 P$

8.2.4 Airframe Noise

The polluted airframe noise is predicted using Fink's empirical method [80]. This method only takes into account the most dominant airframe noise sources as stated before, thereby neglecting for example the external wing tanks mounted under the wing. The far-field mean-square pressure for the airframe components is derived from Equation 142. Like for the jet noise component, the airframe noise spectrum is determined by the Strouhal number at every 1/3 Octave Band central frequency, which is defined in Equation 143. In this equation, L is the characteristics length of a particular airframe component. The acoustic power can be described by Equation 144. The required inputs for computing both quantities are summarized in Table 69 and mostly taken from the designed wing and empennage planform. Finally, the SPL of each component is calculated using Equation 137 and the total airframe noise is obtained by summing all the individual airframe components using Equation 141. The airframe noise spectrum is shown in Figure 67.

$$\langle p_{air}^2\rangle^* = \frac{A^*\Pi^*}{4\pi(r_s^*)^2}\frac{D(\theta,\phi)F(S)}{(1-M_\infty\cos\theta)^4} \tag{142}$$

$$S = \frac{fL}{M_\infty c_\infty}(1-M_\infty\cos\theta) \tag{143}$$

$$\Pi_{air}^* = K(M_\infty)^a G \tag{144}$$

Table 69: Required input to compute the SPL of the airframe noise components

	Spectrum function F(S)	**K [-]**	**G**	**a [-]**	**Directivity $D(\theta,\phi)$**
Clean wing	$0.613(10S)^4\left((10S)^{1.5}+0.5\right)^{-4}$	4.464E-5	$0.37\frac{A_w}{b_w^2}\left(\frac{\rho_\infty M_\infty c_\infty A_w}{\mu_\infty b_w}\right)^{-0.2}$	5	same as clean wing
Horizontal tail	same as clean wing	4.464E-5	$0.37\frac{A_h}{b_h^2}\left(\frac{\rho_\infty M_\infty c_\infty A_h}{\mu_\infty b_h}\right)^{-0.2}\left(\frac{b_h}{b_w}\right)^2$	5	same as clean wing
Vertical tail	same as clean wing	4.464E-5	$0.37\frac{A_v}{b_v^2}\left(\frac{\rho_\infty M_\infty c_\infty A_v}{\mu_\infty b_v}\right)^{-0.2}\left(\frac{b_v}{b_v}\right)^2$	5	$4\sin^2\phi\cos^2\theta/2$
Flaps	$\begin{Bmatrix} 0.0480S, & S<2 \\ 216.49S^{-3}, & S>20 \\ 0.1406S^{-3}, & else \end{Bmatrix}$	2.787E-4	$\frac{A_f}{b_w^2}\sin^2\delta_f$	6	$3(\sin\delta_f\cos\theta+\cos\delta_f\sin\theta\cos\phi)^2$
Nose wheels	$13.59S^2(12.5+S^2)^{-2.25}$	4.349E-4	$n\left(\frac{d}{b_w}\right)^2$	6	$\frac{3}{2}\sin^2\theta$
Nose struts	$5.325S^2(30+S^8)^{-1}$	2.753E-4	$\left(\frac{d}{b_w}\right)^2\frac{l}{d}$	6	$\frac{3}{2}\sin^2\theta\sin^2\phi$
Main wheels	$0.0577S^2(1+0.25S^2)^{-1.5}$	3.414E-4	same as nose gear	6	same as nose gear
Main struts	$1.280S^3(1.06+S^2)^{-3}$	2.753E-4	same as nose gear	6	same as nose gear

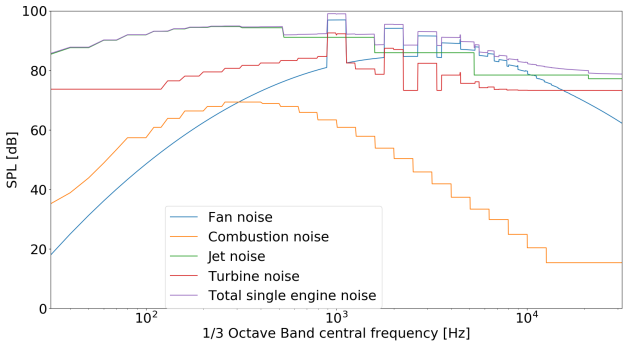

Figure 66: Single engine noise SPL spectrum

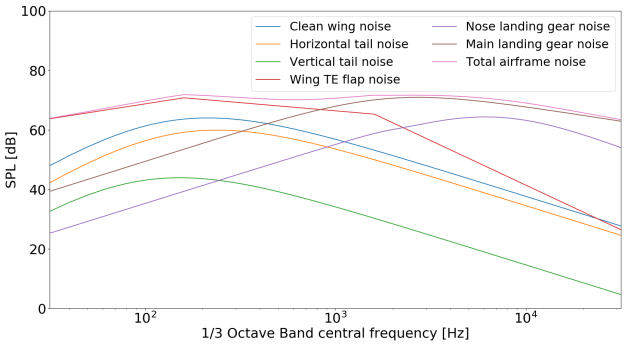

Figure 67: Airframe noise SPL spectrum

8.2.5 Maximum Noise Levels

The above procedure can be repeated for different values of r_s, the distance between noise source and observer. Using the distances for certifying flyover, approach and lateral noise levels, allows for calculating maximum noise levels. This is done by summing the engine noise and airframe noise using Equation 141 and checking the maximum SPL for the central frequencies considered. The total noise spectrum is shown in Figure 68, using the certification distance of approach noise. The resulting maximum noise levels are summarized in Table 70.

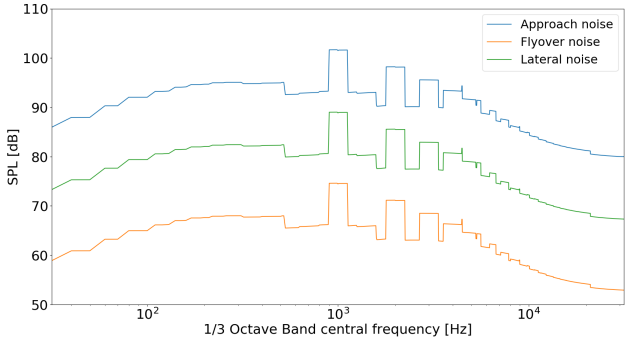

Figure 68: Approach, flyover and lateral noise spectra and stage-5 noise limits

Table 70: Maximum approach, flyover, lateral and cumulative noise levels

	Approach noise	Flyover noise	Lateral noise	Cumulative noise
limit	95	86	91	264 [dB]
RELIGHT	101	74	89	264 [dB]
CRJ700	93	83	89	265 [dB]

8.2.6 Noise Suppression

As stated in [77], the empirical data provided in the various methods do not include noise suppression concepts, like acoustic lining, flow mixers and silencing nozzles. This could suppress jet, inlet and fan noise up to $10dB$ and core and turbine noise even up to to $20dB$. In addition, the noise generated by engine-airframe and engine location interaction is not included, which could increase noise levels up to $2dB$. From this, the conclusion can be drawn that the overall noise footprint can potentially be decreased, if the design is adapted towards these noise suppression concepts.

8.2.7 Verification and Validation

Throughout the noise analysis, the spectral output of each individual noise component is compared to the noise spectra provided in [77]. In addition, the obtained SPLs are directly compared to one another. As expected, engine noise dictates the total noise spectrum by showing higher SPLs compared to airframe noise. Furthermore, fan and jet noise turned out to be the dominant engine noise components, as found in [81]. Finally, also the approach noise level was expected to be the highest, followed by lateral noise and flyover noise. Hence, the code is verified. The code is validated by comparing the maximum approach noise levels to the certification noise levels of reference aircraft [82][31]. The maximum noise levels calculated stay within certification noise levels found by the ICAO. Hence, the code is validated.

8.2.8 Compliance with Requirements

As becomes clear from Table 70, only the approach noise limit is exceeded. This would imply that the aircraft would not fall into the ICAO stage-5 noise level category. However, as stated in Section 8.2.6, the applied empirical methods do not include any noise suppression concepts, which are nowadays current industry stan-

[31] https://www.easa.europa.eu/domains/environment/easa-certification-noise-levels

dards. Therefore, the noise levels obtained have a great potential of improvement by the use of such concepts. The resulting cumulative noise footprint shows only $1dB$, or a 0.4%, difference w.r.t. the CRJ700. Thus requirement SRA-STAKE-ENV-02 is not met without the use of noise suppression concepts. Finally, the interior or cabin noise should be addressed. The CRJ700 has an interior noise level of $93dB$ at take-off and a median noise level of 75-85dB during cruise [83]. The interior noise levels of RELIGHT are expected to be comparable to the CRJ700, due to the low difference in cumulative noise footprint, although the actual compliance with requirement SRA-PROD-PERF-11 should become clear from actual testing or a more sophisticated noise model. Concluding, the noise requirements show high potential of compliance with the use of noise suppression concepts which should be analyzed with an even more detailed noise analysis.

8.3 Aircraft Operational Emissions

Evidently, the emissions aircraft produce during operation take up the largest portion of its environmental footprint. Therefore, it is important to have an estimate for both RELIGHT and the reference aircraft, such that comparison can be done. This should influence the main conclusion of this project as environmental sustainability is the main driver. Before the analysis is Section 8.3.2 discussed first the requirement is presented in Section 8.3.1.

8.3.1 Operational Emission Requirements

The stakeholder requirement for RELIGHT's operational emissions is found in Table 71

Table 71: Requirements related to emissions

Requirement Identifier	Requirement	Compliance
SRA-STAKE-ENV-01.1	The operation of the aircraft shall result in an emissions reduction of at least 25% with respect to the reference aircraft, the Bombardier CRJ700 .	✓

8.3.2 Operational Emissions Analysis

To estimate what the emissions of the aircraft are during operation, pollutants with large impact on the environment are evaluated. These are, with respect to global warming, undoubtedly carbon-dioxide (CO_2), water (H_2O) and nitrogen oxides (NO_x). As each of these particles have a different impact on global warming, they are represented by the Global Warming Potential (GWP). This factor depends on the amount of particles, specific chemical properties and its light-absorption. Also, GWP is quantified to the emission of $1kg$ CO_2, to enhance relative comparison. Moreover, as shown in Figure 69, GWP varies with altitude. In the figure a time span of 100 years is taken, i.e. the impact of the pollutants relative to what $1kg$ CO_2 has over 100 years [84].

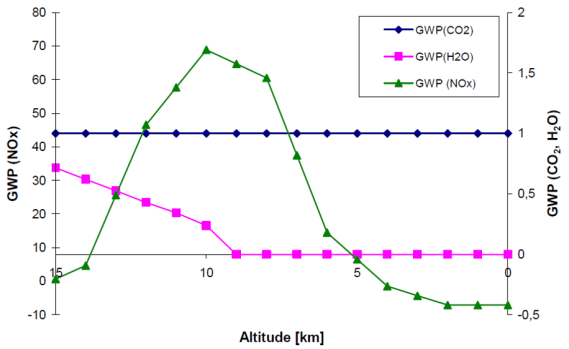

Figure 69: GWP values per kg of pollutant varying with altitude, on a 100-year scale

As can be seen in the figure, NO_x has little impact at low altitude, but increases massively near $10km$. Its impact is so large due to its interaction with complex production and destruction rates of Ozone (O_3) and CH_4. This production or destruction has different impacts on global warming per altitude [84]. Then, the emission of water vapour is negligibly small below 10 km. Then, as altitude increases, water vapour is trapped in the atmosphere and has direct radiative impact [85]. Therefore, it would be advantageous to fly below $10km$. However, the engine used is most efficient at $10km$, and therefore this altitude is still chosen, as long as the emissions with respect to kerosene can be reduced by at least 25%.

Most certainly, aircraft emit a number of other pollutants as well. These include methane (CH_4), dinitrogen oxide (N_2O), unburned Hydrocarbons ($UHC's$), Black Carbon (C) and Carbon monoxide (CO). Even though the GWP of for instance Black Carbon can be as high as 680 [86], $1kg$ of kerosene combustion only emits 0.7 grams [20]. Therefore, when converted to kg of CO_2-equivalent, its score is more than a factor 100 lower than CO_2. This trend is also true for the other minor pollutants.

To relate the emissions of kerosene (Jet-A1) to hydrogen, and thereby the reference aircraft CRJ700 to RELIGHT, a few steps are taken. Firstly, the mass of pollutants emitted per kg of fuel is taken, which is called the Emission Index (EI). These masses are summarized in Table 72 [20].

Table 72: Emission Indices for pollutants from kerosene and hydrogen combustion

Pollutant	**EI Jet-A1 [-]**	**EI H2 [-]**
CO2	3.16	0
H20	1.24	1
NOx	0.02311	6.85e-7

These differences in emissions are the result of the very different combustion reactions with air [87]:

$$2C_{12}H_{26}(l) + 37\{O_2(g) + 3.76N_2(g)\} \rightarrow 24CO_2(g) + 26H_2O + 139.12N_2(g) \tag{145}$$

$$2H_2(g) + \{O_2(g) + 3.76N_2(g)\} \rightarrow 2H_2O + 3.76N_2 \tag{146}$$

The above equations are the theoretical ideal equations, called stoichiometric. In reality, kerosene does not consist of only dodecane, but other hydrocarbons with slightly different compositions as well. Consequently these reactions produce side products, such as NO_x and soot, depending on the fuel-to-air ratio. The fuel-to-air ratio denotes the fuel and air amounts in the combustion chamber, and (f/a) is usually expressed as the equivalence ratio ϕ, where f/a is divided by the stoichiometric f/a. For kerosene combustion ϕ is usually around 0.5, meaning there is more air than fuel: a 'lean' mixture. Around this ϕ the least pollutants are emitted. The pollutant masses for Jet-A1 fuel in Table 72 are the minimum for what is emitted in kerosene combustion [20]. Obtaining the hydrogen combustion pollutant masses is a bit more extensive. First of all, the combustion of hydrogen produces no CO_2, as can be seen in Equation 146. However water vapour is emitted and under non-ideal conditions NO_x is emitted as well. The emission of NO_x depends on the combustion chamber characteristics as described by the empirical Equation 147 [88]. Where:

$$EI_{NO_x} = A'(P_3)^{0.594} exp(T_3/350)(f/a)^{1.6876}(100P_{drop})^{-0.56} \tag{147}$$

- A' is the correlation constant with Jet-A1 combustors (14 for advanced lean-direct-injection technology)
- P_3 is the fuel injector inlet pressure
- T_3 is the fuel injector inlet temperature
- P_{drop} is the percentual fuel injector air flow pressure drop

Now that the emission indices are obtained, Equation 148 is used to obtain a measure of the CF. As such, RELIGHT can be compared with the CRJ700 in terms of operational emissions.

$$CF\left[\frac{kg\ CO_2 - eq}{pax \cdot km}\right] = \sum_p \frac{EI_p \cdot F \cdot GWP_p}{N_{pax} \cdot R_{design}} \tag{148}$$

Table 73: Results of CF analysis for A/C operations

	CF	**Units**
RELIGHT	0.01956	kg CO_2-eq/(pax km)
Bombardier CRJ700	0.08769	kg CO_2-eq/(pax km)

Note how, in Equation 148 the mass equivalent CO_2 is divided by the amount of passenger kilometers, to account for a difference in these numbers.The subscript p is used for the different pollutants. EI is the Environmental Index and F the fuel use. The results are summarized in Table 73.
As such, for the design range of $2000km$ and 75 passengers, compared to the CRJ700 with $2593km$ design range and 78 passengers, RELIGHT has a 77.69% lower Carbon Footprint.

8.3.3 Verification and Validation

For analysis of the operational emissions, the input parameters that were needed regard mainly the the flying altitude and the fuel used. So, if one alters one of these parameters, it is expected that the emissions change accordingly. For instance, when the fuel use is doubled, the Carbon Footprint is twice as high. Also when the cruise altitude is changed to for instance $5km$, almost no pollutants should be emitted according to Figure 69. As expected, the CF is only 7.2E-7. Therefore this part of the code is verified. Also, the emissions are related to passenger kilometers, which allows for relative comparison between different mission characteristics and hence different aircraft. For instance, an aircraft with the same fuel use but less passengers should have a lower CF. Indeed, 50% reduction in passengers results in a 50% larger CF. Therefore this is also verified. Lastly, the emission indices are well-established in literature, and hence no verification for those is needed.

8.3.4 Compliance with Requirements

Evidently, as Table 73 shows, the CF of RELIGHT is substantially lower than the reference aircraft, the Bombardier CRJ700. The requirement (SRA-STAKE-ENV-01.1) was to at least obtain a reduction of 25%. This is fulfilled most certainly with a reduction of about 78%, even though only emissions from flying the aircraft are included. When emissions from the production of fuel are included as well, the operational carbon footprint would change depending on hydrogen production. If hydrogen is assumed to be produced from green energy and H_2O, this would add to the overall performance compared to kerosene refinery.

8.4 Cost Performance

The aviation sector has shown significant growth, and appears to continue to do so. Over the next two decades approximately 450 new regional aircraft are to be shipped out to airlines and other purchasers[32]. According to the reference this would consist of approximately 360 billion dollars, averaging at 18 billion a year. Especially economic development in many countries and increasing wealth are driving the growth in the market. This growth is currently strongest in regions historically lagging behind in the aviation industry, such as Africa and South America. However there is a clear relationship between economic wealth and passenger-kilometers[33]. As already mentioned in Section 2, RELIGHT especially aims to target these regions, hoping to establish themselves as a trusted manufacturer. In order to do so the aircraft needs to be attractive economically.
The following section describes the performance of the aircraft with respect to development, manufacturing and operational costs, as well as highlighting the potential for return on investment and the general market situation. The section concludes by tying the cost performance back to the requirements that were set to ensure competitiveness and how they have been achieved.

8.4.1 Cost Breakdown Structure

The following section shows an estimated breakdown of both the development and manufacturing cost, based on maximum take-off weight and statistical analysis of the industry. A quintessential step in the design process of an aircraft is the estimation and prediction of the total cost of the development. A preliminary estimate on the total cost of the aircraft program -that is to say without knowing the exact masses of each subsystem or part of the aircraft- will be given in Section 8.4.1. Estimating both the development cost and the manufacturing cost is important because a low development cost will result in higher profits. Since RELIGHT takes a novel approach to the propulsion system configuration, development costs can be a difficult to predict. Estimating the expected manufacturing costs is also critical as it allows to put a more realistic pricetag on the aircraft, allowing for changes to be made in time to ensure that the aircraft will be competitive with comparable designs. Ideally this price would be reduced as much as possible as this would translate into a lower purchasing price, higher demand and ultimately higher profits and quicker return on investment.

Aircraft Program Development Cost Estimate The total cost of the development of an aircraft program can be estimated based on the mass fractions of parts of the aircraft relative to the OEW. The estimated mass fractions are shown in Figure 70 [89][34]. With the use of historical data and existing aircraft [90] [1], the mass fractions were established. Previously, the OEW of the Hybrid Hydrogen Concept was estimated to be equal to $21370kg$ [4].

[32] https://www.cleansky.eu/regional-aircraft
[33] https://www.fzt.haw-hamburg.de/pers/Scholz/dglr/hh/text_2001_12_06_Cryoplane.pdf
[34] https://core.ac.uk/download/pdf/4384841.pdf

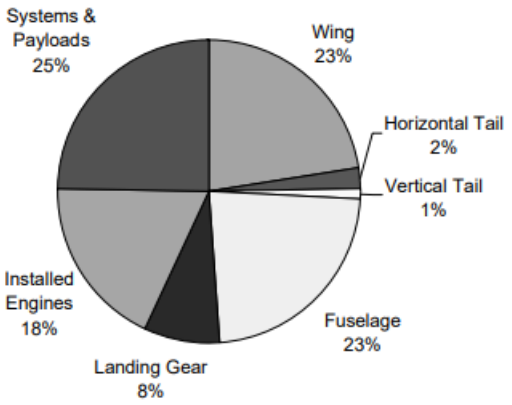

Figure 70: Estimated mass fractions based on OEW

Table 74: Development cost of individual parts of the aircraft

Part	**Mass**	**Cost** [US$ / kg]	**Total Estimated Cost** [US$]
Wing	4915.0	39090.2	192,132,220
Empennage	641.1	114984.4	73,716,493
Fuselage	4915.1	70753.0	347,758,127
Landing Gear	1709.6	5509.4	9,418,796
Installed Engines	3846.6	19160.4	73,716,493
Systems	1068.5	75634.0	80,814,982
Payloads	4274.0	23728.4	50,707,532
Total	21370	-	878,958,042

The development cost of each aircraft part, in American Dollars per pound, has been obtained from the same source and are, after a unit conversion has been applied, tabulated in Table 74. Note that in Figure 70 the payload and systems have been combined in one group; it is assumed that 20% and 5% are taken as mass fraction for payload and systems respectively. The total estimated development cost based on this estimation is 878,958,042 US$.

In order to check whether the obtained cost estimate is reasonable, it is validated against already developed aircraft. The total cost of the development of the Bombardier Challenger 600 series was roughly 1.1b US$ at the time [35]. Bombardier developed, based on the challenger series design, the CRJ100 and 200 series. In turn, the CRJ700 reference aircraft has been developed based on the CRJ200, costing an additional 450 million US$. When comparing the preliminary estimate of the Hybrid Hydrogen Concept development cost with these values, it is concluded that the slightly less than nine hundred million dollar aircraft program is estimated within reason.

Aircraft Manufacturing Cost Estimate An estimation of the expected manufacturing cost is made by determining the cost per kg for each separate subsystem or part of the aircraft from literature [89], identifying the masses of each aircraft part based on their mass fraction with respect to OEW, as has been done in Section 7.2, and lastly the cost per part is obtained by multiplication of the former two.

Table 75: Manufacturing Cost Estimation

Part	**Cost per kg** [US$ / kg]	**Mass** [kg]	**Part Cost** [US$]
Wing	1984.2	4915.0	9,752,355
Empennage	5139.0	641.1	3,294,600
Fuselage	2131.9	4915.1	10,478,363
Landing Gear	487.2	1709.6	832,955
Installed Engines	824.5	3846.6	3,171,635
Systems	996.5	1068.5	1,064,750
Payload	1243.4	4274	5,314,326
Final Assembly	143,3	21370	3,062,334
Total	-	21370	36,971,317

In Table 75 the total estimated manufacturing cost of RELIGHT is given, which approximately equals 37 million US$. Furthermore, this estimate is in compliance with requirement SRA-PROD-PERF-19 [3][36], and therefore is suited as a preliminary estimate. With increased production numbers the cost of manufacture will further decrease, this can be modeled by applying a learning rate model, which might be considered for future analysis.

[35] https://en.wikipedia.org/wiki/Bombardier_Challenger_600_series

[36] Requirement SRA-PROD-PERF-19: The unit-production costs shall not surpass 44.4 million US$

8.4.2 Return on Investment

In order to assess the amount of time it would take for an airline to make the return on investment for an aircraft like this it is necessary to evaluate several parameters to be able to compare them to relevant competitors. This section will first evaluate operational cost, specifically fuel cost and fuel consumption, Block Time and related parameters and finally assess how many flights an aircraft would need to make to generate sufficient profit for a return on investment.

Operational Costs The main downside of using hydrogen, in terms of operational costs, correspond to the large tank volume and the increase in wetted area and therefore drag. Flying hydrogen can increase the operational empty weight of an aircraft by 8% [91] however in this current design configuration no increase in weight has been realized. Therefore the main difference in operational costs result from the difference in fuel burnt, as well as the range and the amount of passengers delivered.

Block Time The block time is total trip time including taxiing, boarding and refueling. It can be described by the following equation:

$$E_B = \frac{R}{V_{cruise}} + \Delta t \quad (149)$$

Table 76: Blocking time for a field operations time of one hour

Parameter	RELIGHT	CRJ700
Design Range [km]	2000	2553
Cruise Speed [km/h]	797	829
Block Time [h]	3.51	4.1

Where R is the range and Δt the time required for field operations. A functional hydrogen infrastructure would not increase refueling time in comparison to kerosene based aircraft [27]. Therefore the difference in blocking time to the reference aircraft CRJ700 only arise out of differences in range and cruise speed. Setting the time required for field operations to 60 minutes one can calculate the following values for both aircraft. This means that the CRJ700 series has a 13% higher transport productivity. The transport productivity is defined as:

$$P_h = \frac{W_{payload} R}{E_B} \quad (150)$$

Table 77: Transport Productivity

Parameter	RELIGHT	CRJ700
Range [km]	2000	2553
Block Time [h]	3.51	4.1
Transport Productivity [kgkm/h]	4554159	5139624

Fuel Burn Since RELIGHT utilizes a different propulsion system, fuel burn and cost need to be taken into account when assessing the operational costs of the aircraft. The design uses hydrogen as a main fuel source and burns $0.1 kg/s$ at full take-off throttle. This is equivalent to $360 kg$ per hour. Taking the General Electric CF34 turbofan engine as a reference engine for the CRJ700, one finds a fuel burn of $0.361 kg/s$ or $1300 kg/h$[37].

The price of hydrogen is approximately 1.70$ per kilogram whilst the price of kerosene is about 0.56$ per kilogram [91][38]. This means that the operating costs for the design are 612$ per hour whilst the CRJ700 series requires fuel worth 728$ per hour. Therefore the price to fly with hydrogen in the current configuration is only 84% of what it would cost to fly the CRJ700 series. The hydrogen design therefore readily makes up for the reduced transport productivity.

Return on Investment Currently the amount of fully hydrogen powered aircraft in operation is very small. Therefore RELIGHT will have a unique value proposition with respect to the competition. In order to meet global demand and keep the aviation industry growing in the future, solutions need to be found that on one hand offer service to the demand for greener and more environmentally sustainable air travel and on the other hand detach the industries dependence on fossil fuels, that will likely begin to run out within this century. Hydrogen produces zero emissions, when generated with green electricity sources and water is readily available everywhere. Currently only small hydrogen powered passenger aircraft are being developed, therefore there

[37] https://link.springer.com/content/pdf/bbm%3A978-1-4614-3532-7%2F1.pdf
[38] https://www.fzt.haw-hamburg.de/pers/Scholz/GF/GF_Paper_DLRK_09-09-08.pdf

is no real competitor using this type of propulsion system[39] many other projects remain in the project analysis and feasibility stages. It seems that the lack of infrastructure is restraining manufacturers and designers from moving forward with such projects. Should airports adopt hydrogen infrastructure, RELIGHT is going to be ready to service it, being the first on the market.

Fuel costs amount to roughly 8% of total operating cost. Decreasing the fuel cost by 16% therefore decreases the total operating cost of RELIGHT by about 1.3%. This could either directly translate into the ticket price, giving the airline a competitive edge, or be used to pay-off the cost of investment. Assuming a block hour cost of roughly 1500 US$ for the CRJ700 and 1481 US$ for RELIGHT, a ticket price of 100 US$ per passenger per flight, at 3 flights per day (12.1 and 10.5 block hours respectively) results in a daily profit of 18150 US$ for a CRJ700 and 15551 US$ for RELIGHT. The performance is summarized in Figure 71. This equates to roughly 6.6 and 5.7 million US$ profit a year. Taking a unit cost of 37 million US$, but a sales cost of 41 million US$ means the return on investment of RELIGHT can be achieved in roughly 7 years assuming continuous utilization at the cost per block hour and the ticket price assumed. Due to the increased unit cost of the CRJ700 at 41 million US$, the reference aircraft itself would only take roughly 3 months less to pay off, under the same circumstances. A sales cost of 41 million would also ensure a return on investment for the project development cost after 220 deliveries.

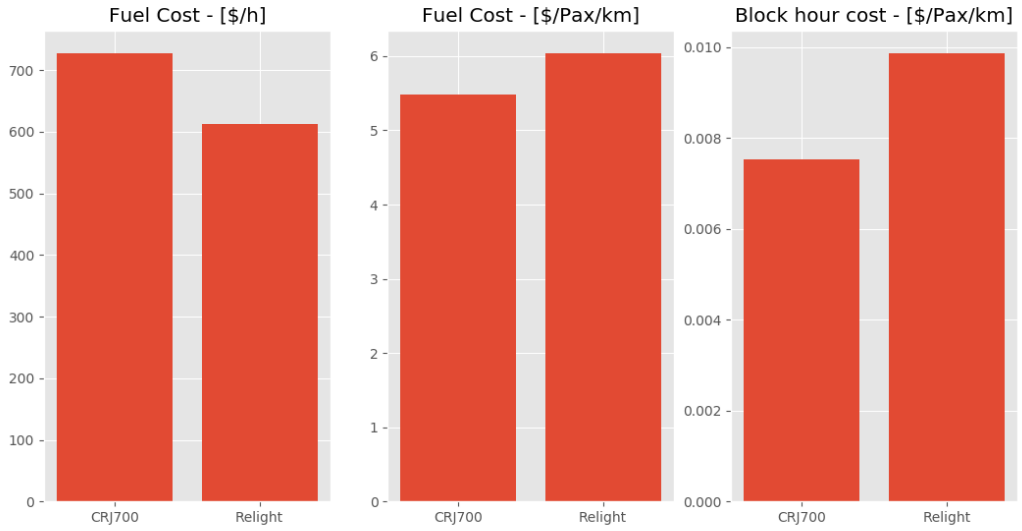

Figure 71: Fuel cost, fuel cost per passenger kilometer and block hour cost per passenger kilometer compared between Bombardier CRJ700 series and Relight aircraft design

Considering the fact that the cost of fossil fuels will likely increase this century, due to decreasing supply, the full hydrogen propulsion design might end up significantly more economical.

[39] https://www.theverge.com/2019/8/14/20804257/zeroavia-hydrogen-airplane-electric-flight

8.4.3 Compliance with Requirements

Table 78: Cost requirements

Requirement Identifier	Requirement	Compliance
SRA-STAKE-AL-05	Operation & Maintenance costs of the aircraft shall not increase more than 25% with respect to the reference aircraft, the Bombardier CRJ700.	✓
SRA-STAKE-AL-07	Purchase costs of the aircraft shall not increase by more than 25% with respect to the reference aircraft, the Bombardier CRJ700 series.	✓
SRA-STAKE-AL-03	The aircraft shall have similar flight crew cost with respect to the reference aircraft, the Bombardier CRJ700 series.	✓/✗
SRA-STAKE-AL-04	The aircraft shall have a similar cabin crew cost with respect to the reference aircraft, the Bombardier CRJ700 series.	✓/✗
SRA-STAKE-AL-06	Airport taxes per passenger shall be similar for the aircraft with respect to the reference aircraft, the Bombardier CRJ700 series.	✓/✗
SRA-PROD-PERF-19	The unit-production costs shall not surpass 44.4 million US$	✓

Table 78 gives an overview over the requirements generated in [3]. These were based on direct comparison with the reference aircraft. RELIGHT retained many conventional features in its configuration. This was done intentionally to ensure that no extensive increases in cost would surface for maintenance, flight control and crew demand. Despite the hydrogen propulsion system the engines remain comparable in their construction, to other high bypass ratio turbofans. One of the main challenges is the inspection and maintenance of the aft fuel tank. Due to the cryogenic nature of the fuel additional stresses maybe introduced due to the temperature gradients. The liners for permeation prevention may need to be exchanged periodically and this will cause and increase in maintenance costs. With respect to the operational aspect of the SRA-STAKE-AL-05 stakeholder requirement it has been shown in the previous section the requirement is met. The unit production cost requirement SRA-PROD-PERF-19, aiming to keep the aircraft competitive economically is also expected to be fulfilled as can be seen by the cost breakdown structure in Section 8.4.

8.5 Aircraft Sustainability

The foregoing sections about noise, emissions and cost contain, respectively, quantification of part of the social, environmental and economical sustainability. To add to this and obtain a stronger baseline for sustainability, two other footprints have been analyzed as well: the Water Footprint (WF) and the Air Pollution Footprint (APF).

8.5.1 Requirements

Table 79 shows the requirements that remain for sustainability.

Table 79: Requirements related to emissions

Requirement Identifier	Requirement	Compliance
SRA-STAKE-ENV-01.0	The aircraft program shall have a minimum of 25% percent lower environmental footprint w.r.t. the Bombardier CRJ700 series.	✓
SRA-STAKE-EOL-01	Serviceable subsystems shall be able to be re-used in operational airframes.	✓/✗
SRA-STAKE-EOL-02	Materials of the airframe shall be recyclable.	✓/✗
SRA-STAKE-ENV-01.2	The disposal of the aircraft after service life shall have a 25% reduction in environmental footprint with respect to the disposal of the reference aircraft, the Bombardier CRJ700.	✗

8.5.2 Footprint Analysis

The two additional footprints are the Water Footprint and the Air Pollution Footprint (Section 8.5.2 and Table 8.5.2. After that, in Section 8.5.3, other aspects of sustainability are touched upon even if they are not quantified in this project.

Water Footprint The WF mainly represents the amount of H_2O used in fuel production. Evidently, hydrogen is to be produced from H_2O and green energy, which has impact on fresh water supplies. However, kerosene production also uses H_2O which allows for comparison. Even though water is widely available, it is important to analyze.
The production of 1 liter of Jet-A1 fuel requires about 0.09 liters water [22], and is thereby one of the least water consuming fossil fuels. In contrast, the production of 1 liter hydrogen, assuming no losses, requires about 0.0012 liters of water per liter of gaseous H_2, which translates to 0.08866 liters of water per liter of LH_2 [92]. Relating this to passenger kilometers, such that the CRJ700 and RELIGHT can be compared, RELIGHT needs 31.3% more H_2O as feedstock for fuel production. The results can be seen in Table 80.

Table 80: Results from the water footprint analysis

	WF [m^3 H_2O / (pax km)]
RELIGHT	5.91e-7
Bombardier CRJ700	4.50e-7

Air Pollution Footprint Air pollution is expressed as the amount of pollutants that have impact on human health, and hence is part of the social footprint of RELIGHT. The main pollutant emitted from kerosene combustion that indirect effects on human health is NO_x. NO_x influences the formation of O_3, which has effects on human health. Kerosene combustion also results in Particulate Matter ($PM_{2.5}$) formation, which are very tiny particles such as soot. These are very damaging to human health and emission of it should be avoided [93][40]. Hence, it is analyzed in what amount these emissions result from hydrogen as well. Hydrogen combustion produces no particulate matter directly as it is a zero carbon fuel [94]. However, NO_x emission has influence on the formation of $PM_{2.5}$ formation [95], which is not included in the analysis. The results are summarized in Table 81.

Table 81: Results from the air pollution footprint analysis

	APF [$kgCO_2 - eq/(paxkm)$]
RELIGHT	0.0277
Bombardier CRJ700	0.0894

8.5.3 Other Sustainability Aspects

Since not all requirements have been touched upon concerning sustainability, they are discussed in this section. These requirements are SRA-STAKE-EOL-01, SRA-STAKE-EOL-02 and SRA-STAKE-ENV-01.2.

Production The overall design follows that of a conventional aircraft closely, meaning the production methods and techniques used are similar. This means that the emissions during production are similar in magnitude. To reduce them the use of recycled material. The higher the complexity of a part the higher the impact on emissions as more time and resources need to be spent, thus increasing waste generated. For example, the winding of the hydrogen tank, a small defect can lead to the whole part needing replacement.

End-of-Life The end-of-life handling of the aircraft still needs to be incorporated into the design. The waste that remains after the aircraft has been retired should be as limited as possible. The structure of the aircraft is made of metal. This allow for great recycling potential, as metals can be sorted, purified, melted and reshaped again with no loss of performance. However, the hydrogen tanks are of Carbon Fiber Reinforced Polymers (CFRP), which are almost non-recyclable. Also, seating materials and plastics are not very applicable for recycling.
Furthermore, as the different aircraft from the model use the same parts, some parts can be reused after they are refurbished from the retired aircraft. That way spare part cost can be reduced also reducing the resourced needed for new parts being produced. This can be done for the flight instruments, fuel pumps, hydraulic system and auxiliary fuel tanks after sufficient tests are performed to ensure the safety and reliability of the parts. Since recycling of the hydrogen tanks is difficult due to the composite used, they should be made applicable for reuse in new aircraft.

Recommended Analyses Firstly, a more extensive analysis on production and manufacturing should be done in terms of emissions. Also, in terms of recyclability, mainly because of the tank materials, RELIGHT will score a little worse than the reference, but more extensive analysis is needed to quantify this. Also

[40] https://www.epa.gov/pm-pollution/health-and-environmental-effects-particulate-matter-pm

quantification is needed on reuse and refurbishment of subsystems. It is also recommended to research how the emission of NO_x from hydrogen combustion has an effect on $PM_{2.5}$ formation, even though not much NO_x is emitted.

8.5.4 Compliance with Requirements and Overall Sustainability

The aforegoing sections have, starting in Section 8.2, made estimations for footprints of environmental, economical and social sustainability. Compliance is obtained with the following requirements: SRA-STAKE-ENV-01.0, SRA-STAKE-ENV-01.1, SRA-STAKE-AL-05, SRA-STAKE-AL-07, SRA-PROD-PERF-11. Not all aspects, such as recyclability, could be quantified and therefore the following requirements are not met in this project: SRA-STAKE-ENV-01.2, SRA-STAKE-ENV-02, SRA-PROD-PERF-10, SRA-STAKE-EOL-01, SRA-STAKE-EOL-02. The result for sustainability is presented in Figure 72. For all categories from left to right holds; the lower the score, the better (except for the profit per year). All footprints are related to passenger kilometers, such that a fair comparison with reference aircraft is possible. Note how a division between the three pillars of sustainability is made. Also, note how the scores of RELIGHT for each footprint-/category are compared on a 0-1 scale with the reference aircraft, the Bombardier CRJ700. Footprints that do not meet the requirements, are highlighted in red.

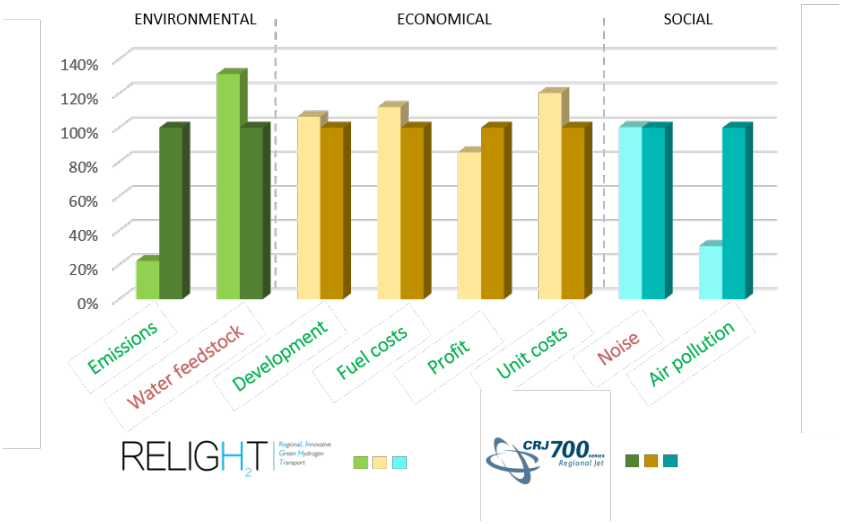

Figure 72: Sustainability comparison between RELIGHT and the Bombardier CRJ700

9 Future Aircraft Development

The design activities performed throughout the DSE merely cover the conceptual phase of the complete aircraft design process. This chapter describes all the steps and processes that will have to be done in order to actually get RELIGHT moving passengers through the skies. These processes can be split in three main categories: design completion in Section 9.1, aircraft testing in Section 9.2 and series production in Section 9.3. Once the aircraft is tested and deemed airworthy, it can enter series production and be shipped to customers. A risk analysis and a mitigation plan for the entire post-DSE process are provided in Section 9.5.

9.1 Continuation of Aircraft Development

RELIGHT is expected to enter service in 2036 at the latest. This is an extremely conservative estimate, and the aircraft is likely to be ready much sooner. Since the aircraft is not based on any pre-existing airframe and brand new hydrogen-based subsystem have to be designed, the development cycle is expected to last about 10 years. In the first three years of design the main aircraft aerodynamic, structural, control and system interaction analysis will be defined in order to meet all the performance requirements. In the following five years the details of the aircraft will be optimized to the highest possible degree. All structural elements such as ribs, rivets, cutouts etc. will be sized with accuracy and systems such as electronics, hydraulic actuators, landing gears and HLDs will be designed thoroughly. Before production can finally start, the manufacturing and production plan will have to be revised to fit all the needs of the finalized design. Once this is done and the aircraft is ready for production, a final assessment of the cost and emissions will be made. The timeline of this complete design process is detailed in Figure 9.4.

9.2 Aircraft Testing Procedures

After the design is finalized, a small number of prototypes will have to be built and tested to ensure airworthiness. The test program is based on Airbus' testing program [96][41]. The first series of tests includes all on-the-ground tests. These include testing the resistance of the aircraft structures and the effectiveness of control surfaces at maximum load conditions, ensuring sufficient fatigue performance by putting the aircraft through an amount of fatigue cycles higher than what it will go through in its operational lifetime. It is also crucial to test extensively for all risks related to the implementation of hydrogen. Insulation tests and fatigue cycling must be done on the tank to make sure it can handle the pressure and temperature stresses. The same goes for the engine feeding system and the hydrogen pumps on the ground. Also, engine ingestion are performed at this stage. Once the worthiness of the airframe has been verified the flight tests can begin. These tests will put the prototype aircraft against the most varied and critical situations it may encounter during its operational lifetime. The aircraft will be tested to operate from/to airports with particular climatic and altitude conditions. After all the tests have been carried out, the results are reviewed critically to see if the aircraft is failing to meet any requirements. Once the aircraft passes all scheduled tests, certifications are issued and series production can begin. The testing process, including construction of the prototype(s), is expected to take about 5 years, and its timeline is specified in Figure 9.4. The testing procedures taking so long are explained by having to integrate an entirely new technology in the commercial aviation sector, namely hydrogen.

[41] https://www.airbus.com/aircraft/how-is-an-aircraft-built/test-programme-and-certification.html

9.3 Manufacturing, Assembly and Integration (MAI) Plan

Table 82: Production requirements

Requirement Identifier	Requirement	Compliance
SRA-STAKE-MNF-02	The manufacturing process shall follow the lean manufacturing methodology.	✓
SRA-STAKE-MNF-04	The manufacturing process shall not require the creation of components with a TRL of 4 or below.	✓
SRA-STAKE-MNF-01	The emissions from the manufacturing process shall be at least 25% lower than those of the Bombardier CRJ700 series.	✓/✗
SRA-STAKE-ENV-01.3	The production of the aircraft shall have a 25% smaller environmental footprint with respect to the reference aircraft, the Bombardier CRJ700.	✓
SRA-STAKE-MNF-03	The throughput time for the production of a single unit shall not exceed six months.	✓

The production plan is displayed in Figure 73. The production plan starts with the manufacturing and procurement of parts. As is standard in the industry, individual workshops produce all single parts and components which will then be joined along an assembly line. Separate sub-assembly lines for subcomponents will assemble components from the workshop and then join the main assembly line where these subcomponents will be attached to the airframe. Since the different sub-assemblies work on independent parts they can be run in parallel to save time. Orders for parts from external suppliers, such as engines and the avionics suite, will be made as soon as series production begins. The final step in the main assembly is to paint the aircraft and this leads integration the final phase of the aircraft assembly plan. During integration the systems displayed in Figure 73 are connected and checks are performed to ensure aircraft functionality before it is sent to testing in case of a prototype or delivered to the customer in case series production has started. According to requirement SRA-STAKE-MNF-03, the total production time for a single unit (once production has been set up and started) will be at most six months and the time frame of each action is shown in Figure 9.4 The production process of RELIGHT will follow the principles of lean production as much as possible. This means that waste of energy and resources is reduced to a minimum by adopting several measures. Some of these measures are making sure that the part production workshops are as physically close as possible to the assembly chain, Just-in-Time (JIT) delivery to minimize storage costs and load leveling to avoid bottlenecks in the assembly process.

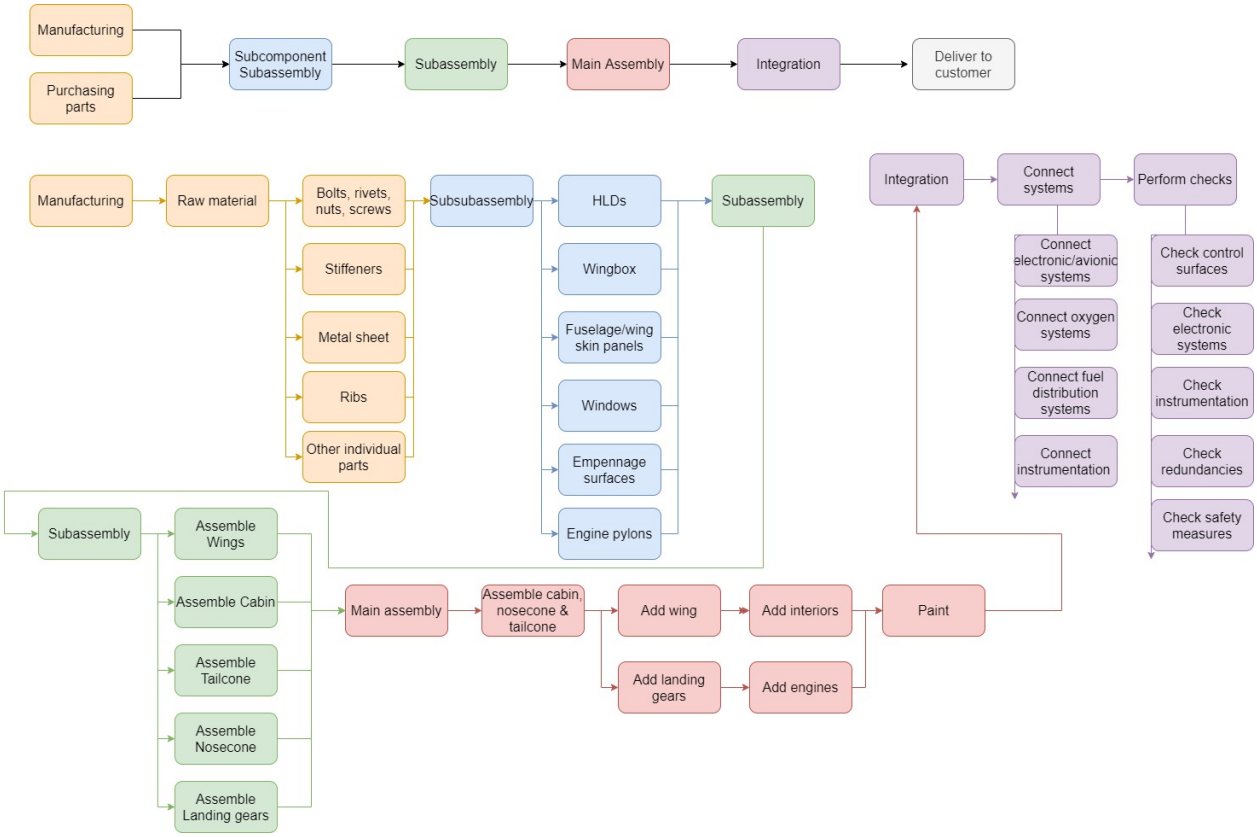

Figure 73: Overview of manufacturing/production/integration process

9.4 Overview of Post-DSE Activities

An overview of all the activities mentioned in Section 9 is shown in Figure 74.

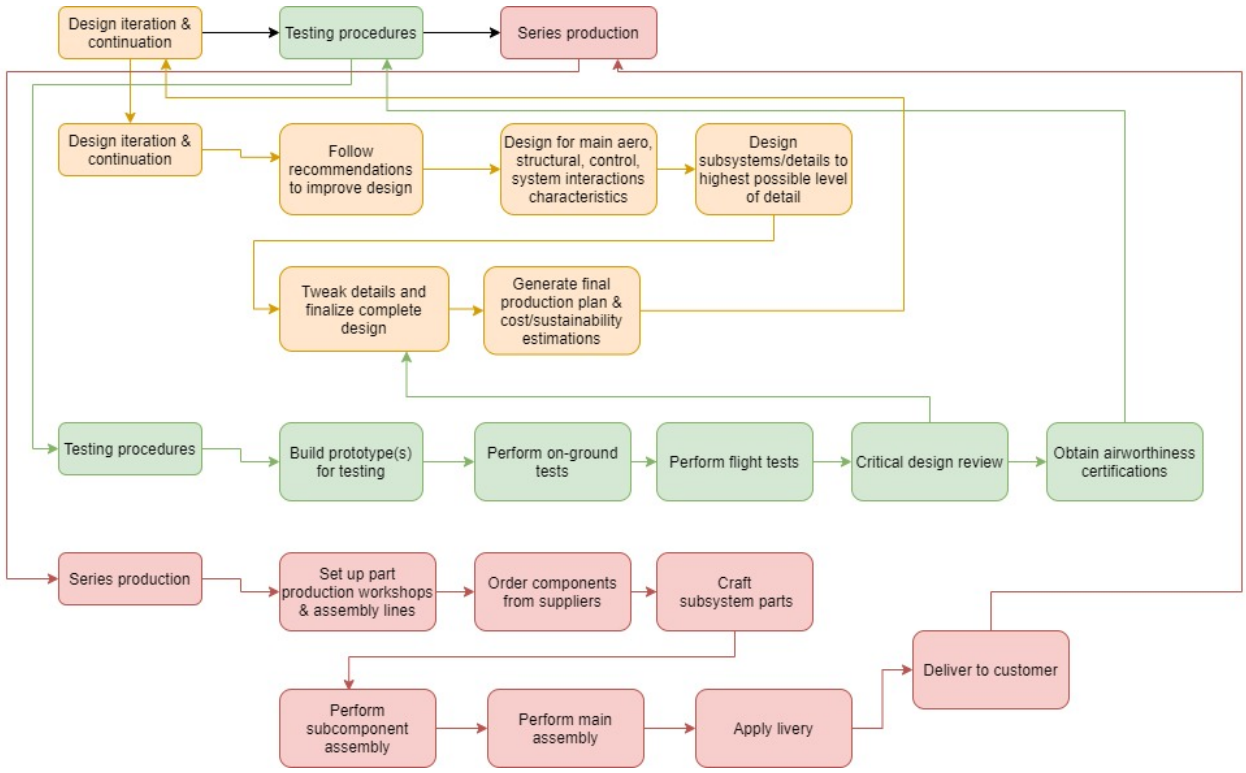

Figure 74: High-level flow chart of post-DSE activities

ID	Task Name	Duration	Start	Finish
1	**Design**	**2644 days**	**Mon 13-7-20**	**Thu 29-8-30**
2	Increase amount of human resources	5 mons	Mon 13-7-20	Fri 27-11-20
3	Design iteration and continuation	5 mons	Fri 17-7-20	Thu 3-12-20
4	Critical design review 1	1 mon	Fri 4-12-20	Thu 31-12-20
5	**Further investigation**	**800 days**	**Fri 1-1-21**	**Thu 25-1-24**
6	Deepen knowledge of regulatic	40 mons	Fri 1-1-21	Thu 25-1-24
7	Perform further market analys	40 mons	Fri 1-1-21	Thu 25-1-24
8	Investigate aircraft design	40 mons	Fri 1-1-21	Thu 25-1-24
9	Deepen knowledge of hydroge	40 mons	Fri 1-1-21	Thu 25-1-24
10	Follow reccomendations to improve design	2 mons	Fri 18-6-21	Thu 12-8-21
11	Design iteration	6 mons	Fri 13-8-21	Thu 27-1-22
12	Critical design review 2	2 mons	Fri 28-1-22	Thu 24-3-22
13	Propose aircraft to customers	24 mons	Fri 25-3-22	Thu 25-1-24
14	Design iteration	10 mons	Fri 25-3-22	Thu 29-12-22
15	**Detailed design**	**1200 days**	**Fri 30-12-22**	**Thu 5-8-27**
16	Design aerodynamics	60 mons	Fri 30-12-22	Thu 5-8-27
17	Design structural components	60 mons	Fri 30-12-22	Thu 5-8-27
18	Design cabin	60 mons	Fri 30-12-22	Thu 5-8-27
19	Design flight deck avionics suit	60 mons	Fri 30-12-22	Thu 5-8-27
20	Design empennage	60 mons	Fri 30-12-22	Thu 5-8-27
21	design control systems	60 mons	Fri 30-12-22	Thu 5-8-27
22	Design subsystems	60 mons	Fri 30-12-22	Thu 5-8-27
23	**Design propulsion system**	**1200 days**	**Fri 30-12-22**	**Thu 5-8-27**
24	Complete design specificatic	18 mons	Fri 30-12-22	Thu 16-5-24
25	give assignment to manufacturer	0 mons	Thu 16-5-24	Thu 16-5-24
26	Design subsystems of engine	42 mons	Fri 17-5-24	Thu 5-8-27
27	Asses system interactions	60 mons	Fri 30-12-22	Thu 5-8-27
28	**Generate detailed production pl**	**300 days**	**Fri 6-8-27**	**Thu 28-9-28**
29	Generate sequence	15 mons	Fri 6-8-27	Thu 28-9-28
30	Sign contracts with part supplie	9 mons	Fri 1-10-27	Thu 8-6-28
31	Design tooling	9 mons	Fri 6-8-27	Thu 13-4-28
32	Schedule production of parts	3 mons	Fri 14-4-28	Thu 6-7-28
33	Schedule integration of system	3 mons	Fri 7-7-28	Thu 28-9-28
34	Tweak design	8 mons	Fri 29-9-28	Thu 10-5-29
35	Freeze design	0 mons	Thu 10-5-29	Thu 10-5-29
36	**Asses aircraft design**	**340 days**	**Fri 11-5-29**	**Thu 29-8-30**
37	Environmental impact	12 mons	Fri 11-5-29	Thu 11-4-30
38	Production cost	12 mons	Fri 11-5-29	Thu 11-4-30
39	Operation cost	12 mons	Fri 11-5-29	Thu 11-4-30
40	safety	12 mons	Fri 11-5-29	Thu 11-4-30
41	passenger comfort	12 mons	Fri 11-5-29	Thu 11-4-30
42	Airport operation	12 mons	Fri 11-5-29	Thu 11-4-30
43	Critical design review 3	5 mons	Fri 12-4-30	Thu 29-8-30
44	Start selling the aircraft	0 mons	Sat 1-1-28	Sat 1-1-28
45				
46	**Testing Procedures**	**1370 days**	**Fri 18-1-30**	**Thu 19-4-35**
85				
86	**Production**	**6 mons**	**Wed 17-6-20**	**Tue 1-12-20**

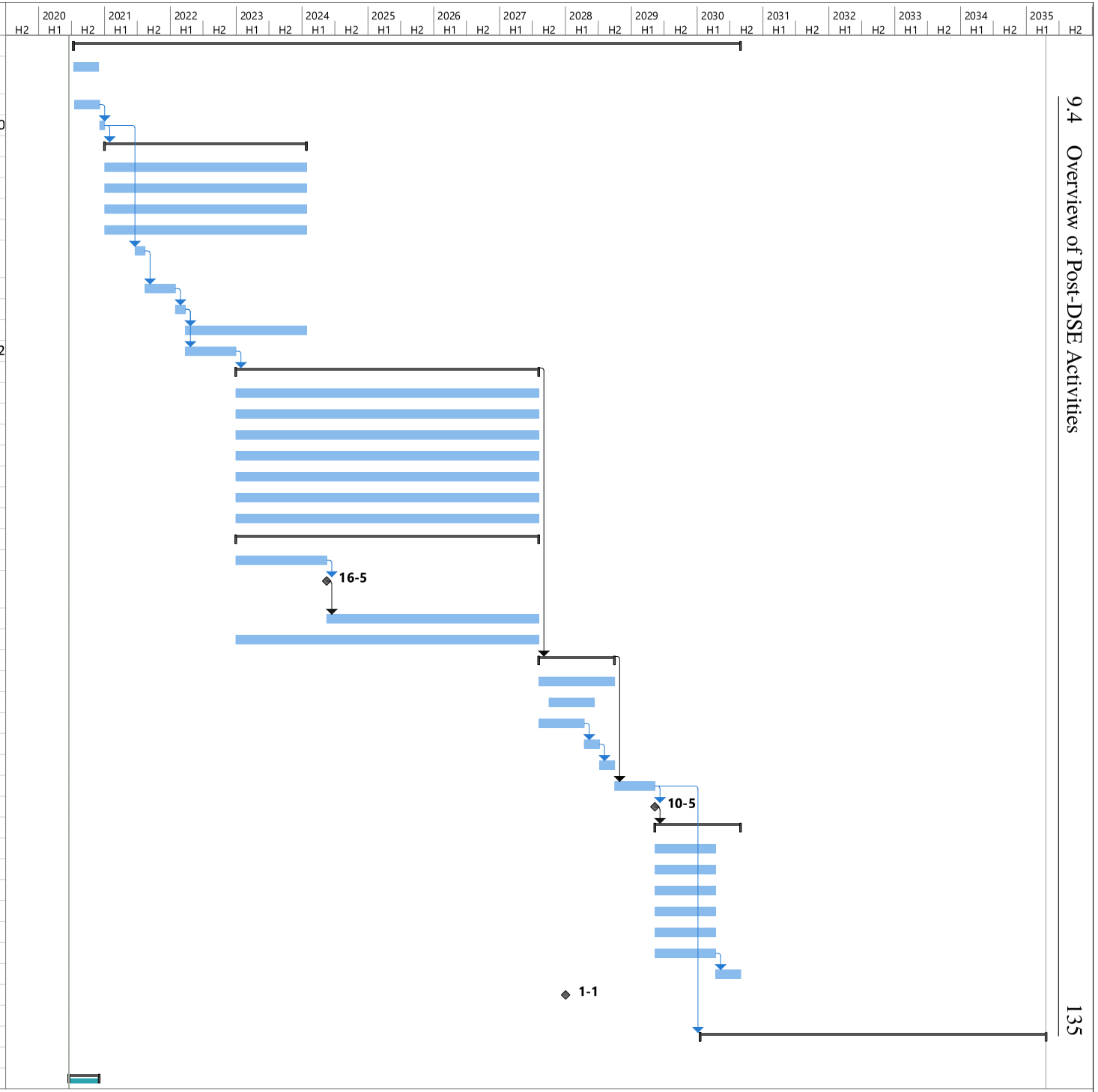

ID	Task Name	Duration	Start	Finish
1	**Design**	**2644 days**	**Mon 13-7-20**	**Thu 29-8-30**
45				
46	**Testing Procedures**	**1370 days**	**Fri 18-1-30**	**Thu 19-4-35**
47	Determine testing and certification program	5 mons	Fri 18-1-30	Thu 6-6-30
48	Perform flight simulator handling tests	9 mons	Fri 18-1-30	Thu 26-9-30
49	**Perform static testing**	**320 days**	**Fri 7-6-30**	**Thu 28-8-31**
50	Build static prototypes	10 mons	Fri 7-6-30	Thu 13-3-31
51	Perform component testing	16 mons	Fri 7-6-30	Thu 28-8-31
52	Perform subsystem testing	16 mons	Fri 7-6-30	Thu 28-8-31
53	perform system testing	16 mons	Fri 7-6-30	Thu 28-8-31
54	**perform static load tests**	**311 days**	**Fri 7-6-30**	**Fri 15-8-31**
55	fuselage	7 mons	Mon 3-2-31	Fri 15-8-31
56	Wing box	12 mons	Fri 7-6-30	Thu 8-5-31
57	Horizontal tail	8 mons	Fri 7-6-30	Thu 16-1-31
58	engine mounting	8 mons	Fri 7-6-30	Thu 16-1-31
59	Wing-fuselage integration	8 mons	Mon 2-9-30	Fri 11-4-31
60	Load floor	4 mons	Fri 7-6-30	Thu 26-9-30
61	gear	8 mons	Mon 2-9-30	Fri 11-4-31
62	fatigue testing of all subsystems and systems	12 mons	Mon 2-9-30	Fri 1-8-31
63	Build initial prototype	12 mons	Fri 25-4-31	Thu 25-3-32
64	**Perform on-ground testing of system**	**280 days**	**Fri 26-3-32**	**Thu 21-4-33**
65	Perform quality inspections	3 mons	Fri 26-3-32	Thu 17-6-32
66	Perform structural integrity testing	12 mons	Fri 26-3-32	Thu 24-2-33
67	Perform initial power on	2 mons	Fri 26-3-32	Thu 20-5-32
68	perform aircraft systems check	6 mons	Fri 21-5-32	Thu 4-11-32
69	perform aircraft backup system checks	6 mons	Fri 21-5-32	Thu 4-11-32
70	perform safety assesment	3 mons	Fri 5-11-32	Thu 27-1-33
71	Perform taxi tests	3 mons	Fri 28-1-33	Thu 21-4-33
72	**Perform flight tests**	**520 days**	**Thu 21-4-33**	**Thu 19-4-35**
73	Perform first flight	0 mons	Thu 21-4-33	Thu 21-4-33
74	Perform maneuverability tests	24 mons	Fri 22-4-33	Thu 22-2-35
75	Perform stall test behaviour	24 mons	Fri 22-4-33	Thu 22-2-35
76	Asses emissions	24 mons	Fri 22-4-33	Thu 22-2-35
77	Asses noise	24 mons	Fri 22-4-33	Thu 22-2-35
78	perform climate tests	24 mons	Fri 22-4-33	Thu 22-2-35
79	asses take-off performance	24 mons	Fri 22-4-33	Thu 22-2-35
80	asses landing performance	24 mons	Fri 22-4-33	Thu 22-2-35
81	asses operational performance	24 mons	Fri 22-4-33	Thu 22-2-35
82	perform route-proving tests	24 mons	Fri 17-6-33	Thu 19-4-35
83	perform critical design review	26 mons	Fri 22-4-33	Thu 19-4-35
84	obtain certification	0 days	Thu 19-4-35	Thu 19-4-35
85				
86	**Production**	**6 mons**	**Wed 17-6-20**	**Tue 1-12-20**

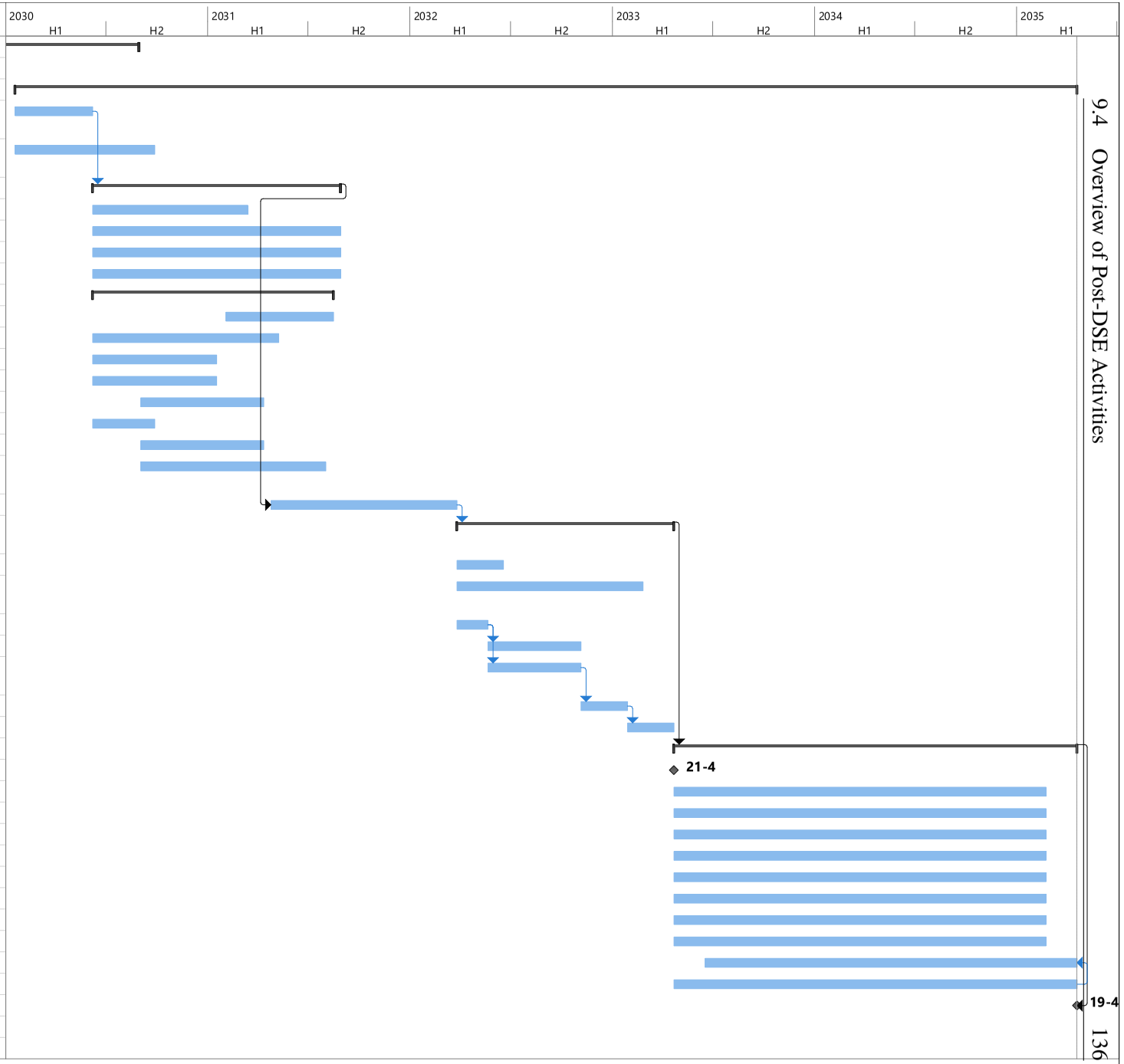

ID	Task Name	Duration	Start
1	**Design**	**2644 days**	**Mon 13-7-20**
45	**Testing Procedures**	**1370 days**	**Fri 18-1-30**
84			
85	**Production**	**6 mons**	**Wed 17-6-20**
86	**Manufacturing**	38 days	**Wed 17-6-20**
87	Raw material production	33 days	Wed 17-6-20
88	Bolts, rivets, nuts screws	20 days	Mon 13-7-20
89	stiffeners	20 days	Mon 13-7-20
90	metal sheets	20 days	Mon 13-7-20
91	ribs	20 days	Mon 13-7-20
92	Avionics, sensors, hydraulics, electronics	20 days	Mon 13-7-20
93	other individual parts	20 days	Mon 13-7-20
94	**subsubassembly**	**80 days**	**Mon 6-7-20**
95	HLD's	25 days	Mon 17-8-20
96	Wingbox	40 days	Mon 27-7-20
97	fuselage/wing skin panels	20 days	Mon 24-8-20
98	windows	10 days	Mon 7-9-20
99	empennage surfaces	30 days	Mon 10-8-20
100	engine pylons	40 days	Mon 27-7-20
101	Engines	80 days	Mon 6-7-20
102	Fuel tanks	30 days	Mon 10-8-20
103	Integrate subsubsystems into subsystems	30 days	Mon 10-8-20
104	System testing	9 days	Mon 21-9-20
105	**Subassembly**	**35 days**	**Mon 7-9-20**
106	Assemble wings	25 days	Mon 21-9-20
107	Assemble cabin	15 days	Mon 21-9-20
108	Assemble tail section	15 days	Mon 21-9-20
109	Assemble nose section	15 days	Mon 21-9-20
110	Assemble landing gears	30 days	Mon 7-9-20
111	**Main assembly**	**16 days**	**Mon 12-10-2**
112	Assemble fuselage	10 days	Mon 12-10-2
113	Add wings	4 days	Mon 26-10-2
114	add landing gears	2 days	Mon 26-10-2
115	add engines	3 days	Wed 28-10-2
116	add interiors	6 days	Mon 26-10-2
117	**Integration**	**32 days**	**Mon 19-10-2**
118	**Connect systems**	**17 days**	**Mon 19-10-2**
119	Connect electronics/avionics	10 days	Mon 19-10-2
120	Connect oxygen systems	3 days	Mon 26-10-2
121	Connect fuel distribution syste	7 days	Mon 2-11-20
122	connect instrumentation	10 days	Mon 19-10-2
123	**Perform system checks**	**22 days**	**Mon 2-11-20**
124	Check control surfaces	10 days	Mon 2-11-20
125	Check electronic systems	10 days	Mon 2-11-20
126	check instrumentation	10 days	Mon 2-11-20
127	check redundancies	10 days	Mon 2-11-20
128	check safety equipment	10 days	Mon 2-11-20
129	Perform flight tests	8 days	Mon 16-11-2
130	paint	8 days	Mon 9-11-20
131	Delivery	0 days	Tue 1-12-20

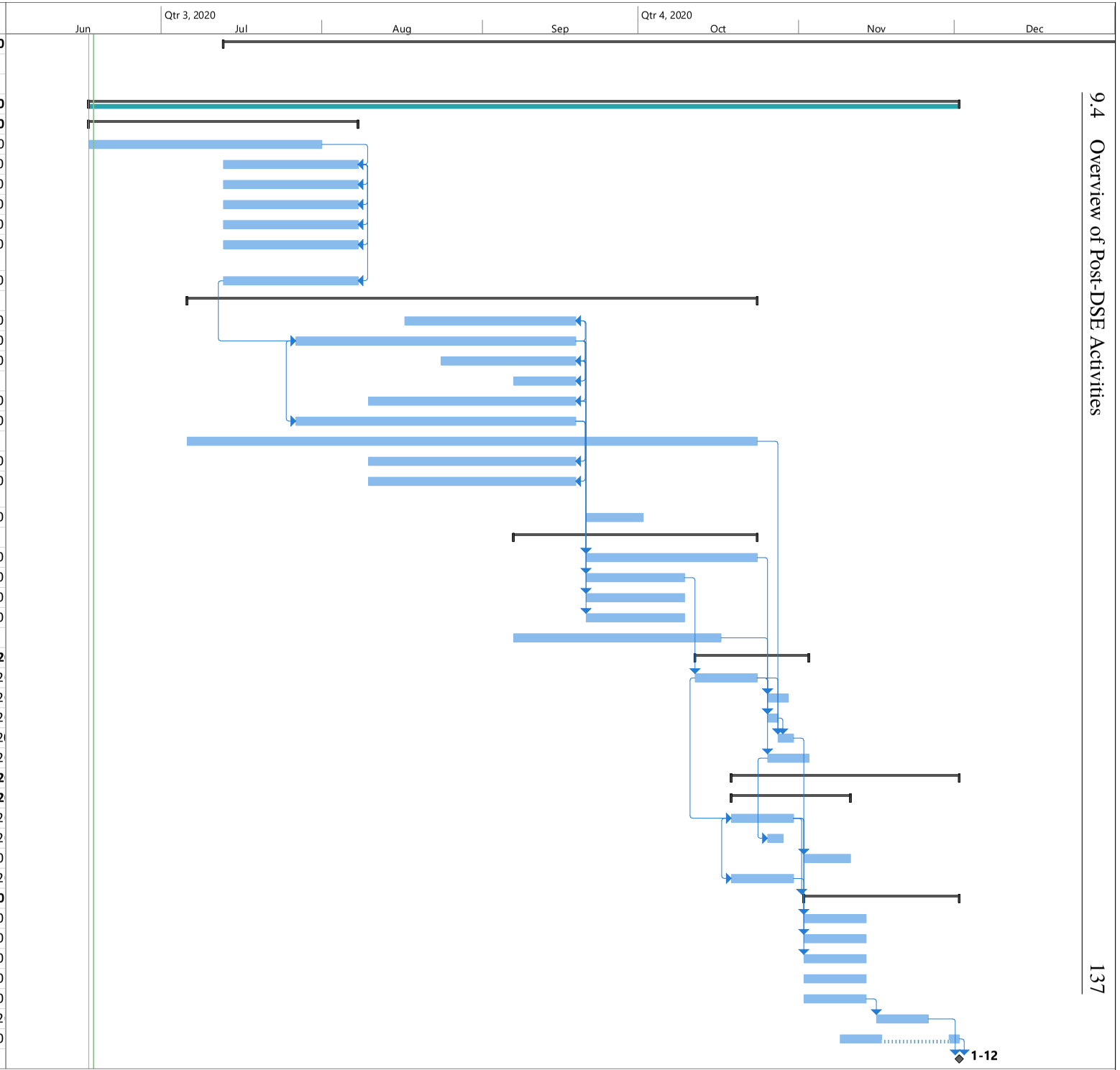

9.5 Technical Risks in the Post-DSE Phase

As for all phases of the RELIGHT program, a technical risk analysis has been performed and a mitigation plan has been devised for the future of the project.

9.6 Risk analysis

The sources of risk for the upcoming phases of the RELIGHT program have been investigated and compiled in the following table. The risks are assessed for all elements of post-DSE development, from the continuation of the design to series production. The risk identifier enumeration starts from $RISK\_39$, earlier risk identifiers correspond to the risks identified in the preliminary stages of the project and design.

Table 83: Technical Risk Assessment

Identifier	Risk	Drivers	Consequences	Likelih.	Impact
RISK_39	Propulsion produced reduced/increased	The assumed efficiency losses are either too large or too small for the propulsion system	Redesign of system	2	3
RISK_40	The stresses are higher than anticipated	Temperature management of cryogenic hydrogen	The fact that the thermodynamic model does not represent reality must be accepted	3	3
RISK_41	The environmental impact larger than anticipated	Increased production of contrails	The sustainability performance is lower	2	1
RISK_42	Subsystem is heavier than anticipated	Class II weight estimation of aircraft	Snowball Effect,Stability Issues / Center of gravity is not within allowable range	3	4
RISK_43	Reduction of aerodynamic performance larger than anticipated, increased drag, decreased lift	Wing twist	more rotational rigidity required, increased in structural weight	2	3
RISK_44	The aircraft does not meet the newly drafted safety requirements during testing	Not established hydrogen aircraft requirements.	Redesign must be done, delays in certification issuing	2	4
RISK_45	The workers go on strike	Worker demands not met	Temporary delay in production and assembly	2	2
RISK_46	Raw material/employee wage price fluctuations	Economic downturn	Cost increase and can lead to strikes	2	4

Identifier	Risk	Drivers	Consequences	Likelih.	Impact
RISK_47	Hydrogen energy cost not decreased	Hyrogen as alternative fuel loses popularity in funding	Emissions not reduced and value proposition massively decreased.	2	5
RISK_48	Bottlenecks in assembly process/ Excessive storage time for completed parts/subassemblies	Discrepancy in time taken to perform different steps of the production process	Increased storage costs and delays in production	2	3
RISK_49	certification delays/not certifiable	propulsion too complicated	delays and cost increase or possible termination of current propulsion system if certification is not possible	2	4
RISK_50	Market difficulties	higher operational cost w.r.t to current competitors, and ground operations limitations	Decrease in overall sales of the aircraft, due to lack of competitiveness	3	3

The table of risks above is summarized in a risk matrix below. The risk matrix shows the the unmitigated risks, after this plans will be made to mitigate as many risks as possible with the goal to lower their likelihood and impact as much as possible.

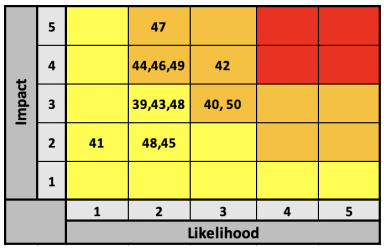

Figure 75: Unmitigated risk matrix

9.6.1 Mitigation Plan

The probability and/or severity of the risk events needs to be lowered as much as possible. To this end, the following mitigation plan has been devised. Some risks are accepted as is since it would not be physically or economically possible to mitigate them.

Table 84: Mitigation Plan

Identifier	Mitigate	Explanation
RISK_39	Accept	The true losses are estimated and uncertainty that comes along with that much just be accepted
RISK_40	Accept	The risk must be accepted that there is a deviation between the thermodynamic model and reality.
RISK_42	Treat	Sensitivity analysis performed to quantify the amount of change introduced if subsystems have a variant in mass and to ensure is acceptable.
RISK_43	Treat	Set a strict angle of twist to reduce the adverse effects
RISK_44	Accept	.
RISK_45	Accept	.
RISK_46	Treat	Set up contracting pinning prices with suppliers on raw materials, passing the risk onto the suppliers and avoid being affected by material price fluctuations.
RISK_47	Accept	.
RISK_48	Treat	Make a production plan to reduce the level of bottlenecking in the production line.
RISK_49	Accept	.
RISK_50	Treat	Investigate government subsidies, due to pollution reduction, to make the product economically more competitive with their kerosene counterparts.

Now that the mitigation plan is made the reduction in likelihood and impact is shown in the mitigated risk matrix.

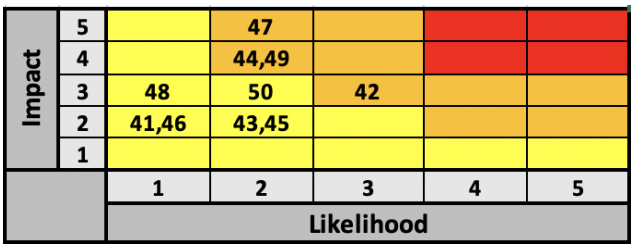

Figure 76: Mitigated risk matrix

Finally a contingency plan is made that covers what plan of action to take if a risk is fulfilled.

Table 85: Contingency planning

Identifier	Contingency plan
RISK_39	Reassess the feasibility of the design with the new changes.
RISK_40	Same contingency plan as Risk_39
RISK_41	The pollution of the contrails is larger that anticipated a reassessment of the sustainability of the aircraft is made.
RISK_45	Set up emergency meeting to to expedite a response plan to appease workers
RISK_47	Reevaluate project viability.

9.7 Risk Mitigation during Design

There are several risks that have been taken care off during the design phase of the aircraft.

Table 86: Contingency planning

Identifier	Contingency plan
RISK_11	Noise compliance we are well below current noise regulations reducing the likelihood of the risk to very unlikely.
RISK_21	The risk to stability due to the tank was solved through the use of podded tanks. Likewise the risk of the fuselage size increasing due to the tank size increase was removed through the means of the podded tanks.
RISK_34	Eliminated by using a full metal aircraft (aluminum) the risk of poor recyclability and re-usability is gone since this only applied to certain composites. It also makes the aircraft more sustainable from a production point of view.

10 Conclusion and Recommendations

The inspiration and objective of the RELIGHT is to provide a sustainable solution to the growing regional flight market. Every single decision that was made during the design process of the aircraft was made to fit that need while keeping the aircraft competitive from an economic point of view.

RELIGHT's superior environmental performance stems from a number of design choices, of which the one with the biggest effect is the use of hydrogen as fuel. Compared to other green fuel options such as biofuels, hydrogen has the advantage of no emissions for CO_2 and minimal emissions for NO_x. The high wing configuration allows for ultra-high bypass ratio turbofans, which have been adapted to work with hydrogen. The wing structure has been designed to use the added weight due to the engines and the wing-mounted tanks to relieve the load caused by the lift, leading to a lighter overall weight. The performance in sustainability during operations have been quantified by the Water Footprint and Air Pollution Footprint. RELIGHT has a 31.3% higher WF than the CRJ700 due to the higher amount of feedstock needed for fuel production. However, the APF is a staggering 69 % lower compared to the CRJ700. While sustainability during operations is paramount, RELIGHT has been designed under the philosophy that emissions and cost for production and end-of-life. That is why materials have been chosen taking into consideration ease of manufacturing and ease of disposal after end-of-life. Furthermore, the aircraft meets all ICAO stage 5 noise requirements, providing a reasonable upper bound to noise pollution.

All these innovations and improvements in performance lead to an aircraft which is capable of fulfilling its' mission of carrying 75 passengers over 2000 km with extremely low emissions while also being cheaper than the reference competition aircraft, the Bombardier CRJ700, at $37 million vs. $41 million per unit cost. According to the post-DSE development and production schedule, the first commercial RELIGHT aircraft is expected to enter service in late 2036. The development stage is expected to take approximately 10 years while the rigorous testing program will take about 5 years. Finally, the throughput time per unit once series production has begun will be six months.

Table 87: General aircraft performance parameters

Cruise Mach	0.74
Cruise altitude	11000 m
Take-off distance - sea level	1037 m
Landing distance - sea level	1049 m
Design range	2000 km

Table 88: General aircraft characteristics

Capacity	75 passengers
Crew	4 (2 cabin + 2 pilots)
Payload	7975.0 kg
Max fuel	1833.0
OEM	18275.6 kg
MTOM	28083 kg
Total length	28.0 m
Aspect Ratio	8.0
Wing span	22.32 m
Wing area	62.25m
Fuselage diameter	3.49 m

10.1 Recommendations

This section contains suggestions for the continuation of the design process.

10.1.1 General Performance

Many of the concepts that were touched upon in the literature study earlier in the DSE were not considered during this conceptual design phase. However, they show significant promise and investigating them further in the future might be the key to breakthroughs. Some of these technologies might also become cheaper and/or more widely available in the future.

10.1.2 Aerodynamics

The current maximum L/D ratio is larger than necessary. While a large L/D ratio is beneficial, this means that the wing might be over-sized. This large L/D ratio also means that there was no need for many leading and trailing edge high-lift devices. For this reason, basic plain flaps were chosen. However, these plain flaps do not provide optimal performance in terms of stall angle of attack and drag, so more complex flap types should be considered. This would have a positive effect on landing and take-off performance, as $C_{L_{max}}$ could be increased, which has effect on the thrust and wing loading.

The wing-mounted tanks have been designed as cylinders with hemispherical caps on both ends. Their drag contribution amounts to about 5.3% and, while quite low already, it could be lowered by analyzing more aerodynamically efficient shapes. Also, shock waves could be minimized by putting more research into Küchemann/anti-shock bodies. Furthermore, it could be investigated whether swap tanks are profitable and usable. This would lower the turnaround time.
Then, to get a better estimate for the aerodynamic properties, computational fluid dynamics or finite element method analysis is necessary. However this was out of the scope of this project.
Finally, modifications to the wing planform could be done to maximize efficiency. Although not very common on high wing aircraft, winglets could provide reductions in induced drag and are thus worth investigating. Other considerations worth looking into are using different airfoils throughout the wingspan, adding twist to the wing and adding kinks or yehudi.

10.1.3 Fuselage Layout

It is worth investigating different seating configurations to allow for more (or less) passengers. Adding seats would have a negative effect on the range, and bigger tanks would also mean more drag and weight. Conversely, removing seats can significantly increase the range, if the weight is exchanged for fuel: by removing 5 passengers and increasing the wing-mounted tanks volume by 50% the range could be extended to $3000km$. Increasing this tank volume comes at a drag penalty, and has an impact on control and stability, which must be reevaluated. Also cabin lighting should be improved and cargo placement can be reconsidered.

10.1.4 Stability & Landing Gear

High wing aircraft usually perform quite poorly in terms of rolling maneuverability. If this turns out to be the case for RELIGHT, a solution could be adding anhedral to the wing. This would exchange some of the excess rolling stability to allow for better maneuverability. The dynamic stability properties of the aircraft in general will also have to be analyzed, along with the possible use of ballasts to optimize both static and dynamic stability. The structural design of the landing gear and adding more plies to the tiresis to be investigated more thoroughly. Also, a more in-depth look into landing gear brakes is recommended

10.1.5 Propulsion & Noise

Gaseous hydrogen is known for its excellent cooling characteristics. A small part of the liquid hydrogen in the tanks could be converted to gaseous form and used to intercool stages in the engine compressor, increasing its efficiency. With regards to the APU, the energy extracted from boil-off gases might not be sufficient. If this turns out to be the case, a system to provide the APU with power from the liquid hydrogen in the tanks will have to be designed. Although the requirements on noise are not expected to become problematic in the detailed design phase, there are plenty of noise suppression concepts that could be studied such as flow mixers, acoustic lining and silencing engine nozzles.

10.1.6 Maintenance

Maintenance can make up us much as 25% of the aircraft operational cost per block hour; it is therefore very important to make sure that all components are designed with ease of inspection in mind. This applies especially to more unconventional components such as the hydrogen external wing tanks. Since the tanks are made of carbon-fiber-reinforced thermoplastics, innovative methods for thermoplastic repair are worth exploring [97]. Using modular components wherever possible may also lead to easier and quicker inspections.

10.1.7 Hydrogen Tanks

The thermodynamic effects of the free-stream airflow on the external wing tanks during flight should be researched and insulation thickness should be added accordingly; requiring weight and drag to be reassessed. Forming of ice must be investigated, as do de-icing mechanisms. The tanks must be designed to cope with bird strikes or ground collisions.

10.1.8 Sustainability

Throughout the project, the emphasis regarding the sustainability approach was set on the operations of the aircraft. Many systems were designed having that in mind. As a sustainable design entails the whole life cycle of the aircraft, considerations regarding each phase need to be taken into account in the design. Continuing work from this point should explore the effect on the other phases of the life such as manufacturing and end-of-life in more detail than it was presented in this report.

References

[1] J Dr. Roskam. *Airplane Design - Part V: Component Weight Estimation*. DARcorporation, 2018.

[2] J. Roskam. *Airplane Design Part V: Component Weight Estimation*. DARcorporation, Kansas, USA, 2018. Fifth printing, in 2018.

[3] DSE Group 20. Sustainable Regional Aircraft Baseline Report final. Technical report, Tu Delft, may 2020.

[4] DSE Group 20. Sustainable Regional Aircraft Midterm Report final. Technical report, Tu Delft, may 2020.

[5] ICAO ENVIRONMENTAL REPORT 2010 - AVIATION and CLIMATE CHANGE. Technical report, International Civil Aviation Organization (ICAO), 2010.

[6] R. Vos, J.A. Melkert, and B.T.C. Zandbergen. Aerospace Design and System Engineering Elements I - A/C Preliminary Sizing.

[7] World air transport statistics. Technical report, International Air Transport Association, 2019.

[8] International Air Transport Association. Iata forecast predicts 8.2 billion air travelers in 2037, 2018.

[9] European Commission. Reducing emissions from aviation, 2020.

[10] International Civil Aviation Orgnization. Trends in emissions that affect climate change, 2019.

[11] International Air Transport Association. Aircraft technology roadmap to 2050. Technical report, 2009.

[12] European Commission. Flightpath 2050 Europe's vision for aviation: Report of the High Level Group on Aviation Research. 2011.

[13] M. Grant. Sustainability, 2020.

[14] J. Morelli. Environmental sustainability: A definition for environmental professionals. *Journal of Environmental Sustainability*, 2011.

[15] R.J. Thomson T.L. Reddy. Environmental, social and economic sustainability: Implications for actuarial science. 2015.

[16] C. Surbeck. Social sustainability from an engineer's perspective, 2013.

[17] European Commission. Labour law, 2020.

[18] L. Meyer R.K. Pachauri. Climate Change 2014: Synthesis Report. 2014.

[19] P. Grammelis. *Energy, Transportation and Global Warming*. 2016.

[20] B. HerbschleB. Conventionele kerosine als vliegtuigbrandstof: Gevolgen voor Klimaat, Gezondheid, Land Water gebruik en Prijsontwikkeling. Technical report, VMB2, March 2019.

[21] V. Himabindu S.S. Kumar. Hydrogen production by PEM water electrolysis – A review. 2019.

[22] M. Wang J. Han R.J. Henderson P. Sun, A. Elgowainy. Estimation of U.S. refinery water consumption and allocation to refinery products. *Fuel*, 2018.

[23] I.H. Lee F. Allroggen A. Ashol F. Caiazzo S.D. Eastham R. Malina S.R.H. Barett S.H.L. Yim, G.L. Leem. Global, regional and local health impacts of civil aviation emissions. *Environmental Research Letters*, 2015.

[24] EIA: U.S. Energy Information Administration. Is ozone a greenhouse gas? 2019.

[25] D. Scholz K. Seeckt. JET VERSUS PROP, HYDROGEN VERSUS KEROSENE FOR A REGIONAL FREIGHTER AIRCRAFT. Technical report, Hamburg University of Applied Sciences.

[26] J. Roskam. *Airplane Design Part I: Preliminary Sizing of Airplanes*. DARcorporation, Kansas, USA, 1997.

[27] Airbus Deutschland GmbH et al. Liquid Hydrogen Fuelled Aircraft – System Analysis. Technical report, may 2002.

[28] GE aviation. CF34-8C turbofan propulsion system. Fact sheet.

[29] A. Colozza. Hydrogen storage for aircraft applications overview. Technical report, NASA Glenn Research Center, September 2002.

[30] R. Thomson et al. Hydrogen: A future fuel for aviation?, 2020.

[31] J. Roskam. *Airplane Design Part VI: Preliminary Calculation of Aerodynamic Thrust and Power Characteristics*. DARcorporation, Kansas, USA, 1987. Fourth printing, in 2004.

[32] J. Roskam. *Airplane Design Part III: Layout design of cockpit, fuselage, wing and empennage: cutaways and inboard profiles*. DARcorporation, Kansas, USA, 2002.

[33] 'Passenger emergency exits, emergency features and escape routes — Harmonisation with FAA' . Technical report, European Aviation Safety Agency, 2010.

[34] D. Scholz. Drag prediction, 2010.

[35] F. Oliviero. Aerospace Design & Systems Engineering Elements - Aircraft Aerodynamic Analysis Fundamentals, 2019.

[36] D.P. Raymer. *Aicraft Design: A Conceptual Approach*. AIAA, 1999.

[37] E. Torenbeek. The computation of characteristic areas and volumes of major aircraft components in project design. 1973.

[38] Stanford University. Fuselage upsweep drag, 2020.

[39] Mihaela Niţă and Dieter Scholz. *Estimating the oswald factor from basic aircraft geometrical parameters*. Deutsche Gesellschaft für Luft-und Raumfahrt-Lilienthal-Oberth eV, 2012.

[40] L.W. Traub. Camber effects on minimum power and thrust relations for propeller aircraft. 2016.

[41] C. D. Cone Jr. The aerodynamic design of wings with camebred span having minimum induced drag. Technical report, NASA, 1964.

[42] R. Babikian. The historical fuel efficiency characteristics of regional aircraft from technological, operational, and cost perspectives, June 2001.

[43] J. Ellerbroek J. Sun, J.M. Hoekstra. Aircraft drag polar estimation based on a stochastic hierarchical model. 2018.

[44] I. Sumner. LOW-DENSITY FOAM FOR INSULATING LIQUID-HYDROGEN TANKS . Technical report, NASA, March 1969.

[45] Wayne Carlsen. Development of transonic area-rule methodology. Technical report, NASA, October 1995.

[46] JEC Group. Carbon fibre-reinforced polymer for cryogenic liquid hydrogen storage systems, Apr 2014.

[47] B. Khandelwal, A. Karakurt, P. Sekaran, V. Sethi, and R. Singh. Hydrogen powered aircraft : The future of air transport. *Progress in Aerospace Sciences*, 60:45–59, Jan 2013.

[48] F. Oliviero. Systems Engineering & Aerospace Design - Weight and Balance in AC design, 2020.

[49] Certification Specifications and Acceptable Means of Compliance for Large Aeroplanes CS-25. Technical report, EASA. Amendment 24.

[50] Dr. F. Oliviero. Aircraft aerodynamic analysis - Mobile surfaces of the wing. Brightspace, 2018.

[51] Dr. Fabrizio Oliviero. Aerospace Design and System Engineering Elements II - Aircraft aerodynamic analysis - fundamentals.

[52] J. Roskam. *Airplane Design Part IV: Layout Design of Landing Gear and Systems*. DARcorporation, Kansas, USA, 1989.

[53] F. Oliviero. Requirement Analysis and Design principles for A/C stability & control (Part 2), 2020.

[54] Torenbeek E. *Synthesis of Subsonic Airplane Design*. Kluwer Boston Inc., 1982.

[55] N.S. Currey. *Aircraft Landing Gear Design: Princilpes and Practices*. American Institue of Aeronautics and Astronautics, Inc., 1988.

[56] Bombardier. Model CL−600−2C10 Series 700 AIRPORT PLANNING MANUAL, 2015.

[57] I.Sen. AIRCRAFT FUSELAGE DESIGN STUDY. Technical report, Delft University of Technology, 2010.

[58] P. Geng, J. Z. Xing, and X. X. Chen. Winding angle optimization of filament-wound cylindrical vessel under internal pressure. *Archive of Applied Mechanics*, 87(3):365–384, Jan 2016.

[59] E.G. Kendall. *METALS AND ALLOYS FOR CRYOGENIC APPLICATIONS - A REVIEW*. Aerospace Corporation, California,USA, 1964.

[60] M. Bauccio. *ASM Metals Reference Book*. ASM International, Ohio, USA, 1993. Third Edition.

[61] E. W. Collings R. Boyer, G. Welsch. *Materials Properties Handbook: Titanium Alloys*. ASM International, Ohio, USA, 1994.

[62] Hexcel. HexTow IM7 Carbon Fiber, 2020.

[63] J. Zhang H. Sun H. Zheng, X. Zeng. The Application of Carbon Fiber Composites in Cryotank, Solidification. *IntechOpen*, March 2018.

[64] Kautex Maschinenbau. Kautex produces 320-liter hydrogen liner in blow molding process.

[65] F. Bonaudi. European Regional Airports. Technical report, Airports Council International. Retrieved from Google Scholar.

[66] Mike Sinnett. Hydrogen powered aircraft : The future of air transport. *Boeing Aero magazine*, 2007.

[67] M.J.L van Tooren R.J. Hamann. Systems engineering & technical management techniques: Part ii, 2006.

[68] M. Voskuijl. AE2230 Flight & Orbital Mechanics (2018/19 Q3). Brightspace, feb 2019.

[69] Ger J.J. Ruijgrok. *Elements of airplane performance*. Delft Academic Press, 2009.

[70] Ozlem Sahin. Calculation of Turn Radius and Bank Angle at Different Altitudes Based on RNP AR. International Journal of Mechanical Engineering and Robotics Research Vol 5, jul 2016.

[71] Dries Verstraete. Long range transport aircraft using hydrogen fuel, 2013.

[72] Federal Aviation Administration. *Airplane Flying Handbook*, volume Chapter 5 Takeoffs and Departure Climbs. Aviation Supplies & Academics, Inc., nov 2016.

[73] Bombardier commercial Aircraft. Bombardier CRJ Series Brochure, 2017.

[74] Procedures for the Noise Certification of Aircraft, jan 2014.

[75] Christoph Zellmann, Jean Wunderli, and Christian Paschereit. The sonair sound source model: Spectral three-dimensional directivity patterns in dependency of the flight condition. 08 2016.

[76] Antonio Filippone. Aircraft noise prediction. Progress in Aerospace Sciences, 2014.

[77] *Aircraft Noise Prediction Program Theoretical Manual*, Hampton, Virginia, 1982. National Aeronautics and Space Admninistration.

[78] M. F. Heidman. Interim Prediction Method for Fan and Compressor Source Noise. NASA TM X-71763, 1975.

[79] Bushell K. W. Smith, M. J. T. Turbine Noise - Its Significance in the Civil Aircraft Noise Problem. Paper 69-WA/GT-12. American Soc. Mech. Eng., nov 1969.

[80] Martin R. Fink. Airframe Noise Prediction Method. FAA-RD-77-29, mar 1977.

[81] Christoph Zellmann Lennart Rossian Ehsan Kian Far Tobias Ring Jan Delfs, Lothar Bertsch and Sabine C. Langer. Aircraft Noise Assessment—From Single Components to Large Scenarios. *Energies*, 11, feb 2018.

[82] EASA. Jet aeroplanes noise database, feb 2020.

[83] Peter DeFazio. Commercial Aviation: Pilots' and Flight Attendants' Exposure to Noise aboard Aircraft. Commercial Aviation, nov 2017.

[84] F. Svensson. Potential of Reducing the Environmental Impact of Civil Subsonic Aviation by Using Liquid Hydrogen. 2005.

[85] J. Moldanova F. Svensson, A. Hasselrot. Reduced environmental impact by lowered cruise altitude for liquid hydrogen-fuelled aircraft. 2004.

[86] H. Sun T. C. Bond. Can Reducing Black Carbon Emissions Counteract Global Warming? *Environmental Science Technology*, 2005.

[87] A. Kuntcky C. Amy. Hydrogen as a Renewable Energy Carrier for Commercial Aircraft. 2019.

[88] K. Kundu C.J. Marek, T.D. Smith. Low Emission Hydrogen Combustors for Gas Turbines Using Lean Direct Injection. 2005.

[89] Jacob Markish. Valuation Techniques for Commercial Aircraft Program Design, 2002. Department of Aeronautics and Astronautics.

[90] D. P. Raymer. *Aircraft Design: A Conceptual Approach*. American Institute of Aeronautics and Astronautics, 1999.

[91] Hamburg University of Applied Sciences Aircraft Design and Systems Group (Aero). JET VERSUS PROP, HYDROGEN VERSUS KEROSENE for a regional freighter aircraft. Technical report, 2009.

[92] M. E. Webber. The water intensity of the transitional hydrogen economy. 2007.

[93] EPA United States Environmental Protection Agency. ealth and Environmental Effects of Particulate Matter (PM), 2020.

[94] R. Balachandran N. Ladommatos M. Talibi, P. Hellier. Effect of hydrogen-diesel fuel cocombustion on exhaust emissions with verification using an in–cylinder gas sampling technique. *International Journal of Hydrogen Energy*, 2014.

[95] N. Kim D.F. Bradford D.L. Mauzerall, B. Sultan. NOx emissions from large point sources: variability in ozone production, resulting health damages and economic costs. *Atmospheric Environment*, 2005.

[96] Airbus SE. Test programme and certifications. Department of Aeronautics and Astronautics.

[97] N. Weidlich F. Seidel, Z.A.K. Leszek. Method of repairing damage of aircraft engine components made of weldable thermoplastic materials, 2016.

Appendix A: Table of Contributions

	Jorn van Beek	Sasho Ivanov	Jari Malfliet	Manuel Martin	Matteo Rebosolan	Rick van Rooijen	Paul Simon Schön	George Tzanetos	Tobias Veselka	Martijn Vroom
Preface				X						
Executive Overview	X	X	X	X	X	X	X	X	X	X
Introduction								X		
Project Objectives						X				
General Objectives						X				
Name of the Aircraft	X					X				
Market Demands							X			
Mission Characteristics						X			X	
Flight Profile						X				
Payload-Range Diagram			X			X				
Operations and Logistics			X						X	
Functional Analysis						X			X	
Sustainable Development Strategy										X
Sustainability Approach										X
Quantification of Sustainability		X								X
Preliminary Concept Description				X		X		X		
Preliminary Concept Trade-off Summary				X		X				
Hydrogen Hybrid Definition			X	X						
Class I Weight Estimation			X	X						
Results Discussion			X							
Concept Selection			X							
Class II Weight Estimation	X				X					
Flight Envelope								X		
Subsystem Development						X		X	X	
Fuselage and Tank Layout Design			X	X			X			
Wing Planform Design		X	X					X		X
Propulsion System Design		X	X	X			X			
Stability and Control	X					X			X	
Materials and Structural Design			X	X	X					
Final Design Characteristics	X							X		
Requirements										
Resource Allocation / Budget Breakdown		X							X	
Aircraft Systems	X	X						X		
RAMS characteristics		X						X		
Aircraft Performance Analysis						X			X	
Take-off, Climb, Cruise, Turning and Landing Performance						X			X	
Aircraft Noise						X				
Aircraft Operational Emissions										X
Cost Performance							X		X	
Aircraft Sustainability		X								X
Future Aircraft Development	X				X					
Continuation of Aircraft Development	X				X					
Aircraft Testing Procedures	X				X					
Manufacturing, Assembly and Integration (MAI) Plan	X	X		X	X					
Overview of Post-DSE Activities	X				X					
Technical Risks in the Post-DSE Phase				X	X					
Conclusion and Recommendations					X	X				
Recommendations		X			X	X				
CATIA			X							
Rendering			X					X		